INTRACELLULAR INFECTIOUS DISEASES

EDITED BY: Feng Lu, Shaobin Shang, Si-Yang Huang and Eun-Taek Han

PUBLISHED IN: Frontiers in Medicine, Frontiers in Cell and Developmental Biology and Frontiers in Public Health

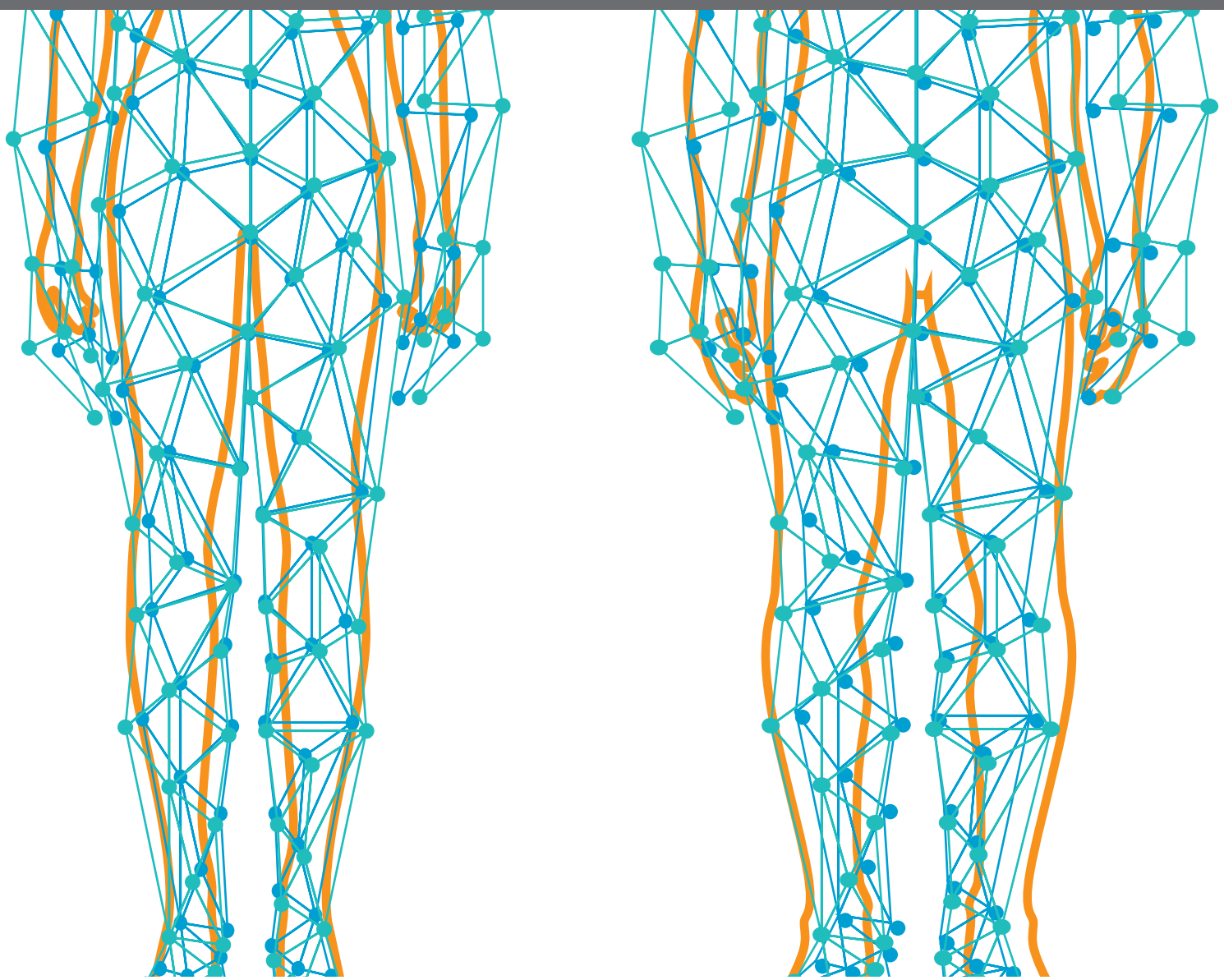

frontiers Research Topics

ISSN 1664-8714
ISBN 978-2-88966-511-2
DOI 10.3389/978-2-88966-511-2

About Frontiers

Frontiers is more than just an open-access publisher of scholarly articles: it is a pioneering approach to the world of academia, radically improving the way scholarly research is managed. The grand vision of Frontiers is a world where all people have an equal opportunity to seek, share and generate knowledge. Frontiers provides immediate and permanent online open access to all its publications, but this alone is not enough to realize our grand goals.

Frontiers Journal Series

The Frontiers Journal Series is a multi-tier and interdisciplinary set of open-access, online journals, promising a paradigm shift from the current review, selection and dissemination processes in academic publishing. All Frontiers journals are driven by researchers for researchers; therefore, they constitute a service to the scholarly community. At the same time, the Frontiers Journal Series operates on a revolutionary invention, the tiered publishing system, initially addressing specific communities of scholars, and gradually climbing up to broader public understanding, thus serving the interests of the lay society, too.

Dedication to Quality

Each Frontiers article is a landmark of the highest quality, thanks to genuinely collaborative interactions between authors and review editors, who include some of the world's best academicians. Research must be certified by peers before entering a stream of knowledge that may eventually reach the public - and shape society; therefore, Frontiers only applies the most rigorous and unbiased reviews.
Frontiers revolutionizes research publishing by freely delivering the most outstanding research, evaluated with no bias from both the academic and social point of view. By applying the most advanced information technologies, Frontiers is catapulting scholarly publishing into a new generation.

What are Frontiers Research Topics?

Frontiers Research Topics are very popular trademarks of the Frontiers Journals Series: they are collections of at least ten articles, all centered on a particular subject. With their unique mix of varied contributions from Original Research to Review Articles, Frontiers Research Topics unify the most influential researchers, the latest key findings and historical advances in a hot research area! Find out more on how to host your own Frontiers Research Topic or contribute to one as an author by contacting the Frontiers Editorial Office: frontiersin.org/about/contact

INTRACELLULAR INFECTIOUS DISEASES

Topic Editors:
Feng Lu, Yangzhou University, China
Shaobin Shang, Yangzhou University, China
Si-Yang Huang, Yangzhou University, China
Eun-Taek Han, Kangwon National University, South Korea

Citation: Lu, F., Shang, S., Huang, S.-Y., Han, E.-T., eds. (2021). Intracellular Infectious Diseases. Lausanne: Frontiers Media SA. doi: 10.3389/978-2-88966-511-2

Table of Contents

frontiers in Cell and Developmental Biology

ORIGINAL RESEARCH
published: 01 November 2019
doi: 10.3389/fcell.2019.00264

TRIBE Uncovers the Role of Dis3 in Shaping the Dynamic Transcriptome in Malaria Parasites

Meng Liu[1†], Binbin Lu[2†], Yanting Fan[2], Xiaohui He[2], Shijun Shen[1], Cizhong Jiang[1,3] and Qingfeng Zhang[2*]*

[1] Institute of Translational Research, Tongji Hospital, Shanghai Key Laboratory of Signaling and Disease Research, The School of Life Sciences and Technology, Tongji University, Shanghai, China, [2] Research Center for Translational Medicine, Key Laboratory of Arrhythmias of the Ministry of Education of China, East Hospital, Tongji University School of Medicine, Shanghai, China, [3] The Research Center of Stem Cells and Ageing, Tsingtao Advanced Research Institute, Tongji University, Shanghai, China

OPEN ACCESS

Edited by:
Feng Lu,
Yangzhou University, China

Reviewed by:
Jianbing Mu,
National Institutes of Health (NIH), United States
Istvan Albert,
Pennsylvania State University, United States

***Correspondence:**
Cizhong Jiang
czjiang@tongji.edu.cn
Qingfeng Zhang
qfzhang@tongji.edu.cn;
qfzhangsh@aliyun.com

[†] These authors have contributed equally to this work

Specialty section:
This article was submitted to Molecular Medicine, a section of the journal Frontiers in Cell and Developmental Biology

Received: *09 September 2019*
Accepted: *18 October 2019*
Published: *01 November 2019*

Citation:
Liu M, Lu B, Fan Y, He X, Shen S, Jiang C and Zhang Q (2019) TRIBE Uncovers the Role of Dis3 in Shaping the Dynamic Transcriptome in Malaria Parasites. Front. Cell Dev. Biol. 7:264. doi: 10.3389/fcell.2019.00264

Identification of RNA targets of RNA-binding proteins (RBPs) is essential for complete understanding of their biological functions. However, it is still a challenge to identify the biologically relevant targets of RBPs through *in vitro* strategies of RIP-seq, HITS-CLIP, or GoldCLIP due to the potentially high background and complicated manipulation. In malaria parasites, RIP-seq and gene disruption are the few tools available currently for identification of RBP targets. Here, we have adopted the TRIBE (Targets of RNA binding proteins identified by editing) system to *in vivo* identify the RNA targets of PfDis3, a key exoribonuclease subunit of RNA exosome in *Plasmodium falciparum*. We generated a transgenic parasite line of *PfDis3-ADARcd,* which catalyzes an adenosine (A)-to-inosine (I) conversion at the potential interacting sites of PfDis3-targeting RNAs. Most of PfDis3 target genes contain one edit site. The majority of the edit sites detected by PfDis3-TRIBE locate in exons and spread across the entire coding regions. The nucleotides adjacent to the edit sites contain ∼75% of A + T. PfDis3-TRIBE target genes are biases toward higher RIP enrichment, suggesting that PfDis3-TRIBE preferentially detects stronger PfDis3 RIP targets. Collectively, PfDis3-TRIBE is a favorable tool to identify *in vivo* target genes of RBP with high efficiency and reproducibility. Additionally, the PfDis3-targeting genes are involved in stage-related biological processes during the blood-stage development. Thus PfDis3 appears to shape the dynamic transcriptional transcriptome of malaria parasites through post-transcriptional degradation of a variety of unwanted transcripts from both strands in the asexual blood stage.

Keywords: malaria, *Plasmodium falciparum*, TRIBE, Dis3, RIP-seq

INTRODUCTION

Plasmodium falciparum, a unicellular apicomplexan parasite, causes the most severe clinical outcome of malaria in human. To date, malaria remains a major global health threat with an estimated 400,000 malaria deaths each year worldwide (World Health Organization [WHO], 2018). The pathogenesis of *P. falciparum* in human results from the intra-erythrocytic developmental cycle (IDC), and each step of which is controlled by a precisely timed cascade of gene

expression. Throughout the 48-h IDC, a majority of mRNAs reach peak abundance at only one time point, suggesting a strong correlation between transcriptome regulation and pathogenesis (Bozdech et al., 2003).

Recent years, post-transcriptional regulation has emerged as an important pathway in orchestrating biological processes on a transcriptome-wide scale throughout the IDC (Rai et al., 2014; Vembar et al., 2016). Nascent RNA sequencing revealed the pervasive distribution of nascent transcripts in the genome of this parasite, supporting the existence of an overlooked post-transcriptional regulation pathway in shaping the steady-state transcriptome in *P. falciparum* (Lu et al., 2017; Painter et al., 2018). For instance, by an inducible gene knockout strategy, the RNA exosome complex-associated 3′-5′ exoribonuclease subunit, PfDis3, was found to degrade different kinds of antisense lncRANs and a few mRNAs (Droll et al., 2018). Moreover, PfRNase II, an ortholog of Dis3, has been reported to silence a subgroup of the primary virulence genes, *var*, by degrading nascent mRNA *in situ* (Zhang et al., 2014). These studies point to a critical regulatory function of RNA exosome in shaping the transcriptome of malaria parasites by surveillance of various transcripts in the life cycle. However, due to the failure to generate and isolate the pure cells of DiCre recombinase-mediated conditional PfDis3 knockout line, the exact targets and related biological role of PfDis3 in regulating transcriptome of malaria parasites remain to be clarified by other approaches.

Conventional methods to identify *in vivo* targets of RNA-binding proteins (RBP) include CLIP (crosslinking and immunoprecipitation) and variants thereof (Ule et al., 2003, 2005; Corden, 2010; Moore et al., 2014) and RIP (RNA immunoprecipitation) (Gilbert and Svejstrup, 2006). These methods are based on immunoprecipitation with specific antibodies recognizing the RBPs. After covalently binding of RBP to its targets, unprotected RNAs are digested and the remaining RBP-bound RNAs are isolated for high throughput sequencing. These approaches need a high-affinity and specific antibody. The low efficiency of crosslinking step (∼ 1–5%) in CLIP also limits the yield of real targets in IP experiments (Darnell, 2010). It therefore requires large amounts of starting materials (almost millions of cells) and may raise the problem of high false-positive rate which is usually observed in IP experiments. *In P. falciparum*, RIP assay is still the main method to identify targets of RBPs since the CLIP-derived techniques such as PAR-CLIP or GoldCLIP are still not established in this organism so far. To overcome the defects of IP-based methods, McMahon et al. has developed a novel technique termed TRIBE (targets of RNA binding proteins identified by editing) to identify the RNA substrates of RBPs *in vivo*. This system fuses a catalytic domain of the RNA-editing enzyme ADAR (ADARcd) to a RBP of interest and expresses the fusion protein *in vivo* (McMahon et al., 2016). ADAR consists of two double-stranded RNA-binding domains (dsRBDs) and a catalytic domain (ADARcd) that deaminates adenosine to inosine (Bass and Weintraub, 1998; Keegan et al., 2004). By coupling the RBP to only ADARcd, the RBP targets are marked with *de novo* editing events which are identified by RNA sequencing (McMahon et al., 2016). Compared to the methods mentioned above, no immunoprecipitation is needed in TRIBE. Thus, problems like low efficiency of crosslinking and requirement of high affinity, specific antibody or terminal tagging of RBP of interest can be avoided (McMahon et al., 2016). Moreover, in TRIBE assay RNA is simply extracted from cells and sequenced by routine RNA-seq assay. Thus, it requires much less cells than RIP-seq. More importantly, it provides a standard but practice-friendly protocol compared with that of CLIPs (McMahon et al., 2016).

In this study, we sought to adopt the TRIBE technique in *P. falciparum*, by which we were able to identify the substrates of PfDis3 *in vivo*. We have generated *Pfdis3-adar* transgenic parasite line by CRISPR-Cas9 gene editing system, and used it to identify PfDis3-targeted transcripts by TRIBE throughout the IDC in *P. falciparum*. Through detecting *de nova* editing events catalyzed by the PfDis3-ADARcd fusion protein, we found that the majority of the editing sites were located in exonic regions. For the 5602 protein-coding genes in the genome of 3D7 strain, we have identified 2032, 2061 and 2303 genes with editing signals on the sense transcripts, whereas 1522, 2119 and 2187 on the antisense transcripts at ring, trophozoite and schizont, respectively. The TRIBE results were further supported by RIP-seq assay with *Pfdis3-tag* transgenic line by comparative analysis. Moreover, our target genes of PfDis3 were validated by inducible *Pfdis3* gene knockdown analysis. Taken together, by development of TRIBE technique in *P. falciparum*, we reveal that PfDis3 targets are enriched in genes involved in multiple biological processes that are highly relevant to their respective time points of development in IDC, indicating a fundamental function of PfDis3 in surveillance of gene expression throughout the asexual stage in malaria parasites.

RESULTS

Generation of Pfdis3-Adar Transgenic Parasite Line by CRISPR-Cas9

To avoid side effect or growth defect by overexpression of PfDis3-ADARcd, we decided to generate an endogenous integration of the catalytic domain of ADAR enzyme from *Drosophila* into *Pfdis3* gene locus (**Figures 1A,B**). In order to use CRISPR/Cas9 gene editing technique to achieve fast endogenous integration of the catalytic domain of ADAR enzyme, we constructed the plasmid pL6-PfDis3-Ty1-ADARcd targeting the C-terminus of *Pfdis3* gene and co-transfected with Cas9 expression vector pUF1-cas9 into 3D7 strain (**Figure 1B**). Approximately 3 weeks after transfection, parasites carrying pL6-PfDis3-Ty1-ADARcd/pUF1-cas9 was obtained by drug selection with both WR99210 (WR) and blasticidin S deaminase (BSD). Next, we cloned this transgenic parasite line and confirmed the integration of Ty1-ADARcd at C-terminus of Pfdis3 gene by PCR (**Figure 1C**). Western blot assay further confirmed the expression of transgenic ADARcd with the expected molecular weight (MW) (**Figure 1D**). The specific recognition of the PfDis3-HA-Ty1 fusion protein by antibodies was critical for reducing the background of RIP-seq assay.

TRIBE technology theoretically can detect adenosine (A)-to-inosine (I) editing events on the target transcripts of

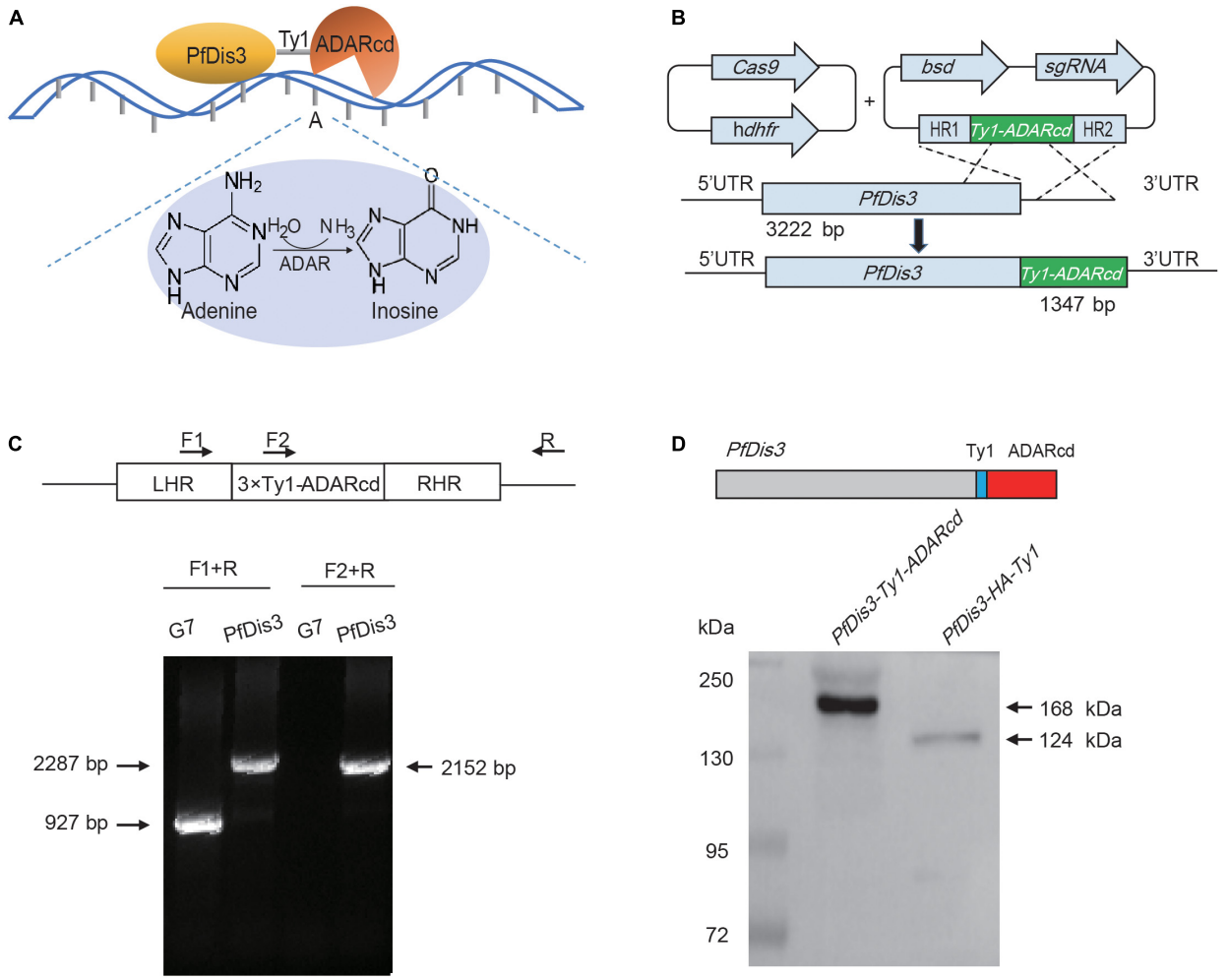

FIGURE 1 | Generation of Pfdis3-adar transgenic parasite line by CRISPR-Cas9. **(A)** PfDis3-ADARcd fusion protein was constructed by attaching a catalytic ADAR protein (ADARcd) to PfDis3. The ADARcd possess a deaminase domain that catalyzes an adenosine-to-inosine conversion. And the editing specificity of the fusion protein is determined by the RNA recognition features of PfDis3. **(B)** Schematic diagram showing the generation of PfDis3-ADARcd transfectant lines by the CRISPR-Cas9 system. The plasmid carrying a single guide RNA (sgRNA) and the Cas9 endonuclease were co-transfected. *bsd*, blasticidin S deaminase. h*dhfr*, human dihydrofolate reductase. HR, homology region. **(C)** qPCR analysis of PfDis3-ADARcd lines. LHR, homology region upstream of Pfdis3-Ty1-ADARcd. RHR, homology region downstream of PfDis3-Ty1-ADARcd. F1, forward primer 1 (5′ gaattgttccatttaagcttttatg 3′). F2, forward primer 2 (5′ cagaagtacatactaaccaagatc 3′). R, reverse primer (5′ acaatgttgttaaattaagtattatg 3′). **(D)** Western blot analysis of PfDis3-ADARcd lines with antibody against Ty1 epitope.

PfDis3 since the PfDis3-ADARcd protein doesn't contain the RNA recognition domain of ADAR (**Figure 1A**). To eliminate the background due to genomic mutation or Single Nucleotide Polymorphism (SNPs), we have re-sequenced the genome sequence of wild-type 3D7-G7 clone for transfection of *PfDis3-ADARcd* construct. Next, by strand-specific RNA sequencing of PfDis3-ADARcd transgenic parasite clone, we were able to identify the *de novo* editing events on the target transcripts of PfDis3 on individual strands of chromosomes. The wild-type 3D7-G7 clone was used as control to exclude endogenous RNA editing events in the parasites. To comprehensively identify the targets of Pfdis3, we harvested the synchronized parasites at ring (R), trophozoite (T) and schizont (S) asexual developmental stages, respectively. Meanwhile, the PfDis3-HA-Ty1 tagging line was collected in parallel for RIP-seq analysis with specific antibody against Ty1 epitope.

PfDis3-ADARcd Edits Evenly Along the Transcripts From 5′UTR to 3′UTR

By nucleotide sequence-based stranded comparative transcriptome analysis between PfDis3-ADARcd and WT 3D7-G7 clone, a total of 3643, 3626, 3387 editing sites on the sense transcripts and 2671, 3765, 3789 editing sites on the antisense transcripts were detected for the three asexual developmental stages (R, T, S), respectively. These editing sites correspond to 2032, 2061, 2303 genes and 1522, 2119, 2187 antisense non-coding RNAs, respectively. Besides the known structured RNAs processed by PfDis3 protein such as rRNAs and

small nucleolar RNAs, we also identified many PfDis3 targets of various functions corresponding to their respective developing stages (**Supplementary Table S1**).

The majority of the *de novo* edit sites of PfDis3-ADARcd locate in exons (**Figure 2A**). Moreover, the edit sites are evenly distributed along the transcripts with minor enrichment in the 3′UTR (**Figures 2B,C**). This enrichment feature is consistent with Dis3's catalytic feature as endonuclease and exonuclease (Lebreton et al., 2008; Schaeffer et al., 2009; Schneider et al., 2009). The number of the edit sites in each transcript ranges from 1 to 15. Most of transcripts contain single edit site (**Figure 2D**). Interestingly, the editing events are highly reproducible both in position and efficiency (**Figure 2D**, inset and **Supplementary Figure S1A**). The median percentage editing levels of *de novo*

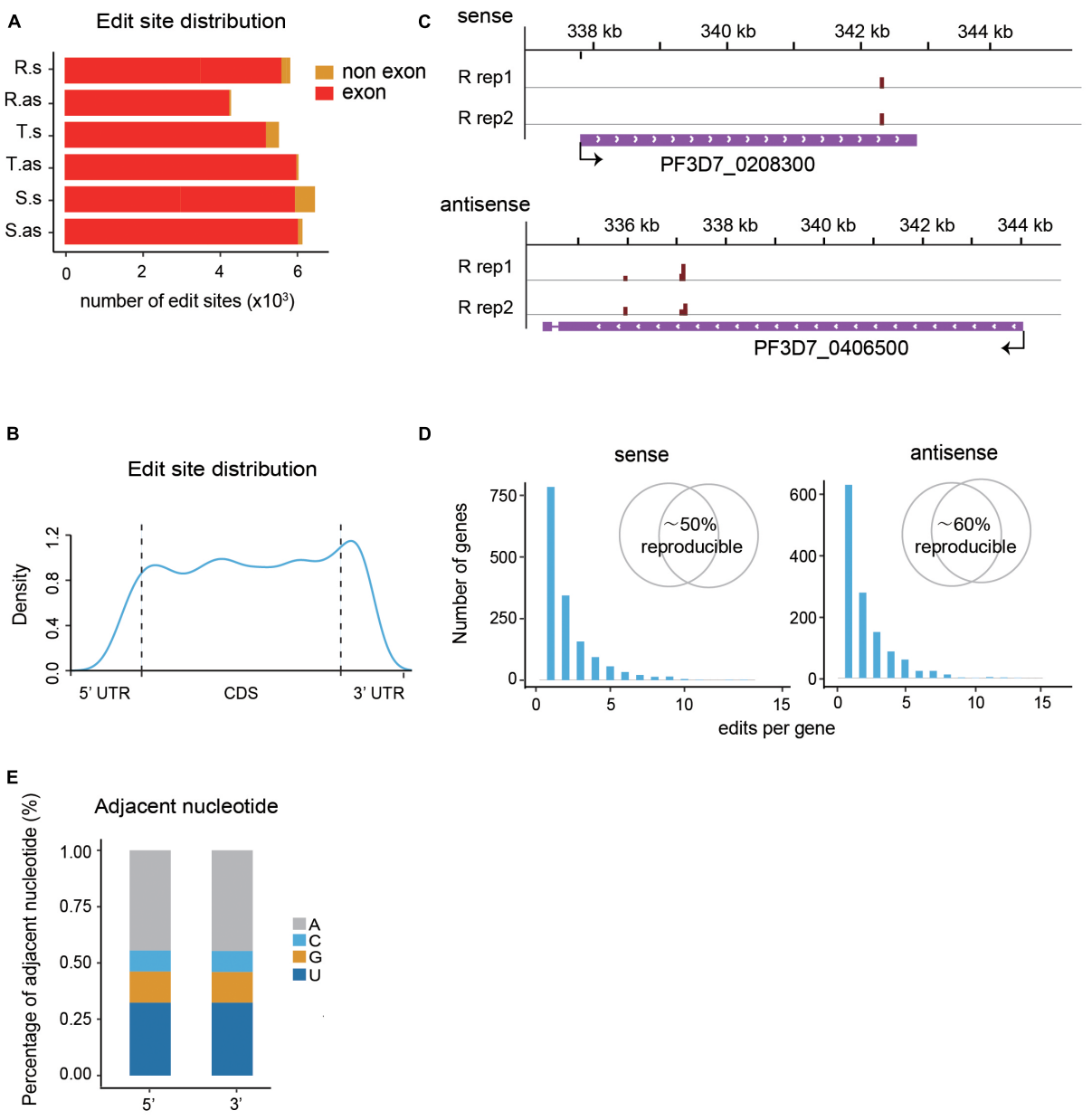

FIGURE 2 | Profiles of PfDis3-ADARcd editing events during the IDC in *P. falciparum*. **(A)** Boxplots showing the numbers of editing events detected in exons and non-exonic regions for sense (s) and antisense (as) transcripts during the IDC, respectively. R.s, T.s, and S.s are sense transcripts at Ring, Trophozoite and Schizont stages. R.as, T.as, and S.as are antisense transcripts at Ring, Trophozoite and Schizont stages. **(B)** Track view of editing events in two representative genes, PF3D7_0208300 (sense) and PF3D7_0406500 (antisense). The data are from the two biological replicates at R stage. The red bars indicate the editing events. The height of the bar indicates the editing ratio in that site. **(C)** Distribution of edit sites along transcripts. **(D)** Frequency histograms indicate the number of edit sites per target transcript for sense and antisense transcripts. The inset Venn diagram showing the percentage of target genes detected in both replicates. **(E)** Barplot showing the sequence composition of the 5′ and 3′ nucleotides adjacent to the PfDis3-ADARcd edit sites.

editing events in both sense and antisense transcripts during the IDC are about 8% (**Supplementary Figure S1B**). To explore whether the number of editing sites in each gene would infect editing ratio, we grouped transcripts by their total number of editing sites and compared their editing ratio among different groups. The results show no obvious correlation between the number of editing sites and editing ratio for both sense and antisense transcripts (**Supplementary Figure S1C**).

It has been reported previously that the *P. falciparum* genome has the highest AT composition among all the organisms sequenced to date (Gardner et al., 2002). Consequently, the mRNA transcriptome possesses higher level of adenosine in *P. falciparum* than other organisms. We wondered whether there is sequence composition bias in flanking sequences of the editing sites. To this end, we examined the adjacent nucleotides of editing sites. Unlike the former study that ADAR preferred an editing sequence of UAG (Rahman et al., 2018), the results show that the most frequent adjacent nucleotide is A, the second T, the third G, then C (**Figure 2E**). The special editing environment of PfDis3-TRIBE may reflect the unique composition of *P. falciparum* genome.

TRIBE Exhibits Higher Sensitivity and Reproducibility in Identification of PfDis3 Targets in *P. falciparum*

To further assess the reliability of our editing result, we performed a series of strand-specific RIP-seq experiments with PfDis3-HA-Ty1 parasite line to identify the potential targets of PfDis3. The RIP enrichment ratio relative to the expression level of transcripts was calculated and normalized. We observed a high correlation of RIP signals in the biological replicates (**Supplementary Figure S2**). The targets identified by RIP are also reproducible (**Supplementary Figure S2**, Venn diagram). Due to the low resolution, RIP signals are broad and spread across the gene body (**Figures 3A,B**). Interestingly, TRIBE detected editing sites in the genes with RIP signals in the gene body. Notably, TRIBE detected editing sites with 1-bp resolution. Surprisingly, the target genes identified by TRIBE are biased toward higher RIP signals when compared to the target genes identified by RIP (**Figure 3C**). Indeed, 36, 39, and 47% of RIP targets are also TRIBE targets at R, T and S stages, respectively (**Figure 3C**, Venn plot). Consistently, it has been reported previously that TRIBE was able to detect high-confidence CLIP targets (McMahon et al., 2016). Moreover, the correlation coefficient between replicates in TRIBE assay is higher and has a much smaller variation than that of RIP assay for either sense or antisense targets (**Figure 3D** and **Supplementary Figures S1A**, **S2**). Collectively, these findings suggest that TRIBE can reliably identify the targets of PfDis3 with high resolution in *P. falciparum*.

PfDis3 Regulates the Dynamical Transcriptional Program During the Asexual Blood Stage in *P. falciparum*

We next investigated the dynamics of PfDis3 targets during the IDC. The results show that there are no editing sites in ∼ one third of genes across the IDC whereas one sixth of genes persistently contain editing sites. The rest of transcripts dynamically contain editing sites (**Figure 4A**). The common targets of PfDis3 across the IDC account for 41, 40, and 36% of sense targets and 52, 37, and 36% of antisense targets for R, T and S stages, respectively. In contrast, only 27, 19, and 28% of sense targets and 15, 21, and 28% of antisense targets are specific to R, T and S stages, respectively (**Figure 4B**). This indicates that the targets of PfDis3 only show stage specificity to a certain extent. We further examined the correlation between the sense targets and antisense targets of PfDis3 at R, T and S stages, respectively. The results show that 26, 38, and 42% of sense targets contain edit site(s) in the corresponding antisense targets for R, T and S stages, respectively. Similarly, 35, 37, and 44% of antisense targets contain edit site(s) in the corresponding sense targets for R, T and S stages, respectively (**Figure 4C**).

To understand the functions of the target genes of PfDis3, we performed Gene Ontology (GO) analysis of the target genes. The results show that the target genes at R, T and S stages are enriched in the stage-related functions (**Figures 5A,B** and **Supplementary Figures S3A,B**). For example, the sense target genes at R stage are enriched for entry into host cell, pathogenesis, invasion, etc. (**Figure 5A**). This is consistent with infection and inhabitation of the parasites in red cells at R stage. In contrast, the antisense target genes at T stage are enriched for DNA replication, protein folding, metabolic process, etc. (**Figure 5B**). This is consistent with proliferation of the parasites at T stage.

We next constructed conditional Pfdis3 knock down (KD) parasite lines PfDis3-DD with ribozyme system (Droll et al., 2018) to investigate how PfDis3 impacts gene transcription. We used RNA-seq to measure gene expression levels that are highly reproducible (**Supplementary Figure S3C**). After Pfdis3 knockdown by drug induction, a number of genes are significantly differentially expressed. Especially, there are much more significantly up-regulated genes than down-regulated genes at R and T stages (**Figure 5C**). Intriguingly, the majority of genes in the GO term "entry into host cell" are up-regulated at R stage upon Pfdis3 knockdown. Similarly, the majority of genes in the GO term "DNA replication" are up-regulated at T stage upon Pfdis3 knockdown (**Figure 5D**). This is consistent with the functions of the target genes (**Figures 5A,B**).

DISCUSSION

The RNA exosome complex is highly conserved in eukaryotic organisms. In *P. falciparum*, the RNA exosome is composed of seven distinct core exosome subunits and two canonical 3′-5′ exoribonuclease factors: PfDis3 and PfRrp6 (Droll et al., 2018). For Dis3 protein, it harbors both processive exonucleolytic and endonucleolytic activities originating from the RNB and PIN domains, respectively (Lebreton et al., 2008; Schaeffer et al., 2009; Schneider et al., 2009). In yeast, Dis3 is present in both the nucleus and cytoplasm (Gudipati et al., 2012; Schneider et al., 2012) and human Dis3 proteins are differently localized (Staals et al., 2010; Tomecki et al., 2010; Lubas et al., 2013). Disruption of human dis3 (hRrp44) gene uncovered the cryptic transcription upstream of active human promoters (Preker et al., 2008). By

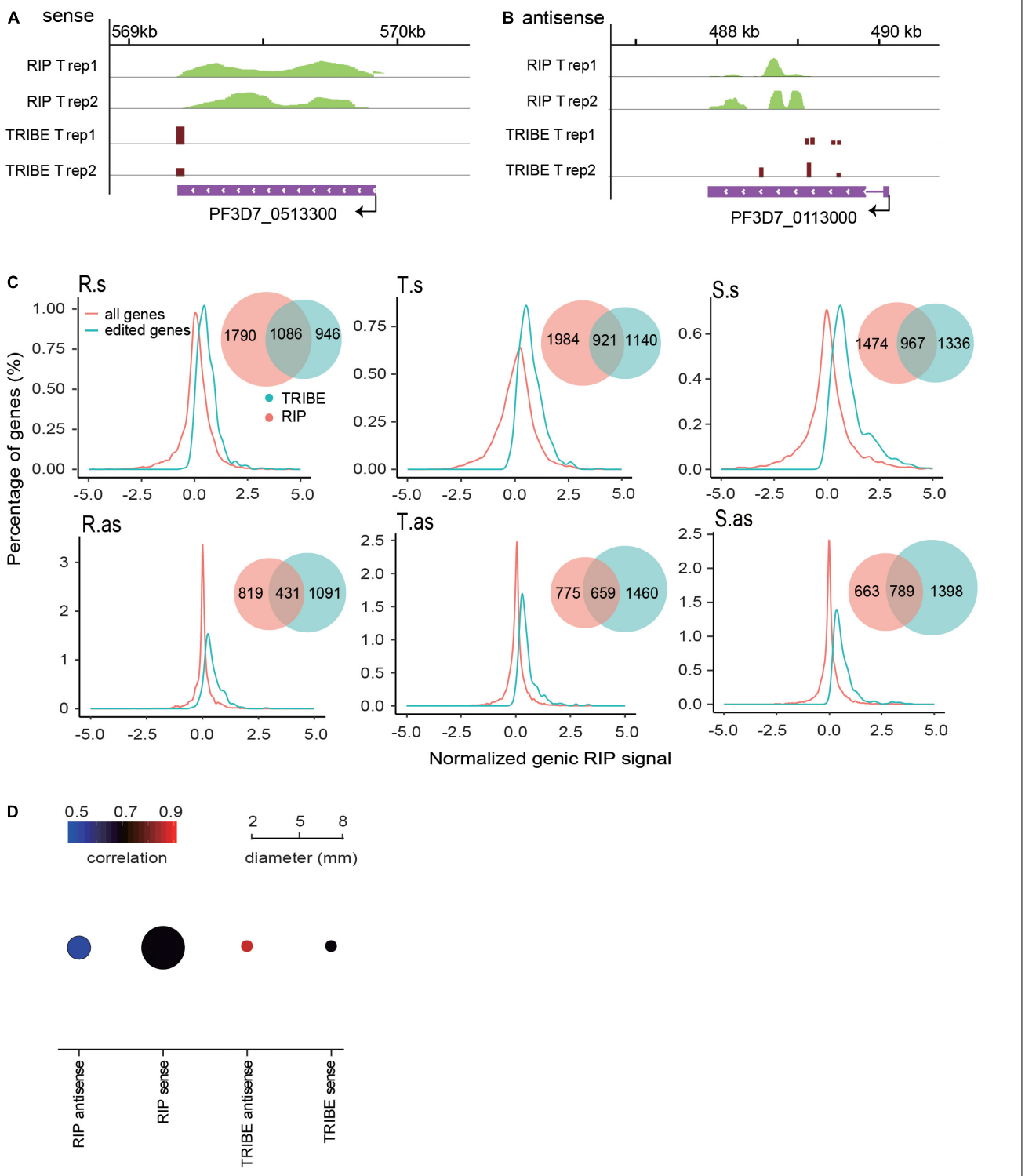

FIGURE 3 | PfDis3-TRIBE identifies targets with higher sensitivity and reproducibility than PfDis3-RIP in *P. falciparum*. **(A,B)** Track view showing RIP signals and editing events in the two representative target genes, PF3D7_0513300 (a, sense) and PF3D7_0113000 (b, antisense). The data are from the two biological replicates of RIP and TRIBE, respectively. **(C)** Distribution of normalized genic RIP signal in all RIP target genes (red) and PfDis3-ADARcd edited genes (green). The inset Venn plot shows the overlap of the target genes identified by both PfDis3-TRIBE (green) and PfDis3-RIP (red). R.s, T.s, and S.s are sense transcripts at Ring, Trophozoite and Schizont stages. R.as, T.as, and S.as are antisense transcripts at Ring, Trophozoite and Schizont stages. **(D)** Bubble plot showing the Pearson correlations between the replicates for PfDis3-TRIBE and PfDis3-RIP at ring (R), trophozoite (T) and schizont (S) stages, respectively. The color indicates the mean value of correlation coefficients. The size of the circle indicates the variance of correlation coefficients.

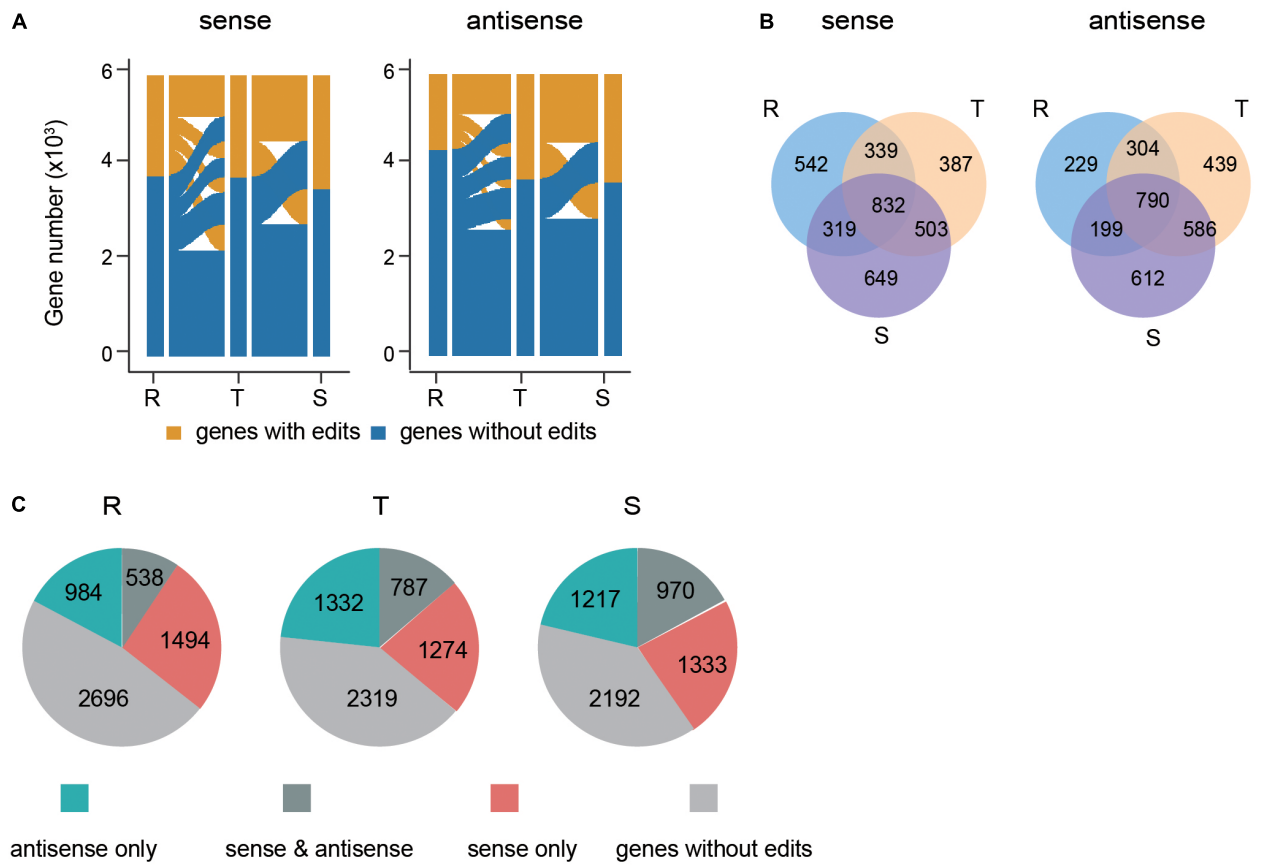

FIGURE 4 | Dynamics and features of PfDis3-TRIBE target genes during the IDC in *P. falciparum*. **(A)** Dynamic change of editing events in sense transcripts and antisense transcripts during the IDC. R, ring. T, trophozoite. S, schizont. **(B)** Overlap of PfDis3-TRIBE sense and antisense target transcripts at ring (R), trophozoite (T) and schizont (S) stages. **(C)** Pie chart showing the number of categorized target genes detected by TRIBE at ring (R), trophozoite (T) and schizont (S) stages, respectively. sense only, Pfdis3 binds to the sense transcripts but not the antisense transcripts of the genes. antisense only, Pfdis3 binds to the antisense transcripts but not the sense transcripts of the genes. sense and antisense, Pfdis3 binds to both antisense and sense transcripts of the genes. Genes without edits, genes with no editing events detected.

combining the transcriptomic analysis of human cell with dis3 gene mutation and Photoactivatable Ribonucleoside-Enhanced Cross-Linking and Immunoprecipitation (PAR-CLIP) assay, the RNA polymerase II transcriptome in humans was found to be controlled by Dis3 through decay of unwanted transcripts associated with ∼50% of transcribed protein-coding genes and unannotated genomic regions covering ∼70% of the genome. In *P. falciprum*, PfDis3 was detected predominately in the cytoplasmic fraction during asexual blood stage, but the majority of target transcripts of PfDis3 were antisense lncRNAs measured by DiCre knockout and RNA-seq (Droll et al., 2018). Here, by using TRIBE analysis, we uncover that PfDis3 is a global post-transcriptional regulator of protein coding and non-coding transcripts over the course of blood-stage development of the parasites. The function of PfDis3 in shaping cellular transcriptome is likely evolutionary conserved in eukaryotes from *Plasmodium* to human.

The human malaria parasite *P. falciparum* has a special nucleotide composition of genome with extremely higher AT content compared to other organisms (Gardner et al., 2002). Moreover, the mRNA transcriptome displays even stronger adenosines bias of about 45% (Baumgarten et al., 2019). The special sequence composition and other reasons make it hard to identify RBP targets in *P. falciparum* with traditional immunoprecipitation-based methods. In CLIP, crosslinking needs to be performed beforehand, raising a bias of preferential crosslinking of uredines (Fecko et al., 2007). It has not been reported any successful CLIP experiment in *P. falciparum* to date. RIP also faces problems like choice of RNase and the fragmentation condition that has a significant impact on the detected targets (Lambert et al., 2014). Many RIP results are not reproducible due to the non-specific binding of antibody in *P. falciparum*. To circumvent these issues, we adopted PfDis3-TRIBE in *P. falciparum* to identify Pfdis3 targets throughout IDC for the first time. We first identified Pfdis3 targeted sense/antisense transcripts at ring, trophozoite and schizont stage, respectively (**Supplementary Table S1**). We found that many Pfdis3 targets were antisense transcripts. Both sense and antisense Pfdis3 targets were enriched in biological processes that are highly relevant for their developmental stages, indicating

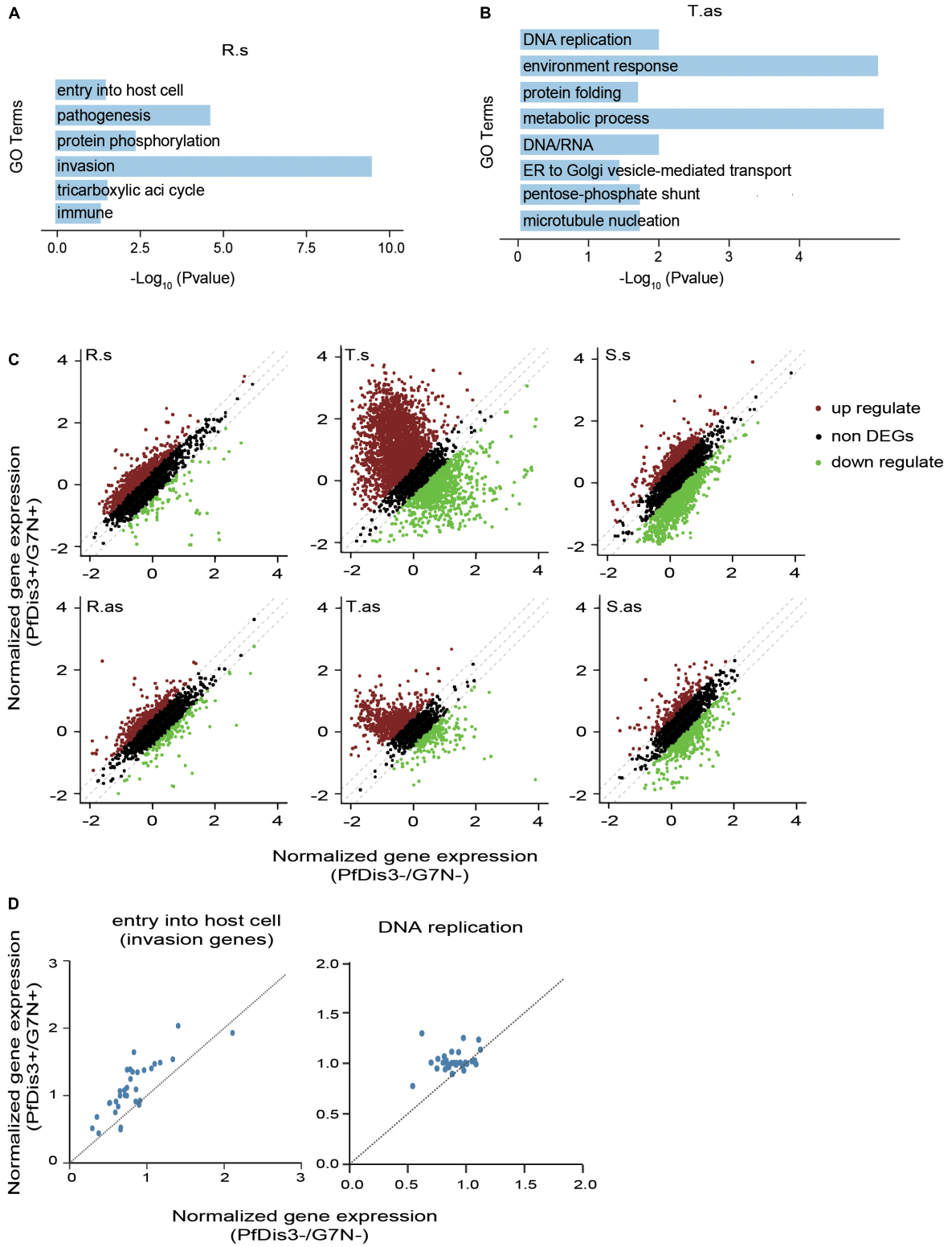

FIGURE 5 | The functions of PfDis3-TRIBE target genes during the IDC in *P. falciparum*. **(A)** Enriched Gene Ontology (biological processes) terms for PfDis3-TRIBE sense target genes at ring stage. **(B)** Enriched GO terms for PfDis3-TRIBE antisense target genes at trophozoite stage. **(C)** Scatter plots showing expression levels of sense (top) and antisense (bottom) transcripts at R, T and S stages with (*Y* axis) and without (*X* axis) Pfdis3 knock down. Transcripts with fold change ≥1.35 are differentially expressed transcripts. **(D)** Scatter plots showing that the majority of the genes in the GO term "entry into host cell" are up-regulated at R stage upon Pfdis3 knockdown (left), and that the majority of the genes in the GO term "DNA replication" are up-regulated at T stage upon Pfdis3 knockdown (right).

that Pfdis3 dynamically regulates the transcriptional program of *P. falciparum* throughout the IDC and maintains the steady state level of transcriptome.

We also performed RIP experiment and conditional Pfdis3 knockdown (KD) to evaluate the reliability of the target genes identified by PfDis3-TRIBE. PfDis3-TRIBE target genes were biased toward higher RIP enrichment, indicating that PfDis3-TRIBE preferentially detects stronger RIP-seq targets (**Figure 3C**). Moreover, most of the identified Pfdis3 target genes across the IDC were upregulated upon Pfdis3 KD (**Figure 5C**). Taken together, all these results suggest that PfDis3-TRIBE is able to identify Pfdis3 targets with higher confidence and better reproducibility than RIP.

MATERIALS AND METHODS

Plasmid Construction

To generate plasmid *Pfdis3-Ty1-ADARcd and Pfdis3-Ty1-ribo* for transfection, we modified the plasmid *pL6-gfp* by replacing the *gfp* box with a ∼1-kb homolog sequence flanking the N- or C-terminus of the target genes which contained three copies of Ty1epitope and ADARcd or *glmS* ribozyme gene, and inserting a guide RNA sequence specific to the *Pfdis3* gene (PF3D7_1359300) by In-Fusion PCR Cloning System, respectively (**Supplementary Table S2**). The resulting plasmids were *pL6-Pfdis3-Ty1-ADARcd* and *pL6-Pfdis3-Ty1-Ribo*. The plasmid pUF1-Cas9-infusion carrying Cas9 expression cassette was modified by replacing the original y*dhodh* gene with h*dhfr*.

Parasite Culture and Transfection

Plasmodium falciparum parasites were cultured in human red blood cell in culture medium (10.44 g/L RPMI-1640, 25 mM HEPES, 10% v/v Albumax I, 0.1 mM hypoxanthine, 20 μg/ml gentamicin) under 5% O_2, 3% CO_2 at 37°C. For synchronization, ring-stage parasites were enriched with 5% sorbitol, late-stage parasites were enriched via 40 and 70% percoll. Fresh red blood cell were electroporated with 100 μg of plasmid sgRNA and Cas9 in cytomix (120 mM KCl, 2 mM EGTA, 10 mM KH_2PO_4, 25 mM HEPES pH7.8, 0.15 mM $CaCl_2$, 5 mM $MgCl_2$) and then the synchronization of late-stage parasites were added. After 2 or 3 cycles, transfected parasites were selected by WR99210 and blasticidin S deaminase drug. The integration DNA was validated by PCR following sequencing and the proteins were identified by Western blot.

Western Blot

Total proteins were extracted with 0.15% saponin, washed with cold PBS (pH 7.4) until the supernatant was clear and then resuspended in 1 × SDS-loading buffer following heating under 100°C for 5 min. Proteins were separated by gel electrophoresis and transferred to a PVDF membrane. The membrane was blocked with 5% milk, incubated with primary antibody, washed with PBST, and then incubated with secondary antibody which could generate a chemiluminescent signal. The proteins were visualized by exposing to an imaging device. The materials used in this study were mouse anti-PfAldolase (1:1000, Abcam), mouse anti-Ty1 (1:500, Sigma), ECL Western blotting kit (GE healthcare) (Freeman, 2013).

RNA Extraction and Stranded RNA-Seq

Red blood cells infected by highly synchronous parasites were collected by centrifugation and resuspended in Trizol that could be stored in −80°C for a long time. After centrifugation, the supernatant was saved and then RNA was extracted according to reagent specification of Direct-zol^{TM} RNA MiniPrep (R2052). The integrality of RNA was validated by 2% agarose gel. Library construction was performed based on KAPA Stranded mRNA-Seq Kit (KK8421).

RIP-Seq

Infected red blood cells (iRBCs) were collected by centrifugation and resuspended in cold PBS (10 volume of iRBC). Parasites were extracted with 0.15% saponin and washed with cold PBS until the supernatant was clear. Lysis buffer (50 mM Tris-Cl pH7.4, 150 mM NaCl, 1 mM EDTA, 1 mM EGTA, 1% Triton X-100/NP-40) with protease inhibitors and RNase inhibitors was added to the parasite pellet [1.5 ml/(1×10^9 parasites)] and incubated with rotation for 1 h at 4°C. Cell debris were spun out at 12000 × *g* for 15 min at 4°C and supernatant was incubated with 10 μg of anti-Ty1 antibodies at 4°C for 3 h with rotation. For preparation of equilibrated protein-G magnetic beads, 50 μl of protein-G magnetic beads were washed once with Wash Buffer (10 mM Tris-Cl pH 7.5, 150 mM $MgCl_2$, 150 mM KCl, 0.1% Triton X-100), then washed once with Elution Buffer, and washed twice with Wash Buffer. Protein-G magnetic beads were mixed with supernatant with protease inhibitors and RNase inhibitors at 4°C overnight with rotation. Beads were washed twice with 500 μl of Wash Buffer and once with PBS and then resuspended in 700 μl of Trizol at 4°C for 10 min. After removal of the beads, 140 μl of chloroform was added to Trizol at room temperature for 5 min and mixture was centrifuged at 12000 × *g* for 30 min at 4°C. Supernatant was added to a new 1.5 ml centrifuge tube and centrifuged at 12000 × *g* for 2 min at 4°C. Supernatant was mixed with 1 μl of glycogen and equal volume of isopropanol on ice for 2 h. Tube was centrifuged at 12000 × *g* for 30 min at 4°C. Pellet was washed twice with 1 ml of 75% (vol/vol) ethanol, then air-dried and resuspended in 20 μl of RNase-free water (Chomczynski and Sacchi, 2006). DNase I was used to digest DNA for 15 min at room temperature. RNase-free water was added up to 100 μl, mixed with equal volume of chloroform/isoamyl alcohol pH < 5.0 (24:1), and then mixture was centrifuged at 12000 × *g* for 5 min. Supernatant was mixed with phenol/chloroform/isoamyl alcohol (25:24:1), and centrifuged at 12000× *g* for 5 min. Supernatant was transferred to a new 1.5 ml centrifuge tube with 1 μl of glycogen, one-tenth volumes of 3 M sodium acetate (pH 5.2), and 2.5 volumes of 100% ethanol and incubated at -80°C for 20 min. Samples were centrifuged at 12000× *g* for 15 min and pellet was washed twice with 1 ml of 75% (vol/vol) ethanol, then air-dried and resuspended in 11 μl of RNase-free water. Construction library was performed using KAPA Stranded mRNA-Seq Kit (KK8421).

RIP Sequencing Analysis

RIP sequencing reads were trimmed with cutadapt (v11) by 10 bp at each end. Reads with average quality score ≥20 and length ≥50 bp were retained. The strand specific reads were aligned with hisat2 (v2.1.0) (Kim et al., 2015) (parameters: –rna-strandness RF –dta –no-discordant –no-mixed –no-unal). Read counts for sense/antisense transcripts were calculated using featureCounts (v1.6.1) with parameters: -M -p -B -C for all; -s 2 for sense transcripts; -s 1 for antisense transcripts (Liao et al., 2014). Both sense and antisense read counts were merged for library normalization between conditions. The final expression levels of sense/antisense transcripts were normalized as FPKM (Fragment Per Kilobase of transcript per Million reads mapped) for further analysis. RIP-seq (i.e., PfDis3-RIP and GFP-RIP) data were normalized with the transcript abundance of their corresponding time point. We also did quantile normalization for former normalized RIP data to make it comparable among samples. Only transcripts with minimum 1.2 fold of PfDis3-RIP versus GFP-RIP were considered as PfDis3-RIP enriched transcripts. As biological replicates of the same treatment and developmental stage were highly correlated (**Supplementary Figure S2**), we combined them for the downstream analysis.

Analysis of Sequencing Data for RNA Editing

RNA editing data was analyzed as the previously published manual (McMahon et al., 2016) with modifications. In brief, pair-end sequencing reads were trimmed with cutadapt (v11) by 10 bp at each end, reads with average quality score ≥20 and length ≥50 bp were retained. Genomic DNA reads were aligned to the *P. falciparum* genome (plasmoDB.org, v3 release 32) (Gardner et al., 2002) using bwa (v 0.7.17-r1188) (Li and Durbin, 2009, 2010; Li, 2012) with default parameter. Strand specific RNA sequencing reads were aligned using Tophat2 (v2.1.1) (Kim et al., 2013) (parameters: -m 1 –g 2 -I 50000 –microexon-search –no-coverage-search –library-type fr-firststrand). PCR duplicates were removed using sambamba (v0.6.6) (Tarasov et al., 2015) for editing analysis and reads were sorted using sambamba (v0.6.6). We next converted the sorted files to a matrix using a previously published perl script sam_to_matrix.pl (McMahon et al., 2016). Genomic nucleotide information and transcript nucleotide information were merged using bedtools (v2.27.1) (Quinlan and Hall, 2010) for further identification of edit sites.

Only sites with minimum 10 coverage and 5% editing ratio were considered to be valid edit sites. gDNA coverage ≥30 and uniformity of nucleotide were also required to avoid SNP. The editing ratios are highly reproducible for the biological replicates (**Supplementary Figure S1A**), therefore, we combined the biological replicates for the downstream analysis. RNA editing data was converted to bedgraph file format for display using R (v3.5.1).

RNA-Seq Data Analysis

Illumina adapters were removed with cutadapt (v11), reads with average quality score ≥20 and length ≥50 bp were retained. RNA sequencing reads were aligned using hisat2 (v2.1.0) (Kim et al., 2015) with strand specific mode (i.e., –rna-strandness RF). Read counts for sense/antisense transcripts were obtained using featureCounts (v1.6.1) (Liao et al., 2014). Both sense and antisense read counts were merged for library normalization between conditions. FPKM of sense/antisense transcripts were calculated using R (v3.5.1). The gene expression levels were highly reproducible for the biological replicates of the same treatment and developmental stage (**Supplementary Figure S3C**), therefore, we used the replicate one for further analysis. Genes with minimum 1.35 fold (Pfdi3 KD versus G7) were considered as differentially expressed genes between two samples.

Gene Ontology Analysis

Gene ontology (GO) enrichment was performed using R (v3.5.1). GO terms database was downloaded from Plasmodb[1]. GO terms with p-value ≥0.05 (Fisher exact test) and enriched gene number ≥5 were considered to be enriched. We next classified our GO terms into different functional categories for better understanding.

DATA AVAILABILITY STATEMENT

The raw sequence data reported in this paper have been deposited in the Gene Expression Omnibus (GEO) under the accession number: GSE133654.

AUTHOR CONTRIBUTIONS

QZ and CJ conceived and designed the experiments. YF and XH generated transgenic parasite lines of PfDis3-ADARcd and PfDis3-DD. BL performed WB, TRIBE, and RNA-seq assay. ML and SS performed informatics analysis. QZ, CJ, and ML wrote the manuscript. All authors read and approved the final manuscript.

FUNDING

This work was supported by the National Natural Science Foundation of China (NSFC) (81630063 and 31671353), National Key R&D Program of China Grant (2018YFA0507300) to QZ, and NSFC (31771419 and 31721003) to CJ.

SUPPLEMENTARY MATERIAL

The Supplementary Material for this article can be found online at: https://www.frontiersin.org/articles/10.3389/fcell.2019.00264/full#supplementary-material

FIGURE S1 | The PfDis3-ADARcd reproducibly edits certain sites in *P.falciparum* during the IDC. **(A)** The edit sites at sense (top) transcripts and antisense (bottom) transcripts are reproducible in editing frequency at ring (R), trophozoite (T) and schizont (S) stages. Pearson correlation between biological replicates are shown. **(B)** Box plot showing the PfDis3-ADARcd editing levels in sense (s) transcripts and

[1]https://plasmodb.org/plasmo/

antisense (as) transcripts at ring (R), trophozoite (T) and schizont (S) stages. **(C)** Box plots showing the editing frequency of sense transcripts and antisense transcripts grouped by the number of edit sites. The middle line in the box indicates the mean of the editing frequency in the transcripts with more than one edit sites.

FIGURE S2 | Reproducibility of PfDis3-RIP assay across developmental stages. Correlation of genic RIP signals in sense (s) transcripts and antisense (as) transcripts between biological replicates. Pearson correlation coefficients between biological replicates are displayed at top left corner. The inset Venn diagram showing the overlap of PfDis3 targets identified by PfDis3-RIP between the two replicates. R, T, S indicates Ring, Trophozoite and Schizont stage, respectively.

FIGURE S3 | Functions of PfDis3-TRIBE target genes during the IDC in *P. falciparum*. **(A)** Enriched Gene Ontology (biological processes) terms for PfDis3 sense target transcripts at T (left panel) and S (right panel) stages, respectively. **(B)** Enriched GO terms for PfDis3 antisense target transcripts at ring R (left panel) and S (right panel) stages, respectively. **(C)** Correlation for expression of sense (top) transcripts and antisense (bottom) transcripts between biological replicates. Pearson correlation coefficients between biological replicates are displayed at top left corner. R, T and S indicates Ring, Trophozoite, Schizont stage, respectively.

TABLE S1 | List of sense/antisense target genes identified by PfDis3-TRIBE during the IDC in *P. falciparum*.

TABLE S2 | Primers and homology sequences for our constructed parasites.

REFERENCES

Bass, B. L., and Weintraub, H. (1998). An unwinding activity that covalently modifies its double-stranded RNA substrate. *Cell* 55:10.

Baumgarten, S., Bryant, J. M., Sinha, A., Reyser, T., Preiser, P. R., Dedon, P. C., et al. (2019). Transcriptome-wide dynamics of extensive m(6)A mRNA methylation during *Plasmodium falciparum* blood-stage development. *Nat. Microbiol.* doi: 10.1038/s41564-019-0521-7 [Epub ahead of print].

Bozdech, Z., Llinas, M., Pulliam, B. L., Wong, E. D., Zhu, J. C., and Derisi, J. L. (2003). The transcriptome of the intraerythrocytic developmental cycle of *Plasmodium falciparum*. *PLoS Biol.* 1:085. doi: 10.1371/journal.pbio.0000005

Chomczynski, P., and Sacchi, N. (2006). The single-step method of RNA isolation by acid guanidinium thiocyanate-phenol-chloroform extraction: twenty-something years on. *Nat. Protoc.* 1, 581–585. doi: 10.1038/nprot.2006.83

Corden, J. L. (2010). Shining a new light on RNA-protein interactions. *Chem. Biol.* 17, 316–318. doi: 10.1016/j.chembiol.2010.04.003

Darnell, R. B. (2010). HITS-CLIP: panoramic views of protein-RNA regulation in living cells. *Wiley Interdiscip. Rev. RNA* 1, 266–286. doi: 10.1002/wrna.31

Droll, D., Wei, G., Guo, G., Fan, Y., Baumgarten, S., Zhou, Y., et al. (2018). Disruption of the RNA exosome reveals the hidden face of the malaria parasite transcriptome. *RNA Biol.* 15, 1206–1214. doi: 10.1080/15476286.2018.1517014

Fecko, C. J., Munson, K. M., Saunders, A., Sun, G., Begley, T. P., Lis, J. T., et al. (2007). Comparison of femtosecond laser and continuous wave UV sources for protein-nucleic acid crosslinking. *Photochem. Photobiol.* 83:1394. doi: 10.1111/j.1751-1097.2007.00179.x

Freeman, L. A. (2013). Western blots. *Methods Mol. Biol.* 1027, 369–385. doi: 10.1007/978-1-60327-369-5_18

Gardner, M. J., Hall, N., Fung, E., White, O., Berriman, M., Hyman, R. W., et al. (2002). Genome sequence of the human malaria parasite *Plasmodium falciparum*. *Nature* 419, 498–511.

Gilbert, C., and Svejstrup, J. Q. (2006). RNA immunoprecipitation for determining RNA-protein associations in vivo. *Curr. Protoc. Mol. Biol.* 27:11. doi: 10.1002/0471142727.mb2704s75

Gudipati, R. K., Xu, Z. Y., Lebreton, A., Seraphin, B., Steinmetz, L. M., Jacquier, A., et al. (2012). Extensive degradation of RNA precursors by the exosome in wild-type cells. *Mol. Cell.* 48, 409–421. doi: 10.1016/j.molcel.2012.08.018

Keegan, L. P., Leroy, A., Sproul, D., and O'connell, M. A. (2004). Adenosine deaminases acting on RNA (ADARs): RNA-editing enzymes. *Genome Biol.* 5:209.

Kim, D., Langmead, B., and Salzberg, S. L. (2015). HISAT: a fast spliced aligner with low memory requirements. *Nat. Methods* 12, 357–360. doi: 10.1038/nmeth.3317

Kim, D., Pertea, G., Trapnell, C., Pimentel, H., Kelley, R., and Salzberg, S. L. (2013). TopHat2: accurate alignment of transcriptomes in the presence of insertions, deletions and gene fusions. *Genome Biol.* 14:R36. doi: 10.1186/gb-2013-14-4-r36

Lambert, N., Robertson, A., Jangi, M., Mcgeary, S., Sharp, P. A., and Burge, C. B. (2014). RNA Bind-n-Seq: quantitative assessment of the sequence and structural binding specificity of RNA binding proteins. *Mol. Cell.* 54, 887–900. doi: 10.1016/j.molcel.2014.04.016

Lebreton, A., Tomecki, R., Dziembowski, A., and Seraphin, B. (2008). Endonucleolytic RNA cleavage by a eukaryotic exosome. *Nature* 456, 993–996. doi: 10.1038/nature07480

Li, H. (2012). Exploring single-sample SNP and INDEL calling with whole-genome de novo assembly. *Bioinformatics* 28, 1838–1844. doi: 10.1093/bioinformatics/bts280

Li, H., and Durbin, R. (2009). Fast and accurate short read alignment with burrows-wheeler transform. *Bioinformatics* 25, 1754–1760. doi: 10.1093/bioinformatics/btp324

Li, H., and Durbin, R. (2010). Fast and accurate long-read alignment with burrows-wheeler transform. *Bioinformatics* 26, 589–595. doi: 10.1093/bioinformatics/btp698

Liao, Y., Smyth, G. K., and Shi, W. (2014). featureCounts: an efficient general purpose program for assigning sequence reads to genomic features. *Bioinformatics* 30, 923–930. doi: 10.1093/bioinformatics/btt656

Lu, X. M., Batugedara, G., Lee, M., Prudhomme, J., Bunnik, E. M., and Le Roch, K. G. (2017). Nascent RNA sequencing reveals mechanisms of gene regulation in the human malaria parasite *Plasmodium falciparum*. *Nucleic Acids Res.* 45, 7825–7840. doi: 10.1093/nar/gkx464

Lubas, M., Damgaard, C. K., Tomecki, R., Cysewski, D., Jensen, T. H., and Dziembowski, A. (2013). Exonuclease hDIS3L2 specifies an exosome-independent 3′-5′ degradation pathway of human cytoplasmic mRNA. *EMBO J.* 32, 1855–1868. doi: 10.1038/emboj.2013.135

McMahon, A. C., Rahman, R., Jin, H., Shen, J. L., Fieldsend, A., Luo, W., et al. (2016). TRIBE: hijacking an RNA-editing enzyme to identify cell-specific targets of RNA-binding proteins. *Cell* 165, 742–753. doi: 10.1016/j.cell.2016.03.007

Moore, M. J., Zhang, C., Gantman, E. C., Mele, A., Darnell, J. C., and Darnell, R. B. (2014). Mapping argonaute and conventional RNA-binding protein interactions with RNA at single-nucleotide resolution using HITS-CLIP and CIMS analysis. *Nat. Protoc.* 9, 263–293. doi: 10.1038/nprot.2014.012

Painter, H. J., Chung, N. C., Sebastian, A., Albert, I., Storey, J. D., and Llinas, M. (2018). Genome-wide real-time in vivo transcriptional dynamics during *Plasmodium falciparum* blood-stage development. *Nat. Commun.* 9:2656. doi: 10.1038/s41467-018-04966-3

Preker, P., Nielsen, J., Kammler, S., Lykke-Andersen, S., Christensen, M. S., Mapendano, C. K., et al. (2008). RNA exosome depletion reveals transcription upstream of active human promoters. *Science* 322, 1851–1854. doi: 10.1126/science.1164096

Quinlan, A. R., and Hall, I. M. (2010). BEDTools: a flexible suite of utilities for comparing genomic features. *Bioinformatics* 26, 841–842. doi: 10.1093/bioinformatics/btq033

Rahman, R., Xu, W., Jin, H., and Rosbash, M. (2018). Identification of RNA-binding protein targets with HyperTRIBE. *Nat. Protoc.* 13, 1829–1849. doi: 10.1038/s41596-018-0020-y

Rai, R., Zhu, L., Chen, H. F., Gupta, A. P., Sze, S. K., Zheng, J., et al. (2014). Genome-wide analysis in *Plasmodium falciparum* reveals early and late phases of RNA polymerase II occupancy during the infectious cycle. *BMC Genomics* 15:18. doi: 10.1186/1471-2164-15-959

Schaeffer, D., Tsanova, B., Barbas, A., Reis, F. P., Dastidar, E. G., Sanchez-Rotunno, M., et al. (2009). The exosome contains domains with specific endoribonuclease, exoribonuclease and cytoplasmic mRNA decay activities. *Nat. Struct. Mol. Biol.* 16, 56–62. doi: 10.1038/nsmb.1528

Schneider, C., Kudla, G., Wlotzka, W., Tuck, A., and Tollervey, D. (2012). Transcriptome-wide analysis of exosome targets. *Mol. Cell.* 48, 422–433. doi: 10.1016/j.molcel.2012.08.013

Schneider, C., Leung, E., Brown, J., and Tollervey, D. (2009). The N-terminal PIN domain of the exosome subunit Rrp44 harbors endonuclease activity and

tethers Rrp44 to the yeast core exosome. *Nucleic Acids Res.* 37, 1127–1140. doi: 10.1093/nar/gkn1020

Staals, R. H., Bronkhorst, A. W., Schilders, G., Slomovic, S., Schuster, G., Heck, A. J., et al. (2010). Dis3-like 1: a novel exoribonuclease associated with the human exosome. *EMBO J.* 29, 2358–2367. doi: 10.1038/emboj.2010.122

Tarasov, A., Vilella, A. J., Cuppen, E., Nijman, I. J., and Prins, P. (2015). Sambamba: fast processing of NGS alignment formats. *Bioinformatics* 31, 2032–2034. doi: 10.1093/bioinformatics/btv098

Tomecki, R., Kristiansen, M. S., Lykke-Andersen, S., Chlebowski, A., Larsen, K. M., Szczesny, R. J., et al. (2010). The human core exosome interacts with differentially localized processive RNases: hDIS3 and hDIS3L. *EMBO J.* 29, 2342–2357. doi: 10.1038/emboj.2010.121

Ule, J., Jensen, K., Mele, A., and Darnell, R. B. (2005). CLIP: a method for identifying protein-RNA interaction sites in living cells. *Methods* 37, 376–386. doi: 10.1016/j.ymeth.2005.07.018

Ule, J., Jensen, K. B., Ruggiu, M., Mele, A., Ule, A., and Darnell, R. B. (2003). CLIP identifies nova-regulated RNA networks in the brain. *Science* 302, 1212–1215. doi: 10.1126/science.1090095

Vembar, S. S., Droll, D., and Scherf, A. (2016). Translational regulation in blood stages of the malaria parasite *Plasmodium spp.*: systems-wide studies pave the way. *Wiley Interdiscip. Rev. RNA* 7, 772–792. doi: 10.1002/wrna.1365

World Health Organization [WHO], (2018). *World Malaria Report*. Geneva: WHO Press.

Zhang, Q., Siegel, T. N., Martins, R. M., Wang, F., Cao, J., Gao, Q., et al. (2014). Exonuclease-mediated degradation of nascent RNA silences genes linked to severe malaria. *Nature* 513, 431–435. doi: 10.1038/nature13468

Conflict of Interest: The authors declare that the research was conducted in the absence of any commercial or financial relationships that could be construed as a potential conflict of interest.

frontiers in Medicine

BRIEF RESEARCH REPORT
published: 19 November 2019
doi: 10.3389/fmed.2019.00267

The Neurotropic Parasite *Toxoplasma gondii* Induces Astrocyte Polarization Through NFκB Pathway

Yu Jin[1], *Yong Yao*[1], *Saeed El-Ashram*[2,3], *Jiaming Tian*[1], *Jilong Shen*[1] *and Yongsheng Ji*[1]*

[1] *Anhui Provincial Laboratory of Microbiology and Parasitology, Laboratory of Tropical and Parasitic Diseases Control, Department of Microbiology and Parasitology, Anhui Medical University, Hefei, China,* [2] *School of Life Science and Engineering, Foshan University, Foshan, China,* [3] *Faculty of Science, Kafrelsheikh University, Kafr El-Shaikh, Egypt*

Background: *Toxoplasma gondii* is a protozoan parasite that chronically infects nearly one-third of the world's human population. In immunosuppressed individuals and fetus, infection with *T. gondii* contributes to a series of devastating conditions, including toxoplasmic encephalitis (TE), which is characterized by neuron damage in the central nervous system (CNS). Astrocyte polarization is currently found in some neurodegenerative diseases, and A1 subtype of astrocyte leads to neuron apoptosis. However, little information has been available on the role of astrocyte polarization in TE.

Methods: In the present study, we established a mouse model to study TE and detected A1 astrocyte in the brains of mice with TE. Expression level of A1 astrocyte-specific marker C3 was evaluated using indirect fluorescent assay (IFA) and Western blotting. Primary mouse astrocytes were incubated with different concentrations of *T. gondii* excreted-secreted antigens (*Tg*ESAs) *in vitro*. Expression level of C3 and A1 astrocyte-specific transcription levels were assessed using Western blotting and qRT-PCR, respectively. Bay11-7082 was used to study nuclear factor (NF) κB pathway in *Tg*ESA-induced astrocyte polarization.

Results: In mice with TE, the proportion of A1 astrocyte ($GFAP^+C3^+$) increased significantly. The results of *in vitro* study showed that *Tg*ESAs induced astrocyte polarization to A1 subtype. Blocking of NFκB pathway by Bay11-7082 inhibited *Tg*ESA-induced astrocyte polarization.

Conclusions: Our preliminary study showed the involvement of A1 astrocyte in the process of TE in mice, and *Tg*ESAs could trigger astrocyte to polarize to A1 subtype. These findings suggest a new mechanism underlying the neuropathogenesis induced by *T. gondii* infection.

Keywords: ***Toxoplasma gondii*, encephalitis, astrocyte, NFκB pathway, neuron**

OPEN ACCESS

Edited by:
Si-Yang Huang,
Yangzhou University, China

Reviewed by:
Marcelo Biondaro Gois,
Federal University of the Recôncavo of Bahia, Brazil
Jing Liu,
China Agricultural University (CAU), China

***Correspondence:**
Yongsheng Ji
jiyongshengkey@hotmail.com

Specialty section:
This article was submitted to Infectious Diseases - Surveillance, Prevention and Treatment, a section of the journal Frontiers in Medicine

Received: *17 September 2019*
Accepted: *31 October 2019*
Published: *19 November 2019*

Citation:
Jin Y, Yao Y, El-Ashram S, Tian J, Shen J and Ji Y (2019) The Neurotropic Parasite Toxoplasma gondii Induces Astrocyte Polarization Through NFκB Pathway. Front. Med. 6:267. doi: 10.3389/fmed.2019.00267

INTRODUCTION

Toxoplasma gondii is an obligate intracellular protozoan parasite that chronically infects the central nervous system (CNS) of up to one-third of the human population in the world (1). Humans get infected with such disease by ingesting water or food contaminated with oocysts shed by cats or consumption of raw or undercooked meat containing a tissue cyst or congenitally by transplacental

transmission of tachyzoites (2). Upon infection with *T. gondii*, fast-replicating tachyzoites infect a wide range of host cells, including neurons. Tachyzoites convert into slow-replicating bradyzoites, which persist as cysts in neurons under the pressure of the immune response.

Although most infected persons show no clinical symptoms, chronic *T. gondii* infection could impair host neuron function and structure (3–5), which may alter the behavior of humans or even increase the risk for neurodegenerative and psychiatric disorders (6, 7). In the developing fetus and immunocompromised individuals, such as AIDS patients or organ transplant recipients, *Toxoplasma* infection can cause a devastating neurologic disease. Symptomatic brain infection with *Toxoplasma* is known as toxoplasmic encephalitis (TE) and can clinically present with dizziness, headaches, and seizures. Currently, TE occurs in untreated or undiagnosed AIDS patients and in patients on new immunomodulants (8). In TE, *T. gondii* bradyzoites within cysts switch to tachyzoites, which infect and destroy brain-resident cells. Previous *in vitro* and *in vivo* evidences suggest that neurons serve as primary target cells for *T. gondii* tachyzoites and bradyzoites (1, 9).

An *in vitro* culture of neurons with *T. gondii* tachyzoites at a low multiplicity of infection (MOI) as previously described (10) induced the formation of a large cyst rather than the lysis of neurons. However, the *in vivo* TE mouse model showed that the neuronal damage was increased in the brain, and *T. gondii* infection induced activated microglia, which contributed to neuronal apoptosis (11). In addition, *T. gondii* excreted-secreted antigens (ESAs) induce apoptosis of the neural stem cells (NSCs) through endoplasmic reticulum stress (ERS) signaling pathways and inhibit differentiation of C17.2 neural stem cells through Wnt/β-catenin signaling pathway (12, 13). Whether other CNS resident cells are involved in neuron loss in TE is still an enigma.

Astrocytes are the most common glial cells within the cerebral cortex, which provide trophic support for neurons, promote formation and function of synapses, and prune synapses by phagocytosis (14–16). These cells also perform a diversity of functions, including participation in the immune response of the brain and undergo a pronounced transformation called reactive astrocytosis after brain injuries and neurodegenerative diseases (17).

Recent studies have demonstrated that proinflammatory microglia induce the formation of a subtype of astrocytes (termed A1 astrocytes), which are characterized by highly upregulated classical complement cascade genes (i.e., C3) shown to be destructive to synapses and are strongly neurotoxic and rapidly kill neurons (18). A1 astrocytes are abundant in various human neurodegenerative diseases, including Alzheimer's disease, Huntington's disease, Parkinson's disease, amyotrophic lateral sclerosis, and multiple sclerosis (18). A1-like astrocyte reactivity is induced in normal aged brains that are vulnerable to injury and cognitive function declines (19). However, whether *T. gondii* infection induces astrocyte polarization to A1 and the role of A1 astrocytes in neuron death in TE are still not clear. In the present study, we aimed to investigate the effects of the ESAs of *T. gondii* (*Tg*-ESAs) on astrocyte polarization and assess the involvement of nuclear factor (NF) κB signaling pathway in *Tg*-ESAs-induced astrocyte polarization. This study provides insight into the underlying molecular mechanisms that regulate neuropathogenesis in TE.

MATERIALS AND METHODS

Cell and Parasite

T. gondii Wh6 strain (avirulent strain) with genotype Chinese 1 (ToxoDB#9) was isolated as previously described (20). Cysts were maintained in the brain of chronically infected mice for *in vivo* infection. To collect cysts, brains from infected mice were mechanically homogenized in 1-ml sterile phosphate-buffered saline (PBS). Cyst numbers were counted in a 10-μl brain suspension using a light microscope (21). Tachyzoites of *T. gondii* were passaged in human foreskin fibroblast (HFF) monolayers for *in vitro* experiments. Mouse primary astrocytes were purchased from FenghuiShengwu (Changsha, China) and cultured in Dulbecco's modified Eagle medium (DMEM) medium supplemented with 10% fetal bovine serum.

Mice and Infection

Mice were divided into three groups (three mice/group): control group (non-infection group), chronic group (chronic infection without cyclophosphamide treatment), and TE group (chronic infection with cyclophosphamide treatment). The Wh6 strain cysts were prepared by homogenization of the brain tissues in phosphate-buffered saline (PBS). Seven-week-old female BALB/c mice were intragastrically administered with 30 cysts. After 6 weeks, mice with latent infection were intraperitoneally injected with cyclophosphamide (50 mg/kg; Baxter Oncology GmbH, Germany) to induce recurrence of toxoplasmosis as previously described (11). Seven days later, all mice of the three groups were euthanized for collection of the brain tissues for further experiments. All experimental procedures were approved by the Institutional Animal Care and Use Committee of Anhui Medical University.

Treatment of Astrocyte With *Tg*ESAs

ESAs from *T. gondii* were prepared as described previously (12). Tachyzoites of *T. gondii* were harvested as described above.

After resuspension with serum-free DMEM, 2×10^7 freshly collected tachyzoites were added into HFF monolayers. *T. gondii*-infected HFFs were further cultured in the serum-free DMEM medium at 37°C in 5% CO_2 for another 48 h. The supernatants of the infected HFFs were collected by centrifugation at 12,000 g for 10 min at 4°C and then filtered through a 0.22-mm membrane filter. Protein concentration in the supernatants was determined by BCA kits according to the manufacturer's instructions (Thermo-Fisher, Boston, MA). Protein samples were stored at −80°C until use. Non-infected HFFs in serum-free DMEM were used as a negative control.

Mouse primary astrocytes were seeded in six-well cell culture plates. Cells were treated with different doses of *Tg*ESAs (0, 0.10, 0.15, and 0.30 mg/ml) for 24 h when the cell confluence reached approximately 70%. Then, C3 protein expression level and A1-specific gene transcription levels were detected by Western blotting and quantitative real-time PCR (qRT-PCR), respectively. In some experiments, astrocytes were pretreated with NFκB inhibitor BAY11-7082 (1 and 5 μM) (22). After 12 h,

*Tg*ESAs (0.30 mg/ml) was added, and cells were co-cultured for further 24 h.

Immunofluorescence Assays

Mice were anesthetized with 1% pentobarbital and transcardially perfused with 20 ml ice-cold 4% paraformaldehyde after an initial flush with 20 ml ice-cold 0.01 M PBS. Brains were removed and post-fixed with 4% paraformaldehyde for 12 h. Brain tissues were subsequently dehydrated in 30% sucrose in 0.01 M PBS for 48 h. Tissues were embedded in optimal cutting temperature compound (OCT Compound, SAKURA, USA) and then sliced coronally (10–20 μm) on a cryostat microtome (CM3050S, Leica, Germany). For immunofluorescence staining, the samples were blocked with 5% bovine serum albumin (BSA) and 0.5% Triton X-100 (containing 0.02% normal goat serum) for 2 h at room temperature. The samples were incubated with primary antibodies overnight at 4°C and then with the appropriate fluorescent secondary antibodies for 2 h at room temperature. Primary antibodies included anti-GFAP (1:50, Abcam) and anti-C3 (1:400, Abcam). Fluorescent images (astrocytes in mouse cortex) were captured using an Olympus BX53 fluorescence microscope (Olympus, Tokyo, Japan) and processed using ImageJ software (ImageJ, National Institutes of Health, Bethesda, MD) for quantification of florescence intensity.

ELISA

Mouse brain tissues (mainly from cortex, 100 mg) were homogenized intensively and centrifuged at 12,000 g for 15 min at 4°C. Concentrations of tumor necrosis factor (TNF)-α and interleukin (IL)-1α in the mouse brain were evaluated using commercial kits according to the manufacturer's instructions (BioLegend, USA).

Western Blotting

Proteins extracted from mouse brains (mainly from cortex) or astrocytes were separated using SDS-PAGE electrophoresis and then transferred to a PVDF membrane (Millipore, USA). After blocking with 5% BSA for 1 h at room temperature, PVDF membrane was incubated with primary antibodies overnight at 4°C and then with the fluorescent secondary antibodies for 1 h at room temperature. Primary antibodies included anti-GFAP (1:1,000, Abcam), anti-C3 (1:2,000, Abcam), anti-β-actin (1:5,000, Abcam), and anti-Neu-N (1:1,000, Cell Signaling Technology). Fluorescent images were captured by the Tacon 5200 (Biotanon, China) and analyzed using ImageJ software.

Quantitative Real-Time PCR Assay

Total RNA was extracted from astrocytes using Trizol reagent (Tiangen Biotech, China) according to the manufacturer's protocols. The concentrations of the extracted RNA were measured using NanoDrop 2000c (ThermoFisher, USA) (23–25). Total RNA (1 μg) was reverse-transcribed to cDNA using a reverse transcription kit (TaKaRa, Japan). QRT-PCR was performed on the QuantStudio® 6 Flex real-time PCR instrument (Applied Biosystems, USA) using SYBR™ Green qPCR Master Mix (ThermoFisher, USA). Gene expression levels were normalized to β-tubulin levels using the $2^{-\Delta\Delta Ct}$ method. All primers for A1 astrocyte-specific genes used in the present study are listed in **Table 1** (18).

Statistical Analysis

All statistical analyses were performed using SPSS (Version 24, IBM, USA). All data are expressed as mean ± SEM (standard error of the mean). Differences between groups were assessed by one-way ANOVA followed by Student-Newman-Keuls (SNK) multiple comparison posttest or Student's *t* test. Differences were considered statistically significant when $P < 0.05$.

RESULTS

Establishment of a Murine Model of TE

To establish a mouse model of TE, BALB/c mice were orally infected with Wh6 tissue cysts. Six weeks later, *Toxoplasma*-infected mice were immunosuppressed by intraperitoneal injection with cyclophosphamide to reactivate chronic *T. gondii* infection. As we can see in **Figure 1A**, mice with TE showed piloerection and hunching posture, which are typical physical characteristics of acute toxoplasmosis. Western blotting results showed that expression levels of neuron marker Neu-N in mice with TE decreased significantly compared to those in the control group (**Figures 1B,C**, Ctrl group vs. TE group, 1.00 ± 0.00 vs. 0.52 ± 0.09, $P < 0.05$). These results indicated that neurons in the central nervous system (CNS) were damaged when the mouse brains were infected with tachyzoites of *T. gondii*.

Astrocyte Polarization to A1 in the Mouse Brain With TE

The proportion of A1 astrocyte ($GFAP^+C3^+$) was significantly higher in the TE group compared to the controls (**Figure 2A**) as detected by immunofluorescent assay (IFA).

TABLE 1 | Primers used for quantitative real-time PCR in the present study.

Gene	Forward	Reverse	Length (bp)
Amigo2	GAGGCGACCATAATGTCGTT	GCATCCAACAGTCCGATTCT	263
Fbln5	CTTCAGATGCAAGCAACAA	AGGCAGTGTCAGAGGCCTTA	281
Ggta1	GTGAACAGCATGAGGGGTTT	GTTTTGTTGCCTCTGGGTGT	115
H2-D1	TCCGAGATTGTAAAGCGTGAAGA	ACAGGGCAGTGCAGGGATAG	204
H2-T23	GGACCGCGAATGACATAGC	GCACCTCAGGGTGACTTCAT	212
Iigp1	GGGGCAATAGCTCATTGGTA	ACCTCGAAGACATCCCCTTT	104
Psmb8	CAGTCCTGAAGAGGCCTACG	CACTTTCACCCAACCGTCTT	121
Serping1	ACAGCCCCCTCTGAATTCTT	GGATGCTCTCCAAGTTGCTC	299

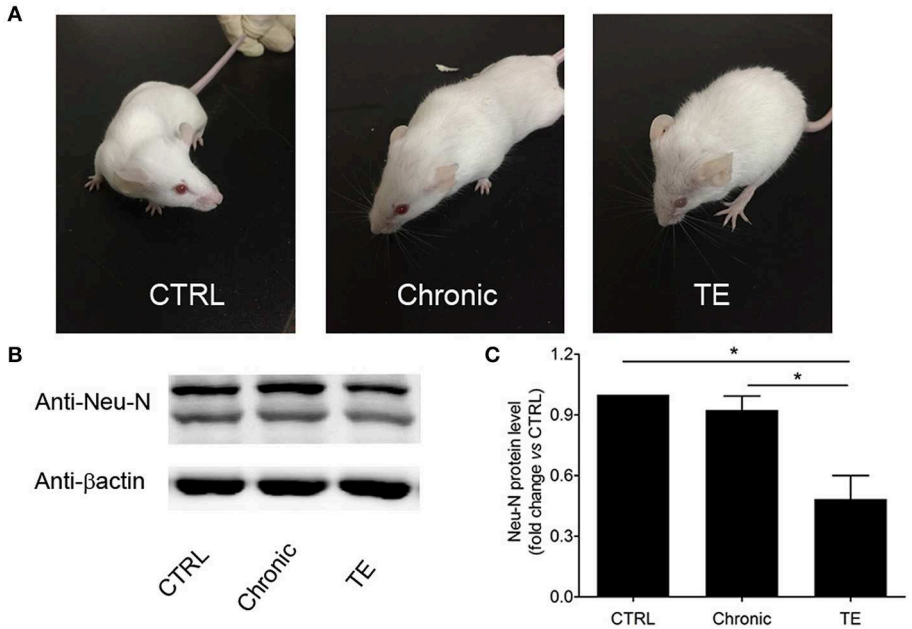

FIGURE 1 | Establishment of a murine model of toxoplasmic encephalitis (TE) **(A)** and identification of neuron damage in the brain of mice with TE **(B,C)**. *$P < 0.05$.

The expression level of A1-specific protein C3 was evaluated using Western blotting. Consistent with IFA result, the expression level of C3 in brains of the TE group increased dramatically (**Figures 2B,C**, Ctrl group vs. TE group, 1.00 ± 0.00 vs. 6.98 ± 1.06, $P < 0.05$), although the expression level of C3 in the chronic group was apparently higher than that of the control group. The concentrations of A1 cytokine inducers (TNF-α and IL-1α) were subsequently measured in the mouse brain using ELISA. The results indicated that TNF-α (Ctrl group vs. TE group, 56.20 ± 19.49 vs. 616.4 ± 104.8, $P < 0.05$) and IL-1α (Ctrl group vs. TE group, 198.2 ± 75.34 vs. $3{,}291 \pm 260.0$, $P < 0.05$) expression levels were remarkably enhanced in mice with TE (**Figures 2D,E**).

*Tg*ESAs Induced Astrocyte Polarization to A1 *via* the NFκb Pathway

Since *T. gondii* tachyzoites can manipulate cells in the mouse brain that they do not productively invade (26), the non-colocalization of tachyzoites and A1 astrocytes prompted us to hypothesize that *Tg*ESAs induced astrocyte polarization. To test this hypothesis, the mouse primary astrocyte was incubated *in vitro* with *Tg*ESAs. Western blotting results showed that the expression level of C3 was robustly elevated in the *Tg*ESA group (Ctrl group vs. 0.30 mg/ml *Tg*ESA group, 1.00 ± 0.00 vs. 11.83 ± 1.32, $P < 0.05$) (**Figures 3A,B**). Then, the transcription levels of A1-specific genes were evaluated using qRT-PCR (18). As shown in **Figure 3C**, after incubation with *Tg*ESAs, the transcription levels of *Amigo2*, *Ggta1*, *H2-D1*, *H2-T23*, and *Psmb8* genes were enhanced apparently, while there was no statistical difference in the transcription levels of *Fbln5*, *Iigp1*, and *Serping1* genes between the control and *Tg*ESA groups. Interestingly, when primary astrocytes were pretreated with NFκB inhibitor BAY11-7082, the C3 expression level decreased significantly comparing to the non-inhibitor treatment group (*Tg*ESA group). Differences in the C3 expression level between the control and BAY11-7082 groups (*Tg*ESA group vs. *Tg*ESA + 5 μM BAY group, 9.87 ± 1.60 vs. 2.30 ± 0.70, $P < 0.05$) suggested that *Tg*ESAs polarized astrocytes to A1 subtype *via* NFκB signaling pathway (**Figures 3D,E**). These results indicated that *Tg*ESAs induced mouse primary astrocyte polarization to A1 subtype *in vitro* through activation of NFκB signaling pathway.

DISCUSSION

Reactivation of chronic *T. gondii* infection can cause life-threatening TE in immunocompromised individuals. Here, we show for the first time that *T. gondii* infection in CNS leads to astrocyte polarization to A1 subtype, which potentially harms neurons.

A1 astrocytes have been reported in the lipopolysaccharide (LPS)-induced CNS inflammation model (18), traumatic brain injury (TBI), and prion diseases (27, 28). In murine models of TE, astrocyte activation and proliferation are prominent, and these cells produce chemokines that can influence the recruitment of T cells and dendritic cells (DCs) as well as microglial cell activation (29). In this study, we found that the majority of activated astrocytes in mice with TE were A1 subtype (C3 positive), indicating that activated astrocytes may function as a double-edged sword in the development of TE. A1 subtype can act as chemokine producers for inflammatory cell recruitment. Additionally, A1 subtype may also release unidentified chemicals toxic for neurons, which needs to be addressed in further studies.

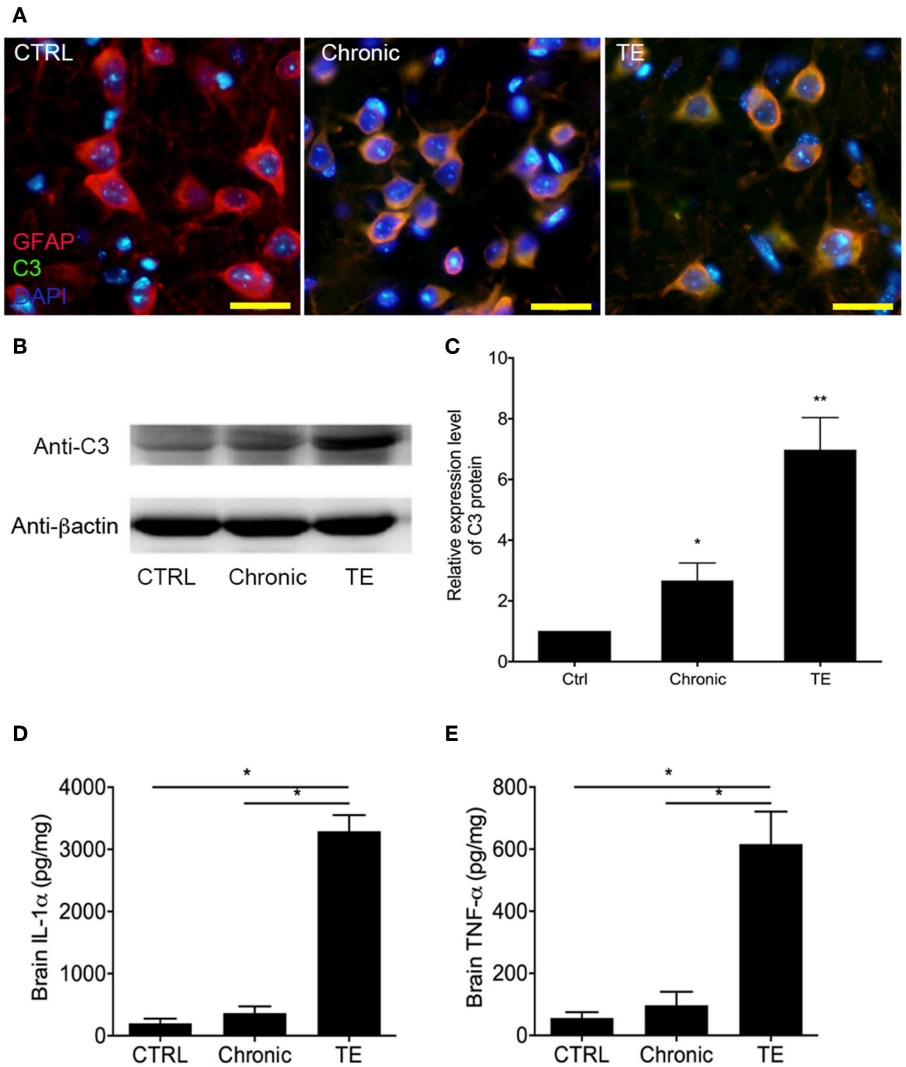

FIGURE 2 | Identification of A1 astrocyte ($GFAP^+C3^+$) in the brain of mice with toxoplasmic encephalitis (TE) using indirect fluorescent assay (IFA) **(A)** and Western blotting analysis of C3 expression level in the mouse brain **(B,C)**. Evaluation of interleukin (IL)-1α and tumor necrosis factor (TNF)-α in the mouse brain using commercial ELISA Kits **(D,E)**. Bar, 50 μm, $^*P < 0.05$ vs. control group.

A previous study has demonstrated reported that activated microglia secrete IL-1α, TNF-α, and C1q in LPS-induced astrocyte polarization. These cytokines were essential for astrocyte polarization to A1 subtype (18). In the present study, increased expression levels of IL-1α and TNF-α were observed. Furthermore, IL-1α and TNF-α could be produced by mouse CNS-resident immune cells, such as $CD11b^+$ microglia cells, since mice were immunosuppressed using cyclophosphamide. The cellular origin of these two cytokines and the cross talk between microglia and astrocytes should be determined in future studies.

A previous report demonstrated that the expression levels of cerebral cortical C1q were significantly elevated during *T. gondii* chronic infection (30). In this study, we found that the expression level of C3 was enhanced in acute TE. Based on our *in vitro* experiment results, the exposure of astrocyte to *Tg*ESAs may contribute to the enhancement of C3. C1q and C3 were mainly expressed by activated astrocytes. We can hypothesize that *T. gondii* chronic infection causes host behavioral changes partially through C1q activation and interaction with bradyzoite cysts. If bradyzoite cysts were disrupted, egressed parasites secrete effector proteins to trigger A1 astrocytes ($C3^+$) resulting in TE. Thus, it is worthy to further study the detailed mechanism of how astrocyte shifts its expression from C1q to C3 at different stages of *T. gondii* infection.

In spinal cord injury (SCI), exosomes derived from mesenchymal stem cells (MSCs) reduced A1 astrocytes *via* downregulation of NFκB pathway (31). Similarly, in this study, we found that inhibition of NFκB pathway by BAY11-7082 significantly reduced the *Tg*ESA-induced C3 expression level in astrocytes. *T. gondii*-derived profilin recognized macrophage TLR-11 and induced the expressions of macrophage chemotactic protein 1 (MCP-1), IL-12, and interferon gamma (IFN-γ) through NFκB activation (32). The

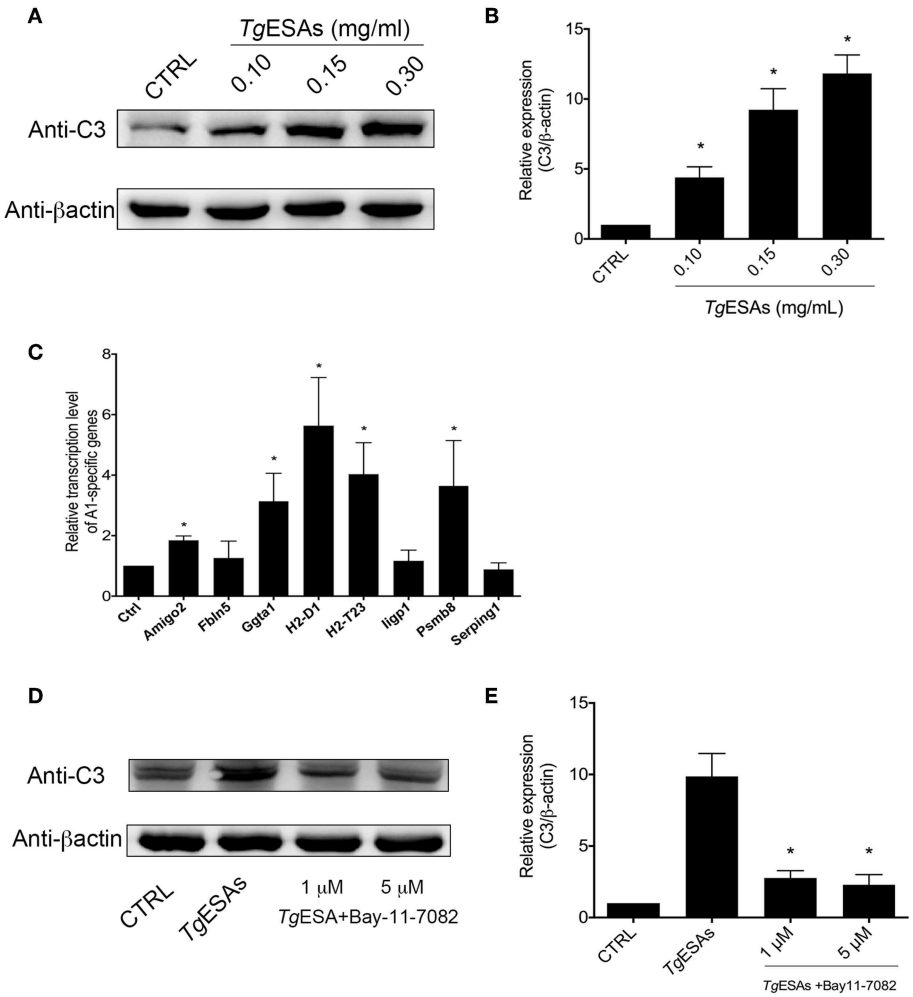

FIGURE 3 | *T. gondii* excreted-secreted antigen (*Tg*ESA) induction of astrocyte to A1 subtype *via* nuclear factor (NF)κB pathway. **(A,B)** *Tg*ESA treatment increased C3 expression level of astrocyte in a dose-dependent manner. **(C)** *Tg*ESA treatment changed A1-specific gene transcript levels. **(D,E)** Blockage of NFκB pathway inhibited *Tg*ESA-induced expression of C3 of astrocyte. *$P < 0.05$ vs. CTRL in **(B,C)**; *$P < 0.05$ vs. *Tg*ESAs in **(E)**.

culture supernatant of *T. gondii* may inhibit THP-1 cell and arrest the cell cycle of THP-1 cells at G_0/G_1 phase mainly by regulating the expression of gene NFκB, cyclin D1 (33), while ROP16 of *T. gondii* could regulate NFκB pathway of A549 cells (34). The effector proteins in *Tg*ESAs linking NFκB activation and astrocyte plasticity need to be determined in further experiments.

In summary, we reported for the first time that neurotoxic A1 astrocytes were involved in TE, and *Tg*ESAs induced astrocyte polarization through NFκB activation. Our results provide new insights into the role of resident cells in the neuropathogenesis in brain toxoplasmosis.

DATA AVAILABILITY STATEMENT

The datasets generated for this study are available on request to the corresponding author.

ETHICS STATEMENT

The animal study was reviewed and approved by the Institutional Animal Care and Use Committee of Anhui Medical University.

AUTHOR CONTRIBUTIONS

YJin, YY, and JT performed the experiments and analyzed the data. SE-A and YJi wrote the manuscript. YJi and JS designed the study.

FUNDING

This study was financially supported by the National Natural Science Foundation of China (YJi, Grant # 81802026) and Anhui Provincial Natural Science Foundation (YJi, Project # 1708085QH222).

REFERENCES

1. Cabral CM, Tuladhar S, Dietrich HK, Nguyen E, MacDonald WR, Trivedi T, et al. Neurons are the primary target cell for the brain-tropic intracellular parasite *Toxoplasma gondii*. *PLoS Pathog.* (2016) 12:e1005447. doi: 10.1371/journal.ppat.1005447
2. El-Ashram S, Yin Q, Barta JR, Khan J, Liu X, Suo X. Immunoproteomic technology offers an extraordinary diagnostic approach for *Toxoplasma gondii* infection. *J Microbiol Methods.* (2015) 119:18–30. doi: 10.1016/j.mimet.2015.09.011
3. Parlog A, Harsan LA, Zagrebelsky M, Weller M, von Elverfeldt D, Mawrin C, et al. Chronic murine toxoplasmosis is defined by subtle changes in neuronal connectivity. *Dis Model Mech.* (2014) 7:459–69. doi: 10.1242/dmm.014183
4. Brooks JM, Carrillo GL, Su J, Lindsay DS, Fox MA, Blader IJ. *Toxoplasma gondii* infections alter GABAergic synapses and signaling in the central nervous system. *MBio.* (2015) 6:e01428–15. doi: 10.1128/mBio.01428-15
5. David CN, Frias ES, Szu JI, Vieira PA, Hubbard JA, Lovelace J, et al. GLT-1-dependent disruption of CNS glutamate homeostasis and neuronal function by the protozoan parasite *Toxoplasma gondii*. *PLoS Pathog.* (2016) 12:e1005643. doi: 10.1371/journal.ppat.1005643
6. Flegr J. How and why Toxoplasma makes us crazy. *Trends Parasitol.* (2013) 29:156–63. doi: 10.1016/j.pt.2013.01.007
7. Torrey EF, Bartko JJ, Yolken RH. *Toxoplasma gondii* and other risk factors for schizophrenia: an update. *Schizophr Bull.* (2012) 38:642–7. doi: 10.1093/schbul/sbs043
8. Kiderlen TR, Liesenfeld O, Schurmann D, Schneider T. Toxoplasmic encephalitis in AIDS-patients before and after the introduction of highly active antiretroviral therapy (HAART). *Eur J Clin Microbiol Infect Dis.* (2011) 30:1521–5. doi: 10.1007/s10096-011-1254-6
9. Schluter D, Deckert M, Hof H, Frei K. *Toxoplasma gondii* infection of neurons induces neuronal cytokine and chemokine production, but gamma interferon- and tumor necrosis factor-stimulated neurons fail to inhibit the invasion and growth of *T. gondii*. *Infect Immun.* (2001) 69:7889–93. doi: 10.1128/IAI.69.12.7889-7893.2001
10. Tanaka N, Ashour D, Dratz E, Halonen S. Use of human induced pluripotent stem cell-derived neurons as a model for Cerebral Toxoplasmosis. *Microbes Infect.* (2016) 18:496–504. doi: 10.1016/j.micinf.2016.03.012
11. Zhang YH, Chen H, Chen Y, Wang L, Cai YH, Li M, et al. Activated microglia contribute to neuronal apoptosis in Toxoplasmic encephalitis. *Parasit Vectors.* (2014) 7:372. doi: 10.1186/1756-3305-7-372
12. Gan X, Zhang X, Cheng Z, Chen L, Ding X, Du J, et al. *Toxoplasma gondii* inhibits differentiation of C17.2 neural stem cells through Wnt/beta-catenin signaling pathway. *Biochem Biophys Res Commun.* (2016) 473:187–93. doi: 10.1016/j.bbrc.2016.03.076
13. Zhou J, Gan X, Wang Y, Zhang X, Ding X, Chen L, et al. *Toxoplasma gondii* prevalent in China induce weaker apoptosis of neural stem cells C17.2 via endoplasmic reticulum stress (ERS) signaling pathways. *Parasit Vectors.* (2015) 8:73. doi: 10.1186/s13071-015-0670-3
14. Clarke LE, Barres BA. Emerging roles of astrocytes in neural circuit development. *Nat Rev Neurosci.* (2013) 14:311–21. doi: 10.1038/nrn3484
15. Chung WS, Clarke LE, Wang GX, Stafford BK, Sher A, Chakraborty C, et al. Astrocytes mediate synapse elimination through MEGF10 and MERTK pathways. *Nature.* (2013) 504:394–400. doi: 10.1038/nature12776
16. Liddelow S, Barres B. SnapShot: astrocytes in health and disease. *Cell.* (2015) 162:1170–e1. doi: 10.1016/j.cell.2015.08.029
17. Sofroniew MV, Vinters HV. Astrocytes: biology and pathology. *Acta Neuropathol.* (2010) 119:7–35. doi: 10.1007/s00401-009-0619-8
18. Liddelow SA, Guttenplan KA, Clarke LE, Bennett FC, Bohlen CJ, Schirmer L, et al. Neurotoxic reactive astrocytes are induced by activated microglia. *Nature.* (2017) 541:481–7. doi: 10.1038/nature21029
19. Clarke LE, Liddelow SA, Chakraborty C, Munch AE, Heiman M, Barres BA. Normal aging induces A1-like astrocyte reactivity. *Proc Natl Acad Sci USA.* (2018) 115:E1896–905. doi: 10.1073/pnas.1800165115
20. Chen ZW, Gao JM, Huo XX, Wang L, Yu L, Halm-Lai F, et al. Genotyping of *Toxoplasma gondii* isolates from cats in different geographic regions of China. *Vet Parasitol.* (2011) 183:166–70. doi: 10.1016/j.vetpar.2011.06.013
21. Biswas A, French T, Dusedau HP, Mueller N, Riek-Burchardt M, Dudeck A, et al. Behavior of neutrophil granulocytes during *Toxoplasma gondii* infection in the central nervous system. *Front Cell Infect Microbiol.* (2017) 7:259. doi: 10.3389/fcimb.2017.00259
22. Juliana C, Fernandes-Alnemri T, Wu J, Datta P, Solorzano L, Yu JW, et al. Anti-inflammatory compounds parthenolide and Bay 11-7082 are direct inhibitors of the inflammasome. *J Biol Chem.* (2010) 285:9792–802. doi: 10.1074/jbc.M109.082305
23. El-Ashram S, Al Nasr I, El-Kemary M, Mehmood R, Hu M, Suo X. Early and late gene expression profiles of the ovine mucosa in response to Haemonchus contortus infection employing Illumina RNA-seq technology. *Parasitol Int.* (2017) 66:681–92. doi: 10.1016/j.parint.2017.05.007
24. El-Ashram S, Li C, Abouhajer F, Mehmood R, Al Nasr I, Zhang Y, et al. An *ex vivo* abomasal ovine model to study the immediate immune response in the context of Haemonchus contortus larval-stage. *Vet Parasitol.* (2018) 254:105–13. doi: 10.1016/j.vetpar.2018.02.042
25. Abouhajer F, El-Ashram S, Karama M, Huang S, Liu JF. An *ex vivo* ruminal ovine model to study the immediate immune response in the context of bacterial lipopolysaccharide. *Funct Integr Genomics.* (2018) 18:277–85. doi: 10.1007/s10142-018-0589-9
26. Koshy AA, Dietrich HK, Christian DA, Melehani JH, Shastri AJ, Hunter CA, et al. Toxoplasma co-opts host cells it does not invade. *PLoS Pathog.* (2012) 8:e1002825. doi: 10.1371/journal.ppat.1002825
27. Clark DPQ, Perreau VM, Shultz SR, Brady RD, Lei E, Dixit S, et al. Inflammation in traumatic brain injury: roles for toxic A1 astrocytes and microglial-astrocytic crosstalk. *Neurochem Res.* (2019) 44:1410–24. doi: 10.1007/s11064-019-02721-8
28. Hartmann K, Sepulveda-Falla D, Rose IVL, Madore C, Muth C, Matschke J, et al. Complement 3(+)-astrocytes are highly abundant in prion diseases, but their abolishment led to an accelerated disease course and early dysregulation of microglia. *Acta Neuropathol Commun.* (2019) 7:83. doi: 10.1186/s40478-019-0735-1
29. Wilson EH, Weninger W, Hunter CA. Trafficking of immune cells in the central nervous system. *J Clin Invest.* (2010) 120:1368–79. doi: 10.1172/JCI41911
30. Xiao J, Li Y, Gressitt KL, He H, Kannan G, Schultz TL, et al. Cerebral complement C1q activation in chronic Toxoplasma infection. *Brain Behav Immun.* (2016) 58:52–6. doi: 10.1016/j.bbi.2016.04.009
31. Wang L, Pei S, Han L, Guo B, Li Y, Duan R, et al. Mesenchymal stem cell-derived exosomes reduce A1 astrocytes via downregulation of phosphorylated NFkappaB P65 subunit in spinal cord injury. *Cell Physiol Biochem.* (2018) 50:1535–59. doi: 10.1159/000494652
32. Chen Q, Zhu W, Liu Z, Yan K, Zhao S, Han D. Toll-like receptor 11-initiated innate immune response in male mouse germ cells. *Biol Reprod.* (2014) 90:38. doi: 10.1095/biolreprod.113.114421
33. Ge P, Peng J, Li C, Liu Y, Ye B. Culture supernatant of *Toxoplasma gondii* inhibits the proliferation of human acute monocytic leukemia cell line THP-1. *Basic Clin Med.* (2011) 31:1129–33 (in Chinese).
34. Su Y, Dong H, Wang Y, Liu X, Zhao Z. Differential expression profiling of A549 cells induced by toxoplasma polymorphism effector ROP16. *Chin J Zoonoses.* (2018) 34:200–206 (in Chinese).

Conflict of Interest: The authors declare that the research was conducted in the absence of any commercial or financial relationships that could be construed as a potential conflict of interest.

frontiers in Medicine

CORRECTION
published: 20 December 2019
doi: 10.3389/fmed.2019.00299

Corrigendum: The Neurotropic Parasite *Toxoplasma gondii* Induces Astrocyte Polarization Through NFκB Pathway

Yu Jin[1], *Yong Yao*[1], *Saeed El-Ashram*[2,3], *Jiaming Tian*[1], *Jilong Shen*[1] *and Yongsheng Ji*[1]*

[1] Anhui Provincial Laboratory of Microbiology and Parasitology, Laboratory of Tropical and Parasitic Diseases Control, Department of Microbiology and Parasitology, Anhui Medical University, Hefei, China, [2] School of Life Science and Engineering, Foshan University, Foshan, China, [3] Faculty of Science, Kafrelsheikh University, Kafr El-Shaikh, Egypt

Keywords: ***Toxoplasma gondii*, encephalitis, astrocyte, NFκB pathway, neuron**

OPEN ACCESS

Edited and reviewed by:
Si-Yang Huang,
Yangzhou University, China

***Correspondence:**
Yongsheng Ji
jiyongshengkey@hotmail.com

Specialty section:
This article was submitted to Infectious Diseases - Surveillance, Prevention and Treatment, a section of the journal Frontiers in Medicine

Received: *20 November 2019*
Accepted: *29 November 2019*
Published: *20 December 2019*

Citation:
Jin Y, Yao Y, El-Ashram S, Tian J, Shen J and Ji Y (2019) Corrigendum: The Neurotropic Parasite Toxoplasma gondii Induces Astrocyte Polarization Through NFκB Pathway. Front. Med. 6:299. doi: 10.3389/fmed.2019.00299

A Corrigendum on

The Neurotropic Parasite *Toxoplasma gondii* Induces Astrocyte Polarization Through NFκB Pathway

by Jin, Y., Yao, Y., El-Ashram, S., Tian, J., Shen, J., and Ji, Y. (2019). Front. Med. 6:267. doi: 10.3389/fmed.2019.00267

In the original article, there was a mistake in **Figure 1** as published. We used the incorrect image for the reference protein in **Figure 1B.** The corrected **Figure 1** appears below.

The authors apologize for this error and state that this does not change the scientific conclusions of the article in any way. The original article has been updated.

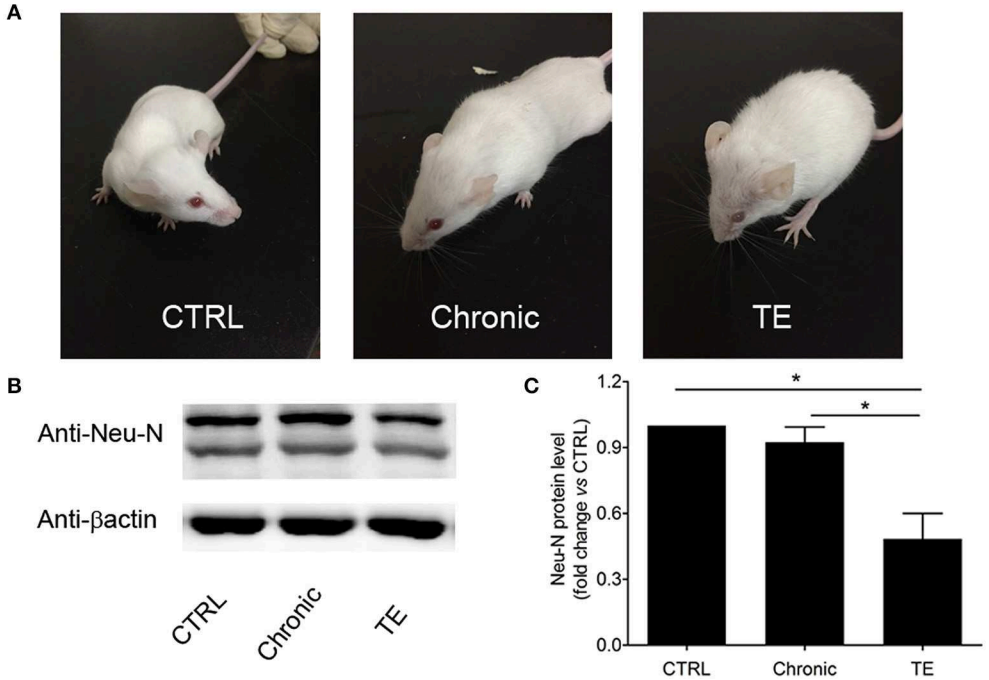

FIGURE 1 | Establishment of a murine model of toxoplasmic encephalitis (TE) **(A)** and identification of neuron damage in the brain of mice with TE **(B,C)**. *$P < 0.05$.

frontiers in Medicine

ORIGINAL RESEARCH
published: 17 December 2019
doi: 10.3389/fmed.2019.00301

Diagnostic Value of Pleural Effusion Mononuclear Cells Count and Adenosine Deaminase for Tuberculous Pleurisy Patients in China: A Case-Control Study

Xiaoli Lei[1], *Junli Wang*[2], *Zhigang Yang*[1]*, *Shengli Zhou*[3] and *Zhiwei Xu*[4]

[1] Department of Respiratory Medicine, Henan Provincial People's Hospital, Henan University People's Hospital, Zhengzhou, China, [2] Henan University People's Hospital, Henan Provincial People's Hospital, Zhengzhou, China, [3] Department of Pathology, Henan Provincial People's Hospital, Henan University People's Hospital, Zhengzhou, China, [4] Department of Clinical-Research Service Center, Henan Provincial People's Hospital, Henan University People's Hospital, Zhengzhou, China

OPEN ACCESS

Edited by:
Shaobin Shang,
Yangzhou University, China

Reviewed by:
Bo Yan,
Fudan University, China
Lely Solari,
National Institute of Health, Peru

***Correspondence:**
Zhigang Yang
18203679389@163.com

Specialty section:
This article was submitted to Infectious Diseases - Surveillance, Prevention and Treatment, a section of the journal Frontiers in Medicine

Received: *09 September 2019*
Accepted: *29 November 2019*
Published: *17 December 2019*

Citation:
Lei X, Wang J, Yang Z, Zhou S and Xu Z (2019) Diagnostic Value of Pleural Effusion Mononuclear Cells Count and Adenosine Deaminase for Tuberculous Pleurisy Patients in China: A Case-Control Study. Front. Med. 6:301. doi: 10.3389/fmed.2019.00301

Background: The diagnostic value of pleural effusion mononuclear cells count for tuberculous pleurisy (TBP) is unclear. We aimed to evaluate the diagnostic value of pleural effusion mononuclear cells count and its combination with adenosine deaminase (ADA) in TBP patients.

Methods: We initially analyzed 296 patients with unknown pleural effusion from the Department of Respiratory Medicine at Provincial People's Hospital during January 2014 to February 2018. Ultimately, 100 tuberculous pleurisy (TBP) patients and 105 non-tuberculous pleurisy (non-TBP) patients with pleural effusion were investigated in the current study. Meanwhile, pleural effusion mononuclear cells count and ADA test were performed to evaluate the diagnostic value for TBP. The sensitivity, specificity, positive predictive value (PPV), negative predictive value (NPV), positive likelihood ratio (LR+), negative likelihood ratio (LR–), accuracy and area under the receiver operating characteristic (ROC) curve (AUC) of pleural effusion mononuclear cells count only and its combination with ADA for TBP diagnosis were investigated.

Results: (i) The best cut-off value of pleural effusion mononuclear cells count for TBP diagnosis was 969.6×10^6/L, with the sensitivity, specificity and accuracy of 76, 57, and 66%, respectively. (ii) Combination of pleural effusion mononuclear cells count and ADA test suggested diagnostic value for TBP. Specifically, serial test showed the sensitivity, specificity, accuracy of 65, 90, 78%, respectively, whereas parallel test revealed the sensitivity, specificity, accuracy of 92, 45, 68%, respectively. The sensitivity of parallel test (92%) was significantly higher than pleural effusion mononuclear cells count alone (76%) ($X^2 = 23.19$, $p < 0.001$). (iii) The area under the ROC of pleural effusion mononuclear cells count and it combined with ADA were 0.66 (95% CI, 0.59–0.72) and 0.83 (95% CI, 0.78–0.89), respectively, with statistically significant difference ($Z = 3.46$, $p < 0.001$).

Conclusion: This retrospective case-control study demonstrated that pleural effusion mononuclear cells count is relatively useful for TBP diagnosis. Furthermore, the pleural effusion mononuclear cells count in combination with ADA can further improve the diagnostic accuracy of TBP.

Keywords: tuberculous pleurisy, pleural effusion, mononuclear cells count, adenosine deaminase, diagnostic accuracy

INTRODUCTION

Tuberculosis (TB) is a serious global public health problem. The World Health Organization estimated that about 10 million people developed TB disease in 2017 globally. China is one of the TB high-risk areas in the world. In 2017, about 889,000 new cases of TB were reported in China, accounting for 9% of new cases worldwide (1). As a common extrapulmonary TB, Tuberculous pleurisy (TBP) accounts for 25% of TB cases in China (2–4). The diagnosis of TBP is difficult (5, 6), with the thoracoscopic pleural pathology as the gold standard method (7). However, thoracoscopic pleural biopsy is an invasive operation with the issues of considerable risks and cost. In addition, yield and complication rate are dependent on the operator's skills (8–10). The operation also has certain limitations in application for elderly patients and hospitals that lack thoracoscopic surgery (10). Further study is needed to investigate less invasive or even non-invasive methods with high accurate diagnosis. Pleural fluid adenosine deaminase (ADA) test is widely used in clinical practice. However, its sensitivity and specificity in the diagnosis of TBP vary greatly (11, 12). Lymphocytes and monocytes in TBP pleural effusions were reported significantly increased. The proportion of lymphocytes and monocytes also had certain clinical significance in the diagnosis of TBP (13, 14). However, lymphocytes and monocytes in pleural effusions are usually not differentiated in clinical practice. Currently, automated blood analyzers are widely used to count mononuclear cells, which include lymphocytes and monocytes (15). Therefore, we hypothesized that, combined with ADA test, pleural effusion mononuclear cells count may contribute to the diagnosis of TBP. This retrospective case-control study aimed to evaluate the diagnostic value of pleural effusion mononuclear cells count and its combination with ADA in TBP patients. We hope to provide a new method for the diagnosis of TBP that is accurate, simple and less invasive.

MATERIALS AND METHODS

Study Design and Subjects

This retrospective case-control study was conducted using pleural effusion samples from 296 patients between January 1, 2014 and February 28, 2018 from Henan Provincial People's Hospital in China. Samples that meet all the following criteria were included: (i) Pleural effusion was indicated by either chest X-ray, chest CT or ultrasound; (ii) Etiology of pleural effusion was undetermined; (iii) Histopathological examination of pleural tissue was performed after obtained through thoracoscopy; (iv) Results of pleural effusion mononuclear cells count and ADA test were obtained; (v) Complete clinical data of the study subjects were acquired. In this study, patients were divided into TBP group and non-tuberculous pleurisy (non-TBP) group by the gold standard of the pathological results of thoracoscopic pleural biopsy (**Figure 1**).

TBP was diagnosed based on any of the criteria as follows (16–18): (i) Pleural biopsy showed granulomatous inflammation with or without staining of mycobacteria; (ii) *Mycobacterium Tuberculosis* (*Mtb*) was positive in pleural by using acid-fast bacilli staining, culture or PCR. Diagnostic criteria for non-tuberculous pleural effusion included: (i) There was no microbiological or histological findings of TB; (ii) Tumor cases were confirmed by pathology or cytology results; (iii) Other cases were diagnosed based on patient symptoms, signs, etiology, imaging findings, and clinical efficacy.

In addition, following medical record information was collected: (i) Basic information of patients, including gender, age, and basic diseases; (ii) Results of thoracoscopic pleural histopathology; (iii) Mononuclear cells count in pleural effusion; (iv) ADA test in Pleural effusion; (v) *Mtb* culture results of pleural tissues or pleural effusin. Basic information, Mononuclear cells count and ADA of patients can be seen in **Supplementary Table 1**.

Test Methods

Thoracoscopy examination of all the enrolled subjects was performed by using Olympus LTF-240 (Olympus Corporation, Japan) in the bronchoscopy room at Henan Provincial People's Hospital. Briefly, the puncture point was determined by chest imaging or ultrasound findings. Conventional disinfection was conducted followed by local anesthesia with 10 ml 2% lidocaine. The standard thoracoscopic procedure was then performed. Finally samples for biopsy at multiple sites in the parietal pleural lesion was taken for further examination. Pleura specimens were fixed with 4% formaldehyde, and followed by HE staining and acid-fast staining. PCR was also applied to detect *Mtb* by PCR instrument ABI 7500 (ABI, USA).

Pleural effusion mononuclear cells count, pleural effusion ADA test, and pleural effusion TB culture test were conducted in accordance with standard operating procedures strictly. Pleural effusion ADA was determined using Siemens ADVIA2400

Abbreviations: ADA, adenosine deaminase; TBP, tuberculous pleurisy; Non-TBP, non-tuberculous pleurisy; PPV, positive predictive value; NPV, negative predictive value; LR+, positive likelihood ratio; LR–, negative likelihood ratio; ROC, receiver operating characteristic; AUC, area under the receiver operating characteristic curve.

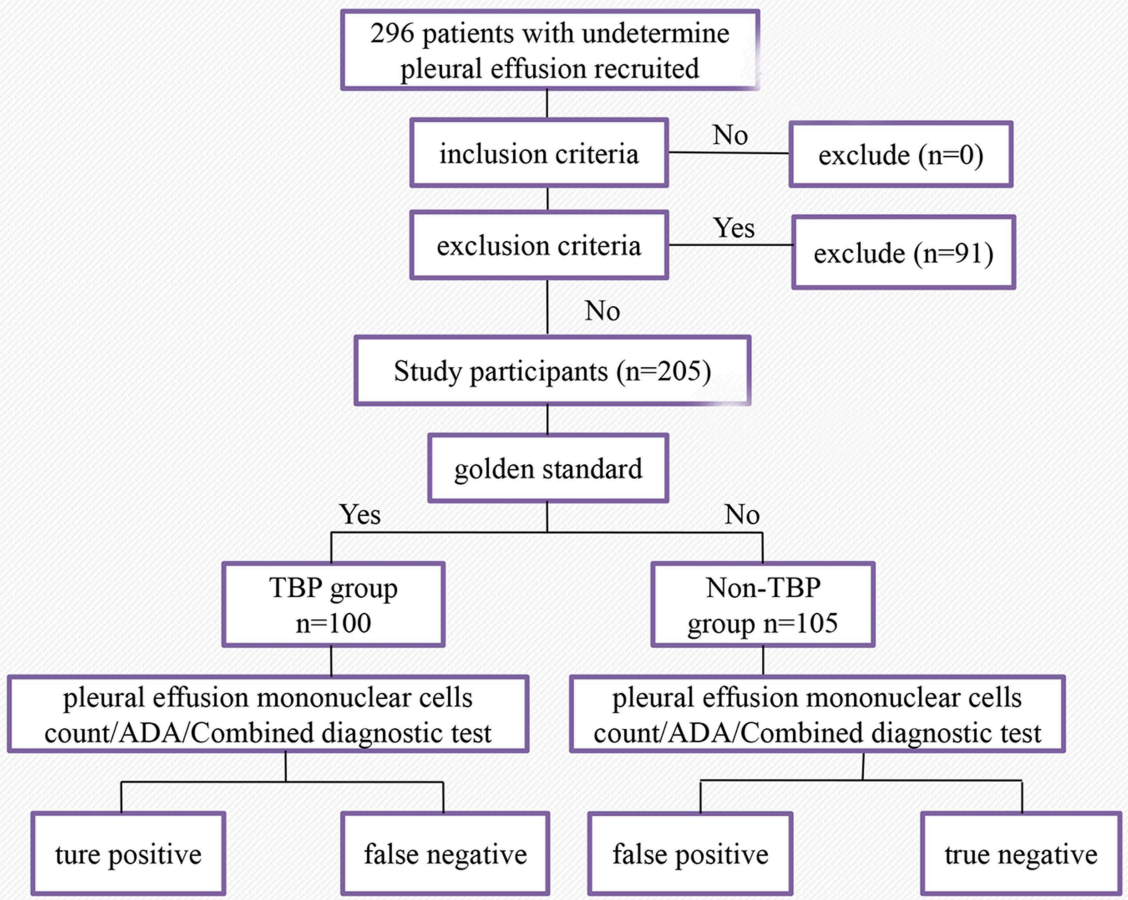

FIGURE 1 | Flowchart of the study population. A total of 296 patients with undetermined pleural effusion were recruited initially. Two hundred and five patients were included in the final analysis.

biochemical analyzer (Siemens, Germany). The pleural effusion mononuclear cells count was measured by Sysmex xn-9000 automatic blood analyzer (Sysmex Corporation, Japan). The pleural effusion *Mtb* culture was performed using BACTECMGIT 960 rapid culture instrument (BD Corporation, USA).

Sample volume was calculated according to the formula of the sample size for diagnostic study $n = [Ua2P(1\text{-}P)]/\delta 2$ (19). 1.96 is the Ua value for a 95% confidence level. P represents sensitivity when used to calculate patients group and specificity when used to calculate the control group. δ is the allowable error, and usually is set at 0.05. Previous studies showed that the sensitivity and specificity of pleural effusion ADA in the diagnosis of tuberculous pleurisy are 93.6 and 90.9%, respectively (20). Our current study eventually included 205 patients, including 100 TBP patients.

Blind Method

The pleural effusion mononuclear cells count and pleural effusion ADA test were operated by laboratory technicians independently. Pleural pathological results were judged independently by two pathologists. The third pathologist would be involved when the opinions were inconsistent. The results of subjects' pleural pathology were unknown to laboratory technicians. The pleural effusion mononuclear cell count and ADA test results were unknown to pathologists either.

Pleural Effusion Mononuclear Cells Count and ADA Test Combination

The receiver operating characteristic (ROC) curve of pleural effusion mononuclear cells count and ADA level for diagnosis of TBP was plotted. When the index was the maximum, the corresponding was the optimal critical value. If the count of pleural effusion mononuclear cells and ADA level were greater than their respective optimal critical values, the diagnosis result was determined to be positive. The combination test includes parallel test and serial test. Parallel test means that two screening tests performed at the same time and the results are subsequently combined. In our current study, parallel test refers to pleural effusion mononuclear cell count and pleural effusion ADA were test simultaneously. The diagnosis is positive as long as one of the results is positive. Serial test means that second screening test is performed only if the result of the first screening test is positive. In our current study, it refers to the pleural effusion mononuclear cell count and pleural effusion ADA were tested serially in order

to conduct diagnosis. The combined diagnosis is positive only when the results of both tests are positive.

Statistical Analysis

Statistical analysis was performed using SPSS version 22.0 (SPSS Inc., Chicago, IL, USA). Continuous variables were defined means ± standard deviation; categorical variables were given as percentage. The independent sample t test or the Mann-Whitney U test was used for the continuous variables and the chi-square test for categorical variables. Diagnostic performance was evaluated using sensitivity, specificity, positive likelihood ratio (LR+), negative likelihood ratio (LR-), positive predictive value (PPV), and negative predictive value (NPV). ROC curves were plotted to assess the diagnostic performance of pleural effusion mononuclear cells and ADA followed by areas under the ROC curve (AUCs) calculation. In addition, optimal cut-off values were obtained by ROC analysis, and ROC analysis based on the multivariate logistic regression model was conducted to assess the diagnostic value of the combined assays. Significance was inferred for $p < 0.05$.

RESULTS

Study Patients

A total of 296 patients with undetermined pleural effusion were enrolled initially. Ninety one patients were excluded for lack of results either thoracoscopic pleural biopsy, pleural effusion mononuclear cells count, or ADA. Finally a total of 100 TBP patients (70 males and 30 females) and 105 non-TBP patients (75 males and 30 females) were investigated in this study. Clinical characteristics of 205 patients with pleural effusion can be seen in **Table 1**. TBP group consisted of one tuberculous pyopneumothorax patient, one tuberculous empyema patient and six TBP patients with pulmonary TB. Details of diseases classification for 105 non-TBP patients with pleural effusion can be seen in **Table 2**.

TABLE 1 | Clinical characteristics of 205 patients with pleural effusion.

Characteristics	TBP group ($n = 100$)	Non-TBP group ($n = 105$)	p-value
Age, y (mean ± SD)	45.9 ± 18.6	61.0 ± 14.3	<0.001
Gender (*n*, %)			
Male	70 (70)	75 (71.4)	0.822
Female	30 (30)	30 (28.6)	
Underlying condition or illness (*n*, %)			
Alcoholism	26 (26)	34 (32.4)	0.316
Tobacco	37 (37)	53 (50.1)	0.052
Diabetes	8 (8)	19 (18.1)	0.033
Hypertension	22 (22)	24 (22.9)	0.883
Arrhythmia	1 (1)	8 (7.6)	0.049
Coronary heart disease	2 (2)	10 (9.5)	0.022
Chronic gastritis	0 (0)	8 (7.6)	0.014
Brain infarction	5 (5)	10 (9.5)	0.214
COPD	0 (0)	2 (1.9)	0.498
Bronchial asthma	1 (1)	2 (1.9)	1.000
Rheumatologic disease	1 (1)	5 (4.8)	0.237
Hyperthyroidism	1 (1)	1 (1)	1.000
Solid tumor	3 (3)	1 (1)	0.579
Chronic viral hepatitis B	2 (2)	4 (3.8)	0.723
Previous TB infection history	0 (0)	4 (3.8)	0.143
Prior TB treatment	11 (11)	12 (11.4)	0.923
Prior glucocorticoid use	2 (2)	0 (0)	0.237

TBP, tuberculous pleurisy; Non-TBP, non-tuberculous pleurisy.

Diagnostic Value of Pleural Effusion Mononuclear Cells Count

When the largest index of the pleural effusion mononuclear cells count for TBP diagnosis was 0.33, the best cut-off of TBP was 969.6×10^6/L. The sensitivity, specificity, positive predictive value, negative predictive value, accuracy, positive likelihood ratio, negative likelihood ratio, and were 76, 57, 63, 71, 66%, 1.77, and 0.42, respectively (**Table 3**).

Diagnostic Value of ADA

When the largest index of the ADA for TBP diagnosis was 0.59, the best cut-off of ADA was 27 U/L. The sensitivity, specificity, positive predictive value, negative predictive value, accuracy, positive likelihood ratio and negative likelihood ratio were 81, 78, 78, 81, 80%, 3.70, and 0.24, respectively (**Table 3**).

Diagnostic Value of the Combination of Pleural Effusion Mononuclear Cells Count and ADA

The sensitivity, specificity, positive predictive value, negative predictive value, accuracy, positive likelihood ratio, and negative likelihood ratio of the serial test were 65, 90, 87, 73, 78%, 6.83, 0.39, respectively; Above evaluation indexes of parallel test were 92, 45, 61, 85, 68%, 1.67, 0.18, respectively (**Table 3**).

The specificity of serial test that pleural effusion mononuclear cells count combined with ADA (90%) for TBP diagnosis was significantly higher than that of pleural effusion mononuclear cells count alone (57%) ($X^2 = 12.27$, $p = 0.000$), the sensitivity (65%) was lesser than that of pleural effusion mononuclear cells count (76%) ($X^2 = 58.65$, $p = 0.000$); The sensitivity of parallel test that pleural effusion mononuclear cells count combined with ADA (92%) for the diagnosis of TBP was significantly higher than that of pleural effusion mononuclear cells count (76%) ($X^2 = 23.19$, $p = 0.000$), the specificity (45%) was lower than that of pleural effusion mononuclear cells count (57%) ($X^2 = 63.82$, $p = 0.000$) (**Table 3**).

The area under the ROC of pleural effusion mononuclear cells count and pleural effusion mononuclear cells count combined with ADA for TBP was 0.66 (95% CI, 0.59–0.72), 0.83 (95% CI, 0.78–0.89), respectively. It was statistically significant difference in area under ROC curve between the pleural effusion

TABLE 2 | Non-tuberculous pleurisy patients with pleural effusion diseases classification.

Classification of diseases	Number	Proportion (%)
Empyema	11	10.48
Pneumonia effusion	23	21.90
Pulmonary embolism	1	0.95
Pulmonary contusion	1	0.95
Thoracic cyst	1	0.95
Sepsis	1	0.95
Liver cirrhosis	1	0.95
Microscopic polyangiitis	1	0.95
Nephrotic syndrome	1	0.95
Acute glomerulonephritis	1	0.95
Constrictive pericarditis	2	1.90
Heart failure	4	3.81
Hypoalbuminemia	1	0.95
Malignant pleural effusion	56	53.33

TABLE 3 | Diagnostic performance of pleural effusion mononuclear cells count, ADA and combination diagnostic test ($n = 205$).

	Sensitivity (%)	Specificity (%)	PPV	NPV	LR+	LR–	Accuracy (%)
Mononuclear cells count	76*	57#	0.63	0.71	1.77	0.42	66
ADA (>27 U/L)	81	78	0.78	0.81	3.70	0.24	80
Serial test	65	90#	0.87	0.73	6.83	0.39	78
Parallel test	92*	45	0.61	0.85	1.67	0.18	68

*PPV, positive predictive value; NPV, negative predictive value; LR+, likelihood ratio for positive test; LR-, likelihood ratio for negative value; #$X^2 = 12.27$, $p = 0.000$, comparison of the specificity among pleural effusion mononuclear cells and Serial test; *$X^2 = 23.19$, $p = 0.000$, comparison of the sensitivity among pleural effusion mononuclear cells and Parallel test.*

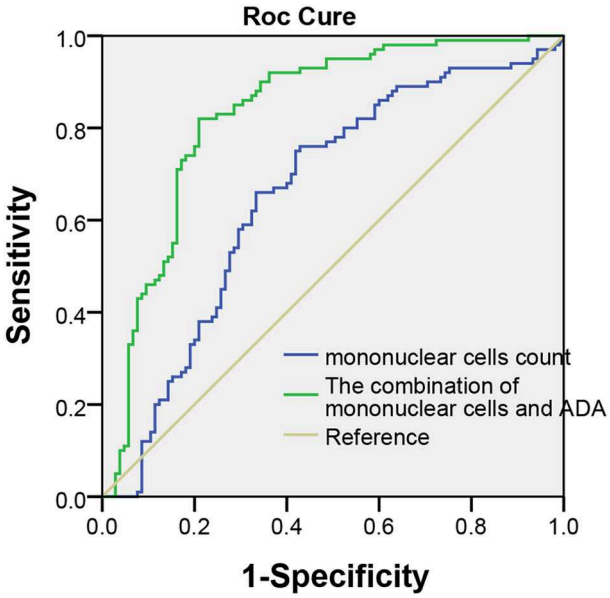

FIGURE 2 | Receiver operating characteristic curve in pleural effusion mononuclear cells and pleural effusion mononuclear cells count combination with ADA for TBP diagnosis. The area under the ROC of pleural effusion mononuclear cells and combined test was 0.66 (95% CI, 0.59–0.72), 0.83 (95% CI, 0.78–0.89) ($Z = 3.46$, $p < 0.05$).

mononuclear cells count and the combination test for TBP diagnosis ($Z = 3.46$, $p < 0.001$) (**Figure 2**).

DISCUSSION

Cellular immunity is the most important immune protection mechanism for Mycobacteria infection. Macrophages in the alveoli secrete a large number of interleukin-1 (IL-1), interleukin-6 (IL-6), tumor necrosis factor-α (TNF-α), and other cytokines, so that lymphocytes and monocytes are accumulated in mycobacterial invasion sites and followed by granulomas formation. TBP could infect the pleura through various routes, causing exudation, hyperplasia, and necrotic inflammation which mainly consisted of lymphocyte and monocyte infiltration. Unlike TB, patients with tuberculous pleural effusion usually have an acute febrile illness with nonproductive cough and pleuritic chest pain, night sweats, chills, weakness, dyspnea, and weight loss can also occur (4, 21). If it is not diagnosed and treated in time, TBP often leads to serious complications such as pleural thickening, calcification, empyema, bronchopleural fistula, etc. (22, 23). However, due to the lack of specificity of the clinical features of this disease, it is difficult to distinguish TBP from malignant pleural effusion and pneumonia-like pleural effusion, making the diagnosis difficult.

Transthoracic pleural biopsy is commonly used in recent years. Pleural pathology showing granulomatous inflammation with acid-fast staining or positive culture of *Mtb* is the gold standard for the diagnosis of TBP (16–18). However, the thoracoscopic pleural biopsy is invasive and expensive operation with certain surgical trauma and postoperative complications. Some elderly patients cannot tolerate the procedure. In addition, a large number of patients in China with TBP are admitted to primary or secondary hospitals lack of thoracoscopy equipment, which made TBP difficult to be diagnosed in a timely manner for the patients in those hospitals. More accurate, simple, and less invasive diagnostic methods are urgently needed. TBP patients often have pleural effusion during the active phase. Therefore, the diagnosis of TBP through thoracentesis with the assistance of cell types measurement, various enzymes and inflammatory factors in pleural effusion has become a hot topic of research.

Lymphocytes and monocytes in pleural effusion increase significantly after Mtb infection (13, 14). The proportion of lymphocytes and the ratio of monocytes have certain diagnostic value for the diagnosis of tuberculous pleurisy. The literature reported that when the pleural effusion lymphocyte is >64%, the sensitivity and specificity of diagnosis of TBP could reach to 89.1 and 76.4% (24). Another report revealed that the sensitivity and specificity of the proportion of lymphocytes (LP ≥ 50%) in pleural effusion combined with ADA greater or equal to 40 U/L

for TBP were 86.3 and 98.3%, respectively (13). In addition, the literature reported the proportion of pleural fluid monocytes cells (%) was 84.5 combined with the pleural effusion ADA value was 28.7 U/L (14), the sensitivity and specificity for TBP were 57.5 and 98%, respectively. The above results suggest that the proportion of lymphocytes and the proportion of monocytes are helpful in the diagnosis of TBP. However, lymphocytes and monocytes in clinical pleural effusions are usually not separately measured. The automatic blood analyzer is widely used to detect the count of mononuclear cells (the main components are lymphocytes, monocytes and a small number of mononuclear cells from other sources), which is simple, rapid and accurate (25, 26). Therefore it has been used as a routine examination item in clinical laboratories. We hypothesized that pleural effusion mononuclear cells count might contribute to the TBP diagnosis. Our study showed that the best cut-off of pleural effusion mononuclear cells count was 969.6×10^6/L. Meanwhile, the sensitivity, specificity, accuracy, area under the ROC of pleural effusion mononuclear cells count for TBP were 76, 57, 66%, 0.66 (95%CI, 0.59–0.72), respectively. Our results suggested the value of pleural effusion mononuclear cells count in the diagnosis of TBP for the first time. To the best of our knowledge, similar studies have not been published.

The pleural effusion ADA is of great value in the diagnosis of TBP (11). In this study, the sensitivity, specificity and accuracy for diagnosis of TBP were 81, 78, and 80%, respectively. The best cut-off value of ADA for TBP was 27 U/L, which is similar to 26.5 U/L (27). Garcia-Zamalloa's study suggested the best cut-off value of ADA for the diagnosis of TBP was 40 U/L (13). The reasons of the difference are not clear yet. Study population, different prevalence rates of TBP, as well as sample sizes might contribute to the difference, further investigation is needed in the future.

This study further explored combination of pleural effusion mononuclear cells count and ADA test in order to improve the accuracy of TBP diagnosis. When combination was used, the area under ROC curve of combination was 0.83 (95% CI, 0.78–0.89), which was significantly higher than that of 0.66 (95% CI, 0.59–0.72) when pleural effusion mononuclear cells count was used only ($p < 0.05$). The difference suggested that combination of pleural effusion mononuclear cells count and ADA test were better than pleural effusion mononuclear cells count was used alone for TBP diagnosis. Our studies also showed that the sensitivity and specificity of combination test was significantly higher than that of sensitivity and specificity when pleural effusion mononuclear cells count was used only for TBP diagnosis ($p < 0.05$). Parallel test has higher sensitivity but lower specificity; as comparison, serial test improves specificity at the cost of lower sensitivity, which was consistent with our results. The likelihood ratio increased from 1.77 to 6.83 when the serial test was used to analyze the results, which indicated that compared with single nuclear cells count, serial test can significantly improve diagnostic value of TBP. Meanwhile, the negative likelihood ratio decreased from 0.42 to 0.18 when the parallel test was used to analyze the results, which indicated that parallel test is more appropriate used to exclude the diagnosis of TBP. The thoracic pleural thickening, adhesion, and even pleural calcification of the affected side lead to thoracic collapse could happen, causing irreversible restrictive ventilation dysfunction if TBP is misdiagnosed. Therefore, it is more important to reduce the rate of misdiagnosis and improve the sensitivity of the diagnostic test. As a result, we recommended parallel test for pleural effusion mononuclear cell count combined with ADA.

In this study, the two study groups were different in age and chronic diseases, such as diabetes, arrhythmia, coronary heart disease, chronic gastritis. One study indicated that pleural tuberculosis was most commonly seen in adolescents and young adults (28), which was similar with this study. Another study found out that, compared with tuberculosis patients who had diabetes, the incidence of pleurisy is reduced in the tuberculosis patients who do not have diabetes (29). That study suggested that diabetes has a certain impact on the occurrence of TBP. No other chronic diseases (arrhythmia, coronary heart disease, chronic gastritis) have been found to affect TBP. Our findings suggested that future research needs to further study the effects of the above chronic diseases on TBP.

Finally, it is worthwhile to note that the quality of the study might be not as good as the cross-sectional study in the same period due to the characteristic of retrospective study. In addition, the patients in this study were enrolled in grade III hospital in China with relatively severe symptoms. Therefore, the selective bias in the population might occur. Simultaneous cross-sectional studies can be used in the future to further investigate the value of combination test of pleural effusion mononuclear cells count and ADA for the diagnosis of TBP.

In summary, pleural effusion mononuclear cells count is helpful in the diagnosis of TBP in our study. Diagnostic accuracy of TBP was improved when combined with ADA test. Our findings provide a new diagnostic method which is more accurate, simple, and less invasive.

DATA AVAILABILITY STATEMENT

The raw data supporting the conclusions of this article will be made available by the authors, without undue reservation, to any qualified researcher.

ETHICS STATEMENT

The studies involving human participants were reviewed and approved by Ethics Committee of Henan Provincial People's Hospital. Written informed consent for participation was not required for this study in accordance with the national legislation and the institutional requirements. Written informed consent was not obtained from the individual(s) for the publication of any potentially identifiable images or data included in this article.

AUTHOR CONTRIBUTIONS

ZY and ZX contributed conception and design of the study. JW and SZ collected the data and organized the database. JW and XL analyzed the data. XL, ZY, and JW wrote the first draft of the manuscript. All authors contributed to the final version of the manuscript.

FUNDING

This research received no specific grant from any funding agency in the public, commercial or not-for-profit sectors.

ACKNOWLEDGMENTS

We would like to thank Mr. Biao Hu at Department of Clinical Laboratory, People's Hospital of Henan Province for his generous help in materials collection and Dr. Hongliang Yang at Houston Methodist Research Institute for his valuable suggestions during the process of manuscript preparation.

SUPPLEMENTARY MATERIAL

The Supplementary Material for this article can be found online at: https://www.frontiersin.org/articles/10.3389/fmed.2019.00301/full#supplementary-material

REFERENCES

1. World Health Organization. *Global Tuberculosis Report 2018*. New York, NY: WHO (2018). p. 34.
2. Jeon D. Tuberculous pleurisy: an update. *Tuberc Respir Dis.* (2014). 76:153–9. doi: 10.4046/trd.2014.76.4.153
3. Abrao FC, de Abreu IR, Miyake DH, Busico MA, Younes RN. Role of adenosine deaminase and the influence of age on the diagnosis of pleural tuberculosis. *Int J Tuberc Lung Dis.* (2014) 18:1363–9. doi: 10.5588/ijtld.14.0257
4. Zhai K, Lu Y, Shi HZ. Tuberculous pleural effusion. *J Thorac Dis.* (2016) 8:E486–94. doi: 10.21037/jtd.2016.05.87
5. Tadele A, Beyene D, Hussein J, Gemechu T, Birhanu A, Mustafa T, et al. Immunocytochemical detection of *Mycobacterium tuberculosis* complex specific antigen, MPT64, improves diagnosis of tuberculous lymphadenitis and tuberculous pleuritis. *BMC Infect Dis.* (2014) 14:585. doi: 10.1186/s12879-014-0585-1
6. Kim MC, Kim SM, Lee SO, Choi SH, Kim YS, Woo JH, et al. A diagnostic algorithm for tuberculous pleurisy using the ELISPOT assay on peripheral blood and pleural effusion. *Infect Dis.* (2016) 48:688–94. doi: 10.1080/23744235.2016.1183816
7. Liu F, Gao M, Zhang X, Du F, Jia H, Yang X, et al. Interferon-gamma release assay performance of pleural fluid and peripheral blood in pleural tuberculosis. *PLoS ONE*. (2013) 8:e83857. doi: 10.1371/journal.pone.0083857
8. Trajman A, Pai M, Dheda K, van Zyl Smit R, Zwerling AA, et al. Novel tests for diagnosing tuberculous pleural effusion: what works and what does not? *Eur Respir J*. (2008) 31:1098–106. doi: 10.1183/09031936.00147507
9. Rahman NM, Ali NJ, Brown G, Chapman SJ, Davies RJ, Downer NJ, et al. Local anaesthetic thoracoscopy: British Thoracic Society Pleural Disease Guideline 2010. *Thorax*. (2010) 65(Suppl 2):ii54–60. doi: 10.1136/thx.2010.137018
10. Dixon G, de Fonseka D, Maskell N. Pleural controversies: image guided biopsy vs. thoracoscopy for undiagnosed pleural effusions? *J Thorac Dis.* (2015) 7:1041–51. doi: 10.3978/j.issn.2072-1439.2015.01.36
11. Gui X, Xiao H. Diagnosis of tuberculosis pleurisy with adenosine deaminase (ADA): a systematic review and meta-analysis. *Int J Clin Exp Med*. (2014) 7:3126–35.
12. Aggarwal AN, Agarwal R, Sehgal IS, Dhooria S. Adenosine deaminase for diagnosis of tuberculous pleural effusion: a systematic review and meta-analysis. *PLoS ONE.* (2019) 14:e0213728. doi: 10.1371/journal.pone.0213728
13. Garcia-Zamalloa A, Taboada-Gomez J. Diagnostic accuracy of adenosine deaminase and lymphocyte proportion in pleural fluid for tuberculous pleurisy in different prevalence scenarios. *PLoS ONE*. (2012) 7:e38729. doi: 10.1371/journal.pone.0038729
14. Zhang X, Tong C. Diagnostic value of hydrothorax mononuclear cell and ADA in tuberculous pleuritis. *Med J Chin People's Health*. (2014) 12:6–8. doi: 10.3969/j.issn.1672-0369.2014.12.003
15. Zhu L, Chen X. *Common Experimental Methods of Immunology*. Beijing: People's Military Medical Press (2000). p. 153–5.
16. Gopi A, Madhavan SM, Sharma SK, Sahn SA. Diagnosis and treatment of tuberculous pleural effusion in 2006. *Chest*. (2007) 131:880–9. doi: 10.1378/chest.06-2063
17. Losi M, Bossink A, Codecasa L, Jafari C, Ernst M, Thijsen S, et al. Use of a T-cell interferon-gamma release assay for the diagnosis of tuberculous pleurisy. *Eur Respir J.* (2007) 30:1173–9. doi: 10.1183/09031936.00067307
18. Aggarwal AN, Agarwal R, Gupta D, Dhooria S, Behera D. Interferon gamma release assays for diagnosis of pleural tuberculosis: a systematic review and meta-analysis. *J Clin Microbiol*. (2015) 53:2451–9. doi: 10.1128/JCM.00823-15
19. Liu X, Wang S, editor. *Clinical Epidemiology and Evidence Based Medicine*, 4th ed. Beijing: People's Medical Publishing House (2016). p. 132.
20. Wang H, Yue J, Yang J, Gao R, Liu J. Clinical diagnostic utility of adenosine deaminase, interferon-γ, interferon-γ-induced protein of 10 kDa, and dipeptidyl peptidase 4 levels in tuberculous pleural effusions. *Heart Lung*. (2012) 41:70–5. doi: 10.1016/j.hrtlng.2011.04.049
21. Bhuniya S, Arunabha DC, Choudhury S, Saha I, Roy TS, Saha M. Role of therapeutic thoracentesis in tuberculous pleural effusion. *Ann Thorac Med*. (2012) 7:215–19. doi: 10.4103/1817-1737.102176
22. Candela A, Andujar J, Hernández L, Martín C, Barroso E, Arriero JM, et al. Functional sequelae of tuberculous pleurisy in patients correctly treated. *Chest*. (2003) 123:1996–2000. doi: 10.1378/chest.123.6.1996
23. Kumar A, Asaf BB, Lingaraju VC, Yendamuri S, Pulle MV, Sood J. Thoracoscopic decortication of stage III tuberculous empyema is effective and safe in selected cases. *Ann Thorac Surg*. (2007) 104:1688–94. doi: 10.1016/j.athoracsur.2017.06.038
24. Sahn SA, Huggins JT, San José ME, Álvarez-Dobaño JM, Valdés L. Can tuberculous pleural effusions be diagnosed by pleural fluid analysis alone? *Int J Tuberc Lung Dis.* (2013) 17:787–93. doi: 10.5588/ijtld.12.0892
25. Fleming C, Brouwer R, Lindemans J, de Jonge R. Validation of the body fluid module on the new Sysmex XN-1000 for counting blood cells in cerebrospinal fluid and other body fluids. *Clin Chem Lab Med*. (2012) 50:1791–8. doi: 10.1515/cclm-2011-0927
26. Buoro S, Mecca T, Azzarà G, Seghezzi M, Dominoni P, Crippa A., et al. Cell population data and reflex testing rules of cell analysis in pleural and ascitic fluids using body fluid mode on Sysmex XN-9000. *Clin Chim Acta*. (2016) 452:92–8. doi: 10.1016/j.cca.2015.11.005
27. Xu HY, Zhang DQ, Ye JR, Su SS, Xie YP, Chen CS, et al. Diagnostic performance of T-SPOT.TB on peripheral blood in combination with adenosine deaminase on pleural fluid for the diagnosis of tuberculous pleurisy within different age group. *Zhonghua Yi Xue Za Zhi*. (2017) 97:1862–6. doi: 10.3760/cma.j.issn.0376-2491.2017.24.004
28. Chakrabarti B, Davies PD. Pleural tuberculosis. *Monaldi Arch Chest Dis*. (2006) 65:26–33. doi: 10.4081/monaldi.2006.582
29. Mamaev IA, Musaeva AM, Abusuev SA, Mamaeva KhI, Untilov GV. The epidemiological features of concomitance of diabetes mellitus and pulmonary tuberculosis. *Probl Tuberk Bolezn Legk*. (2008) 5:23–5.

Conflict of Interest: The authors declare that the research was conducted in the absence of any commercial or financial relationships that could be construed as a potential conflict of interest.

frontiers in Medicine

ORIGINAL RESEARCH
published: 14 February 2020
doi: 10.3389/fmed.2020.00019

Probe Signal Values in mRNA Arrays Imply an Excessive Involvement of Neutrophil FCGR1 in Tuberculosis

Kang Wu[1,2,3], *Meng Li*[4], *Zhen-yan Chen*[1], *Douglas B. Lowrie*[1,3]* *and Xiao-Yong Fan*[2,3]*

[1] Key Laboratory of Medical Molecular Virology of MOE/MOH, Shanghai Public Health Clinical Center, Fudan University, Shanghai, China, [2] School of Laboratory Medicine and Life Science, Wenzhou Medical University, Wenzhou, China, [3] TB Center, Shanghai Emerging and Re-emerging Institute, Shanghai, China, [4] Department of Life Science, Bengbu Medical College, Bengbu, China

The perturbed genes from transcriptomes are often presented in terms of relative expressions against control samples. However, the probe signal values (PSVs) of genes, implying protein abundances, are often ignored. Here, we explored the PSVs in tuberculosis (TB)-relevant signature genes. The signatures from *Mycobacterium tuberculosis*-infected THP-1 cells were defined as induced (T*Mtb*-i, with a derived T*Mtb*-iNet) and repressed (T*Mtb*-r). The signature from human blood was defined as a pulmonary TB (PTB)-specific signature (PTBsig). The analysis showed that before infection, T*Mtb*-i and T*Mtb*-iNet had lower PSVs and T*Mtb*-r genes had average PSVs. In the blood of healthy donors, PTBsig (divided into up-regulated PTBsigUp and down-regulated PTBsigDn) displayed average PSVs. This was partly due to masking by the cellular heterogeneity of blood; diverse PSVs were seen in constituent cell populations (CD4/8+ T, monocytes and neutrophils). Specifically, the PSVs of PTBsigUp in the neutrophils of healthy donors were higher (implying higher protein abundances), and much higher in the neutrophils of PTB (implying excessive protein abundances). Based on the PSV patterns of PTBsigUp in four cell populations, we identified three representative highly homologous genes (*FCGR1A*, *FCGR1B*, and the pseudogene *FCGR1CP*, which were often poorly distinguished), of which the summed PSVs were the highest in the neutrophils of PTB patients and healthy donors. The three genes were all up-regulated and responsive to chemotherapy in the blood of PTB, as validated in an RNA-seq-based analysis. This PSV-based study confirms the excessive involvement of neutrophil FCGR1 in PTB.

Keywords: ***Mycobacterium tuberculosis*, whole blood, neutrophils, gene signature, probe signal value, Fc fragment of IgG receptor I**

OPEN ACCESS

Edited by:
Shaobin Shang,
Yangzhou University, China

Reviewed by:
Sulochana Damodaradas,
National Institute of Research in Tuberculosis (ICMR), India
Daniel Barkan,
Hebrew University of Jerusalem, Israel

***Correspondence:**
Douglas B. Lowrie
lowried@fudan.edu.cn
Xiao-Yong Fan
xyfan008@fudan.edu.cn

Specialty section:
This article was submitted to Infectious Diseases - Surveillance, Prevention and Treatment, a section of the journal Frontiers in Medicine

Received: *19 November 2019*
Accepted: *13 January 2020*
Published: *14 February 2020*

Citation:
Wu K, Li M, Chen Z, Lowrie DB and Fan X-Y (2020) Probe Signal Values in mRNA Arrays Imply an Excessive Involvement of Neutrophil FCGR1 in Tuberculosis. Front. Med. 7:19. doi: 10.3389/fmed.2020.00019

INTRODUCTION

Transcriptome profiling of tuberculosis (TB)-relevant samples, whether from humans (1–3), model animals (4, 5), or immortalized cell lines (6), have been widely utilized to deepen our understanding of TB in many respects, e.g., pathogenesis, diagnosis, and prognosis. The biological samples used for transcriptome profiling have a wide range of purity, ranging from *in vitro* homogeneous cell lines to highly heterogeneous *in vivo*/*ex vivo* samples. Clearly, the readout from the latter is the sum from the various included kinds of cells, which contribute differently.

Irrespective of whether a hybridization-based platform or a sequencing-based platform (7, 8) has been used, the typical premier readout/illustration of transcriptome data has been the relative gene expression between groups of relevant samples and pre-defined groups of control samples (9, 10). However, in contrast to the relative expression, the actual probe signal values (PSVs) of perturbed signature genes have generally been ignored, even though the PSVs of the perturbed signature genes have been reliably detected (technically unreliable/undetected ones have been filtered out prior to bioinformatics analysis). In this study, the term "probes" mean the fluorescently labeled nucleic acids/genes comprising an RNA sample that would hybridize to the corresponding gene-specific DNA fragment of a gene array in a dose-dependent manner. The term PSV means the normalized and then $\log_2$-transformed probe signal strength of any gene in a gene array/sample. We hypothesized that analysis of the PSVs underlying published gene signatures might reveal additional biologically relevant information, since PSVs are taken to broadly reflect the abundance of mRNA, which in turn is a critical determinant of cognate protein abundance. Accordingly, we explored and compared the PSVs of signature genes identified from a homogeneous cell line as a model and then from heterogeneous *in vivo* whole blood. The signatures from the *Mtb*-infected THP-1 cell line were previously identified by us as the induced signature (T*Mtb*-i, from genes that were induced/up-regulated after *Mtb* infection) and its derived network-based signature (T*Mtb*-iNet) and a repressed gene signature (T*Mtb*-r) from genes that were repressed/down-regulated after *Mtb* infection (6, 11). The signature from whole blood was the pulmonary TB (PTB)-specific signature PTBsig identified, by Berry et al. (10), through comparing the transcriptome data of whole blood in PTB patients to those in latent TB-infected (LTBI) donors and healthy control (HC) donors. It was divided into the up-regulated and down-regulated sub-signatures, termed PTBsigUp and PTBsigDn, respectively (10, 12).

The cell line-derived signatures T*Mtb*-i and T*Mtb*-iNet are interferon-related signatures and T*Mtb*-r is a functionally undefined signature (6, 12). The whole blood signature PTBsig is similarly an interferon-inducible blood signature and is present in neutrophils rather than in CD4+ T cells, CD8+ T cells, or monocytes (10). In essence, the numerical predominance and larger gene expression in neutrophils inevitably account for the PTBsig in whole blood (12). However, neutrophils appear to mainly contribute to pathology rather than protection against the bacteria in TB. Furthermore, the determinants of the underlying balance of innate and acquired immunity are not currently resolved and are likely to be complex (13–15). This investigation of PSVs indicates that a high degree of expression of Fc receptor for IgG (i.e., Fc fragments of IgG receptor; FCGR1A, FCGR1B) on neutrophils may be a key signature of pulmonary TB.

RESULTS

T*Mtb*-i and T*Mtb*-iNet Genes Are at Lower PSVs (Implying Lower/Negligible Protein Abundances) in Homogeneous THP-1 Cells Prior to *Mtb* Infection, Whereas T*Mtb*-r Genes Are at Average PSVs

Figure 1 (also see **Figure S1**) shows that in uninfected THP-1 cells (i.e., at 0 h), T*Mtb*-i and T*Mtb*-iNet genes displayed significantly lower PSVs than the whole genome genes (false discovery rate, FDR = 0 in each case). The PSVs of the T*Mtb*-r genes at 0 h were not significantly different from the

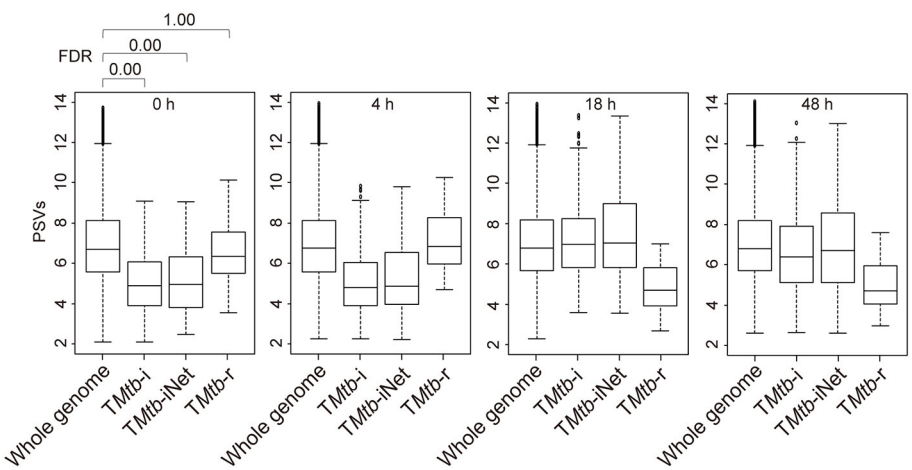

FIGURE 1 | Box plots of the PSVs from THP-1 cells responding to *Mtb* infection. PSVs refer to the normalized and $\log_2$-transformed probe signals. Whole genome: the entire set of technically reliable/detected PSVs in the gene array. T*Mtb*-i: the induced genes of THP-1 responding to *Mtb* infection (6). T*Mtb*-iNet: a network-based signature derived from T*Mtb*-i based on STRING protein–protein interaction information (11). T*Mtb*-r: the repressed genes of THP-1 responding to *Mtb* infection (6). In the box plots, the top and bottom of the box represent the first and third quartile, respectively, and the dividing line represents the median; the lowest horizontal bar represents the smallest datum; the highest horizontal bar represents 1.5 times the third quartile. Each data value larger than 1.5 times the third quartile is shown as a dot above the highest bar. The false discovery rate (FDR) of differences between signature PSVs and whole genome PSVs is shown above the 0 h data panel; FDR $\leq$ 0.05 was regarded as indicating a statistically significant difference.

whole genome genes (FDR = 1). Similar phenomena were also observed in another dataset, in which THP-1 cells were infected for 72 h (**Figure S2**). In summary, T*Mtb*-i and T*Mtb*-iNet genes, as a whole, displayed lower than average PSVs (implying lower/negligible protein abundances) in homogeneous THP-1 cells prior to *Mtb* infection, whereas the T*Mtb*-r genes, as a whole, displayed average PSVs (implying average protein abundances) in the THP-1 cells prior to *Mtb* infection.

PTBsigUp and PTBsigDn Genes Display Average PSVs (Implying Average Protein Abundances) in the Highly Heterogeneous Whole Blood of HC Donors

After exploring the PSVs of signature genes of T*Mtb*-i, T*Mtb*-iNet, and T*Mtb*-r identified in homogeneous THP-1 cells, we then explored the PSVs of signature genes of PTBsig identified in highly heterogeneous whole blood. This analysis would clarify if signature genes, being divided into up-regulated sub-signature (PTBsigUp) and down-regulated sub-signature (PTBsigDn) genes, displayed similar patterns of PSVs in the heterogeneous whole blood of HC donors as compared to the PSVs of T*Mtb*-i, T*Mtb*-iNet, and T*Mtb*-r genes in homogeneous THP-1 cells.

Figure 2 (also see **Figure S3**) shows that in whole blood of HC donors, the PSVs of the PTBsigUp and PTBsigDn genes were not significantly different from the PSVs of the filtered whole genome genes (FDR = 1). This finding was cross-validated in an independent dataset (**Figure S4**). Thus, in contrast to the findings from uninfected THP-1 cells (**Figure 1**), PTBsigUp and PTBsigDn genes, as a whole, displayed average PSVs (implying average protein abundances) in the whole blood of HC donors. However, whole blood is highly heterogeneous in nucleated cell content with various types of white cells in differing proportions. Accordingly, analysis of PSVs in each of the four main white cell populations separately might reveal differences that were masked in the whole-blood data.

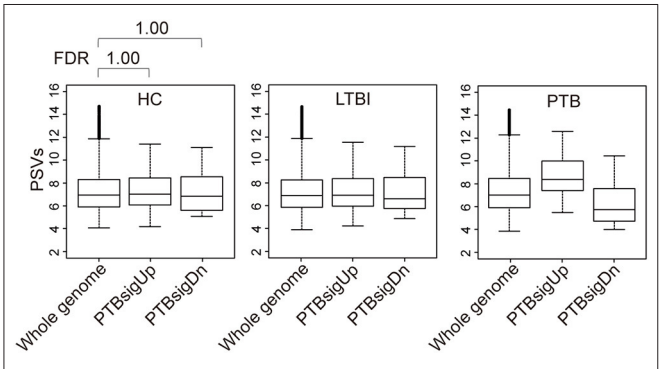

FIGURE 2 | Box plots of the PSVs of PTB-specific signature genes in human whole blood. HC, healthy control donors; LTBI, latent TB infection donors; PTB, pulmonary tuberculosis patients. Whole genome: the entire set of technically reliable/detected PSVs in gene arrays of whole blood. PTBsigUp: the up-regulated genes in the PTB-specific signature PTBsig. PTBsigDn: the down-regulated genes in PTBsig (10). PSV, FDR, and the data plot method are as described in **Figure 1**.

Separation of HC Blood Into Cell Types Reveals Differences in PTBsigUp and PTBsigDn PSVs Compared to Background Whole Genome PSVs

As shown in **Figure 3**, in comparison to HC donors, the PSVs of PTBsigUp genes in the CD4+ T cells and CD8+ T cells were significantly lower (FDR = 0), whereas the PSVs of PTBsigDn genes in the CD4+ T cells were significantly higher (FDR = 0.020) than the PSVs of the HC filtered whole genome genes. The PSVs of PTBsigDn genes in the CD8+ T cells were not significantly different from the HC whole genome PSVs (FDR = 0.291). In the monocytes, the PSVs of PTBsigUp genes were not significantly different from the PSVs of HC filtered whole genome genes whereas the PSVs of PTBsigDn genes were significantly lower (FDRs = 1 and = 0, respectively). In the neutrophils, the PSVs of PTBsigUp genes were statistically higher than the PSVs of the corresponding HC filtered whole genome genes whereas the PSVs of PTBsigDn genes were statistically lower (both FDRs = 0). The data are available for visual comparison in **Figure S5**. In summary, some huge and highly significant differences from HC were seen in the PSVs (implying huge differences in protein abundances) of PTBsigUp and PTBsigDn genes within the four different cell populations, differences that were masked in the average PSVs in the whole blood. Notably, neutrophils displayed the highest PTBsigUp PSVs (implying the highest protein abundances) compared to the abundances in the other three kinds of cells.

The PSV Patterns of *FCGR1* in the Four Cell Populations Are Typical of the PSV Patterns of PTBsigUp Genes in the Four Cell Populations

The up-regulated sub-signature PTBsigUp genes displayed low PSVs in the CD4+ and CD8+ T cells of HC donors, and displayed average and higher PSVs in the monocytes and neutrophils of HC donors, respectively (**Figure 3**). In the light of this, we aimed to identify from the four cell populations those genes that could be typical representatives of the PSV pattern of PTBsigUp.

We used a combination of three selection criteria: median PSVs in the neutrophils of HC donors (HC_neut) being ≥ 7; $\log_2$ (fold change) between PTB_neut and HC_neut being ≥ 3; median PSVs of HC_CD4 and HC_CD8 being ≤ 5. By these criteria, we retrieved only two genes, i.e., *FCGR1A* and *FCGR1B*, represented by the two gene-specific DNA fragments of the gene array (i.e., ILMN_2176063 and ILMN_2261600, respectively). Since *FCGR1A*, *FCGR1B*, and a pseudogene (*FCGR1CP*) are highly homologous (**Figure S6**), we then aligned the sequences of the two gene-specific DNA fragments of the gene array against all human transcripts through the nucleotide BLAST (blastn) of NCBI. The result showed that the two gene-specific DNA fragments of the gene array were both highly homologous to *FCGR1A*, *FCGR1B*, and the pseudogene *FCGR1CP* (**Tables 1**, **2**), which indicated that each of the two gene-specific DNA fragments of the gene array actually detected the summed

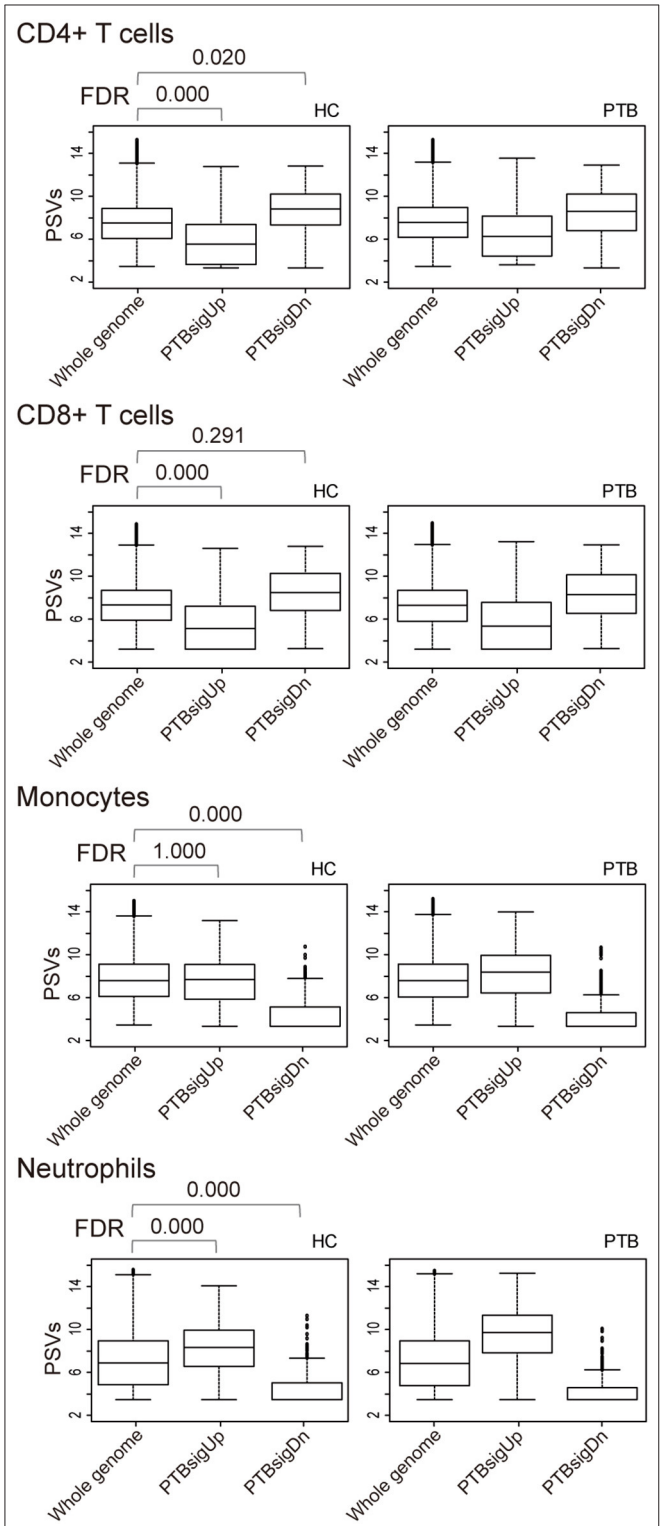

FIGURE 3 | Box plots of the PSVs of PTB-specific signature genes in separated cell populations of human whole blood. HC, healthy control donors; PTB, pulmonary tuberculosis patients. Whole genome, PTBsigUp, and PTBsigDn are as described in **Figure 2**. PSV, FDR, and the data plot method are as described in **Figure 1**.

TABLE 1 | The sequence alignment of ILMN_2176063 against human transcripts using nucleotide BLAST (blastn) of NCBI.

Description	Identity (%)	Accession
PREDICTED: *Homo sapiens* Fc fragment of IgG receptor Ia (*FCGR1A*), transcript variant X2, mRNA	100.00	XM_005244958.4
PREDICTED: *Homo sapiens* Fc fragment of IgG receptor Ia (*FCGR1A*), transcript variant X1, mRNA	100.00	XM_005244957.3
Homo sapiens Fc fragment of IgG receptor Ic, pseudogene (*FCGR1CP*), non-coding RNA	100.00	NR_027484.2
Homo sapiens Fc fragment of IgG receptor Ia (*FCGR1A*), mRNA	100.00	NM_000566.3
PREDICTED: *Homo sapiens* Fc fragment of IgG receptor Ib (*FCGR1B*), transcript variant X3, misc_RNA	98.00	XR_001737041.1
PREDICTED: *Homo sapiens* Fc fragment of IgG receptor Ib (*FCGR1B*), transcript variant X2, misc_RNA	98.00	XR_001737040.1
Homo sapiens Fc fragment of IgG receptor Ib (*FCGR1B*), transcript variant 4, non-coding RNA	98.00	NR_045213.1
Homo sapiens Fc fragment of IgG receptor Ib (*FCGR1B*), transcript variant 3, mRNA	98.00	NM_001244910.1

expressions of *FCGR1A*, *FCGR1B*, and *FCGR1CP* (the three genes together are hereafter termed *FCGR1*). Hence, the two gene-specific DNA fragments of the gene array revealed that *FCGR1* displayed higher PSVs in the whole blood of PTB patients compared to its expression in the whole blood of HC and LTBI donors, and this was markedly reduced during chemotherapy (**Figure S7**). *FCGR1* displayed low PSVs in the CD4+ and CD8+ T cells from both HC and PTB donors (**Figure 4**). In contrast, it had higher PSVs in the monocytes and neutrophils of HC donors and was present at much higher levels in the monocytes and neutrophils of PTB patients, especially in neutrophils (i.e., 5.1- and 13.4-fold higher, respectively, for ILMN_2176063; 4.8- and 9.0-fold, respectively, for ILMN_2261600; **Figure 4**). By implication, there may have been higher expression of the actual receptor on neutrophils than even on monocytes of PTB patients (i.e., 3.29-fold higher for ILMN_2176063 and 2.44-fold for ILMN_2261600). In summary, transcriptome array-based analysis revealed that *FCGR1* can be regarded as a typical representative of PTBsigUp genes in relation to the PSVs patterns in the four cell populations (i.e., CD4+ T cells, CD8+ T cells, monocytes, and neutrophils) and the majority of the receptor may be on neutrophils.

Confirmation That *FCGR1* Genes (i.e., *FCGR1A*, *FCGR1B*, and the Pseudogene *FCGR1CP*) Are All Up-Regulated in the Whole Blood of TB Patients

Definitive evidence for higher mRNA expression levels of *FCGR1A*, *FCGR1B*, and the pseudogene *FCGR1CP* in the whole

blood of PTB patients than in blood of LTBI and HC donors (**Figure S7**) was sought by RNA-seq analysis. The promoter sequences of the three genes (from −2,000 bp upstream to 50 bp downstream of the transcription start sites) are highly homologous, indicating that the three genes likely undergo concordant expression in response to a stimulus such as *Mtb* infection (**Figure S8**). RNA-seq might accurately discriminate differing expression of these highly homologous genes by exploiting differences such as single-nucleotide polymorphisms and/or nucleotide insertion/deletions. For this purpose, we utilized an RNA-seq-based whole blood transcriptome dataset from LTBI donors who had eventually displayed clinical PTB (tagged as progressors) and LTBI donors who did not display clinical PTB (tagged as LTBI controls) (16). As shown in **Figures 5A–C** and **Figure S9**, compared to LTBI controls, the expressions of *FCGR1A*, *FCGR1B*, and *FCGR1CP* were all increasing when progressors were approaching clinical TB and decreasing when progressors were undergoing chemotherapy. In comparison to the median expression in LTBI controls, *FCGR1A* had the highest and *FCGR1CP* had the lowest levels (**Figure 5D** and **Figure S10**). In conclusion, all three *FCGR1* genes displayed up-regulation in the whole blood of PTB patients.

TABLE 2 | The sequence alignment of ILMN_2261600 against human transcripts using nucleotide BLAST (blastn) of NCBI.

Description	Identity (%)	Accession
PREDICTED: *Homo sapiens* Fc fragment of IgG receptor Ia (*FCGR1A*), transcript variant X1, mRNA	100.00	XM_005244957.3
Homo sapiens Fc fragment of IgG receptor Ic, pseudogene (*FCGR1CP*), non-coding RNA	100.00	NR_027484.2
Homo sapiens Fc fragment of IgG receptor Ib (*FCGR1B*), transcript variant 4, non-coding RNA	100.00	NR_045213.1
Homo sapiens Fc fragment of IgG receptor Ib (*FCGR1B*), transcript variant 3, mRNA	100.00	NM_001244910.1
Homo sapiens Fc fragment of IgG receptor Ib (*FCGR1B*), transcript variant 1, mRNA	100.00	NM_001017986.3
Homo sapiens Fc fragment of IgG receptor Ia (*FCGR1A*), mRNA	100.00	NM_000566.3
PREDICTED: *Homo sapiens* Fc fragment of IgG receptor Ib (*FCGR1B*), transcript variant X3, misc_RNA	98.00	XR_001737041.1
PREDICTED: *Homo sapiens* Fc fragment of IgG receptor Ib (*FCGR1B*), transcript variant X2, misc_RNA	98.00	XR_001737040.1
PREDICTED: *Homo sapiens* Fc fragment of IgG receptor Ib (*FCGR1B*), transcript variant X1, mRNA	98.00	XM_017000661.1

DISCUSSION

This investigation appears to confirm our hypothesis: the customary focus on relative expressions between PSVs in transcriptome arrays, rather than on the absolute values of the PSVs, can lead to loss of meaningful information. Although transcript levels by themselves are not sufficient to predict protein levels in many scenarios (17, 18), they are generally accepted to provide a convenient guide to cell phenotype changes. Accordingly, in interpreting the results, we have extrapolated from PSVs, through implied mRNA levels, to potential protein levels.

The concept that analysis of PSVs could be revelatory was first validated by the re-analysis of the published data from TB-infected THP-1 cell line. As might be expected, significant differences in PSVs were only revealed when the up-regulated and down-regulated signature genes were analyzed separately; the PSV differences otherwise tended to cancel out. The genes that were previously shown to be up-regulated in defining the signature of TB infection (T*Mtb*-i) were here found to be expressed at below-average levels before infection (**Figure 1**). This was consistent with the mRNA from these signature genes

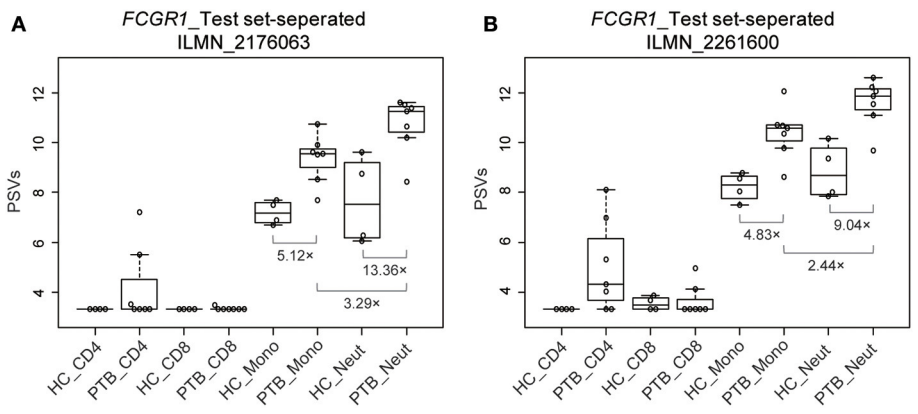

FIGURE 4 | Box plots of the PSVs of *FCGR1* in the separated blood cells. *FCGR1* was revealed by signals from ILMN_2176063 **(A)** and ILMN_2261600 **(B)**. HC_CD4, CD4+ T cells isolated from the whole blood of HC donors; PTB_CD4, CD4+ T cells isolated from the whole blood of PTB patients; other abbreviations are similarly arranged.

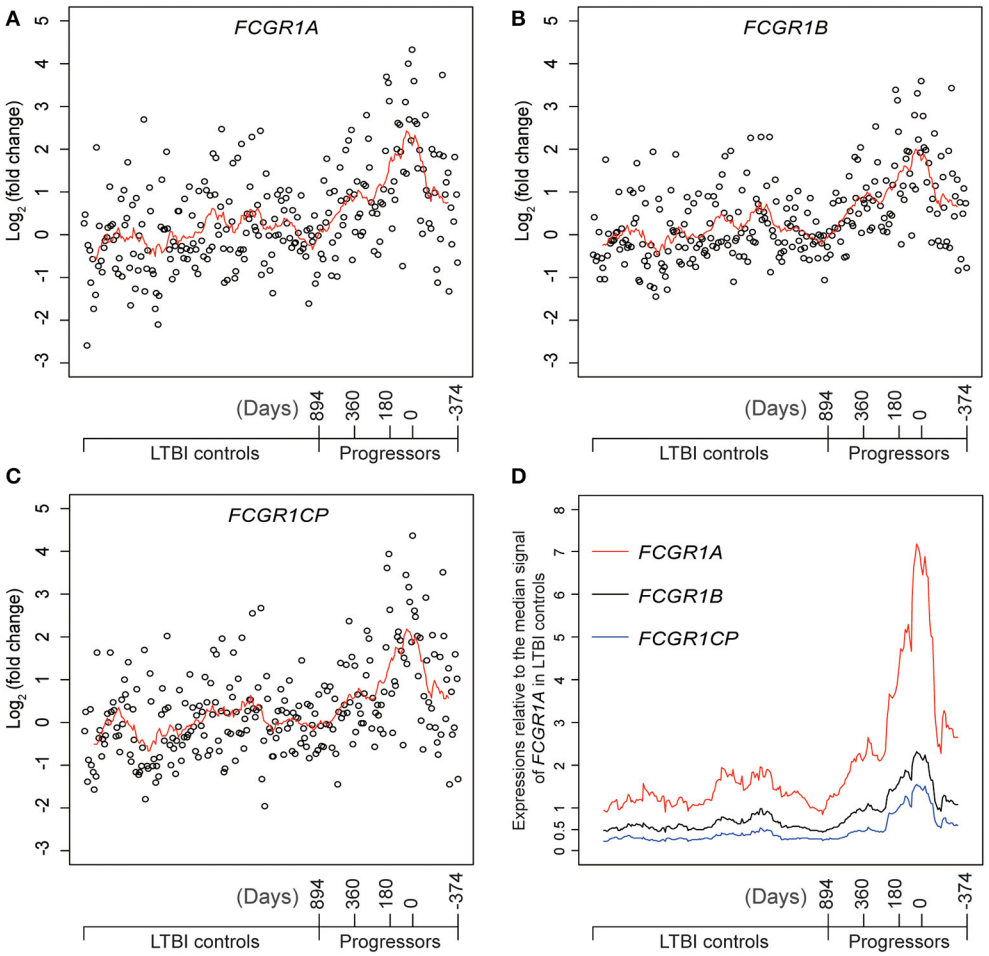

FIGURE 5 | The relative expressions of *FCGR1* in the whole blood of LTBI progressors compared to the whole blood of LTBI controls. **(A–C)** The relative expressions of *FCGR1A*, *FCGR1B*, and *FCGR1CP*, respectively. Each data point represents the PSV from a single individual: LTBI controls were HC and LTBI non-progressors, plotted in arbitrary sequence from left to right; PSVs from progressors were synchronized to the time of PTB diagnosis, with positive value representing days prior to PTB diagnosis and negative value denoting days post PTB diagnosis. **(D)** The PSVs of *FCGR1A*, *FCGR1B*, and *FCGR1CP* relative to the median PSV of *FCGR1A* in LTBI controls. The line in each panel represents the moving average trend line with the interval of 15 (i.e., averaging adjacent 15 data points).

being below the levels needed for translation into protein before infection. For example, *CCL1, IL11, CXCL10, CCL8,* and *CXCL9* are some of these up-regulated signature genes and the cognate proteins in the supernatant of Phorbol 12-myristate 13-acetate (PMA)-differentiated THP-1 cells were barely detectable in a human inflammation antibody array (19). The finding that the mean PSV of the down-regulated signature genes (T*Mtb*-r) was substantially below average after infection suggests that some of these mRNA levels may have dropped below those needed for translation.

In view of the derivation of the PTBsig from whole human blood, it was no surprise to see that the mean PSVs of PTBsigUp and PTBsigDn were significantly different from the average background in PTB (**Figure 2**). However, much bigger differences, including differences in HC donors, were revealed when data for separate cell types were analyzed (**Figure 3**). The concealment in whole blood was largely a consequence of the masking effect imposed by differences of opposite polarity in the different cell types. Furthermore, the signatures were evident in HC donors also, where the pattern was similar but of smaller magnitude. The biggest differences were evident in the neutrophils of HC donors, presumably arising through stimulation by cytokines such as IFN-g and G-CSF since unstimulated neutrophils express little if any surface FCGR1 (20–22). We interpret the presence of the signature in the PSV data from HC subjects as evidence of a background of responses to other infections. This may perhaps limit the practical utility of whole signature PSV data in clinical applications.

However, the selection criteria that we applied to find the most representative PSV signals in the signature led to identification of *FCGR1* as the most robust and analysis of PSVs of the isomers of this gene in the data from separated cell types revealed very large and highly significant differences between HC and PTB datasets (**Figure 4**). The greatest difference between HC and

PTB was in the neutrophil data where, for ILMN_2176063, the PSV of PTB was over 13-fold higher than the PSV of HC. This may point to a practical utility since, even in whole blood data, the PSV of *FCGR1* increased substantially as the status of LTBI transitioned into active PTB disease (**Figure 5**). It is notable that the up-regulation of *FCGR1A* and/or *FCGR1B* has been repeatedly reported as a component of human TB signatures (23–26). Furthermore, recently, *FCGR1A* was found among blood RNA signatures that prospectively discriminated controllers from progressors early after low-dose *Mtb* infection of cynomolgus macaques (27). However, a caveat is indicated regarding extrapolation from the mRNA and protein levels of FCRG1. The reported *FCGR1A* and/or *FCGR1B* signals from high-throughput approaches/platforms reflect a combination of *FCGR1A*, *FCGR1B*, and *FCGR1CP* together since they are highly homologous in their promoter regions (**Figure S8**) and mRNA sequences (**Figure S6**). Neither mRNA nor protein isomers (**Figure S11**) were distinguished by the gene arrays or commercial antibodies employed in the various studies. A possible modulatory effect of pseudogene *FCGR1CP* on the final expression of the receptor remains to be explored. Similarly, because there are three highly homologous genes/pseudogenes in the human genome (all located in chromosome 1), whereas there is only one (*Fcgr1* annotated as human *FCGR1A* ortholog) in mouse genome (located in chromosome 3; **Table S1**), the mouse model is not ideal for precise decipherment of potential functional differences of the three human genes post *Mtb* infection.

Dozens of host-response-based gene signatures, which were identified from human whole blood or peripheral blood mononuclear cells (PBMCs), have been reported to have potential for human TB diagnosis (28). Additional analyses, based on PSVs, could imply/identify the cell types in which the signature genes were sufficiently changed for alteration of cell function. This would aid our limited understanding of TB immunity and immunopathology. It may also guide the cell type-specific implementation of the gene signatures in clinical settings. The role of neutrophils in TB is complex and is likely to vary at different stages of infection and disease (29). Despite their numerical predominance, the functional significance of circulating neutrophils with presumptive high levels of expression of FCGR1 is not known (30). If they reflect the status of neutrophils within TB lesions, then the abundance and high affinity of this IgG receptor may have a key involvement in modulation of innate and acquired immunity in addition to pathology of PTB (31). The predominant infected phagocytes in the airways of TB patients are neutrophils (14) and they are associated with enhanced TB pathology (13). Their FCGR1 receptors may facilitate the phagocytosis that is followed by rapid intracellular replication of *Mtb* and cell necrosis (15). In addition, the cross-linking of the abundant high-affinity receptors by antigen–antibody complexes may generate a cytokine storm that also impairs acquired immunity.

In conclusion, PSVs-based analysis implies an excessive involvement of neutrophil FCGR1 in the impaired balance between protection and pathology in TB.

METHODS

The Transcriptome Datasets Used in This Study

A total of six publically available gene expression datasets with NCBI GEO (32) accession numbers GSE29628 (6), GSE19439 (10), GSE19443 (10), GSE17477 (33), GSE42830 (34), and GSE79362 (16) were utilized in this study.

GSE29628 contains time-course (i.e., 0, 4, 18, and 48 h) transcriptome data of human macrophage-like cells (THP-1 cells treated with PMA) that had then been infected by the *Mtb* lab strain H37Rv or with one of 11 different *Mtb* W-Beijing strains (6). The array platform of GSE29628 is Affymetrix Human Genome U133 Plus 2.0. Based on the dataset GSE29628, we previously reported a highly prominent induced/up-regulated interferon-related gene signature, termed T*Mtb*-i, in addition to a repressed/down-regulated, function-undefined, minor gene signature, termed T*Mtb*-r. Based on STRING protein–protein interaction information (35), we further refined a network-based signature T*Mtb*-iNet from T*Mtb*-i (11).

GSE19439 contains transcriptome data of whole blood from HC donors, LTBI donors, and PTB patients, who were recruited from London, UK. The array platform of GSE19439 is Illumina HumanHT-12 V3.0 expression beadchip. It served as the training set, and is a SubSeries of SuperSeries GSE19491 (10). Only GSE19439 was utilized in this study because the reported PTB-specific blood signature (PTBsig) was defined from GSE19439, and PTBsig could readily distinguish PTB patients from LTBI and/or HC donors in the other two SubSeries of GSE19491 (which served as test set and validation set).

GSE19443 contains transcriptome data of four cell populations (i.e., CD4+ T cells, CD8+ T cells, monocytes, and neutrophils) separated from whole blood of HC donors and PTB patients who were recruited from London, UK. The array platform of GSE19443 is the same as that of GSE19439 (i.e., Illumina HumanHT-12 V3.0 expression beadchip). GSE19443 served as test set_separated, and is also a SubSeries of SuperSeries GSE19491 (10).

GSE17477 contains the transcriptome data of THP-1 cells, THP-1 cells infected with H37Rv (72 h post-infection), THP-1 cells treated with IFN-γ (2 h), or THP-1 cells infected with H37Rv (72 h post-infection) and then treated with IFN-γ (2 h) (33). The array platform of GSE17477 is Affymetrix Human Genome U133A 2.0, of which the gene-specific DNA fragments are identically represented on Affymetrix Human Genome U133 Plus 2.0 used in GSE29628.

GSE42830 contains the transcriptome data of whole blood from HC donors, TB patients, sarcoid patients, pneumonia patients, or lung cancer patients (34). The platform used for GSE42830 is Illumina HumanHT-12 V4.0 expression beadchip, which shares a majority of gene-specific DNA fragments with the Illumina HumanHT-12 V3.0 expression beadchip used in GSE19439 and GSE19443.

GSE79362 contains RNA-seq-based transcriptome data of whole blood from LTBI controls (people who did not display clinical PTB during the period of investigation after diagnosis)

and progressors (LTBI donors who displayed clinical PTB at a later time) (16). See the original research for detailed information of RNA sequencing and the alignment of sequence reads against the human genome (16). The gene expression abundance was monitored based on splice junction counts, which quantify the relative frequency of specific RNA splicing events of expressed genes.

TB-Relevant Gene Signatures and PSV Analysis

The PSVs of published gene signatures from THP-1 cells (i.e., T*Mtb*-i, T*Mtb*-iNet, T*Mtb*-r) together with the PSVs in control THP-1 cells prior to *Mtb* infection were compared to the PSVs of their cognate filtered whole genome genes in the control samples (6). Likewise, the PSVs of gene signatures PTBsigUp (the up-regulated sub-signature of PTBsig) and PTBsigDn (the down-regulated sub-signature of PTBsig) (12) together with their PSVs in control samples (whole blood of HC donors) were compared to the PSVs of their cognate filtered whole genome genes in control samples (10). Since there might be multiple gene-specific DNA fragments for a single gene in a gene signature, we applied the PSV analysis on the basis of an individual gene-specific DNA fragment for each gene. See the original research (6, 10) for the detailed procedures of normalization of transcriptome data and the generation of filtered whole genome gene data. In brief, THP-1-relevant transcriptome data (i.e., dataset GSE29628) were normalized using Robust Multi-array Averaging (RMA) with quantile normalization in R (Bioconductor) (36). Then, gene-specific DNA fragments that had PSVs consistently below the 95th percentile of all the "Absent" call-flagged signals of the entire dataset were filtered out (6). Illumina BeadStudio software and GeneSpring GX software were utilized for the normalization of whole blood-relevant transcriptome data (i.e., GSE19439) and of the separated cell populations-relevant transcriptome data (i.e., GSE19443). Any PSV < 10 was set to 10. A gene-specific DNA fragment was retained when it was called "present" (signal precision < 0.01) in $>10\%$ of all samples in GSE19439 and had a minimum of 2-fold expression change compared to the median intensity in $>10\%$ of all samples in GSE19439 (10).

The dataset GSE17477 (33) was utilized to cross-validate the PSVs of T*Mtb*-i, T*Mtb*-iNet, and T*Mtb*-r genes. The dataset GSE42830 (34) was utilized to cross-validate the PSVs of PTBsigUp and PTBsigDn genes. There are several datasets addressing the transcriptome of THP-1 cells infected with *Mtb* strains (e.g., GSE51029, GSE52819, GSE57028, GSE7870, GSE15539, GSE17477, GSE19052, and GSE6209) and different array platforms were used to generate these datasets. Different array platforms may use different gene-specific DNA sequences to quantify a gene, which might generate platform-specific expression patterns for a gene. To minimize the platform-specific inconsistent expression patterns, we chose the dataset GSE17477, since its array platform was Affymetrix Human Genome U133A 2.0, of which the gene-specific DNA fragments are identically represented on Affymetrix Human Genome U133 Plus 2.0. The Affymetrix Human Genome U133 Plus 2.0 also contains all the gene-specific DNA fragments of Affymetrix Human Genome U133B and many additional gene-specific DNA fragments. The dataset GSE17477 was normalized and filtered exactly the same as for GSE29628 (6). For cross-validating the PSVs of T*Mtb*-i and T*Mtb*-r, we focused on the transcriptome data of THP-1 cells or THP-1 cells infected with H37Rv. The genes of T*Mtb*-i, T*Mtb*-iNet, or T*Mtb*-r could be matched between GSE29628 and GSE17477 through their IDs of gene-specific DNA fragments.

There are a few studies/datasets addressing the transcriptome of PBMCs or whole blood from (pulmonary) TB patients and/or HC donors (1). Of these datasets, only GSE42830 used the Illumina HumanHT-12-relevant platform that contains the transcriptome data of whole blood from both TB patients and HC donors (34), and therefore could be used to validate the PSVs of PTBsigUp and PTBsigDn genes. GSE42830 was normalized and filtered the same way as for GSE19439 (10, 34). For cross-validating the PSVs of PTBsigUp and PTBsigDn genes, we focused on the transcriptome data of whole blood from HC donors and TB patients. The genes of PTBsigUp or PTBsigDn could be matched between GSE19439 and GSE42830 through their IDs of gene-specific DNA fragments.

Also, we retrieved the training set from "GSE79362_primarySampleJunctions.xlsx" and followed the published normalization procedures to normalize the RNA splicing events of expressed genes (16). The expression data of *FCGR1* genes, including *FCGR1A*, *FCGR1B*, and the pseudogene *FCGR1CP*, were extracted from the normalized training set and their expression in LTBI controls and progressors were analyzed.

Statistical Analysis

This approach was to test if signature genes, as a whole, displayed lower, higher, or average PSVs, compared to the PSVs of filtered whole genome genes. The reason for applying PSV analysis is that PSVs could broadly reflect the abundances of mRNAs, which in turn are critical determinants of cognate protein abundances. We believe that the information of protein abundance in cells, even before a stimulation (e.g., *Mtb* infection), could imply the degree of functional involvement of that protein, whereas the often adopted relative expression strategy, which just reflects the relative fold change after a stimulation, simply ignores the information of implied protein abundance.

An FDR was defined for assessing the significance of differences (p-value) between datasets. FDR was calculated as follows: 10,000 randomly sampled gene sets from cognate filtered whole genome genes with the same set size as the gene signature of interest were generated. Then, the PSVs of each of the 10,000 randomly sampled gene sets were iteratively compared to the PSVs of signature genes using the Kolmogorov–Smirnov test (KS test), a process that generated 10,000 p-values. The proportion of p-values larger than the empirically determined value 0.0001 in the 10,000 p-values was treated as the FDR. If the FDR was equal to or <0.05, then the signature genes' PSVs as a whole were said to be significantly different from the PSVs of the filtered whole genome genes.

DATA AVAILABILITY STATEMENT

Publicly available datasets were analyzed in this study. This data can be found here: NCBI GEO accession numbers GSE29628, GSE19439, GSE19443, GSE17477, GSE42830, GSE79362.

AUTHOR CONTRIBUTIONS

KW, DL, and X-YF conceived and designed the experiments and wrote the paper. KW, DL, ML, and ZC analyzed the data. KW and X-YF interpreted the data. KW acquired the data. DL and X-YF gave overall supervision, critical comments, and reviewed the manuscript. All authors read and approved the final manuscript.

FUNDING

This work was supported by grants from the Chinese National Mega Science and Technology Program on Infectious Diseases (2018ZX10731301 and 2018ZX10302301), the National Key R&D Program of China (2018YFD0500900), the National Natural and Science Foundation of China (31771004, 81301407, and 81770011), and Shanghai Science and Technology Commission (19XD1403100, 18411970700, and 17ZR1423900).

SUPPLEMENTARY MATERIAL

The Supplementary Material for this article can be found online at: https://www.frontiersin.org/articles/10.3389/fmed.2020.00019/full#supplementary-material

REFERENCES

1. Berry MP, Blankley S, Graham CM, Bloom CI, O'Garra A. Systems approaches to studying the immune response in tuberculosis. *Curr Opin Immunol.* (2013) 25:579–87. doi: 10.1016/j.coi.2013.08.003
2. Arlehamn CL, Seumois G, Gerasimova A, Huang C, Fu Z, Yue X, et al. Transcriptional profile of tuberculosis antigen-specific T cells reveals novel multifunctional features. *J Immunol.* (2014) 193:2931–40. doi: 10.4049/jimmunol.1401151
3. Tailleux L, Waddell SJ, Pelizzola M, Mortellaro A, Withers M, Tanne A, et al. Probing host pathogen cross-talk by transcriptional profiling of both *Mycobacterium tuberculosis* and infected human dendritic cells and macrophages. *PLoS ONE.* (2008) 3:e1403. doi: 10.1371/journal.pone.0001403
4. Orlova MO, Majorov KB, Lyadova IV, Eruslanov EB, M'lan CE, Greenwood CM, et al. Constitutive differences in gene expression profiles parallel genetic patterns of susceptibility to tuberculosis in mice. *Infect Immun.* (2006) 74:3668–72. doi: 10.1128/IAI.00196-06
5. Beisiegel M, Mollenkopf HJ, Hahnke K, Koch M, Dietrich I, Reece ST, et al. Combination of host susceptibility and *Mycobacterium tuberculosis* virulence define gene expression profile in the host. *Eur J Immunol.* (2009) 39:3369–84. doi: 10.1002/eji.200939615
6. Wu K, Dong D, Fang H, Levillain F, Jin W, Mei J, et al. An interferon-related signature in the transcriptional core response of human macrophages to *Mycobacterium tuberculosis* infection. *PLoS ONE.* (2012) 7:e38367. doi: 10.1371/journal.pone.0038367
7. Mortazavi A, Williams BA, McCue K, Schaeffer L, Wold B. Mapping and quantifying mammalian transcriptomes by RNA-Seq. *Nat Methods.* (2008) 5:621–8. doi: 10.1038/nmeth.1226
8. Schulze A, Downward J. Navigating gene expression using microarrays—a technology review. *Nat Cell Biol.* (2001) 3:E190–5. doi: 10.1038/35087138
9. Xue Z, Huang K, Cai C, Cai L, Jiang CY, Feng Y, et al. Genetic programs in human and mouse early embryos revealed by single-cell RNA sequencing. *Nature.* (2013) 500:593–7. doi: 10.1038/nature12364
10. Berry MP, Graham CM, McNab FW, Xu Z, Bloch SA, Oni T, et al. An interferon-inducible neutrophil-driven blood transcriptional signature in human tuberculosis. *Nature.* (2010) 466:973–7. doi: 10.1038/nature09247
11. Wu K, Fang H, Lyu LD, Lowrie DB, Wong KW, Fan XY. A Derived network-based interferon-related signature of human macrophages responding to *Mycobacterium tuberculosis*. *Biomed Res Int.* (2014) 2014:713071. doi: 10.1155/2014/713071
12. Wu K, Wong KW, Deng WL, Zhang H, Li J, Lowrie DB, Fan XY, et al. The numerical predominance and large transcriptome differences of neutrophils in peripheral blood together inevitably account for a reported pulmonary tuberculosis signature. *Int J Genomics.* (2017) 2017:5830971. doi: 10.1155/2017/5830971
13. Dallenga T, Schaible UE. Neutrophils in tuberculosis—first line of defence or booster of disease and targets for host-directed therapy? *Pathog Dis.* (2016) 74:1–7. doi: 10.1093/femspd/ftw012
14. Eum SY, Kong JH, Hong MS, Lee YJ, Kim JH, Hwang SH, et al. Neutrophils are the predominant infected phagocytic cells in the airways of patients with active pulmonary TB. *Chest.* (2010) 137:122–8. doi: 10.1378/chest.09-0903
15. Corleis B, Korbel D, Wilson R, Bylund J, Chee R, Schaible UE. Escape of *Mycobacterium tuberculosis* from oxidative killing by neutrophils. *Cell Microbiol.* (2012) 14:1109–21. doi: 10.1111/j.1462-5822.2012.01783.x
16. Zak DE, Penn-Nicholson A, Scriba TJ, Thompson E, Suliman S, Amon LM, et al. A blood RNA signature for tuberculosis disease risk: a prospective cohort study. *Lancet.* (2016) 387:2312–22. doi: 10.1016/S0140-6736(15)01316-1
17. Pascal LE, True LD, Campbell DS, Deutsch EW, Risk M, Coleman IM, et al. Correlation of mRNA and protein levels: cell type-specific gene expression of cluster designation antigens in the prostate. *BMC Genomics.* (2008) 9:246. doi: 10.1186/1471-2164-9-246
18. Liu Y, Beyer A, Aebersold R. On the dependency of cellular protein levels on mRNA abundance. *Cell.* (2016) 165:535–50. doi: 10.1016/j.cell.2016.03.014
19. Wang T, Xiang Z, Wang Y, Li X, Fang C, Song S, et al. (-)-Epigallocatechin gallate targets notch to attenuate the inflammatory response in the immediate early stage in human macrophages. *Front Immunol.* (2017) 8:433. doi: 10.3389/fimmu.2017.00433
20. Graziano RF, Fanger MW. Fc gamma RI and Fc gamma RII on monocytes and granulocytes are cytotoxic trigger molecules for tumor cells. *J Immunol.* (1987) 139:3536–41.
21. Repp R, Valerius T, Sendler A, Gramatzki M, Iro H, Kalden JR, et al. Neutrophils express the high affinity receptor for IgG (Fc gamma RI, CD64) after *in vivo* application of recombinant human granulocyte colony-stimulating factor. *Blood.* (1991) 78:885–9. doi: 10.1182/blood.V78.4.885.885
22. Hokibara S, Kobayashi N, Kobayashi K, Shigemura T, Nagumo H, Takizawa M, et al. Markedly elevated CD64 expression on neutrophils and monocytes as a biomarker for diagnosis and therapy assessment in kawasaki disease. *Inflamm Res.* (2016) 65:579–85. doi: 10.1007/s00011-016-0942-1
23. Maertzdorf J, Repsilber D, Parida SK, Stanley K, Roberts T, Black G, et al. Human gene expression profiles of susceptibility and resistance in tuberculosis. *Genes Immun.* (2011) 12:15–22. doi: 10.1038/gene.2010.51
24. Jacobsen M, Repsilber D, Gutschmidt A, Neher A, Feldmann K, Mollenkopf HJ, et al. Candidate biomarkers for discrimination between infection and disease caused by *Mycobacterium tuberculosis*. *J Mol Med.* (2007) 85:613–21. doi: 10.1007/s00109-007-0157-6
25. Sutherland JS, Loxton AG, Haks MC, Kassa D, Ambrose L, Lee JS, et al. Differential gene expression of activating Fcgamma receptor classifies active tuberculosis regardless of human immunodeficiency virus status or ethnicity. *Clin Microbiol Infect.* (2014) 20:O230–8. doi: 10.1111/1469-0691.12383
26. Sambarey A, Devaprasad A, Mohan A, Ahmed A, Nayak S, Swaminathan S, et al. Unbiased identification of blood-based biomarkers for pulmonary tuberculosis by modeling and mining molecular interaction networks. *EBioMedicine.* (2017) 15:112–26. doi: 10.1016/j.ebiom.2016.12.009
27. Thompson EG, Shankar S, Gideon HP, Braun J, Valvo J, Skinner J, et al. Prospective discrimination of controllers from progressors early after low-dose *Mycobacterium tuberculosis* infection of cynomolgus macaques using blood RNA signatures. *J Infect Dis.* (2018) 217:1318–22. doi: 10.1093/infdis/jiy006

28. Warsinske H, Vashisht R, Khatri P. Host-response-based gene signatures for tuberculosis diagnosis: a systematic comparison of 16 signatures. *PLoS Med*. (2019) 16:e1002786. doi: 10.1371/journal.pmed.1002786
29. Kang DD, Lin Y, Moreno JR, Randall TD, Khader SA. Profiling early lung immune responses in the mouse model of tuberculosis. *PLoS ONE*. (2011) 6:e16161. doi: 10.1371/journal.pone.0016161
30. Nancy HJ, Das S. Neutrophil CD64, TLR2 and TLR4 expression increases but phagocytic potential decreases during tuberculosis. *Tuberculosis*. (2018) 111:135–42. doi: 10.1016/j.tube.2018.06.010
31. Nimmerjahn F, Ravetch JV. Fcgamma receptors as regulators of immune responses. *Nat Rev Immunol*. (2008) 8:34–47. doi: 10.1038/nri2206
32. Barrett T, Wilhite SE, Ledoux P, Evangelista C, Kim IF, Tomashevsky M, et al. NCBI GEO: archive for functional genomics data sets–update. *Nucleic Acids Res*. (2013) 41:D991–5. doi: 10.1093/nar/gks1193
33. Salamon H, Qiao Y, Cheng JC, Yamaguchi KD, Soteropoulos P, Weiden M, et al. Evidence for postinitiation regulation of mRNA biogenesis in tuberculosis. *J Immunol*. (2013) 190:2747–55. doi: 10.4049/jimmunol.1202185
34. Bloom CI, Graham CM, Berry MP, Rozakeas F, Redford PS, Wang Y, et al. Transcriptional blood signatures distinguish pulmonary tuberculosis, pulmonary sarcoidosis, pneumonias and lung cancers. *PLoS ONE*. (2013) 8:e70630. doi: 10.1371/annotation/7d9ec449-aee0-48fe-8111-0c110850c0c1
35. Snel B, Lehmann G, Bork P, Huynen MA. STRING: a web-server to retrieve and display the repeatedly occurring neighbourhood of a gene. *Nucleic Acids Res*. (2000) 28:3442–4. doi: 10.1093/nar/28.18.3442
36. Gentleman RC, Carey VJ, Bates DM, Bolstad B, Dettling M, Dudoit S, et al. Bioconductor: open software development for computational biology and bioinformatics. *Genome Biol*. (2004) 5:R80. doi: 10.1186/gb-2004-5-10-r80

Conflict of Interest: The authors declare that the research was conducted in the absence of any commercial or financial relationships that could be construed as a potential conflict of interest.

frontiers in Public Health

SYSTEMATIC REVIEW
published: 13 March 2020
doi: 10.3389/fpubh.2020.00076

Building the Evidence Base for the Prevention of Raw Milk-Acquired Brucellosis: A Systematic Review

*Shakirat A. Adetunji[1], Gilbert Ramirez[2], Allison R. Ficht[3], Ligia Perez[4], Margaret J. Foster[5] and Angela M. Arenas-Gamboa[1]**

[1] Department of Veterinary Pathobiology, Texas A&M University, College Station, TX, United States, [2] School of Public Health, Texas A&M University, College Station, TX, United States, [3] College of Medicine, Texas A&M University Health Science Center, Bryan, TX, United States, [4] Department of Student Life Studies, Texas A&M University, College Station, TX, United States, [5] Medical Sciences Library, Texas A&M University, College Station, TX, United States

OPEN ACCESS

Edited by:
Si-Yang Huang,
Yangzhou University, China

Reviewed by:
Ni Hong Bo,
Heilongjiang Bayi Agricultural University, China
Sascha Al Dahouk,
Federal Institute for Risk Assessment (BfR), Germany

***Correspondence:**
Angela M. Arenas-Gamboa
aarenas@cvm.tamu.edu

Specialty section:
This article was submitted to Infectious Diseases - Surveillance, Prevention and Treatment, a section of the journal Frontiers in Public Health

Received: 02 November 2019
Accepted: 25 February 2020
Published: 13 March 2020

Citation:
Adetunji SA, Ramirez G, Ficht AR, Perez L, Foster MJ and Arenas-Gamboa AM (2020) Building the Evidence Base for the Prevention of Raw Milk-Acquired Brucellosis: A Systematic Review. Front. Public Health 8:76. doi: 10.3389/fpubh.2020.00076

Background: The scientific evidence of the health risks associated with the consumption of raw milk has been known for a long time. However, less clear is the impact of acquiring infectious diseases from raw milk consumption in the United States (US) due to incomplete reporting of cases and the complex factors associated with the sale and consumption of raw milk. Investigations of this current study focused on human brucellosis, one of the infectious diseases commonly acquired through the consumption of raw milk and milk products, and which continues to be a public health threat worldwide.

Methodology: A qualitative systematic review of the sources of opinions that contribute to the increased trend of raw milk sales and consumption in the US was conducted.

Results: Interestingly, opinions about the sale of raw milk and/or the benefits arising from its consumption varied by US region, with the proportion of messages supporting raw milk consumption being highest in the Northeast compared to other US regions. Several evidence gaps and factors that possibly contribute to the increased prevalence of raw milk-acquired brucellosis were identified including inadequate monitoring of the raw milk sales process and lack of approved diagnostic methods for validating the safety of raw milk for human consumption.

Conclusions: The unavailability of data specifying brucellosis cases acquired from raw milk consumption have precluded the direct association between raw milk and increased brucellosis prevalence in the United States. Nevertheless, the evidence gaps identified in this study demonstrate the need for intensified surveillance of raw-milk acquired infectious diseases including human brucellosis; establishment of safety and quality control measures for the process of selling raw milk; and design of an effective strategy for the prevention of raw milk-acquired infectious diseases including brucellosis. Overall, for the first time, this study has not only shown the gaps in evidence that require future investigations, but also, variations in the perception of raw milk consumption that may impact disease acquisition in different US regions.

Keywords: brucellosis, evidence, gaps, raw milk, systematic review

INTRODUCTION

Brucellosis, one of the world's most common bacterial zoonosis, is an ancient disease that dates as far back as the 1800s (1–3). The discovery of the disease was by David Bruce, a military physician stationed in the island of Malta in the 1880s. During this period, Bruce noted the increased manifestation of a disease characterized by undulant fever and joint pains that debilitated many British soldiers. Autopsy of the deceased soldiers led to the recovery of the causative organism from the spleens, livers, and kidneys. To confirm that the recovered organism was the cause of the disease, Sir Bruce reproduced the infection in monkeys using bacterial cultures from the spleen of infected soldiers. A common practice at that time in Malta was the consumption of fresh raw goat milk (4). Raw goat milk was later confirmed to be the source of the bacteria, and the first consideration of brucellosis as a zoonosis arose from the isolation of its causative agent, *Brucella melitensis*, from goat milk (2, 3, 5). Subsequently, the prohibition of goat milk and cheese in military establishments led to a significant reduction of the disease incidence among the soldiers of Malta (2).

In the United States, brucellosis was reported as early as the 1900s where 29 cases of brucellosis (*B. melitensis*) were reported in Houston among Mexican immigrants that had consumed goat cheese before the onset of their symptoms. Additionally, between 1965 and 1978 in the US, over 3,000 cases of brucellosis were reported, and 4% of these cases were attributed to raw dairy products from Mexico, predominantly from the consumption of fresh cheese from unpasteurized goat milk (2, 6).

Although, brucellosis incidence has been attributed to varying factors, the consumption of unpasteurized dairy products accounts for a large number of cases, particularly in endemic countries such as Asia, Middle East, Africa, Central and South America (7–9). Further, in non-endemic countries, brucellosis has also been reported to occur after travel to, and consumption of raw dairy products in endemic countries (10).

In developed countries, the emerging interests in natural foods and products have led to the increased preference for raw milk consumption due to its acclaimed health benefits that are believed to be destroyed upon pasteurization (11, 12). Pasteurization, a process which dates back to the 1800s, involves the heating of raw milk to a defined temperature for a specific period of time to inactivate live, disease-causing organisms such as *Brucella*, *Salmonella*, *Listeria*, *Campylobacter*, *E. coli*, amongst others that pose significant health risk to consumers (13, 14). The process has been invaluable in the improvement of the safety of milk and other food products for human consumption. Another added advantage of pasteurization is that it destroys organisms that cause food spoilage, thereby increasing shelf-life and enhancing food security in low to middle income countries (11, 14–16). The presence of harmful pathogens in milk or dairy products can occur from either a direct passage from the animal, contamination of the expressed milk by animal excreta, or unsanitary handling of the milking process (13). For many years, several outbreaks of diseases resulting from the consumption of raw dairy products have been reported to the Centers for Disease Control and Prevention (CDC) (6, 15, 17–19). In recent times, at least three cases of human brucellosis have been confirmed by the CDC resulting from an exposure to the live-attenuated vaccine strain *Brucella abortus* RB51 following the consumption of raw milk (18, 19). In the most recent outbreak, it is believed that hundreds of persons in approximately 19 states may have been exposed in connection to the consumption of raw milk from a farm in Pennsylvania (19).

Interestingly, despite the significant public health risk that raw milk presents to consumers, the sale of raw milk for human consumption is not prohibited in all states in the US (11, 14, 20). Currently, 13 states allow raw milk to be sold in retail stores, 17 states allow raw milk to be sold only on farms where the milk is produced, 8 states allow raw milk to be obtained via the cow-share program (which involves the leasing of cows to obtain a percentage of a cow's milk production), while 21 states prohibit the sale of raw milk for human consumption (6). Interestingly, outbreaks of raw milk-related diseases including brucellosis have been reported mostly in states that legalize the sale of raw milk (11, 17, 19, 21, 22).

Previous studies have highlighted the varying motivations that drive raw milk consumers including consuming food items in their pure natural forms, better tastes and flavors, the belief that pasteurization destroys the natural components of milk, support of local farmers, and lack of trust of the state government as regards regulation of safe foods for consumption (16, 21, 23).

To date, scientific validation of the health benefits of consuming raw milk is very limited, and it has been extensively demonstrated that the health risks associated with the consumption of raw milk significantly outweigh the unfounded proclaimed health benefits (6, 21, 24, 25). Additionally, information exchanged via social media and networks have been shown to influence the attitudes and decisions of consumers (16, 21, 23, 26). Currently, there is a gap in knowledge about the variables by which consumers evaluate the information exchanged in their food safety and preference conversations, or how consumers perceive the varying recommendations regarding raw milk.

Despite the significant health risks posed by the consumption of unpasteurized milk and dairy products, there is still an increased trend in the purchase and consumption of raw milk (21), which may consequently lead to an increased prevalence of raw-milk acquired brucellosis as well as other diseases in the US. In order to design a more effective approach to educate consumers on the public health risks associated with this practice, the significance of the sources of information related to the purchase and consumption of raw milk and milk products must be critically evaluated to enhance or come up with an effective strategy in the control and prevention of raw milk-acquired brucellosis. Therefore, the objectives of this report are to identify the evidence gaps for future investigations that will facilitate informed policy decision about the sale and consumption of raw milk and milk products in the US, and to systematically review the sources of information that contribute to the increased trend of raw milk sale and consumption in the US, and associate the findings with the rising prevalence of raw milk-acquired brucellosis cases in the country. Results from this current study will facilitate efforts that are necessary to

enhance research into the development of innovative approaches to disseminate information about the dangers of raw milk consumption; intensify the surveillance of human brucellosis as a differential diagnosis to enable physicians to better control the disease; establish a quality control of the sales process; and highlight the significance of collecting and analyzing data about nation-wide raw milk sales, which will help to frame food safety policies for the benefit of the human population.

MATERIALS AND METHODS

Eligibility Criteria

To systematically review public opinions about the consumption of raw dairy products in the US, potential sources of public opinion including newspapers, magazines, and newsletters were searched using the EBSCO information services. The search was restricted to the US and a span years (2012 to 2017). Information sources expressing an opinion that was neutral, supportive or against the consumption of raw milk were included in the study. Peer-reviewed scientific publications, reports, or conference proceedings were excluded. The systematic review was conducted according to the Joanna Briggs Institute Critical Appraisal Tools for the systematic review of texts and opinions (27).

Search Strategy

Five databases were searched: Alt HealthWatch, Health Source—consumer edition magazines, Newspaper Source, Business Source Complete, and Academic Search. The searches included two concepts: raw or unpasteurized milk. The search was restricted to English Language reports and included all the states in the US and the Virgin Islands.

Screening

Citations were uploaded to Rayyan, an application designed for sorting citations. The titles were screened, and those that seemed relevant were added to RefWorks and the full-texts were reviewed.

Data Extraction

Equivalent information was extracted from all included reports. This information was comprised of the publication type; publishing regions [Federal Information Processing System (FIPS) 2015 codes were used to organize data by state and region/division]; the date, month, and year of publication; the category of opinions (supportive, against, or neutral); accessibility of information by the public (online, print, or both); and the frequency of publication (daily or monthly).

Theoretical and Analytical Frameworks

In order to identify evidence gaps and future research needs, theoretical and analytical frameworks were designed and subsequently used to guide this review. For the current study, theoretical framework represents an explanation of the factors related to the likelihood of raw-milk acquired brucellosis while analytical framework is the visual representation of the complex factors associated with the increased prevalence of raw milk-acquired brucellosis in the United States.

Analytic Framework of Direct and Indirect Measures

Google searches were used to identify direct and indirect measures of the elements identified in the analytical framework. Specifically, results were presented in a user-friendly format such as graphs and maps. Federal Information Processing System (FIPS) 2015 codes were used to organize data by state and region/division (28). FIPS grouped states into four regions with two or more divisions: Northeast (New England Division and Middle Atlantic Division); Midwest (East North Central Division and West North Central Division); South (South Atlantic Division, East South-Central Division, and West South-Central Division); and West (Mountain Division and Pacific Division). Maps were created using SPSS version 25.

Public opinions were coded as supportive, neutral, or against raw milk consumption. Within each state, an opinion message ratio was created by dividing the number of supportive/neutral messages within a state, by the total number of messages. Reported cases of brucellosis in the US (2012-2017) were obtained from the Centers for Disease Control and Prevention through the National Notifiable Diseases Surveillance System (NDSS).

Statistical Analysis

Statistical analyses including univariate and bivariate analyses, as well as Chi-Square tests were conducted using the STATA statistical software (STATA, STATACorp LP, College Station, Texas, USA).

RESULTS

Theoretical Framework

The theoretical framework that was used to guide this review is illustrated in **Figure 1**. We proposed that varying factors contribute to the prevalence of raw milk-acquired brucellosis. For example, raw milk sales promotion through advertisement and media advocacy could lead to the increased awareness of its availability for human consumption, as well as a surge in purchases, thereby leading to the increased prevalence of raw milk-acquired diseases such as brucellosis.

Study Characteristics

In this study, a total of 745 information sources were identified and analyzed for a qualitative systematic review. **Figure 2** details the process of screening and selection of opinion messages, which was performed according to the Preferred Reporting Items for Systematic Review and Meta-Analyses guidelines (PRISMA) (29).

One hundred and thirty-six opinion messages met the inclusion criteria, and they cut across 33 states including the District of Columbia. The publishing regions of the journals were grouped according to the US Census Bureau regional and divisional coding. The messages were coded (with respect to opinions about raw milk consumption) as "supportive (43/133)," "against (86/133)," or "neutral (4/133)" during the 6-year range 2012–2017 (each region or division was represented in the database with three cases of missing data for "state"). The majority of messages appeared in dual-format publications (print

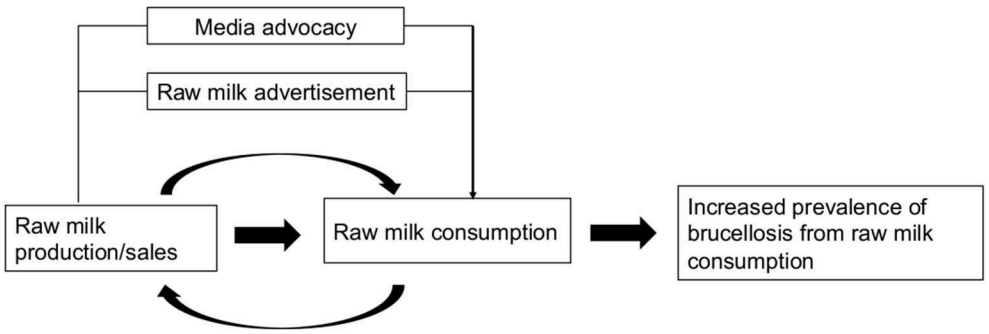

FIGURE 1 | Theoretical framework of the factors related to the likelihood of raw-milk acquired brucellosis. An increase in raw milk sales and promotion through media advocacy could lead to increased purchase and consumption, ultimately leading to an increase of prevalence of raw milk-acquired brucellosis.

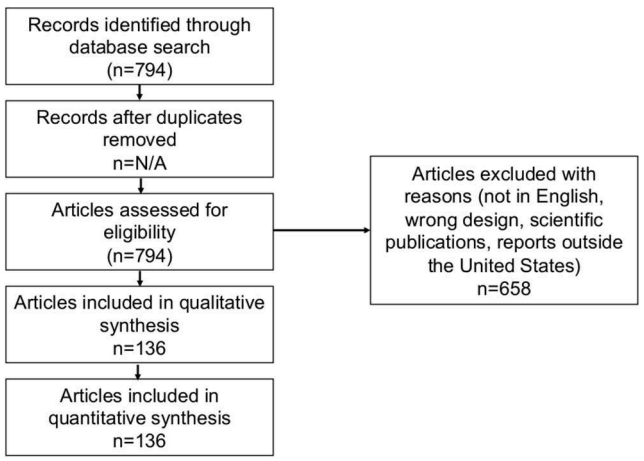

FIGURE 2 | PRISMA flow chart of the systematic review of public opinions about raw milk consumption in the United States.

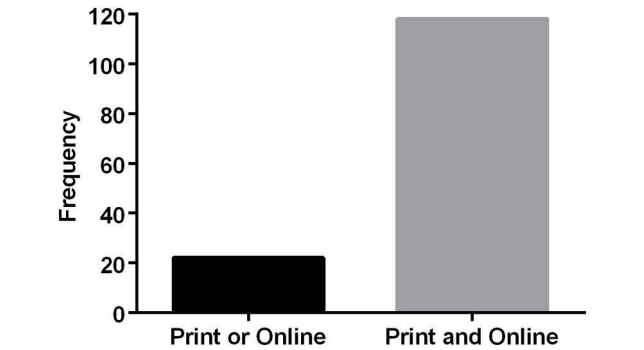

FIGURE 3 | Accessibility of the public to the varying information sources that support or are against the consumption of raw milk.

and online) (**Figure 3**), however we did not verify that within each of these dual-format publications any specific message did in fact appear in both formats. The vast majority (>80%) of publications had daily (sometimes twice a day) distributions with the remainder weekly, monthly, or quarterly. Most message authors contributed a message only once, and most publications also only contributed once.

Data Analyses

The Federal Information Processing System (FIPS) coding, which comprises four US Census Bureau Regions was used in this current study. Each region or division was represented in the database with two cases of missing data for "state." The (%) denotes the percentage representation of the 134 cases with state/FIPS identification, such that the sum of the division percentages within a region equal the region percentage (less rounding differences) (**Table 1**).

Bivariate Analyses of Groupings

To determine the distribution of opinion messages by US regions, bivariate analysis of groupings was used. Opinion messages that indicated a support for or indifference about raw milk consumption were categorized as "Supportive" or "Neutral", respectively, and those that were against raw milk consumption were categorized as "Against." The region with the highest percentage of "against" messages (of messages within the region) was the West (91.3%), followed by the Midwest (69.2%), South (56.0%), and the Northeast (52.2%); chi-square = 11.461, 3 df, $p = 0.009$. The West region had the highest milk production and, among West messages, the highest percentage of "against" messages, but had the lowest percentage of total messages observed (**Table 2**).

Univariate Analyses of Groupings

To determine the proportion of opinion messages that support or are against raw milk consumption, univariate analysis of groupings was used. Interestingly, the proportion of messages against raw milk consumption was higher than the messages that support it.

However, the proportion of supportive messages appeared to be higher than those of neutral (**Figure 4**), indicating the trend and preference for raw milk consumption. In an attempt to characterize the regional distribution of the opinion messages, the messages were grouped based on the FIPS divisional coding as previously stated. The number of opinion messages that

TABLE 1 | Regional/divisional analyses.

United States Regions	State FIPS code	Number of cases	Percentage of cases (%)	Milk production	
				Rank	Percentage (%)
Northeast		**46**	**34.3**	**3**	**14**
New England Division:		*16*	*11.9*	*8*	*2*
Connecticut	9	1	0.7	34	0.2
Maine	23	12	9	33	0.3
Massachusetts	25	1	0.7	39	0.1
New Hampshire	33	0	-	37	0.1
Rhode Island	44	0	-	49	0.01
Vermont	50	2	1.5	17	1.3
Middle Atlantic Division:		*30*	*22.4*	*4*	*12*
New Jersey	34	1	0.7	44	0.1
New York	36	12	9	4	6.8
Pennsylvania	42	17	12.7	5	5.2
Midwest		**40**	**29.9**	**2**	**35.2**
East North Central Division:		*29*	*21.6*	*1*	*24.3*
Indiana	18	1	0.7	14	1.9
Illinois	17	7	5.2	22	0.9
Michigan	26	2	1.5	7	4.9
Ohio	39	1	0.7	11	2.6
Wisconsin	55	18	13.4	2	13.9
West North Central Division:		*11*	*8.2*	*5*	*11*
Iowa	19	1	0.7	12	2.3
Kansas	20	0	-	16	1.5
Minnesota	27	6	4.5	8	4.5
Missouri	29	2	1.5	25	0.7
Nebraska	31	0	-	26	0.6
North Dakota	38	1	0.7	35	0.2
South Dakota	46	1	0.7	20	1.1
South		**25**	**18.7**	**4**	**10.6**
South Atlantic Division:		*17*	*12.7*	*7*	*4.1*
Delaware	10	0	-	46	0.1
D.C.	11	1	0.7	-	-
Florida	12	0	-	18	1.2
Georgia	13	1	0.7	23	0.9
Maryland	24	2	1.5	29	0.5
North Carolina	37	0	-	28	0.5
South Carolina	45	0	-	38	0.1
Virginia	51	0	-	24	0.9
West Virginia	54	13	9.7	42	0.1
East South-Central Division:		*1*	*0.7*	*9*	*1*
Alabama	1	0	-	45	0.1
Kentucky	21	0	-	27	0.5
Mississippi	28	1	0.7	41	0.1
Tennessee	47	0	-	30	0.4
West South-Central Division:		*7*	*5.2*	*6*	*5.4*
Arkansas	5	0	-	47	0.04
Louisiana	22	2	1.5	40	0.1
Oklahoma	40	1	0.7	31	0.4
Texas	46	4	3	6	4.9
West		**23**	**17.2**	**1**	**40.2**
Mountain Division:		*10*	*7.5*	*3*	*16.2*
Arizona	4	0	-	13	2.3
Colorado	8	1	0.7	15	1.8
Idaho	16	0	-	3	6.8
New Mexico	35	1	0.7	9	3.8
Montana	30	5	3.7	36	0.1
Utah	49	1	0.7	21	1.1
Nevada	32	1	0.7	32	0.3
Wyoming	56	1	0.7	43	0.1
Pacific Division:		*13*	*9.7*	*2*	*24*
Alaska	2	0	-	50	0
California	6	5	3.7	1	19.6
Hawaii	15	0	-	48	0.02
Oregon	41	4	3	19	1.2
Washington	53	4	3	10	3.2

The table denotes the number or percentage representation of the opinion messages included in the study [States (FIPS code) by Division (SPSS Code) by Region (SPSS Code)—not all states were represented in database]. Milk production was also ranked by states or regional division.

FIPS, Federal Information Processing Standard. The bold values represent the number of opinion messages per region; percentage of that per region; the rank of each region in milk production; and percentage of milk production per region.

advocated raw milk consumption were highest in the Northeast (**Figure 5**).

Confirmed Brucellosis Cases in the US

Consumption of raw milk can lead to the acquisition of diseases that significantly impact the health of consumers, including brucellosis. Unfortunately, data demonstrating the proportion of raw milk-acquired brucellosis in the US is unavailable. Therefore, it was not possible to use this in further data analyses in the current study. However, for graphical representation, we used the confirmed cases of human brucellosis provided by the CDC, which represented the total number of cases irrespective of the source of acquisition. We found that brucellosis was also mostly reported in the states that had a high proportion of opinion messages supporting raw milk consumption (**Figure 6**). However, other factors that possibly contribute to the prevalence of brucellosis in some US states including immigration and close proximity to brucellosis-endemic countries like Mexico were not examined in this study.

Analytical Framework

In summary, the current study has identified several evidence gaps and factors that can possibly contribute to the increased prevalence of raw milk-acquired infectious diseases such as brucellosis (**Figure 7**). One of the primary goals of this study was

TABLE 2 | CenRegion crosstabulation.

Percentage (%) within CenRegion		CenRegion				Total (%)
		Northeast (%)	Midwest (%)	South (%)	West (%)	
Opinion	Neutral or Supportive	47.8	30.8	44.0	8.7	35.3
	Against	52.2	69.2	56.0	91.3	64.7
Total	100.0	100.0	100.0	100.0	100.0	

	Value	*df*	Asymptotic significance (2-sided)
Chi-Square Tests			
Pearson chi-square	11.461[a]	3	0.009
Likelihood ratio	13.057	3	0.005
Linear-by-linear association	6.880	1	0.009
N of valid cases	133		

[a]*0 cells (0.0%) have expected count <5. The minimum expected count is 8.13.*

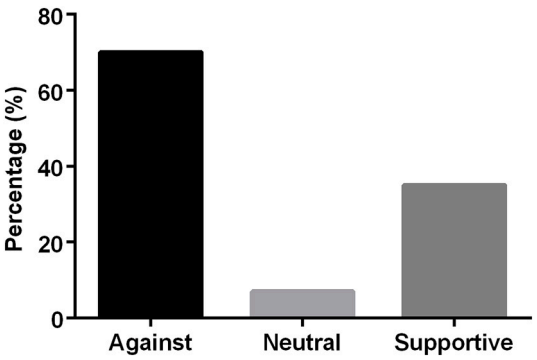

FIGURE 4 | Sources of information categorized based on varying reactions to the consumption of raw milk in the United States. The graph represents the percentage of messages that are against, neutral or in support of the consumption of raw milk.

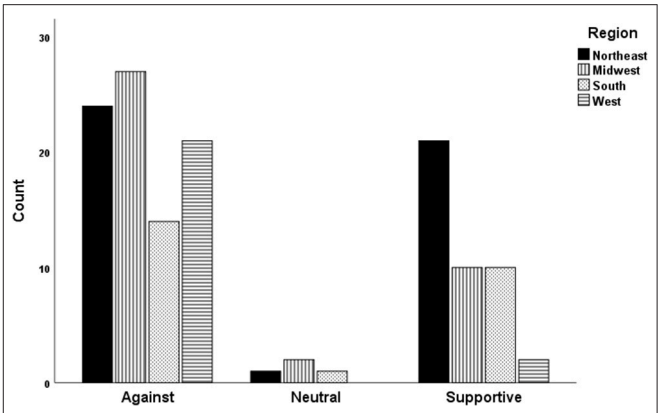

FIGURE 5 | Public opinions categorized based on varying reactions to raw milk consumption in the United States. Neutral or Supportive: The graph represents the number of publications that were indifferent about or advocated the consumption of raw milk. Media from the Northeast had the most promotion of raw milk consumption.

to correlate raw milk supportive messages with increased sales and purchases of raw milk as well as the increased prevalence of raw milk-acquired brucellosis in US regions. Unfortunately, the conclusions from this study have been limited by the inaccessibility of pertinent data such as an estimate of regional or national raw milk sales, demographics of consumers, and particularly, cases of human brucellosis resulting from raw milk consumption. Availability of these data will facilitate efforts to design an effective strategy for the prevention of raw milk-acquired brucellosis through the regulation of sales, increased awareness of disease risks associated with consumption, and the establishment of safety and quality control measures.

DISCUSSION

The scientific evidence of the health risks associated with the consumption of raw milk and products has been known for a long time (30, 31). However, less clear is the impact of acquiring infectious diseases including brucellosis from raw milk consumption in the US due to incomplete reporting of cases and the complex factors associated with the sale and consumption of raw milk, including inconsistent policies that range from total prohibition to legal sales in retail stores. One of the aims of this current study was to determine if increase in sales and consumption of raw milk in the US is directly associated with increased media advocacy and public opinions about the benefits of consuming raw milk. Interestingly, we found that the majority of public opinion published by newspapers and magazines in the Northeastern, Midwestern, Southern, and Western regions of the US were against the sale and consumption of raw milk due to the associated health risks. Hence, the rise in the trend of raw milk consumption may be a result of other factors such as the dissemination of misleading information that are neither evidence nor science-based on other social media networks like Facebook, Twitter, and other social interactive platforms. Previous studies have shown that discussions on these types of social platforms have severe implications in influencing consumer behaviors (32).

Another important finding in this current study was that majority of the media advocacy and public opinion in favor of raw milk consumption were published in the Northeast compared to other US regions. Why the Northeast had more favorable public opinion is not known, but it may be due to a stronger commitment of individuals in this US region to healthy local foods as indicated by Lovacore Index which ranks states based on the support of natural products or food (**Figure 6**). Additionally, the favorable raw milk regulations in the Northeast also facilitates the ease of access to raw milk via various means including availability in retail stores and farms where raw milk is produced (**Figure 6**). Moreover, media advocacy and public opinion were also accessible via both printed and online, making it possible to reach a larger audience. Therefore, efforts should be intensified for the adoption of media advocacy as well as social networks to increase awareness and educate the public about the disease risks associated with raw milk consumption. It is important to bear

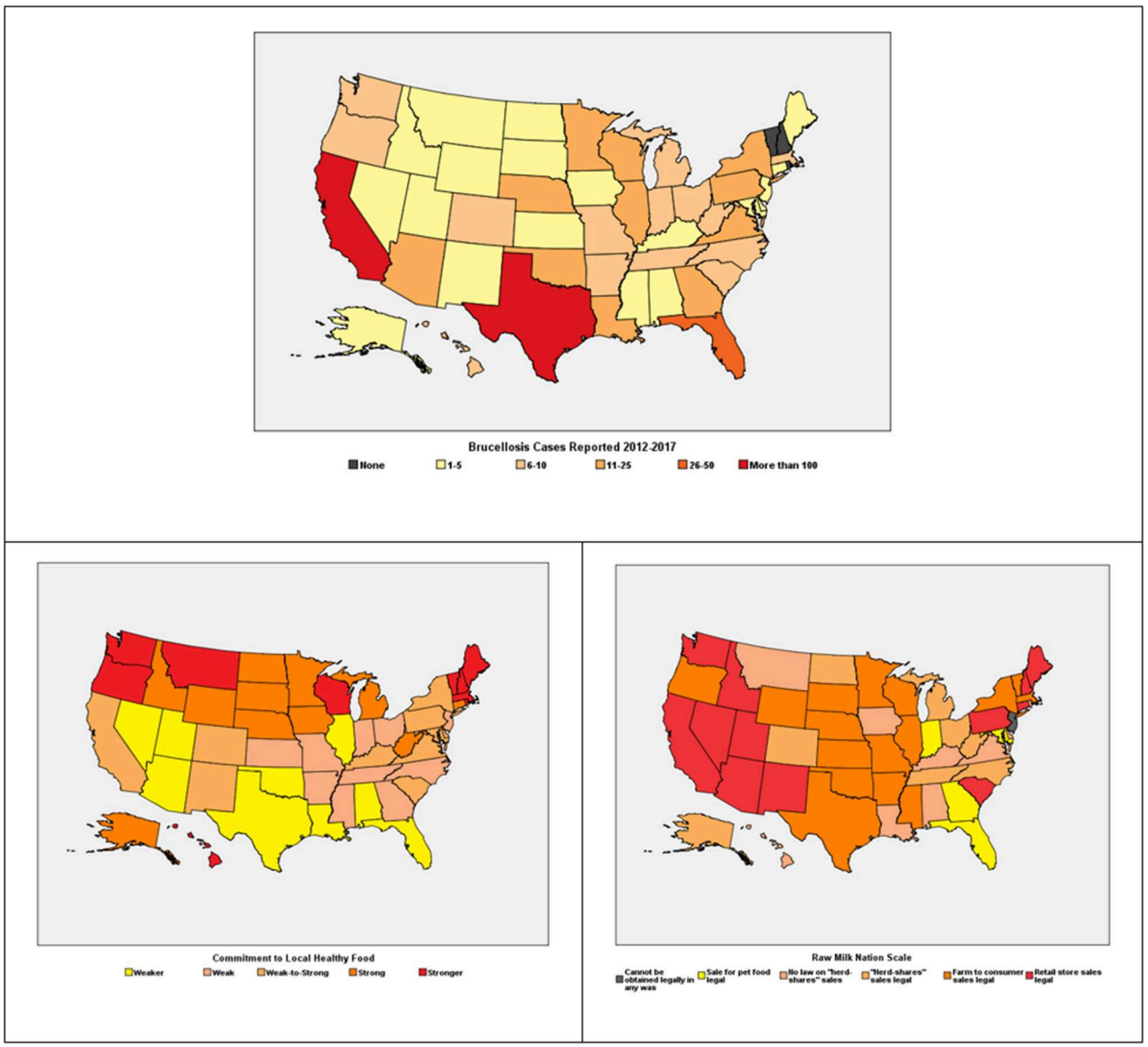

FIGURE 6 | Number of confirmed cases of brucellosis in the US reported to the CDC. Outbreak of raw milk related diseases including brucellosis have been reported mostly in states that permit the sale of raw milk. Lovacore Index—A measure of the commitment of individuals to local healthy food. Legal status of the sale of raw milk in the United States.

in mind that the more favorable public opinion in the Northeast does not directly correlate with increased incidence of brucellosis when compared to other regions like the southern states. A possible explanation for this might be the interplay of factors that contribute to disease incidence and prevalence in different regions including immigration and interaction with wild animals that serve as reservoir hosts.

What prompted the investigation of this current study were the recent increase in the number of confirmed human brucellosis cases resulting from the consumption of raw milk and products. Interestingly, human brucellosis is an almost nonexistent disease in the US, but endemic in countries where the consumption of raw milk is greatest and unregulated. Symptoms in infected individuals are non-specific and can include fever, sweats, arthralgia, myalgia, and in complicated cases, miscarriage or spontaneous abortion (1, 33–35). In this study, an attempt to directly correlate confirmed human brucellosis cases with the consumption of raw milk and products was impossible, which demonstrates a gap in evidence of unavailable data reporting human brucellosis acquired from raw milk consumption. Therefore, we cannot prove that raw milk consumption contributed to increased prevalence of brucellosis in the US. It is notable that apart from raw milk consumption, there are several other factors that increase the risk of acquisition of human brucellosis including occupations that allow direct contact with animals (e.g., veterinarians, butchers,

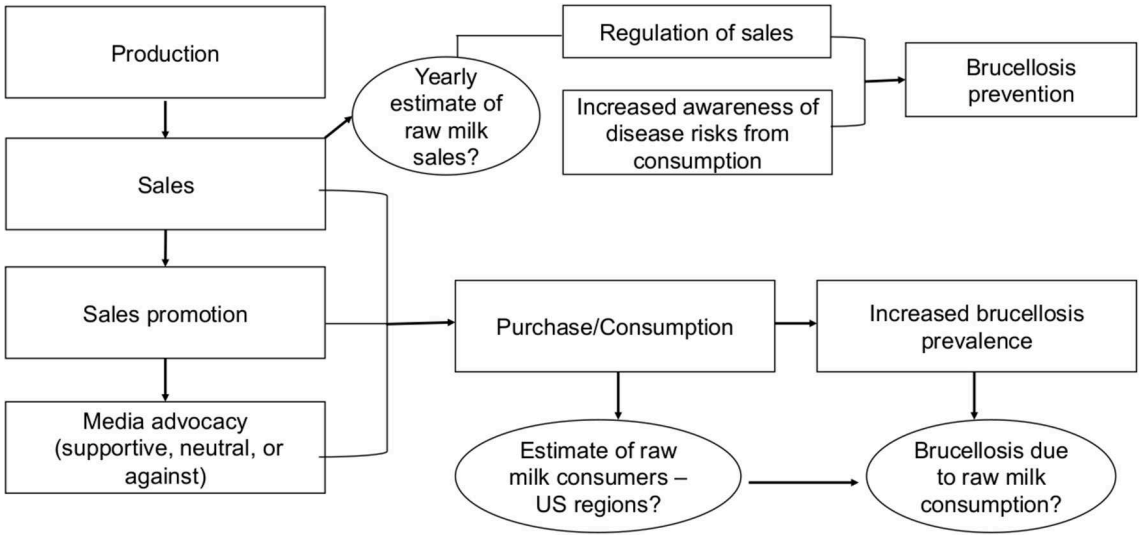

FIGURE 7 | An analytical framework is proposed for understanding the complex factors associated with the increased prevalence of raw milk-acquired brucellosis in the United States. The circles represent priority areas and gaps in evidence that require additional research to facilitate the establishment of the safety and quality control measures for the raw milk sales process, and also design an effective strategy for the prevention of raw milk-acquired brucellosis.

ranchers, animal care givers, etc.), laboratory personnel or research scientists that have direct exposure to animal samples, immigration, as well as feral swine hunting that results in species-specific infections. An important issue for future research is to unravel how raw milk consumption specifically contributes to the prevalence of brucellosis in the US. However, in endemic regions, raw milk consumption accounts for the most common cause of human brucellosis (36, 37). For this study, the number of brucellosis cases publicly provided by the CDC did not delineate the cases based on the source of infection. Therefore, the ease of access to cases of raw milk-acquired brucellosis is paramount to further generate effective brucellosis control and prevention strategies so as to avoid a backward trend of disease outbreaks due to raw milk consumption that occurred in the 1900s. Moreover, in order to reduce the incidence of raw milk-acquired brucellosis, several measures must be implemented including but not limited to promoting pasteurization, restricting the sale and access to raw milk, establishing rigorous quality control of the raw milk sale process, and the development of diagnostic tests for validating the safety of raw milk. This is crucial due to the fact that no diagnostic tests are available or approved for raw milk and milk products in the US or globally (US—Food and Drug Administration). Because of the current difficulty in restricting the sale of and access to raw milk, a better approach to limiting the associated disease risks may be an effective regulation of the quality of raw milk provided for human consumption, which will involve integrated efforts from veterinary services, regulations from the Federal Department of Agriculture (FDA), as well as effective training of physicians, farmers, ranchers, and consumers.

To facilitate informed policy decisions about restricting the sale and consumption of raw milk and products in the US, and ultimately reduce the risk of raw milk acquired diseases including brucellosis, an analytical framework was proposed (**Figure 7**). One of the research priority areas identified was the lack of regional or nation-wide data reporting the sales and purchases of raw milk in the US. This lack of raw milk sales data precluded the probable analyses and conclusions that may demonstrate the direct association of the magnitude of sales and purchases of raw milk with an increased brucellosis prevalence. We argue that data reporting the US regional or state-wide raw milk sales will help to establish the influence of the sales process on disease prevalence in the country. In addition, information about the purchases and demographics of raw milk consumers will help to further understand consumer attitude and behavior toward the consumption of raw milk, and also help to increase awareness about the potential risks of raw-milk acquired diseases. In other words, to formulate policies on the reduction of raw milk sales and distribution, the impact of raw milk production, sales promotion, consumer attitudes, and behavioral patterns must all be critically evaluated (12).

Additionally, we propose that raw milk sales promotion may influence consumer behavior and motivation by contributing to increased awareness of the availability of raw milk for purchases. Previous studies have shown that the purchase and consumption of raw milk are not restricted to a particular age group, income, education level of consumers, or distance to the place of purchase. In fact, in these studies, there was no association between these factors and raw milk consumption (21). Therefore, sales promotion, possibly through social media networks, likely presents a huge influence on consumer attitude and motivation for raw milk consumption.

The findings in this current study have demonstrated that media advocacy and public opinion possibly contribute to increased trend of raw milk consumption in different US regions, and that several factors might be involved in the prevalence of raw milk-acquired diseases like brucellosis. Additionally,

the evidence gaps identified in this study have provided a strong basis for future investigations and the development of effective strategies to alleviate the risks associated with raw milk-acquired infectious diseases including brucellosis. This will help to prevent outbreaks of human brucellosis in the US, which can have both direct and indirect implications including increased healthcare costs and potential threats to food safety and security due to the loss of livestock production. Evidence-informed health policies are most effective when guided by science, consumer preferences, and political reality. Hence, we strongly recommend an interdisciplinary approach and effort toward the building of the raw milk consumption evidence base.

DATA AVAILABILITY STATEMENT

All datasets generated for this study are included in the article/supplementary material.

AUTHOR CONTRIBUTIONS

SA, AF, GR, and AA-G: conceptualization. SA, MF, and GR: data curation. SA, GR, and LP: formal analysis. SA, GR, and AA-G: investigation. SA, GR, MF, and LP: methodology. SA, AF, MF, LP, and AA-G: resources. AA-G: supervision. SA, GR, and AA-G: writing—original draft. SA, AF, MF, LP, and AA-G: writing—review and editing.

FUNDING

This work was supported by National Institutes of Health (NIH) International Research Scientist Development Award (IRSDA/K01) (Award number: K01 TW009981-01). President's Excellence Funds (T3: Texas A&M Triads for Transformation), Texas A&M University, College Station, Texas, USA. The funders had no role in study design, data collection, and analysis, decision to publish, or preparation of the manuscript.

REFERENCES

1. Pappas G, Papadimitriou P, Akritidis N, Christou L, Tsianos EV. The new global map of human brucellosis. *Lancet Infect Dis*. (2006) 6:91–9. doi: 10.1016/S1473-3099(06)70382-6
2. Kiel FW, Khan MY. Brucellosis in Saudi Arabia. *Social Sci Med*. (1989) 29:999–1001.
3. Seleem MN, Boyle SM, Sriranganathan N. Brucellosis: a re-emerging zoonosis. *Vet Microbiol.* (2010) 140:392–8. doi: 10.1016/j.vetmic.2009.06.021
4. Christie A. Brucellosis, undulant fever, Malta or Mediterranean fever. In: Christ A, editor. *Infectious Disease: Epidemiology and Clinical Practice*. 3rd ed. London: Churchill Livingstone (1980). p. 824–47.
5. Bruce D. discoverer of brucellosis. *Singapore Med J.* (2011) 52:138.
6. Langer AJ, Ayers T, Grass J, Lynch M, Angulo FJ, Mahon BE. Nonpasteurized dairy products, disease outbreaks, and state laws—United States, 1993–2006. *Emerging Infect Dis*. (2012) 18:385. doi: 10.3201/eid1803.111370
7. Colmenero JD, Reguera J, Martos F, Sanchez-De-Mora D, Delgado M, Causse M, et al. Complications associated with *Brucella melitensis* infection: a study of 530 cases. *Medicine.* (1996) 75:195–211. doi: 10.1097/00005792-199607000-00003
8. Pourbagher A, Pourbagher MA, Savas L, Turunc T, Demiroglu YZ, Erol I. Epidemiologic, clinical, and imaging findings in brucellosis patients with osteoarticular involvement. *Am J Roentgenol.* (2006) 187:873–80. doi: 10.2214/AJR.05.1088
9. Guler S, Kokoglu OF, Ucmak H, Gul M, Ozden S, Ozkan F, et al. Human brucellosis in Turkey: different clinical presentations. *J Infect Dev Ctries.* (2014) 8:581–8. doi: 10.3855/jidc.3510
10. Al Dahouk S, Nöckler K, Hensel A, Tomaso H, Scholz HC, Hagen RM, et al. Human brucellosis in a nonendemic country: a report from Germany, 2002 and 2003. *European J Clin Microbiol Infect Dis.* (2005) 24:450–6. doi: 10.1007/s10096-005-1349-z
11. Buzby JC, Hannah GL, Kendall ME, Jones TF, Robinson T, Blayney DP. Characteristics of consumers of unpasteurized milk in the United States. *J Consumer Affairs.* (2013) 47:153–66. doi: 10.1111/joca.12001
12. Kearney J. 2010. Food consumption trends and drivers. *Philos Trans R Soc B Biol Sci.* (2010) 365:2793–807. doi: 10.1098/rstb.2010.0149
13. Oliver SP, Jayarao BM, Almeida RA. Foodborne pathogens in milk and the dairy farm environment: food safety and public health implications. *Foodbourne Pathog Dis*. (2005) 2:115–29. doi: 10.1089/fpd.2005.2.115
14. Angulo FJ, LeJeune JT, Rajala-Schultz PJ. Unpasteurized milk: a continued public health threat. *Clin Infect Dis*. (2009) 48:93–100. doi: 10.1086/595007
15. Headrick ML, Korangy S, Bean NH, Angulo FJ, Altekruse, SF, Potter ME, et al. The epidemiology of raw milk-associated foodborne disease outbreaks reported in the United States, 1973 through 1992. *Am J Public Health*. (1998) 88:1219–21. doi: 10.2105/AJPH.88.8.1219
16. Leamy RJ, Heiss SN, Roche E. The impact of consumer motivations and sources of information on unpasteurized milk consumption in Vermont, 2013. *Food Protect Trends.* (2013) 34:216–25.
17. Cossaboom, CM, Kharod GA, Salzer JS, Tiller RV, Campbell LP, Wu K, et al. Notes from the field: *Brucella abortus* vaccine strain RB51 infection and exposures associated with raw milk consumption—Wise County, Texas, 2017. *Morb Mortal Wkly Rep.* (2018) 67:286. doi: 10.15585/mmwr.mm6709a4
18. Sfeir MM. Raw milk intake: beware of emerging brucellosis. *J Med Microbiol.* (2018) 67:681–2. doi: 10.1099/jmm.0.000722
19. Negrón ME, Kharod GA, Bower WA, Walke H. Notes from the Field: Human *Brucella abortus* RB51 infections caused by consumption of unpasteurized domestic dairy products—United States, 2017–2019. *Morb Mortal Wkly Rep*. (2019) 68:185. doi: 10.15585/mmwr.mm6807a6
20. Steele JH. History, trends, and extent of pasteurization. *J Am Vet Med Assoc.* (2000) 217:175–8. doi: 10.2460/javma.2000.217.175
21. Katafiasz AR, Bartlett P. Motivation for unpasteurized milk consumption in Michigan, 2011. *Food Prot Trends*. (2012) 32:124–8.
22. Mungai EA, Behravesh CB, Gould LH. Increased outbreaks associated with nonpasteurized milk, United States, 2007–2012. *Emerg Infect Dis.* (2015) 21:119. doi: 10.3201/eid2101.140447
23. Rahn WM, Gollust SE, Tang X. Framing food policy: the case of raw milk. *Pol Stud J.* (2017) 45:359–83. doi: 10.1111/psj.12161
24. Alvarez VB, Parada-Rabell F. Health benefits, risk and regulations of raw and pasteurizes milk. *Factsheet Extension*. (2005) 3:5.
25. Potter ME, Kaufmann AF, Blake PA, Feldman RA. Unpasteurized milk: the hazards of a health fetish. *JAMA*. (1984) 252:2048–52.
26. Rogers EM. (1962). *Diffusion of Innovations.* New York, NY: Free Press.
27. McArthur A, Klugarova J, Yan H, Florescu S. Innovations in the systematic review of text and opinion. *Int J Evid Based Health*. (2015) 13:188–95. doi: 10.1097/XEB.0000000000000060
28. FIPS Codes. *United States Census and Bureau.* Available online atL https://www.census.gov/geographies/reference-files/2015/demo/popest/2015-fips.html
29. Moher D, Liberati A, Tetzlaff J, Altman DG. Preferred reporting items for systematic reviews and meta-analyses: the PRISMA statement. *Ann Internal Med.* (2009) 151:264–9. doi: 10.7326/0003-4819-151-4-200908180-00135
30. Abbas BA, Aldeewan AB. Occurrence and epidemiology of *Brucella* spp. in raw milk samples at Basrah province, Iraq. *Bulgarian J Vet Med.* (2009) 12:2.
31. Rijpens NP, Jannes G, Van Asbroeck MA, Rossau R, Herman LM. Direct detection of Brucella spp. in raw milk by PCR and reverse hybridization with 16S-23S rRNA spacer probes. *Appl Environ Microbiol.* (1996) 62:1683–8.

32. Schmidt AL, Zollo F, Scala A, Betsch C, Quattrociocchi W. Polarization of the vaccination debate on Facebook. *Vaccine.* (2018) 36:606–12. doi: 10.1016/j.vaccine.2018.05.040
33. Young EJ. An overview of human brucellosis. *Clin Infect Dis*. (1995) 21:283–9.
34. Khan MY, Mah MW, Memish, Z.A., 2001. Brucellosis in pregnant women. *Clin Infect Dis*. (2001) 32:1172–7. doi: 10.1086/319758
35. Arenas-Gamboa AM, Rossetti CA, Chaki SP, Garcia-Gonzalez DG, Adams LG, Ficht TA. Human brucellosis and adverse pregnancy outcomes. *Curr Trop Med Rep.* (2016) 3:164–72. doi: 10.1007/s40475-016-0092-0
36. Lulu AR, Araj GF, Khateeb MI, Mustafa MY, Yusuf AR, Fenech FF. Human brucellosis in Kuwait: a prospective study of 400 cases. *QJM*. (1988) 66:39–54.
37. Ramos JM, Bernal E, Esguevillas T, Lopez-Garcia P, Gaztambide MS, Gutierrez F. Non-imported brucellosis outbreak from unpasteurized raw milk in Moroccan immigrants in Spain. *Epidemiol Infect*. (2008) 136:1552–5. doi: 10.1017/S0950268807000210

Conflict of Interest: AF is a managing partner of NanoRelease Technologies (NRT), LLC Inc., has a 95% equity interest in NRT, a company involved in vaccine delivery platforms. The terms of this arrangement have been reviewed and approved by TXAgriLife Research and Texas A&M University in accordance with their conflict of interest policies.

The remaining authors declare that the research was conducted in the absence of any commercial or financial relationships that could be construed as a potential conflict of interest.

frontiers in Public Health

ORIGINAL RESEARCH
published: 17 March 2020
doi: 10.3389/fpubh.2020.00077

$CD19^{+}CD1d^{hi}CD5^{hi}$ B Cells Can Downregulate Malaria ITV Protection by IL-10 Secretion

*Hongli Guan, Jiacong Peng, Liping Jiang, Gang Mo, Xiang Li and Xiaohong Peng**

Department of Parasitology, Guilin Medical University, Guilin, China

Infection treatment vaccine (ITV) can lead to sterile protection against malaria infection in mice and humans. However, parasite breakthrough is frequently observed post-challenge. The mechanism of rapid decline in protection after the last immunization is unclear. Herein, C57BL/6 mice were immunized with 10^3, 10^5, or 10^7 ITV thice at 14-day intervals. Mice were challenged with 10^3 parasites at 1, 3, and 6 months after last immunization and the protection was checked using blood smear. The phenotypes of B cells were analyzed by flow cytometry. The levels of serum cytokines were quantified using cytometric bead array. The 10^3 ITV vaccination group exhibited 100% protection at 1 month after last immunization, and the 10^5 group showed sterile protection at 3 months after last immunization. However, the 10^7 group showed only partial protection. Further, the protection declined to 16.7% at 6 months after last immunization in 10^5 and 10^7 groups, whereas it maintained for more than 60% in 10^3 group. The number of memory B cells (MBC) decreased along with the decline in protection. However, programmed cell death protein 1 (PD-1) expressed on MBCs did not show significant variation among the three groups. Interestingly, $CD19^{+}CD1d^{hi}CD5^{hi}$ B cells, defined as B10 cells, exhibited negative regulation with respect to protection. The numbers of $CD19^{+}CD1d^{hi}CD5^{hi}$ B cells in the 10^3 group at 1 months and in the 10^5 group at 3 months post-immunization were the lowest compared to those in the other groups. Moreover, the serum levels of interleukin 10 (IL-10) in these two groups were also significantly lower than those in other groups. We conclude that higher immunization dose may not lead to better protection with the malaria vaccine as $CD19^{+}CD1d^{hi}CD5^{hi}$ B cells can downregulate ITV protection against malaria via IL-10 secretion. These results could facilitate the design of an effective long-lasting malaria vaccine with the aim of maintaining MBC function.

Keywords: Plasmodium, memory B cells, B10 cells, infection treatment vaccine (ITV), IL-10, malaria vaccine

OPEN ACCESS

Edited by:
Si-Yang Huang,
Yangzhou University, China

Reviewed by:
Marisa Silvia Castro,
Institute of Studies on Humoral Immunity (IDEHU), Argentina
Pedro Xavier-Elsas,
Federal University of Rio de Janeiro, Brazil

****Correspondence:***
Xiaohong Peng
pxh815@163.com

Specialty section:
This article was submitted to Infectious Diseases - Surveillance, Prevention and Treatment, a section of the journal Frontiers in Public Health

Received: *17 December 2019*
Accepted: *25 February 2020*
Published: *17 March 2020*

Citation:
Guan H, Peng J, Jiang L, Mo G, Li X and Peng X (2020) $CD19^{+}CD1d^{hi}CD5^{hi}$ B Cells Can Downregulate Malaria ITV Protection by IL-10 Secretion. Front. Public Health 8:77. doi: 10.3389/fpubh.2020.00077

INTRODUCTION

Malaria is still one of the three most important infectious diseases worldwide, resulting in 228 million clinical cases and 405,000 deaths in 2018, mostly in Africa in children under 5 years of age (1). The emergence and spread of insecticides and anti-malarial drug resistance (2) have posed severe challenges in the prevention and control of malaria. An effective and long-lasting malaria vaccine is urgently needed to eliminate this disease.

The blood stage of the malarial parasite life cycle is responsible for all the clinical symptoms of malaria (3). The goal of blood stage malaria vaccines is to inhibit the proliferation of intraerythrocytic malaria parasites, so as to control the symptoms of malaria and prevent the disease. The protection of blood stage malaria vaccines depends on acquisition of antibodies against parasite target antigens (4). However, maintaining the antibodies is still a bottleneck for effective vaccine design. Infrequent malaria infections can induce antigen-specific, long-lived antibody, and antigen-specific memory B cell (MBC) responses in a significant proportion of malaria-exposed individuals (5). The role of MBCs in the maintenance of protection conferred by the vaccine has also been confirmed in a mouse model (6). However, the protection conferred by blood stage vaccines is not sterile and quickly wanes if an individual leaves the endemic area (7). Therefore, inadequate maintenance of the function of long-term, effective malaria parasite-specific MBCs is an urgent problem that needs to be solved.

A malaria infection-treatment-vaccine (ITV) as anti-malaria drug prophylaxis is effective against the blood stage of Plasmodium (8). Human experiments have confirmed that ITV can induce sterile protection against homogeneous *Plasmodium falciparum*-infected mosquitoes, and this protection can last for approximately 2 years (9, 10). Related studies have shown that ITV immunization with an extremely low dose of the parasite (in cases where no parasitemia has been found in routine blood smears) can induce stronger protection than drug control after parasite infection (11). This indicates that low-dose immunization may confer better protection.

Over the past decade, a number of studies have demonstrated that regulatory B cells (Bregs) are crucial in the maintenance of immune tolerance and suppression of inflammation (12). B10 cells, a Breg subset, have been shown to limit immune response to pathogen infection via the release of interleukin-10 (IL-10) (13). $CD19^{+}CD1d^{hi}CD5^{hi}$ B cells are defined as B10 cells in mice (14–16) as well as $CD19^{+}CD24^{hi}CD38^{hi}$ B cells in humans (17). The number of B10 cells is significantly increased during acute infections resulting in decrease in inflammation (18). However, B10 cells are functionally impaired or their abundance is lower in autoimmune diseases or chronic infections (19–21). Thus, we speculate that high-dose *Plasmodium* immunization induces B10 cells to increase in number similar to that in acute infections, and subsequently accelerates the decline in protection.

In this study, we mainly explored the role of MBCs and B10 cells in immune dose-mediated long-term protection decline of malaria blood stage ITV, and clarified the role of PD-1 in MBC and B10-related cytokines in this process. This study will thus provide a new research direction to explore the mechanism of decline in long-term protection of ITV, and provide a theoretical basis for improving the long-term protection of malaria vaccine as well as for the design and application of a more effective vaccine.

METHODS

Mice and Malaria Parasite Strain

Female C57BL/6 mice and BALB/c mice were obtained from the Hunan Silaike Jingda Laboratory Animal Co. Ltd. All mice ranged in age from 6 to 8 weeks when the experiments were initiated. All mice were maintained in the experimental animal centers of Guilin Medical University. The lethal strain of *Plasmodium yoelii* 265 was originally obtained from the Department of Human Parasitology at Guilin Medical University and was maintained as cryopreserved stabilates. All animal studies were reviewed and approved by the Animal Ethics Committee of the Guilin Medical University Institute of Medical Research.

Vaccination

First, cryopreserved *P. yoelii 265* were thawed and 100 μL of this suspension was inoculated into mice by intraperitoneal (i.p.) injection. Four days later, the blood of infected mice was harvested by cardiac puncture and parasitemia was determined. Then, naïve mice were immunized thrice by intravenous (i.v.) injection with a 10^3, 10^5, or 10^7 dose of *P. yoelii* 265-infected red blood cells (Py-iRBCs) at 2-week intervals. All mice were then i.p. injected with 100 μL of 8 mg/mL chloroquine (CQ; Sigma-Aldrich, St. Louis, MO, USA) diluted in saline daily for 14 days, starting on the day of iRBC injection. The absence of parasites was confirmed by Giemsa-staining of blood smears from all treated mice since the beginning of CQ treatment.

Challenge

Before challenge, the absence of blood stage parasite infection was confirmed by Giemsa staining of thin blood smears. Mice were challenged with 10^3 Py-iRBCs by intravenous (i.v.) injection at 1, 3, and 6 months (mo) after the last immunization. Blood stage infection was examined daily from 3 days post-challenge to the days until parasitemia disappeared or the mice died. Parasitemia was calculated as the percentage of iRBCs.

Flow Cytometric Analysis

Spleens were collected at 1, 3, and 6 months after the last immunization, and splenocytes were prepared as described previously (8). Phenotypic analysis of lymphocytes was performed by flow cytometry. Cells were stained using fluorescein isothiocyanate (FITC)-conjugated anti-mouse CD19, PE-Cy5.5 anti-mouse-CD27, and phycoerythrin (PE)-conjugated anti-mouse-CD279 [also known as programmed cell death protein 1 (PD-1)] to detect the PD-1 expression on MBCs (**Figure 2A**). B10 cells were stained with FITC-conjugated anti-mouse CD19, PE-conjugated anti-mouse-CD5, and allophycocyanin (APC)-conjugated anti-mouse-CD1d. All antibodies were purchased from BioLegend.

Initially, 10^6 cells were resuspended in 50 μL fluorescence-activated cell sorting (FACS) buffer (phosphate-buffered saline (PBS) supplemented with 2% heat-inactivated fetal bovine serum (FBS); Gemini Bio-Products). Then, the mixture was incubated for 10–15 min at 4°C. Next, 50 μL of the 2X antibody cocktail was added to each tube (for the unstained sample, 50 μL of FACS buffer was added), vortexed gently or tapped to mix, and incubated at 4°C for 20–40 min in dark. Next, after washing with FACS buffer, 200 μL FACS buffer was added to resuspend the cells. The cells were analyzed using FACSCanto II instrument (BD Biosciences, San Jose, CA, USA), and the data were analyzed with FlowJo version 10 software.

Serum Cytokine Detection

The whole blood of mice was obtained by cardiopuncture before euthanization, and serum was harvested by centrifugation. The levels of the proinflammatory cytokines interleukin 6 (IL-6), monocyte chemoattractant protein-1 (MCP-1), interferon γ (IFN-γ), tumor necrosis factor α (TNF-α), IL-12p70, and the anti-inflammatory cytokine, IL-10, in serum samples were quantified using the cytometric bead array (CBA) Mouse Inflammation Kit (BD Biosciences), according to the manufacturer's instructions. Briefly, mouse inflammation standards were prepared with 2 mL of assay diluent, and by doubling the dilution to 1:2, 1:4, 1:8, 1:16, 1:32, 1:64, 1:128, 1:256, 1:512, and 1:1,024. Six mouse inflammation capture beads were mixed thoroughly. Next, 50 μL of mixed capture beads were incubated with the same volume of each mouse inflammation standard dilution or each sample. Then, 50 μL mouse inflammation PE detection reagent was added to all assay tubes and incubated for 2 h at room temperature, in dark. After washing with washing buffer, samples were analyzed on a FACSCanto II instrument (BD Biosciences), and the data were analyzed with FCAP Array version 3 software (22).

TABLE 1 | Protection against 10^3 *Plasmodium yoelii* 265-infected red blood cells (iRBC) challenge in infection treatment vaccine (ITV)-immunized mice of two strains—BALB/c and C57BL/6.

Mice	Immunogens	1 month	3 months	6 months
BALB/c	PBS	0% (0/5)	0% (0/5)	0% (0/5)
	10^5 ITV	100% (5/5)	100% (5/5)	80% (4/5)
C57BL/6	PBS	0% (0/5)	0% (0/5)	0% (0/5)
	10^5 ITV	100% (5/5)	40% (2/5)	20% (1/5)

Statistical Analysis

The data were analyzed using GraphPad Prism version 5 software. Non-parametric tests (Mann-Whitney test) and two-way analysis of variance (ANOVA) were used to compare groups, and $P < 0.05$ were considered statistically significant. Pearson correlation analysis was performed using SPSS 17.0.

RESULTS

C57BL/6 Mice Showed Quicker Protection Decline Than BALB/c Mice

First, we investigated the protection against *P. yoelii* challenge in different mice strains. C57BL/6 and BALB/c mice were immunized with 10^5 *P. yoelii* ITV and challenged with 10^3 homogeneous iRBC at 1, 3, and 6 months after the last immunization. As shown in **Table 1**, both C57BL/6 and BALB/c mice showed sterile protection against 10^3 iRBC challenge at 1 month. However, the protection quickly dropped to 40% in C57BL/6 mice at 3 months, whereas it was maintained in BALB/c mice. At 6 months, C57BL/6 mice only showed 20% protection compared to 80% in BALB/c mice.

Low Immunization Dose Group Gained Better Protection Than High-Dose Group

To explore the protection resulting from immune doses, we immunized groups of C57BL/6 mice with 10^3, 10^5, and 10^7 ITV and challenged them with 10^3 parasite iRBCs by i.v. injection at 1, 3, and 6 months after the last immunization (**Figure 1A**). Parasitemia was detected by thin blood film smear from 3 days post-challenge until the parasitemia disappeared or the mice died, and parasitemia was calculated as the percentage of

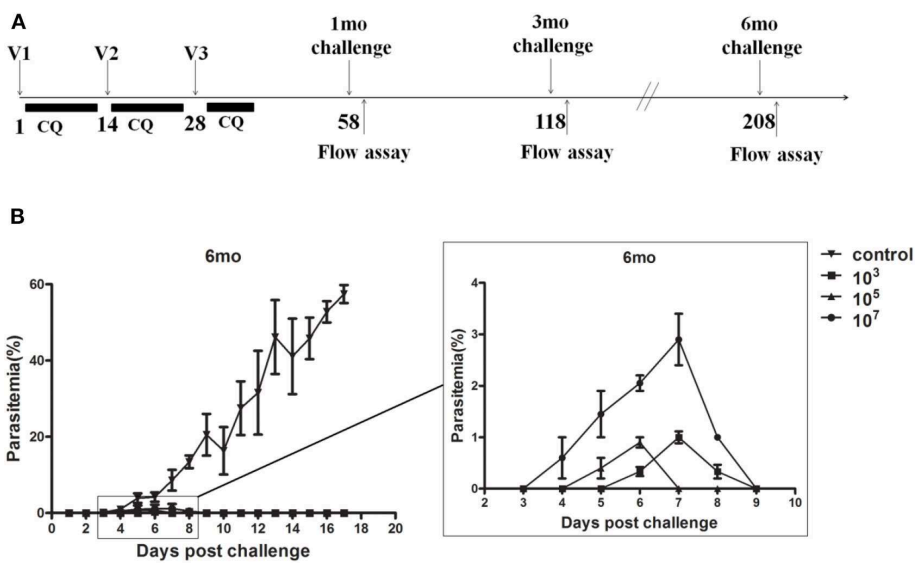

FIGURE 1 | (A) The procedure for ITV immunization and experiment operation. **(B)** Naive or immunized mice ($n = 5$) were challenged intravenously (i.v.) with 10^3 *Plasmodium yoelii* 265-infected red blood cells (iRBC) at 6 months. Parasitemia was recorded. The results are representative of two independent experiments. The Y-axis shows the percentage of erythrocytes infected with parasites, as determined by microscopy of Giemsa-stained thin blood smears, and the X-axis corresponds to days post-infection (p.i.). The data are presented as mean ± standard deviation (SD).

iRBCs. The protection rates and peak parasitemia of the three immunized groups at three different times were compared after a blood stage challenge, as depicted in **Table 2**.

Mice in the control group showed detectable blood stage parasitemia 4 days after challenge and died at 19–21 days post-challenge. However, in immunized groups, the infection started from 3 to 7 days post-challenge and lasted with low-dose parasitemia only for 3–6 days (**Figure 1B**). The peak parasitemia gradually increased over time in all three groups. Remarkably, the 10^7 group revealed the highest peak parasitemia compared to the other two lower dose groups. In addition, the 10^3 group gained sterile protection in the 1-month challenge, and maintained more than 60% protection for at least 6 months. However, the 10^5 and 10^7 immunized groups only exhibited 16.7% protection after 6 months (**Table 2**).

In other words, malaria blood stage ITV long-term protection of the 10^7 group was generally worse than that of the 10^3 and 10^5 groups, and the long-term protection of ITV decreased with the prolongation of immunization time.

TABLE 2 | Protection assay of different immunization dose groups.

Groups	% Protection (peak parasitemia*)		
	1 month ($n = 10$)	3 months ($n = 10$)	6 months ($n = 6$)
Control	0% (>60%)	0% (>60%)	0% (>60%)
10^3	100% (–)	60% (0.50%)	66.7% (1.00%)
10^5	60% (0.5%)	100% (–)	16.7% (0.90%)
10^7	20% (1.86%)	70% (2.50%)	16.7% (2.90%)

**C57BL/6 mice were immunized three times with 10^3, 10^5, or 10^7 ITV at 2-week intervals and were challenged with 10^3 parasite iRBCs by i.v. injection at 1, 3, and 6 months after last immunization. Peak parasitemia represents the highest parasitemia of challenged mice. Data of two independent experiments combined are exhibited.*

$CD19^+CD27^{mid}$ Memory B Cells Decreased With the Prolongation of Immunization Time

To characterize the protection resulting from immunization dose, we first observed the number of MBC variations in spleen. The results showed that the number of $CD19^+CD27^{mid}$ MBCs in the three experimental groups decreased gradually over time (**Figure 2B**). The number of MBCs in all three groups at 6 months was significantly lower than that at 3 months (10^3: $p = 0.0023$; 10^5: $p = 0.0007$; 10^7: $p = 0.001$), but the number of MBCs at 3

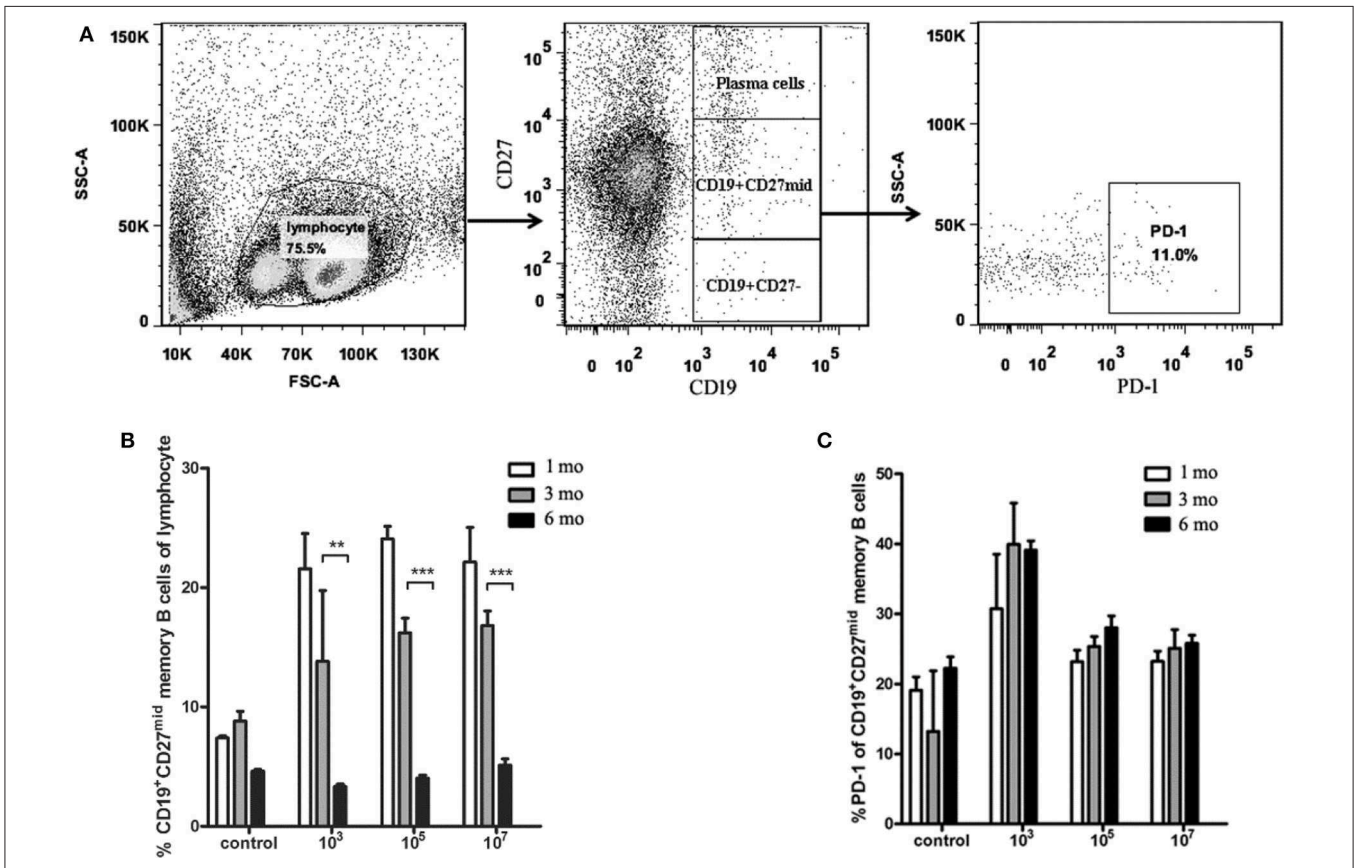

FIGURE 2 | The number of memory B cells and PD-1^+ memory B cells in the spleens of the ITV-immunized mice. **(A)** Gating strategy of PD-1^+ memory B cells. **(B)** The number of memory B cells declined with immunization time in each group. **(C)** PD-1^+ memory B cells exhibited no significant variation at different observation time points. Two individual experiments were performed and combined. The data are presented as mean ± SD. $^{**}p < 0.01$ and $^{***}p < 0.005$.

months was not significantly different from that at 1 month ($p > 0.05$). Next, we analyzed if PD-1 expressed on MBCs played a role in the difference in protection. We found no significant difference in PD-1 expression on $CD19^{+}CD27^{mid}$ MBCs in the three immunized groups at different times ($p > 0.05$; **Figure 2C**). This result indicated that the number of MBCs decreased with the prolongation of immunization time.

Low Immunization Dose Group Displayed Low Number of $CD19^{+}CD1d^{hi}CD5^{hi}$ B Cells During Sterile Protection Phase Compared With the High Immunization Dose Group

In order to explore whether the immune dose could affect the increase in B10 cell abundance, splenocytes were collected and the number of $CD19^{+}CD1d^{hi}CD5^{hi}$ B cells was counted by flow cytometry. The results showed that at 1 month, the number of B10 cells of ITV-immunized mice in 10^3 and 10^5 groups was significantly lower than that in the control group (10^3: $p = 0.0497$, 10^5: $p = 0.0232$), and that in the 10^7 group was significantly higher than that in the 10^3 ($p = 0.0471$), and 10^5 ($p = 0.0128$) groups (**Figure 3**). This was in accordance with the protection assay at 1 month. At 3 months, the number of B10 cells in 10^5 group was significantly lower than that in control ($p = 0.0275$), 10^3 ($p = 0.0075$), and 10^7 groups ($p = 0.0071$).

The results showed that the immunized group with the best protective effect expressed the lowest number of B10 cells. This suggests that the expansion of B10 cells in ITV-immunized mice may result in reduced long-term protective efficacy of ITV.

The Amount of IL-10 in Mouse Serum Was Positively Correlated With the Number of B10 Cells, Whereas the Amounts of IL-6 and IFN-γ Were Negatively Correlated With the Amount of IL-10

Considering the important role of cytokines in the immunosuppressive effects of B10 cells (23–25), cytokine

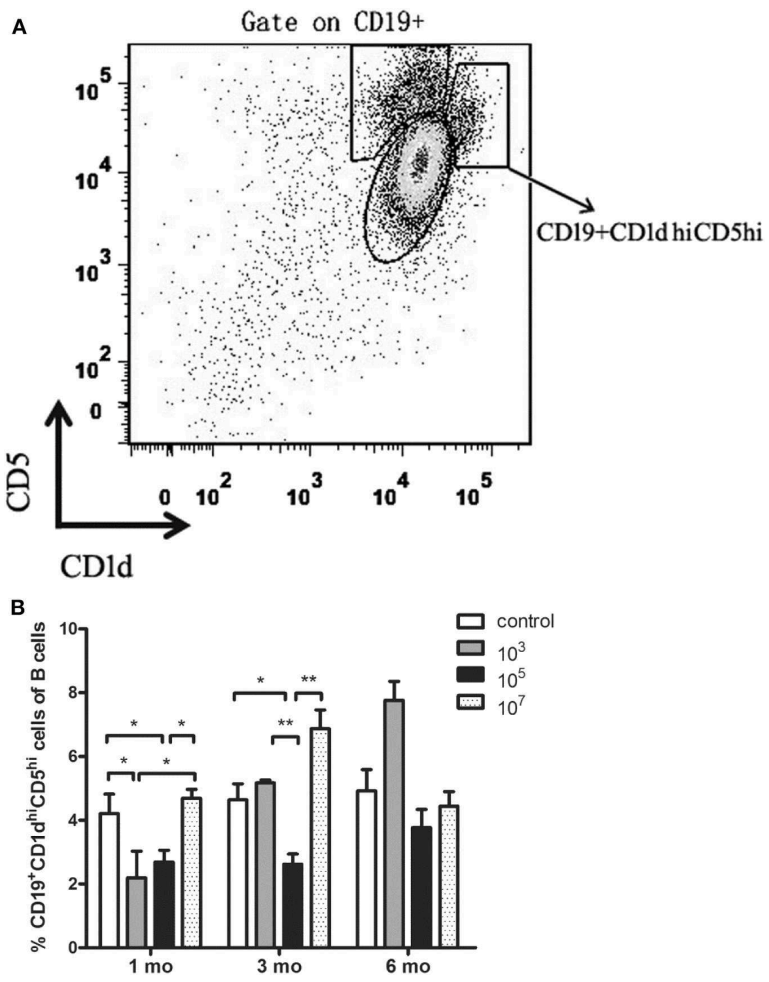

FIGURE 3 | (A) Gating strategy of $CD19^{+}CD1d^{hi}CD5^{hi}$ B cells. **(B)** Statistical analysis of the total number of $CD19^{+}CD1d^{hi}CD5^{hi}$ B cells in the spleen from ITV-immunized mice at 1, 3, and 6 months after the last immunization. Data from two independent experiments combined is exhibited. The data are presented as mean ± SD. $^{*}p < 0.05$ and $^{**}p < 0.01$.

levels in serum were investigated. The concentrations of IL-6, MCP-1, IFN-γ, TNF-α, IL-12p70, and IL-10 in serum were measured by CBA. As shown in **Figure 4**, the level of IL-10 in the control group was significantly higher than that in the three immunized groups, especially at 1 month (10^7: $p = 0.0029$). The level of IL-10 in the 10^5 group was lower than that in the 10^3 ($p = 0.0155$) and 10^7 groups ($p = 0.0022$) at 3 months. However, no significant variation was found among the three experimental groups at 6 months. Therefore, Pearson correlation analysis showed that the level of IL-10 was proportional to the number of B10 cells ($r = 0.41$, $p = 0.015$). Interestingly, the amount of IL-6 was inversely proportional to the amount of IL- 10 ($r = -0.626$, $p < 0.001$). At 1 and 3 months, the amount of IL- 6 in the control group was significantly lower than that in the three experimental groups. The level of IL-6 in the 10^3 group was higher than that in the control ($p = 0.0053$) and 10^7 ($p = 0.0236$) groups at 1 month. Meanwhile, the 10^5 group exhibited higher IL-6 levels than the 10^3 ($p = 0.0051$) and 10^7 ($p = 0.0052$) groups at 3 months. No significant difference was found at 6 months among all the four groups.

In addition, the level of IFN-γ was also inversely proportional to the level of IL-10 ($r = -0.638$, $p < 0.001$). The level of IFN-γ in the control group was significantly lower than that in 10^3 group ($p = 0.011$) as well as other immunized groups at 1 month. Although no significant difference was found among three immunized groups at different time points, 10^5 group tended to express higher IFN-γ level than other three groups at 3 months. The levels of TNF-α, MCP-1, and IL-12p70, which could be negatively regulated by IL-10 (26–28), were not significantly correlated with the level of IL-10.

Taken together, the amount of IL-10 in mouse serum was positively correlated with the number of B10 cells, whereas the amount of IL-6 and IFN-γ was negatively correlated with the amount of IL-10. Thus, these data suggest that increased level of IL-10 may lead to decline in protection. The role of IL-6 and IFN-γ in this process needs to be verified by further experiments.

DISCUSSION

All clinical symptoms of malaria mainly occur due to the blood phase of the malaria parasite life cycle (3). Therefore, the goal

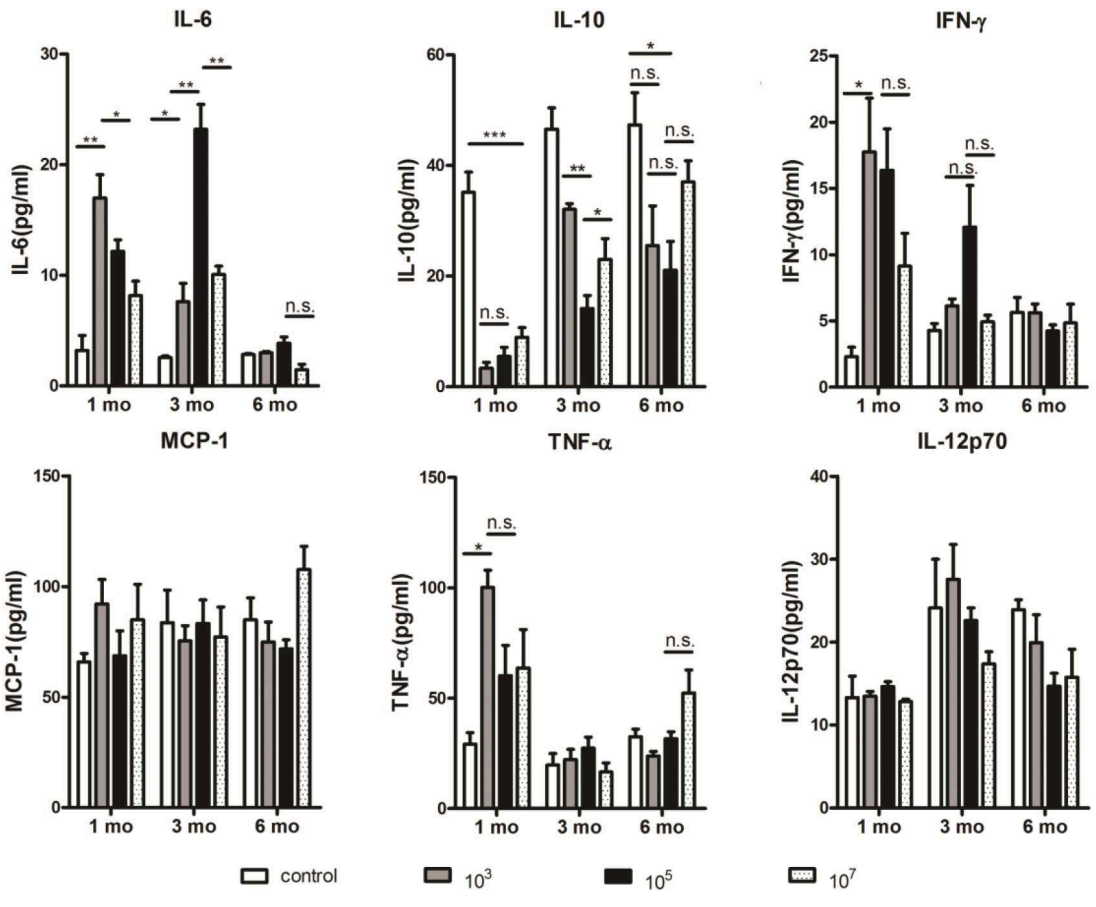

FIGURE 4 | At 1 and 3 months, the amount of IL-10 in the 10^3 and 10^5 groups was the lowest, respectively. Serum samples were collected from immunized mice at the indicated time points after the final immunization and the concentrations of cytokines were measured serially by a cytometric bead array (CBA). Two individual experiments were performed. The data are presented as the mean ± SD. Data were compared with the two-way analysis of variance (ANOVA). *$p < 0.05$, **$p < 0.01$, ***$p < 0.005$, and n.s., not significant.

of blood stage malaria vaccines is to inhibit the proliferation of intraerythrocytic malaria parasites so as to control the symptoms of malaria and prevent the disease. However, there is still no effective malaria vaccine for humans because the protection of blood stage vaccine is not sterile and wanes quickly; moreover, there may be a risk of malaria parasite infection caused by the vaccine (29). Thus, exploring the mechanism of long-term protection decline of malaria vaccine will be helpful for designing a more effective malaria vaccine. Our previous results have shown that the long-term protective efficacy of malaria vaccine in the low immunization dose group was better than that in the high immunization dose group (30). Previous studies have shown that ITV immunized at an extremely low dose of the parasite can induce stronger protection than high doses (11). Therefore, it was unclear whether the immunization dose also affects the long-term protection of the blood stage malaria vaccine.

Herein, we explored the influence of immune dose on Plasmodium ITV protection longevity. C57BL/6 mice are more sensitive to *P. yoelii* than other mouse strains. Theoretically, they could generate more antigens than other mouse stains. However, our experiment found that ITV-immunized C57BL/6 mice have a quicker protective decline than BALB/c mice (**Table 1**). Thus, C57BL/6 mice were chosen for further dosage associate investigation. C57BL/6 mice were immunized with different doses of parasites and were challenged at 1, 3, or 6 months post-immunization. Although immunization with different dosages conferred partial protection against the challenge, variations in protection were observed. The highest immunization dose, the 10^7 group, showed the highest peak parasitemia and lowest protection rate at all three challenge phases (**Table 1**, **Figure 1B**). However, it is challenging to compare the 10^3 and 10^5 groups because the 10^3 group showed sterile protection at 1 month, whereas the 10^5 group exhibited 100% protection at 3 months. Nevertheless, the 10^5 group had a lower protection rate than the 10^3 group at 6 months. These results indicated that the immunization dose could mediate the long-term protection of malaria ITV in C57BL/6 mice, and that a higher immunization dose could not exert a better long-term protective effect.

Studies have found that splenic MBCs played the most important role in the immune protection induced by Plasmodium blood stage ITV vaccine. The number of malaria parasite-specific MBCs is proportional to the immune protection of the host, and decrease of the number of specific MBCs leads to decrease in immune protection (5). Our results also showed that with the increase in immunization time, the number of MBCs decreased gradually in all the three immunization groups. Therefore, the regression of ITV long-term protection may be related to the decrease in the number of MBCs of mice with an increase in immunization time.

B10 cells, a small subset of $CD19^+CD24^{hi}CD38^{hi}$ B cells as well as $CD19^+CD1d^{hi}CD5^{hi}$ B cells in mice, are an immunosuppressive B cell type that stop the expansion of pathogenic, proinflammatory lymphocytes and play a significant role in suppressing autoimmune responses and preventing autoimmunity through the secretion of IL-10, IL-35, and transforming growth factor β (TGF-β) (31). Previous studies have shown that the number of B10 cells is significantly increased during acute infection, resulting in decreased inflammation (18). However, B10 cells are functionally impaired or their abundance is decreased in autoimmune disease or chronic infection (19–21). Therefore, we hypothesize that high-dose *Plasmodium* immunization could induce B10 cells to increase in number and subsequently mediate a decline in protection. Our results showed that the number of B10 cells in the 10^3 and 10^5 group mice was the lowest at 1 and 3 months, respectively. This was in accordance with the protection results. The number of B10 cells in the 10^7 group was higher than that in the 10^5 and 10^3 groups at 1 and 3 months, respectively, after the last immunization. Meanwhile, the number of B10 cells in the 10^3 and 10^5 groups at 6 months was higher than that at 1 and 3 months. This confirmed that B10 cells could downregulate the long-term protection conferred by ITV. Therefore, it can be concluded that worse ITV long-term protection mediated by high immunization dose is related to an increase in the number of B10 cells in the mouse spleen.

A previous study indicated that the main mechanism of the inhibitory action of B10 cells is IL-10 production (32). In addition, some studies indicate that increased IL-10 levels are accompanied by decreased levels of other cytokines, such as IL-6 and IFN-γ (33, 34). Our results thus show that the amount of IL-10 in the 10^3 and 10^5 groups of mice was the lowest at 1 and 3 months, respectively. This correlated with the number of B10 cells. On the contrary, the amount of IL-6 and IFN-γ of the 10^3 and 10^5 groups was the highest at 1 and 3 months, respectively. This was negatively correlated with the amount of IL-10. Therefore, an increased level of IL-10 secreted by B10 cells may lead to a decline of long-term protection by malaria ITV. However, the role of IL-6 and IFN- γ in this process needs to be verified by further experiments.

In conclusion, we demonstrated that the immunization dose could mediate the long-term protection of Plasmodium blood stage ITV in C57BL/6 mice, and that a higher immunization dose could not produce a better long-term protective effect. The long-term protection of ITV was shown to be related to the increase in the number of $CD19^+CD1d^{hi}CD5^{hi}$ B (B10) cells, which may negatively regulate the long-term protective effect of malaria ITV by secreting IL-10. In addition, the decrease in long-term protection of ITV may be related to the decline of MBCs in the spleen of mice with an increase in immunization time. Our study thus elucidates the mechanism of high immunization doses inhibiting long-term immunity protection in a model of long-term protection decline of malaria blood stage ITV mediated by the immunization dose due to the regulatory role of B10 cells, thus providing a theoretical basis for the design of malaria vaccine.

DATA AVAILABILITY STATEMENT

All datasets generated for this study are included in the article/supplementary material.

ETHICS STATEMENT

This animal study was reviewed and approved by Animal Ethics Committee of the Guilin Medical University Institute of Medical Research.

AUTHOR CONTRIBUTIONS

HG, JP, and XL performed this study. HG analyzed the data. LJ collected samples. GM provided technical support. XP designed this work, supervised this study, and final revised the manuscript. HG drafted the work. JP, XL, LJ, and GM revised the work. All of the authors listed have approved the final version for published and agreed to be accountable for all aspects of the work in ensuring that questions related to the accuracy or integrity of any part of the work are appropriately investigated and resolved.

FUNDING

This work was supported by Guangxi Natural Science Foundation (Nos. 2017GXNSFAA198229 and AD18281029), Innovation Project of Guangxi Graduate Education (YCSW2019212), and National undergraduate training program for innovation and entrepreneurship (201710601030).

REFERENCES

1. World Health Organization. *World Malaria Report 2019*. WHO Global Malaria Programme (2019). Available online at: https://www.who.int/malaria/publications/world-malaria-report-2019/en/
2. Ashley EA, Dhorda M, Fairhurst RM, Amaratunga C, Lim P, Suon S, et al. Spread of artemisinin resistance in Plasmodium falciparum malaria. *N Engl J Med.* (2014) 371:411–23. doi: 10.1056/NEJMoa1314981
3. Vijayan A, Chitnis CE. Development of blood stage malaria vaccines. *Methods Mol Biol.* (2019) 2013:199–218. doi: 10.1007/978-1-4939-9550-9_15
4. Teo A, Feng G, Brown GV, Beeson JG, Rogerson SJ. Functional antibodies and protection against blood-stage malaria. *Trends Parasitol.* (2016) 32:887–98. doi: 10.1016/j.pt.2016.07.003
5. Wipasa J, Suphavilai C, Okell LC, Cook J, Corran PH, Thaikla K, et al. Long-lived antibody and B Cell memory responses to the human malaria parasites, *Plasmodium falciparum* and *Plasmodium vivax*. *PLoS Pathog.* (2010) 6:e1000770. doi: 10.1371/journal.ppat.1000770
6. Stephens R, Albano FR, Quin S, Pascal BJ, Harrison V, Stockinger B, et al. Malaria-specific transgenic CD4(+) T cells protect immunodeficient mice from lethal infection and demonstrate requirement for a protective threshold of antibody production for parasite clearance. *Blood.* (2005) 106:1676–84. doi: 10.1182/blood-2004-10-4047
7. Mura M, Ruffie C, Combredet C, Aliprandini E, Formaglio P, Chitnis CE, et al. Recombinant measles vaccine expressing malaria antigens induces long-term memory and protection in mice. *NPJ Vaccines.* (2019) 4:12. doi: 10.1038/s41541-019-0106-8
8. Liu T, Lu X, Zhao C, Fu X, Zhao T, Xu W. PD-1 deficiency enhances humoral immunity of malaria infection treatment vaccine. *Infect Immun.* (2015) 83:2011–7. doi: 10.1128/IAI.02621-14
9. Meta Roestenberg MD, Matthew McCall MD, Joost Hopman MD. Protection against a malaria challenge by sporozoite inoculation. *N Engl J Med.* (2009) 361:468–77. doi: 10.1056/nejmoa0805832
10. Roestenberg M, Teirlinck AC, McCall MB, Teelen K, Makamdop KN, Wiersma J, et al. Long-term protection against malaria after experimental sporozoite inoculation: an open-label follow-up study. *Lancet.* (2011) 377:1770–76. doi: 10.1016/S0140-6736(11)60360-7
11. Elliott SR, Kuns RD, Good MF. Heterologous immunity in the absence of variant-specific antibodies after exposure to subpatent infection with blood-stage malaria. *Infect Immun.* (2005) 73:2478–85. doi: 10.1128/IAI.73.4.2478-2485.2005
12. Mauri C, Menon M. Human regulatory B cells in health and disease: therapeutic potential. *J Clin Invest.* (2017) 127:772–79. doi: 10.1172/JCI85113
13. Neves P, Lampropoulou V, Calderon-Gomez E, Roch T, Stervbo U, Shen P, et al. Signaling via the MyD88 adaptor protein in B cells suppresses protective immunity during salmonella typhimurium infection. *Immunity.* (2010) 33:777–90. doi: 10.1016/j.immuni.2010.10.016
14. DiLillo DJ, Matsushita T, Tedder TF. B10 cells and regulatory B cells balance immune responses during inflammation, autoimmunity, and cancer. *Ann N Y Acad Sci.* (2010) 1183:38–57. doi: 10.1111/j.1749-6632.2009.05137.x
15. Zhu HQ, Xu RC, Chen YY, Yuan HJ, Cao H, Zhao XQ, et al. Impaired function of CD19(+) CD24(hi) CD38(hi) regulatory B cells in patients with pemphigus. *Br J Dermatol.* (2015) 172:101–10. doi: 10.1111/bjd.13192
16. Sheng JR, Rezania K, Soliven B. Impaired regulatory B cells in myasthenia gravis. *J Neuroimmunol.* (2016) 297:38–45. doi: 10.1016/j.jneuroim.2016.05.004
17. Menon M, Rosser EC, Mauri C. Identification and isolation of regulatory B cells in mouse and human. *Methods Mol Biol.* (2019) 1899:55–66. doi: 10.1007/978-1-4939-8938-6_5
18. Zhao MQ, Wang LH, Lian GW, Lin ZF, Li YH, Guo M, et al. Characterization of lymphocyte subsets in peripheral blood cells of children with EV71 infection. *J Microbiol Immunol Infect.* (2019). doi: 10.1016/j.jmii.2019.03.001. [Epub ahead of print].
19. Blair PA, Norena LY, Flores-Borja F, Rawlings DJ, Isenberg DA, Ehrenstein MR, et al. CD19+CD24hiCD38hi B cells exhibit regulatory capacity in healthy individuals but are functionally impaired in systemic lupus erythematosus patients. *Immunity.* (2010) 32:129–40. doi: 10.1016/j.immuni.2009.11.009
20. Staun-Ram E, Miller A. Effector and regulatory B cells in multiple sclerosis. *Clin Immunol.* (2017) 184:11–25. doi: 10.1016/j.clim.2017.04.014
21. Busse M, Campe KJ, Nowak D, Schumacher A, Plenagl S, Langwisch S, et al. IL-10 producing B cells rescue mouse fetuses from inflammation-driven fetal death and are able to modulate T cell immune responses. *Sci Rep.* (2019) 9:9335. doi: 10.1038/s41598-019-45860-2
22. Liu T, Cheng X, Ding Y, Zhu F, Fu Y, Peng X, et al. PD-1 deficiency promotes TFH cells expansion in ITV-immunized mice by upregulating cytokines secretion. *Parasit Vectors.* (2018) 11:397. doi: 10.1186/s13071-018-2984-4
23. Yanaba K, Bouaziz JD, Matsushita T, Tsubata T, Tedder TF. The development and function of regulatory B cells expressing IL-10 (B10 cells) requires antigen receptor diversity and TLR signals. *J Immunol.* (2009) 182:7459–72. doi: 10.4049/jimmunol.0900270
24. Matsushita T, Tedder TF. Identifying regulatory B cells (B10 cells) that produce IL-10 in mice. *Methods Mol Biol.* (2011) 677:99–111. doi: 10.1007/978-1-60761-869-0_7
25. Mavropoulos A, Liaskos C, Simopoulou T, Bogdanos DP, Sakkas LI. IL-10-producing regulatory B cells (B10 cells), IL-17+ T cells and autoantibodies in systemic sclerosis. *Clin Immunol.* (2017) 184:26–32. doi: 10.1016/j.clim.2017.04.013
26. Vestergaard C, Gesser B, Lohse N, Jensen SL, Sindet-Pedersen S, Thestrup-Pedersen K, et al. Monocyte chemotactic and activating factor (MCAF/MCP-1) has an autoinductive effect in monocytes, a process regulated by IL-10. *J Dermatol Sci.* (1997) 15:14–22. doi: 10.1016/s0923-1811(96)00589-0
27. Peng JC, Abu BS, Richardson MM, Jonsson JJ, Frazer IH, Nielsen LK, et al. IL10 and IL12B polymorphisms each influence IL-12p70 secretion by dendritic cells in response to LPS. *Immunol Cell Biol.* (2006) 84:227–32. doi: 10.1111/j.1440-1711.2006.01419.x
28. Iwata Y, Matsushita T, Horikawa M, Dilillo DJ, Yanaba K, Venturi GM, et al. Characterization of a rare IL-10-competent B-cell subset in

humans that parallels mouse regulatory B10 cells. *Blood*. (2011) 117:530–41. doi: 10.1182/blood-2010-07-294249
29. Olotu, Ibrahim A. *Long Term Efficacy of a Pre-Erythrocytic Malaria Vaccine and Correlates of Protection in Children Residing in a Malaria Endemic Country*. University of Oxford (2013). Available online at: https://ora.ox.ac.uk/objects/uuid:3fcbab1a-689a-41bd-8685-4762941f7b0c
30. Guan HL, Jiang LP, Mo G. Decreased expression of miR-106b induced malaria vaccine protection decline. *Immunol J.* (2018) 34:313–18. doi: 10.13431/j.cnki.immunol.j.20180048
31. Mavropoulos A, Simopoulou T, Varna A, Liaskos C, Katsiari CG, Bogdanos DP, et al. Breg cells are numerically decreased and functionally impaired in patients with systemic sclerosis. *Arthritis Rheumatol.* (2016) 68:494–504. doi: 10.1002/art.39437
32. Holan V, Zajicova A, Javorkova E, Trosan P, Chudickova M, Pavlikova M, et al. Distinct cytokines balance the development of regulatory T cells and interleukin-10-producing regulatory B cells. *Immunology*. (2014) 141:577–86. doi: 10.1111/imm.12219
33. Chabaud M, Fossiez F, Taupin JL, Miossec P. Enhancing effect of IL-17 on IL-1-induced IL-6 and leukemia inhibitory factor production by rheumatoid arthritis synoviocytes and its regulation by Th2 cytokines. *J Immunol.* (1998) 161:409–14. Available online at: http://www.jimmunol.org/content/161/1/409
34. Pak JH, Lee JY, Jeon BY, Dai F, Yoo WG, Hong SJ. Cytokine production in cholangiocarcinoma cells in response to clonorchis sinensis excretory-secretory products and their putative protein components. *Korean J Parasitol.* (2019) 57:379–87. doi: 10.3347/kjp.2019.57.4.379

Conflict of Interest: The authors declare that the research was conducted in the absence of any commercial or financial relationships that could be construed as a potential conflict of interest.

frontiers in Cell and Developmental Biology

ORIGINAL RESEARCH
published: 28 April 2020
doi: 10.3389/fcell.2020.00247

Inhibitory Effects of Fosmidomycin Against *Babesia microti in vitro*

*Sen Wang[1,2], Muxiao Li[1,2], Xiaoying Luo[1,2], Long Yu[1,2], Zheng Nie[1,2], Qin Liu[1,2], Xiaomeng An[1,2], Yangsiqi Ao[1,2], Qin Liu[3], Jiaxu Chen[3], Yu Tian[1], Junlong Zhao[1,2,4] and Lan He[1,2,4]**

[1] State Key Laboratory of Agricultural Microbiology, College of Veterinary Medicine, Huazhong Agricultural University, Wuhan, China, [2] Key Laboratory of Preventive Veterinary Medicine in Hubei Province, Wuhan, China, [3] National Institute of Parasitic Diseases, Chinese Center for Disease Control and Prevention, Shanghai, China, [4] Key Laboratory of Animal Epidemical Disease and Infectious Zoonoses, Ministry of Agriculture, Huazhong Agricultural University, Wuhan, China

Babesia microti, the main pathogen causing human babesiosis, has been reported to exhibit resistance to the traditional treatment of azithromycin + atovaquone and clindamycin + quinine, suggesting the necessity of developing new drugs. The methylerythritol 4-phosphate (MEP) pathway, a unique pathway in apicomplexan parasites, was shown to play a crucial function in the growth of *Plasmodium falciparum*. In the MEP pathway, 1-deoxy-D-xylulose 5-phosphate reductoisomerase (DXR) is a rate-limiting enzyme and fosmidomycin (FSM) is a reported inhibitor for this enzyme. DXR has been shown as an antimalarial drug target, but no report is available on *B. microti* DXR (BmDXR). Here BmDXR was cloned, sequenced, analyzed by bioinformatics, and evaluated as a potential drug target for inhibiting the growth of *B. micorti in vitro*. Drug assay was performed by adding different concentrations of FSM in *B. microti in vitro* culture. Rescue experiment was done by supplementing 200 μM isopentenyl pyrophosphate (IPP) or 5 μM geranylgeraniol (GG-ol) in the culture medium together with 5 μM FSM or 10 μM diminazene aceturate. The results indicated that FSM can inhibit the growth of *B. microti* in *in vitro* culture with an IC50 of 4.63 ± 0.12 μM, and growth can be restored by both IPP and GG-ol. Additionally, FSM is shown to inhibit the growth of parasites by suppressing the DXR activity, which agreed with the reported results of other apicomplexan parasites. Our results suggest the potential of DXR as a drug target for controlling *B. microti* and that FSM can inhibit the growth of *B. microti in vitro*.

Keywords: *Babesia microti*, fosmidomycin, DXR, isoprenoid, babesiosis, methylerythritol 4-phosphate

OPEN ACCESS

Edited by:
Si-Yang Huang,
Yangzhou University, China

Reviewed by:
Audrey Ragan Odom John,
Washington University in St. Louis, United States
Mohamed Abdo Rizk,
Mansoura University, Egypt
Mahmoud Rezk Ali AbouLaila,
Damanhour University, Egypt

***Correspondence:**
Lan He
helan@mail.hzau.edu.cn

Specialty section:
This article was submitted to Molecular Medicine, a section of the journal Frontiers in Cell and Developmental Biology

Received: *16 December 2019*
Accepted: *24 March 2020*
Published: *28 April 2020*

Citation:
Wang S, Li M, Luo X, Yu L, Nie Z, Liu Q, An X, Ao Y, Liu Q, Chen J, Tian Y, Zhao J and He L (2020) Inhibitory Effects of Fosmidomycin Against Babesia microti in vitro. Front. Cell Dev. Biol. 8:247. doi: 10.3389/fcell.2020.00247

INTRODUCTION

Parasites of the genus *Babesia* are prevalent apicomplexan pathogens transmitted by ticks and infect many mammalian and avian species (Yabsley and Shock, 2013). Human babesiosis is primarily caused by the parasite *Babesia microti*, with most people being infected by ticks and some by blood transfusion (Goethert et al., 2003; Hildebrandt et al., 2007; Young et al., 2012).

Abbreviations: DXR, 1-deoxy-D-xylulose 5-phosphate reductoisomerase; FSM, fosmidomycin; DA, diminazene Aceturate; IPP, isopentenyl pyrophosphate; GG-ol, geranylgeraniol; ORF, open reading frame; MEP, 2-C-methylerythritol 4-phosphate; IC50, half-maximum inhibition concentration; PPE, percent parasitized erythrocytes.

The infection is characterized by fever and hemolytic anemia and can result in death in severe cases from complications, such as heart failure, respiratory distress, and pulmonary edema (Rosner et al., 1984). Due to the increasing number of people infected with *Babesia*, *B. microti*-related infection has been classified as a nationally notifiable disease since 2011 by the Center for Disease Control (United States) (Herwaldt et al., 2011). Babesiosis is usually treated with atovaquone and azithromycin, but resistance to these drugs has been reported (Krause et al., 2000; Wormser et al., 2010; Simon et al., 2017). Therefore, it is very urgent to develop new anti-*Babesia* drugs.

Apicomplexan parasites contain a vestigial plastid called the apicoplast (McFadden et al., 1996), which plays an important role in the biosynthesis of isoprenoid precursors, fatty acids, and part of the heme (Ralph et al., 2004). However, the apicoplast of *Babesia* is only found in isoprenoid biosynthesis (Brayton et al., 2007; Silva et al., 2016). Apicomplexan parasites utilize the methylerythritol 4-phosphate (MEP) pathway to get isopentenyl pyrophosphate (IPP) and dimethylallyl pyrophosphate (DMAPP) (Imlay and Odom, 2014), which are the basic units of synthetic isoprenoids and essential for parasite growth (Gershenzon and Dudareva, 2007).

Isoprenoids comprise a large family and have an important function in membrane structure, cellular respiration, and cell signaling (Gershenzon and Dudareva, 2007). IPP in living organisms can be synthesized by two pathways [mevalonate (MVA) pathway and MEP pathway] (Odom, 2011). Humans use the MVA pathway to synthesize IPP from acetyl-CoA (Endo, 1992). However, there is no MVA pathway in the genus of *Apicomplexa*, which thus synthesizes IPP by the MEP pathway (Cassera et al., 2004). The MEP pathway was first reported to be present in *Plasmodium falciparum* in 1999 (Jomaa et al., 1999). With the deepening of research, the MEP pathway was found to be crucial for parasites (Cassera et al., 2004). For instance, the deoxyxylose-5-phosphate reductoisomerase (DXR) of *P. falciparum* was shown to contribute to the erythrocyte stage, and inhibiting the DXR activity reduced the growth and the development of the parasites (Odom and Van Voorhis, 2010; Zhang et al., 2011). Additionally, by knocking out the DXR genes of *Toxoplasma gondii*, the parasites were found unable to survive, proving the essentiality of the MEP pathway for their survival (Nair et al., 2011).

The first dedicated step in MEP isoprenoid biosynthesis is accomplished by the bifunctional enzyme DXR (Imlay and Odom, 2014). DXR is competitively inhibited *in vitro* by the antibiotic fosmidomycin (Koppisch et al., 2002; Sangari et al., 2010). Fosmidomycin has been shown to be a clinical prospect for antimalarial drugs due to its inhibition on the recombinant *Plasmodium* DXR to kill *Plasmodium*, and the current clinical trial of malaria treatment with clindamycin is in phase II (Olliaro and Wells, 2009). *Babesia* and *Plasmodium* have many similarities, and they both live in red blood cells (RBCs). In this study, we have found that *B. microti* DXR (BmDXR) has conserved binding sites of fosmidomycin (FSM), and FSM can inhibit the growth of *B. microti in vitro*, suggesting its potential as a new anti-*Babesia* drug.

MATERIALS AND METHODS

Parasites

A *B. microti* strain ATCC PRA-99TM® (Ruebush and Hanson, 1979) was obtained from the National Institute of Parasitic Diseases, Chinese Center for Disease Control and Prevention (Shanghai, China), and maintained in our laboratory (State Key Laboratory of Agricultural Microbiology, College of Veterinary Medicine, Huazhong Agricultural University, China). The parasites were isolated at parasitemia of 30–40% as determined by Giemsa staining of thin blood smears.

RNA Extraction and cDNA Synthesis

Total RNA was extracted from infected blood by using the TRIZOL reagent (Invitrogen, Shanghai, China) and treated with RNase-free DNase I (TaKaRa, Dalian, China). RNA concentration was measured by NanoDrop 2000 (Thermo, China). The cDNA was prepared from 1 μg of the total RNA using a PrimeScript™ RT reagent kit with gDNA eraser (TaKaRa, Dalian, China).

Cloning of the BmDXR Gene

Primer pairs of BmDXR were designed based on the sequences of the *B. microti* strain R1: BmDXR-F (5'-ATGACAAATTATTTAAAACTC-3') and BmDXR-R (5'-TTAACACTTAATTTTTTTTGC-3'). Complete sequences of the BmDXR were amplified by PCR from cDNA separately. The PCR reaction was performed at 95°C for 5 min, followed by 35 cycles of 95°C for 30 s, 47°C for 30 s, 72°C for 1 min 30 s, and finally at 72°C for 10 min. The PCR products were purified and ligated into the cloning vector pEASY-Blunt (Trans, Beijing, China). Three positive colonies of each gene were sent for sequencing analysis by Invitrogen (Shanghai, China).

Sequence Analysis

The amino acid sequence of BmDXR was aligned with the selected amino acid sequences from other organisms by MAFFT online[1], then edited by BioEdit v7.25, and phylogenetically analyzed by using the Maximum Likelihood method in MEGA 7 (Kumar et al., 2016). The structure of BmDXR was predicted by SWISS-MODEL[2] (Guex et al., 2009; Bienert et al., 2017; Waterhouse et al., 2018). The 3D structure of BmDXR was virtually docked with FSM through Molecular Operating Environment (MOE) version 2014.09 (Chemical Computing Group).

B. microti Short-Term *in vitro* Cultivation

To cultivate *B. microti in vitro*, infected RBCs and healthy mouse RBCs were collected in tubes containing EDTA-2K solution (solution/RBCs = 1:9; 10% EDTA-2K), followed by centrifugation to pellet the cells at 1,000 *g* for 10 min at room temperature), two washes in PSG solution, resuspension of RBCs in the same volume of PSG + G solution, and storage at 4°C until use. The infected RBCs were diluted

[1]https://mafft.cbrc.jp/alignment/software/

[2]https://swissmodel.expasy.org/

with healthy RBCs to 3%, followed by cultivation in the presence of HL-1 supplemented with 10 μg/mg AlbuMax I (Gibco Life Technologies), 1% HB101 (Irvine Scientific, Shanghai, China), 200 μM L-glutamine (ATLANTA Biologicals, Shanghai, China), 2% antibiotic/antimycotic 100 × (Corning, Shanghai, China), and 20% fetal bovine serum at 37°C in a microaerophilous stationary phase (5% CO_2, 2% O_2, and 93% N_2) (Abraham et al., 2018).

Fosmidomycin Treatment and Rescue Assay

Drug stock solutions of FSM (Sigma-Aldrich, Shanghai, Chain) and diminazene aceturate (DA) (Sigma-Aldrich, Shanghai, Chain) were prepared in sterile water. Geranylgeraniol (Sigma-Aldrich, Shanghai, Chain) stocks were prepared in 100% ethanol. Isopentenyl pyrophosphate triammonium salt solution (Sigma-Aldrich, Shanghai, Chain) was used directly without any additional treatment. For the growth inhibition assay, *B. microti* cultures (20 μl of RBCs plus 100 μl of culture medium) were grown in 96-well flat-bottomed plates, and the susceptibility of *B. microti in vitro* to FSM was evaluated at concentrations up to 500 μM. The results were further confirmed by the IC50 values calculated using the Käber method. All the experiments were repeated three times.

In the rescue experiments, IPP or geranylgeraniol (GG-ol, alcohol of geranylgeranyl diphosphate) was added to the medium containing different drugs. IPP is one of the products in the MEP pathway (He et al., 2018), and GG-ol is the alcohol analog of the downstream isoprenoids (Yeh and DeRisi, 2011; Imlay and Odom, 2014). DA was used as a positive control, and ethanol was used as a negative control. The group of control is only medium. Each drug test was performed in triplicate.

In order to test the parasitemia, three smears were prepared from each well after 72 h of incubation. After air-drying, thin blood smears were fixed with methanol, followed by staining with Giemsa (Sigma-Aldrich, Shanghai, China), and measuring the parasitemia by microscopy. The data were analyzed using GraphPad Prism 7 (San Diego, CA, United States) by two-way analysis of variance (ANOVA), followed by Tukey's multiple-comparison test. The results are shown as mean ± SD (NS, $P > 0.05$ not significant at 5%; $^{*}P < 0.05$ significant at 5%; $^{**}P < 0.01$ significant at 1%; and *** $P < 0.001$ significant at 0.1%; error bars represent the standard deviations).

RESULTS

Cloning and Characterization of *B. microti* DXR

The open reading frame of BmDXR was cloned from *B. microti* PRA99 cDNA by conventional PCR. The results showed that BmDXR is 1,401 bp in length, encoding 466 amino acids with a predicted size of 51.8 kDa. The sequence was submitted to GenBank, with accession number MK673989. BLASTn indicated that BmDXR PRA99 (MK673989) is identical to that of *B. microti* R1 strain (XP_021338225).

Bioinformatic Analysis

The obtained BmDXR sequence was characterized by bioinformatic analysis. SignalP4.1 analysis indicated that BmDXR has a 22-amino-acid signal peptide in N-terminus[3], and a 48-amino-acid transit peptide right after the signal peptide. The amino acid sequence of BmDXR was aligned with the DXR amino acid sequences of other apicomplexan parasites by MAFFT. The results showed that BmDXR has the highest similarity to the DXR sequence of *P. falciparum* (AAD03739) with a percent identity of 41.71%, and the lowest similarity to that of *Mycobacterium tuberculosis* (NP_217386), with a percent identity of 36.59% (**Figure 1A**).

DXR amino acid sequences were characterized by phylogenetic analysis with MEGA6, and *B. microti* was shown to fall in the piroplasma clade in the same category of *Plasmodium*. In contrast, bacteria, plant, algae, and sarcocystis are grouped in the same category (**Figure 1B**). In the piroplasma clade, *B. microti* is significantly different from the other species, including *B. bigemina*, *B. ovata*, *B. bovis*, *T. equi*, *T. orientalis*, *T. parva*, and *T. annulata*.

The 3D structure of BmDXR was predicted by SWISS-MODEL, and BmDXR is shown as a dimeric structure with a metal ion binding site consisting of amino acids D216, E218, and E298. The 3D structure of BmDXR was virtually docked with FSM using MOE2014.0901. The results showed that FSM can form hydrogen bonds with Ser217, Asp216, Cys253, Met281, Ser289, Asn294, and Lys295 of BmDXR (**Figure 1C**).

Fosmidomycin Inhibits the Growth of *B. microti in vitro*

The effect of FSM on the growth of *B. microti in vitro* was tested by adding different concentrations of FSM into the *in vitro* culture medium at an initial percent parasitized erythrocytes (PPE) of 3%. Parasitemia was counted at 72 h post-treatment by microscopy. The parasitemia of the FSM groups is 4.27 ± 0.28%, 3.60 ± 0.16%, 3.09 ± 0.25%, 2.49 ± 0.33%, 1.67 ± 0.18%, and 1.45 ± 0.45% at the concentration of 5, 50, and 500 nM and 5, 50, and 500 μM, respectively, in contrast to an increase from 3% to 4.83 ± 0.8% for the negative control group (the group without drug) after 72 h of culture. After the 72-h treatment, the parasitemia is significantly lower ($P < 0.05$) in the 50 nM FSM group than in the negative control group, with a significant difference ($P < 0.01$) between 5 and 50 or 500 nm FSM groups, but no difference between the 50- and 500-μM FSM groups (**Figure 2**). The test results indicated that the drug efficacy is dose dependent, and FSM could not completely inhibit the growth of *B. microti* even at a drug concentration as high as 500 μM (inhibition rate of 70%). Compared to the negative control group, FSM exhibited a potential anti-*B. microti* activity at a low micromolar concentration, with an IC50 of 4.63 ± 0.12 μM.

[3]http://www.cbs.dtu.dk/services/SignalP/

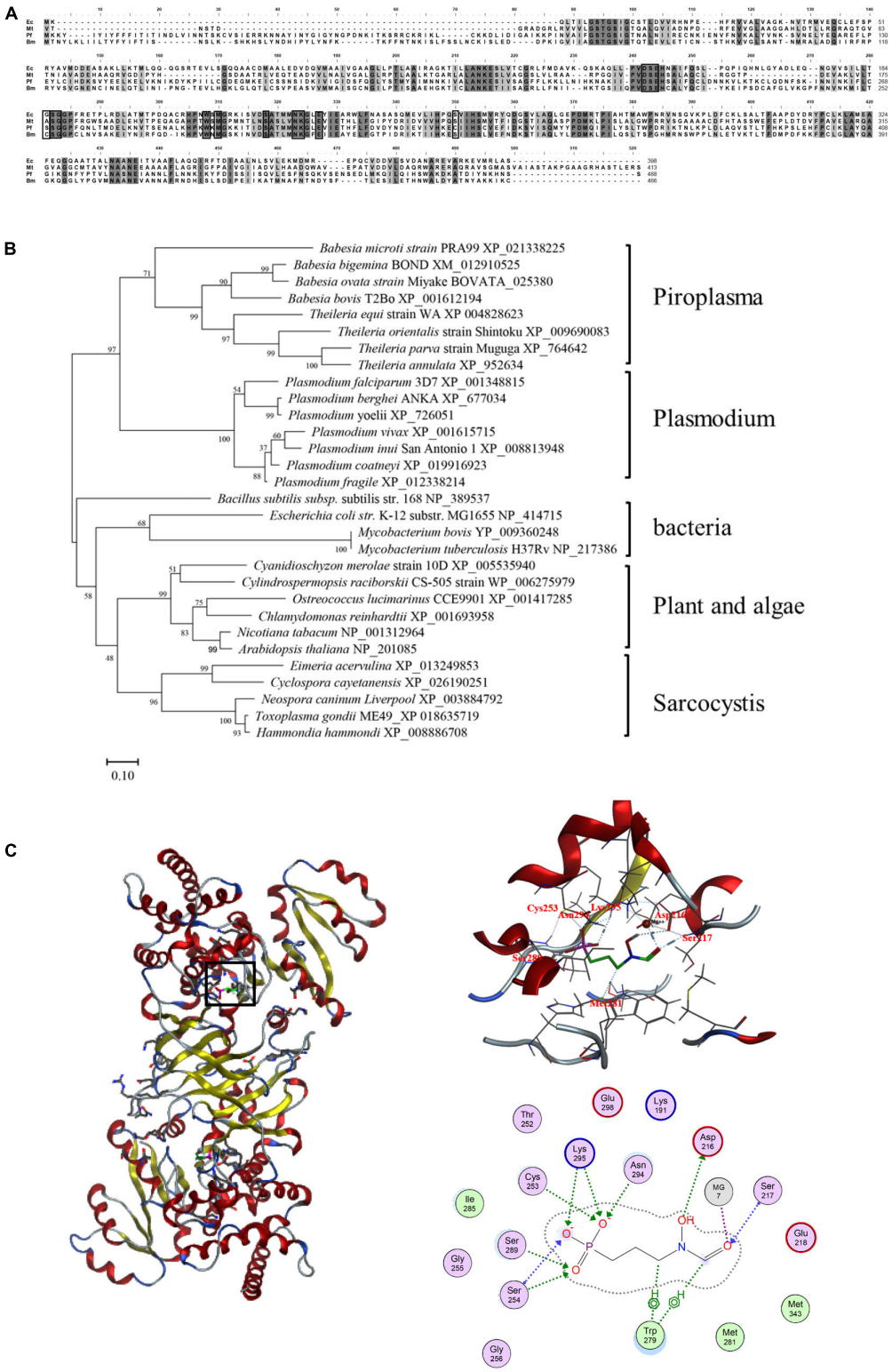

FIGURE 1 | Bioinformatics analysis of the amino acid sequence of DXR. **(A)** Multiple alignment of DXR amino acid sequences. Ec, *Escherichia coli* (NP_414715); *Mt*, *Mycobacterium tuberculosis* (NP_217386); *Pf*, *Plasmodium falciparum* (AAD03739); *Bm*, *Babesia microti* (XP_021338225). Black shading indicates a similarity in four or in more than four species; gray shading indicates a similarity in three species. Black pane indicates the reported fosmidomycin binding site. **(B)** Neighbor-joining phylogenetic tree based on DXR amino acid sequences. The organism names and sequence accession numbers are indicated. **(C)** Prediction of the structure of BmDXR by SWISS-MODEL. The 3D structure of BmDXR is virtually docked with FSM through MOE2014.0901, and FSM can form hydrogen bonds with Ser217, Asp216, Cys253, Met281, Ser289, Asn294, and Lys295 of BmDXR.

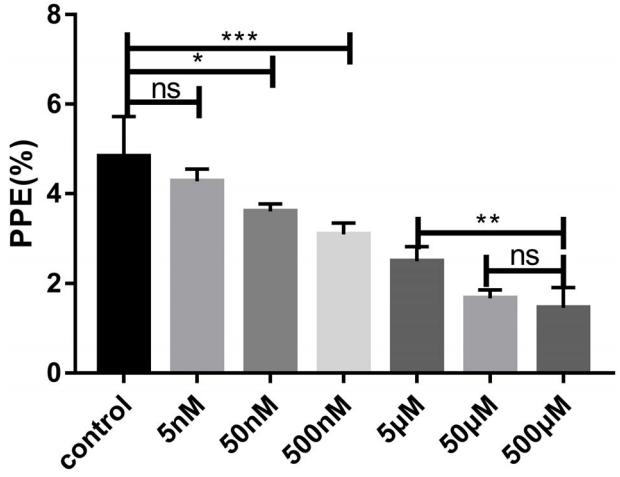

FIGURE 2 | Parasitemia of different drug concentrations after 72 h of treatment. Evaluation of the susceptibility of *B. microti in vitro* to fosmidomycin at concentrations from 5 to 500 μM. Giemsa staining assay at 72 h after the addition of the drug. PPE, pollen productivity estimate; Ns, not significant ($P > 0.05$); *$P < 0.05$, **$P < 0.01$, ***$P < 0.001$.

IPP and GG-ol Can Rescue *B. microti* Treated by Fosmidomycin

The inhibition of FSM on the growth of *B. mitroti* was investigated through rescue experiments in *B. microti in vitro* cultivation with 200 μM IPP and 5 μM GG-ol added separately into 5 μM FSM and 10 μM DA using the latter as a positive control. The 5 μM FSM and 10 μM DA showed 53.8 and 58.6% inhibition on the growth of the parasites (**Figure 3A**) in the rescue experiment. The growth in 5 μM FSM could be restored by adding 200 μM IPP or 5 μM GG-ol into culture media as indicated by having no difference ($P < 0.001$) in the relative growth rate among FSM + IPP, GG-ol, and the control (**Figures 3B,C**). However, the growth in 10 μM DA could not be rescued by adding IPP or GG-ol, as shown by a significant difference ($P < 0.001$) in the relative growth rate among DA + IPP, DA + GG-ol, and the control [ANOVA, $F(2, 6) = 259.2$, $P < 0.0001$; ANOVA, $F(2, 6) = 65.1$, $P < 0.0001$] (**Figures 3B,C**).

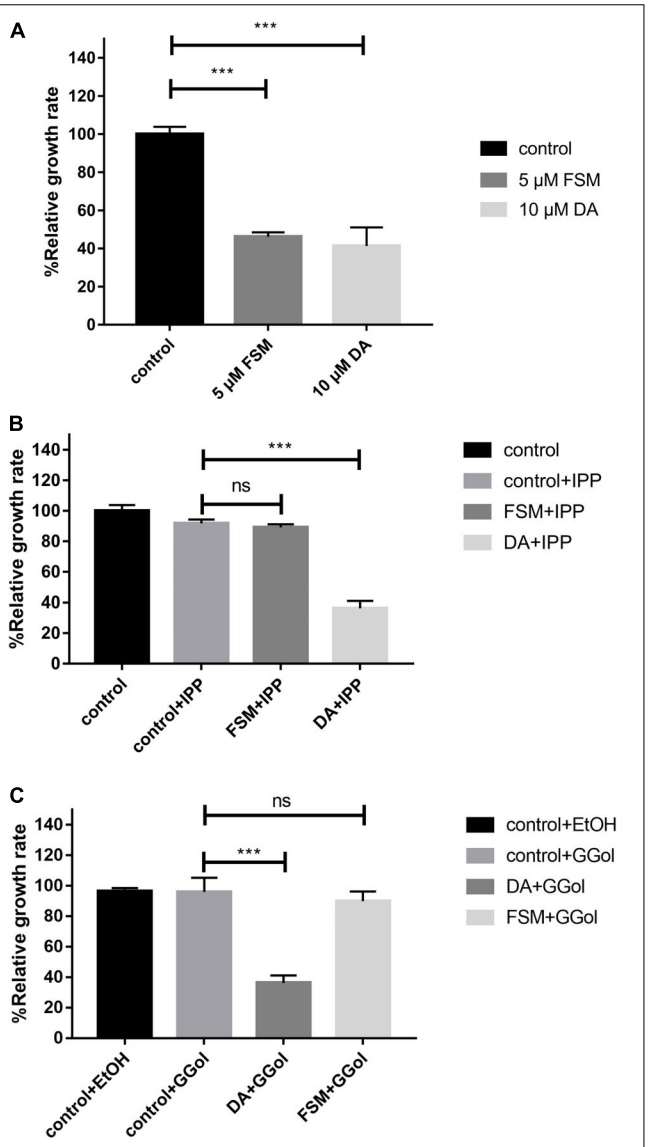

FIGURE 3 | IPP and GGol can rescue *B. microti* treated by fosmidomycin and Giemsa staining assay at 72 h after the addition of the drugs. **(A)** Effect of 5 μM fosmidomycin and 10 μM diminazene aceturate on the growth of *B. microti in vitro*. The group of control is only medium. **(B)** Rescue of *B. microti* by adding isopentenyl pyrophosphate. **(C)** Rescue of *B. microti* by adding geranylgeraniol. ***$P < 0.001$.

DISCUSSION

The MEP pathway, an essential route in apicomplexan parasites, plays a vital role in the growth of parasites by synthesizing IPP (Imlay and Odom, 2014); however, very few effective inhibitors have been studied. Currently, the MEP inhibitors with lower IC50 for *Plasmodium* are FSM and 1R, 3S MMV008138 (Ghavami et al., 2018). DXR is the second and also a rate-limiting enzyme in the MEP pathway (Imlay and Odom, 2014). The inhibitors of DXR enzymes, such as FSM, suppress the synthesis of IPP in the MEP pathway of multiple organisms *in vitro* (**Figure 4**; Jomaa et al., 1999). It has been reported that FSM can inhibit *B. divergen*, *B. bovis*, and *B. orientalis in vitro* (Baumeister et al., 2011; Caballero et al., 2012; He et al., 2018). As shown by the reported *P. falciparum* and *M. tuberculosis* crystal structures of inhibitor-free and FSM-bound complete quaternary complexes of DXR (Mac Sweeney et al., 2005; Andaloussi et al., 2011; Umeda et al., 2011), a large cleft was closed between NADPH-binding and catalytic domains upon inhibitor binding, which means that FSM inhibits DXR activity by competing with DOXP. The FSM binding site is conservative, and BmDXR is similar in structure to PfDXR and EcDXR. We speculate that FSM can inhibit the DXR activity in *B. microti* due to its inhibition on the growth of *B. microti* in *in vitro* culture with an FSM IC50

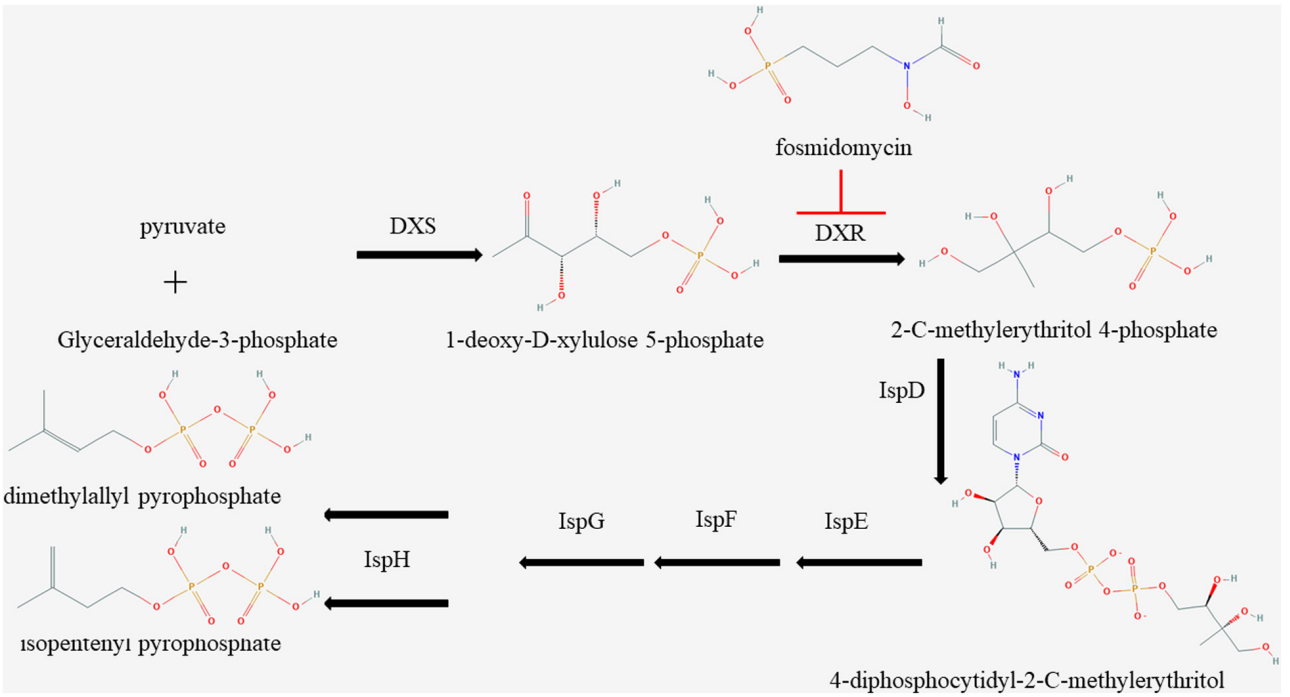

FIGURE 4 | Schematic of isoprenoid metabolism through the non-mevalonate pathway. The methylerythritol 4-phosphate pathway is a unique route to isoprenoid biosynthesis in apicomplexan, and fosmidomycin is a specific inhibitor to 1-deoxy-D-xylulose 5-phosphate reductoisomerase.

value of 4.63 ± 0.12 μM, which is higher than that of *B. bovis* and *B. bigemina* (3.87 and 2.4 μM, respectively) (Sivakumar et al., 2008). The growth of *B. microti* can be rescued by adding IPP or GG-ol in the culture medium, which agreed with the report that GG-ol can rescue the growth of *B. orientalis* inhibited by FSM (He et al., 2018). These results further suggest that FSM inhibits *B. microti* growth by suppressing the MEP pathway. It is reported that *B. microti*, an obligate parasite of red blood cells (Silva et al., 2016), obtains most of the nutrition materials for parasite survival from host red blood cells, but it cannot obtain IPP from host cells due to the small amount of IPP in RBCs (Wiback and Palsson, 2002). In this case, FSM may inhibit the growth of *B. microti* by suppressing the synthesis of IPP.

FSM can cause the death of *P. falciparum* in the first life cycle (Howe et al., 2013), but we failed to observe the death of *B. microti* after 24 h of treatment at 5 μM FSM. According to the results of Giemsa staining (**Supplementary Figure S1**), we selected the parasites in the period of merozoites and compared their morphologies. All the merozoites in the control group have an obvious contour and a complete shape, while those treated by FSM have lost their contour and complete shape which, however, can be recovered upon addition of IPP or GG-ol in the medium. This is consistent with the observation in *B. bovis* and *B. bigemina* treated with FSM, with obvious changes in the shape of the parasites (Sivakumar et al., 2008). These results indicate that IPP is important for *Babesia* to keep a normal shape. Meanwhile, the merozoites treated by DA present a pointed shape, which could not be restored to a normal shape after adding IPP or GG-ol. These morphologies indicate a milder efficacy of FSM than DA because DA made the merozoites of *B. microti* point-like, while FSM caused the parasite to lose its normal form. FSM-treated *P. falciparum* was shown to reduce protein prenylation, leading to marked defects in food vacuolar morphology and integrity (Howe et al., 2013). However, no food vacuole has been reported in *B. microti* (Rudzinska et al., 1976), suggesting that the impact of FSM on *B. microti* may be different from its influence mechanism on malaria parasites.

Traditionally, azithromycin + atovaquone was used to treat babesiosis in humans and clindamycin + quinine as a treatment strategy for patients with resistance to atovaquone (Simon et al., 2017). Meanwhile, many patients have adverse reactions to chloroquine (Krause et al., 2000; Rozej-Bielicka et al., 2015). Generally, traditional treatments cannot eliminate *B. microti* parasitemia completely, suggesting the high recurrence potential of *B. microti*. Despite being a safe and effective inhibitor, FSM has some limitations to clinical applications. First of all, it is an unmodified compound which is very costly. Secondly, FSM has a poor pharmacokinetics profile with a plasma half-life of 3.5 h (Na-Bangchang et al., 2007); it will need multiple shots for clinic use. This limitation of FSM can be solved by drug modification. For example, FR9008 is a derivative of FSM, which has a better effect on *P. falciparum* than FSM. Currently, it is necessary to improve the ability of FSM in entering cells and extend its half-life for clinical applications. We believe that the limitations of FSM can be overcome by drug modification. For drug development, modified drugs have better clinical results; for example, dihydroartemisinin has a better effect than artemisinin in treating *Plasmodium* (Li et al., 1983). About

combination therapy, clindamycin + FSM can play a better effect in the treatment of *Plasmodium* (Borrmann et al., 2006), but clindamycin has less effect to *B. microti in vitro* (Lawres et al., 2016). Other drugs could be used as combination therapy with FSM if required. Our future work will focus on modifying FSM and the combination therapy of FSM.

CONCLUSION

The MEP pathway is a favorable target for drug development. In this study, it is shown that FSM can inhibit the growth of *B. microti in vitro*, which can be rescued by a medium supplemented with IPP or GG-ol. These results indicate that DXR is a potential drug target for designing anti-*Babesia* drugs and that the DXR function and FSM structure contribute to the design of such drugs.

DATA AVAILABILITY STATEMENT

The datasets generated for this study can be found in the NCBI GenBank under the accession number MK673989.

ETHICS STATEMENT

This study was approved by the Scientific Ethic Committee of Huazhong Agricultural University (permit number: HZAUMO-2017-040). All mice were handled in accordance with the Animal Ethics Procedures and Guidelines of the People's Republic of China.

AUTHOR CONTRIBUTIONS

SW, LH, and JZ designed the study and wrote the draft of the manuscript. ML, XL, LY, ZN, QL, XA, YA, QL, JC, and YT performed the experiments and analyzed the results. All the authors have read and approved the final manuscript.

FUNDING

This work was supported by the National Natural Science Foundation of China (31772729), the National Key Research and Development Program of China (2017YFD0501201), the National Key Basic Research Program (973 Program) of China (2015CB150302), and the Natural Science Foundation of Hubei Province (2017CFA020).

SUPPLEMENTARY MATERIAL

The Supplementary Material for this article can be found online at: https://www.frontiersin.org/articles/10.3389/fcell.2020.00247/full#supplementary-material

FIGURE S1 | Morphology of merozoites cultured *in vitro* for 72 h. 5 μM FSM and 10 μM DA caused changes in merozoite morphology, and 200 μM IPP or 5 μM GG-ol can restore merozoite morphology treated by FSM.

REFERENCES

Abraham, A., Brasov, I., Thekkiniath, J., Kilian, N., Lawres, L., Gao, R., et al. (2018). Establishment of a continuous in vitro culture of *Babesia duncani* in human erythrocytes reveals unusually high tolerance to recommended therapies. *J. Biol. Chem.* 293, 19974–19981. doi: 10.1074/jbc.AC118.005771

Andaloussi, M., Henriksson, L. M., Wieckowska, A., Lindh, M., Bjorkelid, C., Larsson, A. M., et al. (2011). Design, synthesis, and X-ray crystallographic studies of alpha-aryl substituted fosmidomycin analogues as inhibitors of *Mycobacterium tuberculosis* 1-deoxy-D-xylulose 5-phosphate reductoisomerase. *J. Med. Chem.* 54, 4964–4976. doi: 10.1021/jm2000085

Baumeister, S., Wiesner, J., Reichenberg, A., Hintz, M., Bietz, S., Harb, O. S., et al. (2011). Fosmidomycin uptake into *Plasmodium* and *Babesia*-infected erythrocytes is facilitated by parasite-induced new permeability pathways. *PLoS One* 6:e19334. doi: 10.1371/journal.pone.0019334

Bienert, S., Waterhouse, A., de Beer, T. A., Tauriello, G., Studer, G., Bordoli, L., et al. (2017). The SWISS-MODEL repository-new features and functionality. *Nucleic Acids Res.* 45, D313–D319. doi: 10.1093/nar/gkw1132

Borrmann, S., Lundgren, I., Oyakhirome, S., Impouma, B., Matsiegui, P. B., Adegnika, A. A., et al. (2006). Fosmidomycin plus clindamycin for treatment of pediatric patients aged 1 to 14 years with *Plasmodium falciparum* malaria. *Antimicrob. Agents Chemother.* 50, 2713–2718. doi: 10.1128/aac.00392-396

Brayton, K. A., Lau, A. O., Herndon, D. R., Hannick, L., Kappmeyer, L. S., Berens, S. J., et al. (2007). Genome sequence of *Babesia bovis* and comparative analysis of apicomplexan hemoprotozoa. *PLoS Pathog.* 3, 1401–1413. doi: 10.1371/journal.ppat.0030148

Caballero, M. C., Pedroni, M. J., Palmer, G. H., Suarez, C. E., Davitt, C., and Lau, A. O. (2012). Characterization of acyl carrier protein and LytB in *Babesia bovis* apicoplast. *Mol. Biochem. Parasitol.* 181, 125–133. doi: 10.1016/j.molbiopara.2011.10.009

Cassera, M. B., Gozzo, F. C., D'Alexandri, F. L., Merino, E. F., del Portillo, H. A., Peres, V. J., et al. (2004). The methylerythritol phosphate pathway is functionally active in all intraerythrocytic stages of *Plasmodium falciparum*. *J. Biol. Chem.* 279, 51749–51759. doi: 10.1074/jbc.M408360200

Endo, A. (1992). The discovery and development of HMG-CoA reductase inhibitors. *J. Lipid Res.* 33, 1569–1582.

Gershenzon, J., and Dudareva, N. (2007). The function of terpene natural products in the natural world. *Nat. Chem. Biol.* 3, 408–414. doi: 10.1038/nchembio.2007.5

Ghavami, M., Merino, E. F., Yao, Z. K., Elahi, R., Simpson, M. E., Fernandez-Murga, M. L., et al. (2018). biological studies and target engagement of the 2- C-Methyl-d-Erythritol 4-Phosphate Cytidylyltransferase (IspD)-Targeting Antimalarial Agent (1 R,3 S)-MMV008138 and analogs. *ACS Infect. Dis.* 4, 549–559. doi: 10.1021/acsinfecdis.7b00159

Goethert, H. K., Lubelcyzk, C., LaCombe, E., Holman, M., Rand, P., Smith, R. P., et al. (2003). Enzootic *Babesia microti* in Maine. *J. Parasitol.* 89, 1069–1071. doi: 10.1645/ge-3149rn

Guex, N., Peitsch, M. C., and Schwede, T. (2009). Automated comparative protein structure modeling with SWISS-MODEL and Swiss-PdbViewer: a historical perspective. *Electrophoresis* 30(Suppl. 1), S162–S173. doi: 10.1002/elps.200900140

He, L., He, P., Luo, X., Li, M., Yu, L., Guo, J., et al. (2018). The MEP pathway in *Babesia orientalis* apicoplast, a potential target for anti-babesiosis drug development. *Parasit Vectors* 11:452. doi: 10.1186/s13071-018-3038-3037

Herwaldt, B. L., Linden, J. V., Bosserman, E., Young, C., Olkowska, D., and Wilson, M. (2011). Transfusion-associated babesiosis in the United States: a description of cases. *Ann. Intern. Med.* 155, 509–519. doi: 10.7326/0003-4819-155-8-201110180-201110362

Hildebrandt, A., Hunfeld, K. P., Baier, M., Krumbholz, A., Sachse, S., Lorenzen, T., et al. (2007). First confirmed autochthonous case of human *Babesia microti*

infection in Europe. *Eur. J. Clin. Microbiol. Infect. Dis.* 26, 595–601. doi: 10.1007/s10096-007-0333-331

Howe, R., Kelly, M., Jimah, J., Hodge, D., and Odom, A. R. (2013). Isoprenoid biosynthesis inhibition disrupts Rab5 localization and food vacuolar integrity in *Plasmodium falciparum*. *Eukaryot Cell* 12, 215–223. doi: 10.1128/ec.00073-12

Imlay, L., and Odom, A. R. (2014). Isoprenoid metabolism in apicomplexan parasites. *Curr. Clin. Microbiol. Rep.* 1, 37–50. doi: 10.1007/s40588-014-0006-7

Jomaa, H., Wiesner, J., Sanderbrand, S., Altincicek, B., Weidemeyer, C., Hintz, M., et al. (1999). Inhibitors of the nonmevalonate pathway of isoprenoid biosynthesis as antimalarial drugs. *Science* 285, 1573–1576. doi: 10.1126/science.285.5433.1573

Koppisch, A. T., Fox, D. T., Blagg, B. S., and Poulter, C. D. (2002). E. *coli MEP* synthase: steady-state kinetic analysis and substrate binding. *Biochemistry* 41, 236–243. doi: 10.1021/bi0118207

Krause, P. J., Lepore, T., Sikand, V. K., Gadbaw, J., Burke, G., Telford, S. R., et al. (2000). Atovaquone and azithromycin for the treatment of babesiosis. *N. Engl. J. Med.* 343, 1454–1458. doi: 10.1056/nejm200011163432004

Kumar, S., Stecher, G., and Tamura, K. (2016). MEGA7: molecular evolutionary genetics analysis version 7.0 for bigger datasets. *Mol. Biol. Evol.* 33, 1870–1874. doi: 10.1093/molbev/msw054

Lawres, L. A., Garg, A., Kumar, V., Bruzual, I., Forquer, I. P., Renard, I., et al. (2016). Radical cure of experimental babesiosis in immunodeficient mice using a combination of an endochin-like quinolone and atovaquone. *J. Exp. Med.* 213, 1307–1318. doi: 10.1084/jem.20151519

Li, Z. L., Gu, H. M., Warhurst, D. C., and Peters, W. (1983). Effects of qinghaosu and related compounds on incorporation of [G-3H] hypoxanthine by Plasmodium falciparum in vitro. *Trans. R. Soc. Trop. Med. Hyg.* 77, 522–523. doi: 10.1016/0035-9203(83)90129-90123

Mac Sweeney, A., Lange, R., Fernandes, R. P., Schulz, H., Dale, G. E., Douangamath, A., et al. (2005). The crystal structure of *E.coli* 1-deoxy-D-xylulose-5-phosphate reductoisomerase in a ternary complex with the antimalarial compound fosmidomycin and NADPH reveals a tight-binding closed enzyme conformation. *J. Mol. Biol.* 345, 115–127. doi: 10.1016/j.jmb.2004.10.030

McFadden, G. I., Reith, M. E., Munholland, J., and Lang-Unnasch, N. (1996). Plastid in human parasites. *Nature* 381:482. doi: 10.1038/381482a0

Na-Bangchang, K., Ruengweerayut, R., Karbwang, J., Chauemung, A., and Hutchinson, D. (2007). Pharmacokinetics and pharmacodynamics of fosmidomycin monotherapy and combination therapy with clindamycin in the treatment of multidrug resistant falciparum malaria. *Malar. J.* 6:70. doi: 10.1186/1475-2875-6-70

Nair, S. C., Brooks, C. F., Goodman, C. D., Sturm, A., McFadden, G. I., Sundriyal, S., et al. (2011). Apicoplast isoprenoid precursor synthesis and the molecular basis of fosmidomycin resistance in *Toxoplasma gondii*. *J. Exp. Med.* 208, 1547–1559. doi: 10.1084/jem.20110039

Odom, A. R. (2011). Five questions about non-mevalonate isoprenoid biosynthesis. *PLoS Pathog.* 7:e1002323. doi: 10.1371/journal.ppat.1002323

Odom, A. R., and Van Voorhis, W. C. (2010). Functional genetic analysis of the *Plasmodium falciparum* deoxyxylulose 5-phosphate reductoisomerase gene. *Mol. Biochem. Parasitol.* 170, 108–111. doi: 10.1016/j.molbiopara.2009.12.001

Olliaro, P., and Wells, T. N. (2009). The global portfolio of new antimalarial medicines under development. *Clin. Pharmacol. Ther.* 85, 584–595. doi: 10.1038/clpt.2009.51

Ralph, S. A., van Dooren, G. G., Waller, R. F., Crawford, M. J., Fraunholz, M. J., Foth, B. J., et al. (2004). Tropical infectious diseases: metabolic maps and functions of the *Plasmodium falciparum* apicoplast. *Nat. Rev. Microbiol.* 2, 203–216. doi: 10.1038/nrmicro843

Rosner, F., Zarrabi, M. H., Benach, J. L., and Habicht, G. S. (1984). Babesiosis in splenectomized adults. Review of 22 reported cases. *Am. J. Med.* 76, 696–701. doi: 10.1016/0002-9343(84)90298-5

Rozej-Bielicka, W., Stypulkowska-Misiurewicz, H., and Golab, E. (2015). Human babesiosis. *Przegl. Epidemiol.* 69, 489–494.

Rudzinska, M. A., Trager, W., Lewengrub, S. J., and Gubert, E. (1976). An electron microscopic study of *Babesia microti* invading erythrocytes. *Cell Tissue Res.* 169, 323–334.

Ruebush, M. J., and Hanson, W. L. (1979). Susceptibility of five strains of mice to *Babesia microti* of human origin. *J. Parasitol.* 65, 430–433.

Sangari, F. J., Perez-Gil, J., Carretero-Paulet, L., Garcia-Lobo, J. M., and Rodriguez-Concepcion, M. (2010). A new family of enzymes catalyzing the first committed step of the methylerythritol 4-phosphate (MEP) pathway for isoprenoid biosynthesis in bacteria. *Proc. Natl. Acad. Sci. U.S.A.* 107, 14081–14086. doi: 10.1073/pnas.1001962107

Silva, J. C., Cornillot, E., McCracken, C., Usmani-Brown, S., Dwivedi, A., Ifeonu, O. O., et al. (2016). Genome-wide diversity and gene expression profiling of *Babesia microti* isolates identify polymorphic genes that mediate host-pathogen interactions. *Sci. Rep.* 6:35284. doi: 10.1038/srep35284

Simon, M. S., Westblade, L. F., Dziedziech, A., Visone, J. E., Furman, R. R., Jenkins, S. G., et al. (2017). Clinical and molecular evidence of atovaquone and azithromycin resistance in relapsed *Babesia microti* infection associated with rituximab and chronic lymphocytic leukemia. *Clin. Infect. Dis.* 65, 1222–1225. doi: 10.1093/cid/cix477

Sivakumar, T., AbouLaila, M., Khukhuu, A., Iseki, H., Alhassan, A., Yokoyama, N., et al. (2008). In vitro inhibitory effect of fosmidomycin on the asexual growth of *Babesia bovis* and *Babesia bigemina*. *J. Protozool. Res.* 18, 71–78.

Umeda, T., Tanaka, N., Kusakabe, Y., Nakanishi, M., Kitade, Y., and Nakamura, K. T. (2011). Molecular basis of fosmidomycin's action on the human malaria parasite *Plasmodium falciparum*. *Sci. Rep.* 1:9. doi: 10.1038/srep00009

Waterhouse, A., Bertoni, M., Bienert, S., Studer, G., Tauriello, G., Gumienny, R., et al. (2018). SWISS-MODEL: homology modelling of protein structures and complexes. *Nucleic Acids Res.* 46, W296–W303. doi: 10.1093/nar/gky427

Wiback, S. J., and Palsson, B. O. (2002). Extreme pathway analysis of human red blood cell metabolism. *Biophys. J.* 83, 808–818. doi: 10.1016/s0006-3495(02)75210-75217

Wormser, G. P., Prasad, A., Neuhaus, E., Joshi, S., Nowakowski, J., Nelson, J., et al. (2010). Emergence of resistance to azithromycin-atovaquone in immunocompromised patients with *Babesia microti* infection. *Clin. Infect. Dis.* 50, 381–386. doi: 10.1086/649859

Yabsley, M. J., and Shock, B. C. (2013). Natural history of Zoonotic *Babesia*: role of wildlife reservoirs. *Int. J. Parasitol. Parasites Wildl.* 2, 18–31. doi: 10.1016/j.ijppaw.2012.11.003

Yeh, E., and DeRisi, J. L. (2011). Chemical rescue of malaria parasites lacking an apicoplast defines organelle function in blood-stage *Plasmodium falciparum*. *PLoS Biol.* 9:e1001138. doi: 10.1371/journal.pbio.1001138

Young, C., Chawla, A., Berardi, V., Padbury, J., Skowron, G., and Krause, P. J. (2012). Preventing transfusion-transmitted babesiosis: preliminary experience of the first laboratory-based blood donor screening program. *Transfusion* 52, 1523–1529. doi: 10.1111/j.1537-2995.2012.03612.x

Zhang, B., Watts, K. M., Hodge, D., Kemp, L. M., Hunstad, D. A., Hicks, L. M., et al. (2011). A second target of the antimalarial and antibacterial agent fosmidomycin revealed by cellular metabolic profiling. *Biochemistry* 50, 3570–3577. doi: 10.1021/bi200113y

Conflict of Interest: The authors declare that the research was conducted in the absence of any commercial or financial relationships that could be construed as a potential conflict of interest.

frontiers in Cell and Developmental Biology

MINI REVIEW
published: 09 June 2020
doi: 10.3389/fcell.2020.00439

Epithelial Haven and Autophagy Breakout in Gonococci Infection

*Ana Clara Mendes†, Marcone Ciccone†, Bruna Gazolla† and Diana Bahia**

Departamento de Genética, Ecologia e Evolução, Instituto de Ciencias Biológicas, Universidade Federal de Minas Gerais, Belo Horizonte, Brazil

The World Health Organization (WHO) has estimated that in 2016, there were 87 million new cases of gonorrhea. Gonorrhea is caused by the sexually transmitted human-exclusive agent *Neisseria gonorrhoeae*, a Gram-negative diplococcus that causes cervicitis in females and urethritis in males and may lead to more severe complications. Currently, there is no vaccine against *N. gonorrhoeae*. Its resistance to antibiotics has been increasing in the past few years, reducing the range of treatment options. *N. gonorrhoeae* requires a surface protein/receptor (Opa proteins, porin, Type IV pili, LOS) to adhere to and invade epithelial cells. During invasion and transcytosis, *N. gonorrhoeae* is targeted by the autophagy pathway, a cellular maintenance process which balances sources of energy at critical times by degrading damaged organelles and macromolecules in the lysosome. Autophagy is an important host defense mechanism which targets invading pathogens. Based on transmission electron microscopy (TEM) analysis, the intracellular bacteria occupy the autophagosome, a double-membraned vesicle that is formed around molecules or microorganisms during macroautophagy and fuses with lysosomes for degradation. Most of the gonococci end up in autolysosomes for degradation, but a subpopulation of the intracellular bacteria inhibits the maturation of the autophagosome and its fusion with lysosomes by activating mTORC1 (a known suppressor of the autophagy signaling), thus escaping autophagic elimination. This mini review focuses on the cellular features of *N. gonorrhoeae* during epithelial cell invasion, with a particular focus on how *N. gonorrhoeae* evades the autophagy pathway.

Keywords: *N. gonorrhoeae*, autophagy, epithelial cell, intracellular pathogen, epithelial cell invasion

OPEN ACCESS

Edited by:
Si-Yang Huang,
Yangzhou University, China

Reviewed by:
Chihiro Aikawa,
Kyoto University, Japan
Ravi Manjithaya,
Jawaharlal Nehru Centre for Advanced Scientific Research, India

****Correspondence:***
Diana Bahia
dianabahia@hotmail.com

†These authors share first authorship

Specialty section:
This article was submitted to Molecular Medicine, a section of the journal Frontiers in Cell and Developmental Biology

Received: *06 February 2020*
Accepted: *11 May 2020*
Published: *09 June 2020*

Citation:
Mendes AC, Ciccone M, Gazolla B and Bahia D (2020) Epithelial Haven and Autophagy Breakout in Gonococci Infection. Front. Cell Dev. Biol. 8:439. doi: 10.3389/fcell.2020.00439

INTRODUCTION

Neisseria gonorrhoeae, also known as gonococcus, is the causative agent of gonorrhea, a sexually transmitted infection that occurs exclusively in humans. In 2016, The World Health Organization (WHO) estimated that 86.9 million new cases of gonorrhea occurred globally. In 2017, the WHO included *N. gonorrhoeae* in its list of bacteria for which new antibiotics are urgently needed[1]. *N. gonorrhoeae* is a major global public health concern due to its increasing resistance to antibiotics, which leads to the possibility of untreatable gonorrhea infections (World Health Organization [WHO], 2017; Rowley et al., 2019). *N. gonorrhoeae* is a Gram-negative diplococcus that usually infects urogenital epithelia, but it is also able to infect rectal, pharynx, and conjunctival mucosa (Britigan et al., 1985).

[1]https://www.who.int/medicines/news/bacteria-antibiotics-needed/en/

At the sites of gonococci colonization, the activation of the innate immune response causes the symptoms of gonorrhea, including discomfort in the affected area and purulent urethral or cervical discharge. Acute gonorrhea results in an intensely inflammatory exudate, which contains macrophages, exfoliated epithelial cells, and polymorphonuclear neutrophils (Hook, 2012). Many studies have shown that asymptomatic infections are common in both men and women, but are more prevalent in women than in men (Muzny et al., 2017). This may be due to the relative ease in diagnosing symptoms in men, as the purulent exudate causes painful urination in men. Symptoms in women are mostly unnoticed and/or non-specific and are often mistaken for symptoms of bacterial vaginosis, hormonal alterations, or normal vaginal secretions (Grimley et al., 2006; Quillin and Seifert, 2018). Untreated gonorrhea may result in pelvic inflammatory disease, infertility, ectopic pregnancies, or neonatal blindness as a consequence of vertical transmission. In addition, untreated gonorrhea can lead to gonococcal dissemination and enhanced transmission of HIV (Masi and Eisenstein, 1981; Sandstrom, 1987; Little, 2006).

ADHERENCE AND INVASION

Neisseria gonorrhoeae adheres to urogenital tract by attaching to surface structures as Type IV pili (Tfp) (Pearce and Buchanan, 1978), opacity (Opa) proteins, LOS, or outer membrane protein porin (PorB) (Stern et al., 1986; van Putten and Paul, 1995). Type IV pili (Tfp) mediate initial cellular adherence, its retraction brings the bacteria closer to the epithelial cell surface and activates Ca^{2+} flux, PI3K/Akt, and the ERK/MAP kinase pathways (Ayala et al., 2005; Lee et al., 2005). The Opa family of proteins includes two classes: the Opa50 protein, which binds to surface heparan sulfate proteoglycan (HSPG) receptors; and Opa51-60, which bind to carcinoembryonic antigen-related cellular adhesion molecules (CEACAMs) and mediate the complex interactions between the gonococci and epithelial cells or phagocytes after Tfp adhesion (van Putten and Paul, 1995). After adhesion, *N. gonorrhoeae* replicates in microcolonies, which are collections of bacteria formed from a few diplococci after the initial adhesion on epithelial cells, competes with the local microbiota, and is able to invade and disseminate by transmigrating across the epithelial cell monolayer (Quillin and Seifert, 2018). Gonococcal microcolonies can move and promote interaction between bacterial cells, helping them to deal with environmental pressures. In addition, microcolonies play a role in gonococci-host interactions (Higashi et al., 2007).

The gonococci initiate cross-talk with host cells using multiple surface molecules, resulting in activation of signaling pathways and changes in gene expression in the host cells and in the gonococci themselves (Stein et al., 2015). Interactions between CEACAMs and Opa proteins can induce phagocytosis, triggering the engulfment of the bacteria into the epithelial cells and neutrophils (Fox et al., 2014).

Neisseria gonorrhoeae facilitates its invasion into host cells by modulating the activity and distribution of host epidermal growth factor receptor (EGFR), which is a signaling receptor that pathogens can manipulate for their survival in host cells (Zhang et al., 2004). The gonococcal microcolonies recruit EGFR to the site of microcolony adherence. The kinase activity of EGFR is necessary for gonococcal invasion into epithelial cells. The gonococci activate EGFR by inducing the production of EGFR ligands. This suggests that microcolonies are important for invasion of *N. gonorrhoeae* into epithelial cells. Studies have shown that EGFR kinase inhibition reduces gonococcal invasion, further indicating an important role for EGFR in gonococci invasion (Swanson et al., 2011).

Apicella et al. (1996) analyzed urethral exudates from men infected with *N. gonorrhoeae* and observed that bacteria were clustered within vacuoles upon invasion. However, they also found bacteria in the cytosol without evidence of a surrounding vacuole. Harvey et al. (1997) studied primary human urethral epithelial cell cultures infected with *N. gonorrhoeae* and showed that after the invasion, the gonococci appeared to reside and multiply within vacuoles close to the apical layers of the epithelial cells and were later released from the epithelial cell monolayer either in membrane-bound vacuoles or after rupturing the infected cells (Mosleh et al., 1997). Gonococcal infection of the urethral epithelium modulates host anti-apoptotic factors, thereby promoting bacterial survival within the epithelial tissue (Binnicker et al., 2003).

WHAT IS AUTOPHAGY?

Autophagy is a cellular mechanism that can be upregulated in response to stress conditions and lack of nutrients. It is a pathway that delivers organelles and cytoplasmic proteins to the lysosome for degradation (Yang et al., 2005).

Mammalian cells have three types of autophagy: microautophagy, in which the lysosome captures the molecules by invagination of the lysosomal membrane; chaperone-mediated autophagy (CMA), in which chaperone proteins identify molecules that contain a particular pentapeptide motif and transport them directly to lysosomes; and macroautophagy, referred to in this text as autophagy, which involves the formation of cytosolic vesicles to transport the molecules, including damaged organelles or pathogens, to the lysosome for degradation. Upon activation of autophagy, a membrane structure known as a phagophore forms and expands, eventually closing to form a double-membrane vesicle called autophagosome (Parzych and Klionsky, 2014).

Autophagosomes fuse with lysosomes (autolysosomes), and the sequestered cargo is digested. The initial formation of the autophagosomes requires the activation of the unc-51-like kinase 1 (ULK1) complex. Then, ULK activates the Vps34 (class III phosphatidylinositol 3-kinase) complex, which comprises Vps34, associated to Beclin 1, VPS15, and ATG14L, triggering vesicle nucleation. The subsequent steps involve the ATG12 and the LC3 (microtubule-associated light chain 3) conjugation systems. Both systems promote the elongation of the isolation membrane (Joubert et al., 2009; Rubinsztein et al., 2012).

An important regulator of autophagy is the target of rapamycin (TOR), which inhibits multiple autophagy-promoting

proteins via phosphorylation. TOR is a phosphatidylinositol-related kinase involved in regulatory pathways that control the responses to nutrients and energy metabolism changes. In mammalian cells, mTOR nucleates two structurally and functionally different complexes termed mTORC2, which regulates cytoskeleton organization and cell survival, and mTORC1, which is essential to sense and respond to intracellular and extracellular nutrients, amino acids, growth factors, energy, and oxygen levels. In the presence of stimuli, mTORC1 phosphorylates the ULK1 complex, inhibiting autophagy. On the contrary, when mTORC1 is inactive, ULK1 is released and autophagy is initiated (Yang et al., 2005; Huang and Brumell, 2014; Rabanal-Ruiz et al., 2017).

Although autophagy can be induced to control infection upon intracellular pathogen invasion, many pathogens have developed strategies to avoid or subvert autophagy for their own benefit. Bacteria are targets of selective autophagy, a process known as xenophagy. Xenophagy is a mechanism that targets and removes pathogens after cellular invasion (Bauckman et al., 2015; Escoll et al., 2016). It can be induced upon bacterial infection and involves the formation of autophagosomes, which target bacteria and transport them to lysosomes for degradation. Some bacteria can inhibit autophagy signaling pathways, avoid autophagy recognition, inhibit fusion of the autophagosome with the lysosome, or escape targeting by interfering with the autophagy machinery (Gomes and Dikic, 2014; Bauckman et al., 2015).

CD46 acts as an immunomodulatory protein and plays a role in autophagy signaling. CD46 is a glycoprotein expressed on the surface of every nucleated human cell, and it has isoforms that contain one of two short cytoplasmic tails (cyt), cyt-1 or cyt-2, the most abundant CD46 isoform (Meiffren et al., 2010). CD46 is a cellular receptor for several pathogens, including measles virus, human herpes virus 6, adenovírus B and D, group A *Streptococcus* (GAS), and *Neisseria* bacteria (Cattaneo, 2004).

Joubert et al. (2009) demonstrated that CD46 is connected to autophagy. They found an interaction between the scaffold protein GOPC and cyt-1. GOPC contains two coiled-coil domains (CC) and a PDZ domain, and it interacts with cyt-1 through the PDZ domain. GOPC is reported to interact with Beclin-1, (an important molecule in autophagy induction, part of the Vps34 complex) through CC domains. The CD46-cyt-1/GOPC interaction is associated with the autophagosome formation complex Vps34/Beclin-1, recruiting this complex to initiate autophagy (Joubert et al., 2009).

AUTOPHAGY INDUCTION AND ESCAPE

Very little is known about *N. gonorrhoeae*'s interaction with autophagy and its impact on intracellular survival, and recent studies have demonstrated that autophagy does affect the survival of intracellular gonococci. As a consequence of cellular invasion, *N. gonorrhoeae* is targeted by the autophagy pathway: *N. gonorrhoeae* was found within double-membrane autophagic structures by transmission electron microscopy (TEM), suggesting that the gonococcus ended up in autophagosomes (Lu et al., 2019).

Kim et al. (2019) reported that *N. gonorrhoeae* (MS11 strain and only piliated and Opa non-expressing bacteria) infection led to autophagosome formation and activation of autophagy in the endocervical cell lines ME180 and Hec1B, induced through CD46-cyt1/GOPC in host cells. The gonococcus interacts with CD46-cyt1 via the Type IV pilus (Tfp), recruiting CD46-cyt1 at the site of infection (**Figure 1**). Thus, *N. gonorrhoeae* stimulates matrix metalloproteinases, which are host extracellular sheddases that cleave the CD46-cyt1 ectodomain. After the cleavage of the CD46-cyt1 ectodomain, the presenilin/γ-secretase complex, a host membrane protease complex that modifies type I transmembrane protein function and signaling, cleaves the transmembrane domain, resulting in the release of the cytoplasmic domain. Consequently, this complex gradually reduces the pool of intracellular CD46-cyt1, which decreases the ability of infected cells to initiate autophagy (Weyand et al., 2010).

Autophagosome maturation and fusion with the lysosome is inhibited by *N. gonorrhoeae*. Studies have shown that *Legionella pneumophila* (Choy et al., 2012; Arasaki and Tagaya, 2017) and *Mycobacterium tuberculosis* (Vergne et al., 2005) are also able to inhibit autophagosome maturation. Additionally, *N. gonorrhoeae* secrets IgAP, a protein which cleaves the major lysosomal membrane protein LAMP1. IgAP cleaves LAMP1 gradually, remodels lysosomes, and blocks lysosome/autophagosome fusion. This dual interference in the autophagy pathway promotes the survival of *N. gonorrhoeae* until the later stages of infection (Kim et al., 2019).

Lu et al. (2019) quantified intracellular and extracellular bacteria (American Type Culture Collection 49226) in order to evaluate the escape of gonococci from autophagy in HeLa cells. After initial gonococci invasion, the authors added gentamicin in the culture medium to eliminate extracellular bacteria, showing that the extracellular bacteria in the later stages of infection are the subpopulation of the intracellular *N. gonorrhoeae* that survived autophagy degradation and underwent exocytosis, the process through bacteria are transported inside vesicles to extracellular environment. When *N. gonorrhoeae* invades cells, many gonococci end up in autophagosomes for elimination, showing that the autophagy pathway affects gonococcus survival in the early stages of invasion. However, a subpopulation of bacteria evades the autophagy pathway (Lu et al., 2019). In the same study, they found that *N. gonorrhoeae* also activates the autophagy repressor mTORC1 during the intracellular stages, resulting in suppression of autophagy signaling and thus subverting autophagy for its own benefit (**Figure 1**). This strategy is also used by other intracellular pathogens, including *Legionella* sp., *Shigella flexneri,* and *S*almonella *typhimurium* (Ogawa et al., 2005; Choy et al., 2012; Tattoli et al., 2012). In addition, *N. gonorrhoeae* also inhibited autophagosome maturation and autophagolysosome formation in a way independent of mTORC1 activation through a mechanism that remains unclear (Lu et al., 2019).

In order to grow inside epithelial cells, *N. gonorrhoeae* uses host sources to acquire iron, resulting in interruption of iron homeostasis in the cells and liberation of bioavailable iron from ferritin storage compartments. This supports the intracellular

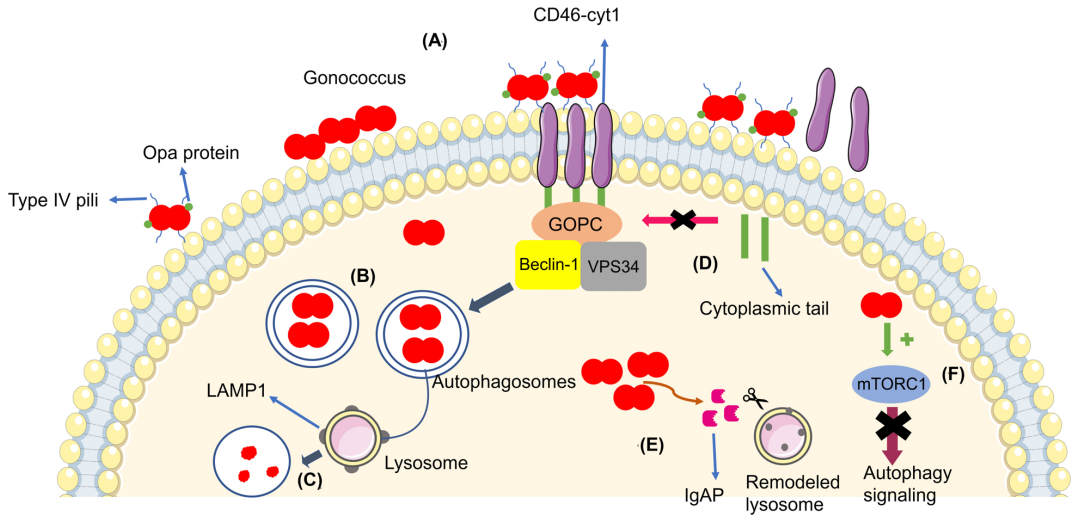

FIGURE 1 | (A) Gonococci (in red) adhere to the cellular membrane and form a microcolony, triggering the autophagy pathway through CD46-cyt1/GOPC, which recruits the Beclin-1/Vps34 complex. **(B)** Bacteria become enveloped in the autophagosome (blue arrow). **(C)** The autophagosome fuses with the lysosome in order to kill the bacteria. **(D)** Gonococci evade the autophagy pathway by inducing the cleavage of the CD46-cyt ectodomain via metalloproteinases and by inducing the cleavage and release of the cytoplasmic tail via presenilin/γ-secretase, decreasing intracellular CD46-cyt1 and the cell's ability to initiate autophagy (pink arrow). **(E)** Bacteria secrete IgAP, (orange arrow) which cleaves LAMP1, resulting in remodeling of the lysosomal membranes and prevention of autophagosome/lysosome fusion, therefore increasing the survival of the gonococci. **(F)** Gonococci activate mTORC1 (green arrow), therefore suppressing autophagy signaling (purple arrow).

growth of *N. gonorrhoeae* in the late stages of infection, since autophagy mediates ferritin degradation. Therefore, the autophagic flux in the early stages of invasion may increase iron availability in the cell, resulting in the growth of intracellular *N. gonorrhoeae* in the later stages of infection (Bonnah et al., 2000; Larson et al., 2004; Dowdle et al., 2014).

Transcytosis is the transit across cellular epithelium monolayers into the subepithelial space by a bacterium and usually requires endocytic recycling and vesicular transport systems. The epithelial invasion of *N. gonorrhoeae* and its transcytosis is related to disseminated gonococcal infection and results in complications. The importance of epithelial cell invasion and transcytosis in uncomplicated infections is not clear and needs further investigation (Quillin and Seifert, 2018).

CONCLUSION

Neisseria gonorrhoeae is already resistant to most antibiotics, which makes the treatment of this disease difficult. In addition, the lack of immunologic memory due to surface antigenic variation complicates the development of an efficient vaccine. Consequently, new studies related to the survival, proliferation, and permanence strategies used by *N. gonorrhoeae* are important. However, studies on the pathogenesis of the bacteria are challenging because *N. gonorrhoeae* is an exclusive human pathogen, which means that it needs specific human proteins to interact and nutrients to grow. As a consequence, animal or culture models that mimic human tissue are needed to better study the pathogenesis of *N. gonorrhoeae*. Some studies have developed such models, although they still have limitations and may not represent all human conditions.

The recent studies of autophagy and *N. gonorrhoeae* infection show that in the early stages of invasion, bacteria survival is impaired by the autophagy pathway. However, in the later stages of infection, some gonococci are capable of subverting autophagy signaling and maintaining the infection. Consequently, targeting specific bacterial proteins related to autophagy inhibition could be another strategy to control the infection. The development of drugs that affect the bacterial-host interactions and not only the bacteria itself would be promising given that it would allow the host innate immune system to respond to the infection upon autophagy reactivation. We can propose, for instance, the development of drug or antibody to antagonize IgAP, which would prevent the blockage of lysosome/autophagosome fusion. Nonetheless, more studies are needed to better understand the interactions between *N. gonorrhoeae* and host autophagy.

AUTHOR CONTRIBUTIONS

AM, MC, BG, and DB conceived and wrote the manuscript.

ACKNOWLEDGMENTS

The authors wish to thank the following funding sources: FAPEMIG (PPM-00604-16), CNPq (404182/2016-0), and CAPES. DB is a recipient of CNPq fellowship. The authors also thank BioMed Proofreading for English language editing of this manuscript.

REFERENCES

Apicella, M. A., Ketterer, M., Lee, F. K. N., Zhou, D., Rice, P. A., and Blake, M. S. (1996). The pathogenesis of gonococcal urethritis in men: confocal and immunoelectron microscopic analysis of urethral exudates from men infected with *Neisseria gonorrhoeae*. *J. Infect.* 173, 636–646. doi: 10.1093/infdis/173.3.636

Arasaki, K., and Tagaya, M. (2017). *Legionella* blocks autophagy by cleaving STX17 (syntaxin 17). *Autophagic Punctum.* 13, 2008–2009. doi: 10.1080/15548627.2017.1371395

Ayala, P., Wilbur, J. S., Wetzler, L. M., Tainer, J. A., Snyder, A., and So, M. (2005). The pilus and porin of *Neisseria gonorrhoeae* cooperatively induce Ca(2+) transients in infected epithelial cells. *Cell Microbiol.* 7, 1736–1748. doi: 10.1111/j.1462-5822.2005.00586.x

Bauckman, K. A., Owusu-Boaitey, N., and Mysorekar, I. U. (2015). Selective autophagy: xenophagy. *Methods* 75, 120–127. doi: 10.1016/j.ymeth.2014.12.005

Binnicker, M. J., Williams, R. D., and Apicella, M. A. (2003). Infection of human urethral epithelium with *Neisseria gonorhoeae* elicits an upregulation of host anti-apoptotic factors and protects cells from staurosporine-induced apoptosis. *Cell Microbiol.* 5, 549–560. doi: 10.1046/j.1462-5822.2003.00300.x

Bonnah, R. A., Lee, S. W., Vasquez, B. L., Enns, C. A., and So, M. (2000). Alteration of epithelial cell transferrin-iron homeostasis by *Neisseria meningitidis* and *Neisseria gonorrhoeae*. *Cell Microbiol.* 2, 207–218. doi: 10.1046/j.1462-5822.2000.00042.x

Britigan, B. E., Cohen, M. S., and Sparling, P. F. (1985). Gonococcal infection: a model of molecular pathogenesis. *N. Engl. J. Med.* 312, 1683–1694. doi: 10.1056/NEJM198506273122606

Cattaneo, R. (2004). Four viruses, two bacteria, and one receptor: membrane cofactor protein (CD46) as pathogens'. *Magnet. J. Virol.* 78, 4385–4388. doi: 10.1128/jvi.78.9.4385-4388.2004

Choy, A., Dancourt, J., Mugo, B., O'Connor, T. J., Isberg, R. R., Melia, T. J., et al. (2012). The *Legionella* effector RavZ inhibits host autophagy through irreversible Atg8 deconjugation. *Science* 338:6110. doi: 10.1126/science.1227026

Dowdle, W. E., Nyfeler, B., Nagel, J., Elling, R. A., Liu, S., Triantafellow, E., et al. (2014). Selective VPS34 inhibitor blocks autophagy and uncovers a role for NCOA4 in ferritin degradation and iron homeostasis in vivo. *Nat. Cell Biol.* 16, 1069–1079. doi: 10.1038/ncb3053

Escoll, P., Rolando, M., and Buchrieser, C. (2016). Modulation of host autophagy during bacterial infection: sabotaging host munitions for pathogen nutrition. *Front. Immunol.* 7:81. doi: 10.3389/fimmu.2016.00081

Fox, D. A., Larsson, P., Lo, R. H., Kroncke, B. M., Kasson, P. M., and Columbus, L. (2014). Structure of the *Neisseria*l outer membrane protein Opa60: loop flexibility essential to receptor recognition and bacterial engulfment. *J. Am. Chem. Soc.* 136, 9938–9946. doi: 10.1021/ja503093y

Gomes, L. C., and Dikic, I. (2014). Autophagy in antimicrobial immunity. *Mol. Cell* 54, 224–233. doi: 10.1016/j.molcel.2014.03.009

Grimley, D. M., Annang, L., Lewis, I., Smith, R. W., Aban, I., Hooks, T., et al. (2006). Sexually transmitted infections among urban shelter clients. *Sex Transm. Dis.* 33, 666–669. doi: 10.1097/01.olq.0000223285.18331.4d

Harvey, H. A., Ketterer, M. R., Preston, A., Lubaroff, D., Williams, R., and Apicella, M. A. (1997). Ultrastructural analysis of primary human urethral epithelial cell cultures infected with *Neisseria gonorrhoeae*. *Infect. Immun.* 65, 2420–2427. doi: 10.1128/iai.65.6.2420-2427.1997

Higashi, D. L., Lee, S. W., Snyder, A., Weyand, N. J., Bakke, A., and So, M. (2007). Dynamics of *Neisseria gonorrhoeae* attachment: microcolony development, cortical plaque formation, and cytoprotection. *Infect. Immun.* 75, 4743–4753. doi: 10.1128/IAI.00687-07

Hook, E. W. III (2012). Gender differences in risk for sexually transmitted diseases. *Am. J. Med. Sci.* 343, 10–11. doi: 10.1097/MAJ.0b013e31823ea276

Huang, J., and Brumell, J. H. (2014). Bacteria-autophagy interplay: a battle for survival. *Nat. Rev. Microbiol.* 12, 101–114. doi: 10.1038/nrmicro3160

Joubert, P. E., Meiffren, G., Grégoire, I. P., Pontini, G., Richetta, C., Flacher, M., et al. (2009). Autophagy induction by the pathogen receptor CD46. *Cell Host Microbe* 6, 354–366. doi: 10.1016/j.chom.2009.09.006

Kim, W. J., Mai, A., Weyand, N. J., Rendón, M. A., Van Doorslaer, K., and So, M. (2019). *Neisseria gonorrhoeae* evades autophagic killing by downregulating CD46-cyt1 and remodeling lysosomes. *PLoS Pathog.* 15:e1007495. doi: 10.1371/journal.ppat.1007495

Larson, J. A., Howie, H. L., and So, M. (2004). *Neisseria meningitidis* accelerates ferritin degradation in host epithelial cells to yield an essential iron source. *Mol. Microbiol.* 53, 807–820. doi: 10.1111/j.1365-2958.2004.04169.x

Lee, S. W., Higashi, D. L., Snyder, A., Merz, A. J., Potter, L., and So, M. (2005). PilT is required for PI(3,4,5)P3-mediated crosstalk between *Neisseria gonorrhoeae* and epithelial cells. *Cell Microbiol.* 7, 1271–1284. doi: 10.1111/j.1462-5822.2005.00551.x

Little, J. W. (2006). Gonorrhea: update. *Oral Surg. Oral Med. Oral Pathol. Oral Radiol. Endod.* 101, 137–143. doi: 10.1016/j.tripleo.2005.05.077

Lu, P., Wang, S., Lu, Y., Neculai, D., Sun, Q., and Van Der Veen, S. (2019). A subpopulation of intracellular *Neisseria gonorrhoeae* escapes autophagy-mediated killing inside epithelial cells. *J. Infect.* 219, 133–144. doi: 10.1093/infdis/jiy237

Masi, A. T., and Eisenstein, B. I. (1981). Disseminated gonococcal infection (DGI) and gonococcal arthritis (GCA): II. Clinical manifestations, diagnosis, complications, treatment, and prevention. *Semin. Arthritis Rheum.* 10, 173–197. doi: 10.1016/s0049-0172(81)80002-9

Meiffren, G., Joubert, P. E., Grégoire, I. P., Codogno, P., Rabourdin-Combe, C., and Faure, M. (2010). Pathogen recognition by the cell surface receptor CD46 induces autophagy. *Autophagy* 6, 299–300. doi: 10.4161/auto.6.2.11132

Mosleh, I. M., Boxberger, H. J., Sessler, M. J., and Meyer, T. F. (1997). Experimental infection of native human ureteral tissue with *Neisseria gonorrhoeae*: adhesion, invasion, intracellular fate, exocytosis, and passage through a stratified epithelium. *Infect. Immun.* 65, 3391–3398. doi: 10.1128/iai.65.8.3391-3398.1997

Muzny, C. A., Harbison, H. S., Austin, E. L., Schwebke, J. R., Van Der Pol, B., and Hook, E. W. III (2017). Sexually transmitted infection risk among women is not fully explained by partner numbers. *South Med. J.* 110, 161–167. doi: 10.14423/SMJ.0000000000000621

Ogawa, M., Yoshimori, T., Suzuki, T., Sagara, H., Mizushima, N., and Sasakawa, C. (2005). Escape of Intracellular *Shigella* from Autophagy. *Science* 307:5710. doi: 10.1126/science.1106036

Parzych, K. R., and Klionsky, D. J. (2014). An overview of autophagy: morphology, mechanism, and regulation. *Antioxid. Redox Sign.* 20, 460–473. doi: 10.1089/ars.2013.5371

Pearce, W. A., and Buchanan, T. M. (1978). Attachment role of gonococcal pili. Optimum conditions and quantitation of adherence of isolated pili to human cells in vitro. *J. Clin. Invest.* 61, 931–943. doi: 10.1172/JCI109018

Quillin, S. J., and Seifert, H. S. (2018). *Neisseria gonorrhoeae* host adaptation and pathogenesis. *Nat. Rev. Microbiol.* 16, 226–240. doi: 10.1038/nrmicro.2017.169

Rabanal-Ruiz, Y., Otten, E. G., and Korolchuk, V. I. (2017). MTORC1 as the main gateway to autophagy. *Essays Biochem.* 61, 565–584. doi: 10.1042/EBC20170027

Rowley, J., Hoorn, S. V., Korenromp, E., Low, N., Unemo, M., Abu-Raddad, L. J., et al. (2019). Chlamydia, gonorrhoea, trichomoniasis and syphilis: global prevalence and incidence estimates, 2016. *Bull. World Health Organ.* 97, 548–562. doi: 10.2471/BLT.18.228486

Rubinsztein, D. C., Shpilka, T., and Elazar, Z. (2012). Mechanisms of autophagosome biogenesis. *Curr. Biol.* 22, R29–R34. doi: 10.1016/j.cub.2011.11.034

Sandstrom, I. (1987). Etiology and diagnosis of neonatal conjunctivitis. *Acta. Paediatrica.* 79, 221–227. doi: 10.1111/j.1651-2227.1987.tb10451.x

Stein, D. C., LeVan, A., Hardy, B., Wang, L. C., Zimmerman, L., and Song, W. (2015). Expression of opacity proteins interferes with the transmigration of *Neisseria gonorrhoeae* across polarized epithelial cells. *PLoS One* 10:e013434. doi: 10.1371/journal.pone.013434

Stern, A., Brown, M., Nickel, P., and Meyer, T. F. (1986). Opacity genes in *Neisseria gonorrhoeae*: control of phase and antigenic variation. *Cell* 47, 61–71. doi: 10.1016/0092-8674(86)90366-1

Swanson, K. V., Griffiss, J. M., Edwards, V. L., Stein, D. C., and Song, W. (2011). *Neisseria gonorrhoeae*-induced transactivation of EGFR enhances gonococcal invasion. *Cell. Microbiol.* 13, 1078–1790. doi: 10.1111/j.1462-5822.2011.01603.x

Tattoli, I., Philpott, D. J., and Girardin, S. E. (2012). The bacterial and cellular determinants controlling the recruitment of mTOR to the *Salmonella*-containing vacuole. *Biol. Open* 1, 1215–1225. doi: 10.1242/bio.20122840

van Putten, J. P., and Paul, S. M. (1995). Binding of syndecan-like cell surface proteoglycan receptors is required for *Neisseria gonorrhoeae* entry into human mucosal cells. *EMBO J.* 14, 2144–2154. doi: 10.1002/j.1460-2075.1995.tb07208.x

Vergne, I., Chua, J., Lee, H. H., Lucas, M., Belisle, J., and Deretic, V. (2005). Mechanism of phagolysosome biogenesis block by viable *Mycobacterium tuberculosis*. *Proc. Natl. Acad. Sci. U.S.A.* 102, 4033–4038. doi: 10.1073/pnas.0409716102

Weyand, N. J., Calton, C. M., Higashi, D. L., Kanack, K. J., and So, M. (2010). Presenilin/gamma-secretase cleaves CD46 in response to *Neisseria* infection. *J. Immunol.* 184, 694–701. doi: 10.4049/jimmunol.0900522

World Health Organization [WHO] (2017). *WHO Publishes List of Bacteria for Which New Antibiotics are Urgently Needed*. Avaiable online at: https://www.who.int/medicines/news/bacteria-antibiotics-needed/en/ (accessed April 20, 2020).

Yang, Y. P., Liang, Z. Q., Gu, Z. L., and Qin, Z. H. (2005). Molecular mechanism and regulation of autophagy. *Acta Pharmacol. Sin.* 26, 1421–1434. doi: 10.1111/j.1745-7254.2005.00235.x

Zhang, J., Li, H., Wang, J., Dong, Z., Mian, S., and Yu, F. S. (2004). Role of EGFR transactivation in preventing apoptosis in *Pseudomonas aeruginosa*-infected human corneal epithelial cells. *Invest. Ophthalmol. Vis. Sci.* 45, 2569–2576. doi: 10.1167/iovs.03-1323

Conflict of Interest: The authors declare that the research was conducted in the absence of any commercial or financial relationships that could be construed as a potential conflict of interest.

frontiers in Cell and Developmental Biology

MINI REVIEW
published: 10 June 2020
doi: 10.3389/fcell.2020.00396

The Parasitic Intracellular Lifestyle of Trypanosomatids: Parasitophorous Vacuole Development and Survival

*Marina Ferreira Batista†, Carlos Alcides Nájera†, Isabela Meneghelli† and Diana Bahia**

Departamento de Genética, Ecologia e Evolução, Instituto de Ciências Biológicas, Universidade Federal de Minas Gerais, Belo Horizonte, Brazil

The trypanosomatid (protozoan) parasites *Trypanosoma cruzi* and *Leishmania* spp. are causative agents of Chagas disease and *Leishmaniasis*, respectively. They display high morphological plasticity, are capable of developing in both invertebrate and vertebrate hosts, and are the only trypanosomatids that can survive and multiply inside mammalian host cells. During internalization by host cells, these parasites are lodged in "parasitophorous vacuoles" (PVs) comprised of host cell endolysosomal system components. PVs effectively shelter parasites within the host cell. PV development and maturation (acidification, acquisition of membrane markers, and/or volumetric expansion) precede parasite escape from the vacuole and ultimately from the host cell, which are key determinants of infective burden and persistence. PV biogenesis varies, depending on trypanosomatid species, in terms of morphology (e.g., size), biochemical composition, and parasite-mediated processes that coopt host cell machinery. PVs play essential roles in the intracellular development (i.e., morphological differentiation and/or multiplication) of *T. cruzi* and *Leishmania* spp. They are of great research interest as potential gateways for drug delivery systems and other therapeutic strategies for suppression of parasite multiplication and control of the large spectrum of diseases caused by these trypanosomatids. This mini-review focuses on mechanisms of PV biogenesis, and processes whereby PVs of *T. cruzi* and *Leishmania* spp. promote parasite persistence within and dissemination among mammalian host cells.

Keywords: *Trypanosoma cruzi*, *Leishmania*, vacuole, parasitophorous vacuole, intracellular pathogen

OPEN ACCESS

Edited by:
Si-Yang Huang,
Yangzhou University, China

Reviewed by:
Wanderley De Souza,
Federal University of Rio de Janeiro, Brazil
Rubem Figueiredo Sadok Menna-Barreto,
Oswaldo Cruz Foundation (Fiocruz), Brazil

****Correspondence:***
Diana Bahia
dianabahia@hotmail.com

†These authors share first authorship

Specialty section:
This article was submitted to Molecular Medicine, a section of the journal Frontiers in Cell and Developmental Biology

Received: *13 February 2020*
Accepted: *29 April 2020*
Published: *10 June 2020*

Citation:
Batista MF, Nájera CA, Meneghelli I and Bahia D (2020) The Parasitic Intracellular Lifestyle of Trypanosomatids: Parasitophorous Vacuole Development and Survival. Front. Cell Dev. Biol. 8:396. doi: 10.3389/fcell.2020.00396

INTRODUCTION

Trypanosoma cruzi and *Leishmania* spp. are evolutionarily closely related trypanosomatid protozoan parasites and the causative agents of Chagas disease and leishmaniasis, respectively, (Chagas, 1909; Brener, 1997; Harmer et al., 2018). These are classified by WHO as neglected tropical diseases (NTDs), and collectively affect over 20 million people worldwide – mainly populations living in remote, poorly developed areas (WHO, 2020a,b). *T. cruzi* and *Leishmania* spp. have complex and distinctive life cycles, and both are transmitted by insect vectors (triatomine bugs and phlebotomine flies, respectively) to various mammalian species (including humans) that act as persistent hosts (Ashford, 2000; Zingales et al., 2012; Kaufer et al., 2017). Trypanosomatids display remarkable plasticity in adapting to distinctive host organisms and environments, and in adapting and developing resistance to the action of drugs intended to control infection,

thus presenting a challenge to any therapeutic strategy (Genois et al., 2014; Reis-Cunha et al., 2015; Laffitte et al., 2016; Reis-Cunha et al., 2018; Kaufer et al., 2019). Such adaptability is based on morphological and biochemical changes. For example, *T. cruzi* has five morphologically distinct developmental forms: non-infectious multiplicative epimastigote and infectious less-replicative metacyclic trypomastigote forms that colonize the insect vector, an intracellular amastigote form that multiplies within mammalian host cells, and infectious extracellular amastigote and trypomastigote forms that enter the mammalian host bloodstream (Lima et al., 2010; Ferreira et al., 2012).

Leishmania spp. have two clearly defined developmental forms: promastigote forms that colonize insect vectors (divided into non-infectious procyclic and infectious metacyclic subgroups), and amastigote forms that multiply within mammalian host cells (primarily macrophages; Tomlinson et al., 1995; Kaufer et al., 2017). The host cell interior is thus an important developmental environment for trypanosomatids, and they have developed various strategies for entering host cells. For this purpose, *T. cruzi* can utilize "passive" pathways such as endocytosis (Mortara et al., 2005, 2008; de Souza et al., 2010; Fernandes et al., 2015), or "active" parasite-mediated invasive pathways such as actin depolymerization induced in either phagocytic or non-phagocytic cells by extracellular amastigotes (Mortara, 1991; Mortara et al., 2008; Caradonna and Burleigh, 2011; Fernandes et al., 2013, 2015) or induction of lysosome-mediated membrane repair that promotes internalization (Fernandes et al., 2011).

In contrast, entry of *Leishmania* spp. into host cells occurs mainly via endocytosis, primarily by "professional phagocytes" such as macrophages and neutrophils. Neutrophils act as "Trojan horses," they deliver parasites into host cells after being phagocytosed by macrophages (Farah et al., 1975; Chang and Dwyer, 1976; Ribeiro-Gomes et al., 2004). In addition, *Leishmania amazonensis* was recently reported to enter non-phagocytic cells (e.g., fibroblasts) using a Ca^{2+}-dependent mechanism similar to one utilized by *T. cruzi*, involving membrane damage and repair via lysosomal exocytosis (Fernandes et al., 2015; Cavalcante-Costa et al., 2019).

Following cell invasion, intracellular obligate parasites use various strategies to withstand host cell immune responses and persist in the host cell. One such strategy, commonly observed in medically relevant infectious diseases, is formation of pathogen-containing vacuoles within host cells after pathogen internalization. Among trypanosomatids, only *T. cruzi* and *Leishmania* spp. are intracellular parasites of mammals.

After entering host cells, they are sheltered within a type of vacuole termed "parasitophorous vacuoles" (PVs), an essential preliminary step in further intracellular development of the parasites. PVs act as filters for nutrients to the detriment of host cell immune response factors, creating a niche for parasite differentiation, and/or multiplication. PVs also function as intermediary chambers facilitating development of parasites until they reach the cell cytoplasm, where they multiply and then exit the host cell (the case for *T. cruzi*; Basu and Ray, 2005; Barrias et al., 2013 for reviews), or until they are transferred safely from cell to cell without contacting the extracellular milieu (the case for *L. amazonensis*; Real et al., 2014). This mini-review focuses on mechanisms of PV biogenesis, and processes whereby PVs of *T. cruzi* and *Leishmania* spp. promote parasite persistence within and dissemination among mammalian host cells.

PARASITOPHOROUS VACUOLE DEVELOPMENT IN TRYPANOSOMATIDS IS AN EVOLUTIONARY ADAPTATION FOR INTRACELLULAR PARASITISM

Trypanosomatids, in their evolutionary history, were initially non-parasitic free-living organisms, as evidenced by their common ancestor *Bodo saltans*, and subsequently underwent selective pressure leading to development of the capacity to colonize host organisms, as either extracellular or intracellular parasites (Jaskowska et al., 2015). Ability to live inside host cells was a key evolutionary adaptation toward parasitism in mammalian hosts. For example, *T. brucei* (which is more closely related to *T. cruzi* than to *Leishmania*) does not require an intracellular/vacuolar environment in order to parasitize mammals, and exists exclusively as an extracellular parasite in the bloodstream of its mammalian host during its life cycle (Stevens et al., 1998; Hamilton et al., 2007). Adaptation to such an intracellular lifestyle has apparently involved genome reduction during the evolutionary history of many parasitic microorganisms (Casadevall, 2008). Genomes of the PV-forming intracellular parasites *Leishmania* spp. and *T. cruzi* are smaller than those of extracellular parasites such as *T. brucei*, indicating that PV biogenesis was a later adaptation that was beneficial to previously exclusively extracellular parasites (Jaskowska et al., 2015). *T. cruzi* likely appeared earlier than *Leishmania* spp. during trypanosomatid evolutionary history, which could account for the persistence of *T. cruzi* in mammalian host organisms as both extracellular (like *T. brucei*) and intracellular forms (like *Leishmania* spp.). From an evolutionary point of view, PV biogenesis may be a refined adaptation for parasitism that enhanced the fitness of trypanosomatid parasites involved in medically relevant pathologies.

Although both *T. cruzi* and *Leishmania* spp. depend on PV development to persist inside host cells, the former is sheltered transiently by PVs and then is released to host cell cytosol where it multiplies, whereas the latter is sheltered permanently by PVs throughout its intracellular life cycle, and multiplies within PVs (Fernandes et al., 2011; Fernandes and Andrews, 2012). Its release from these PVs to cytoplasm depends on an acid pH-dependent signaling event promoted by lysosome recruitment toward PV; this leads to parasite exit into cytosol, where they differentiate into replicative amastigote forms and multiply (Ley et al., 1990; Andrade and Andrews, 2004; Fernandes and Andrews, 2012). *Leishmania* spp., on the other hand, take advantage of PVs to differentiate into amastigotes and also to multiply. Analogously to the diverse spectrum of disease outcomes in leishmaniasis (Burza et al., 2018), PVs of *Leishmania* spp. display diverse morphologies depending on species: the great majority of *Leishmania* spp. (including *L. major* and *L. donovani*) develop

in single compact PVs, whereas members of the *L. mexicana* complex (*L. amazonensis*, *L. mexicana*) multiply within larger PVs (Real and Mortara, 2012).

Thus, PVs are customized to fulfill the requirements of parasites for their intracellular development, as reflected by the construction of doubly infected, chimeric PVs, i.e., single pathogen-containing vacuoles that host different parasite species simultaneously. In a model system of chimeric vacuoles hosting *L. amazonensis* amastigotes (primo-infection) and *L. major* promastigotes (superinfection), the latter was unable to differentiate into amastigote form (Real et al., 2010). In another model of chimeric vacuoles using *L. amazonensis* large PVs as recipient vacuoles for *T. cruzi*, the latter differentiated into replication-competent amastigote forms not in cytosol but within phagolysosome-like *L. amazonensis* large PVs, indicating that trypomastigote-to-amastigote differentiation of *T. cruzi* occurs under the acidic pH of PVs and precedes the release from PV to cytosol (Pessoa et al., 2016). This finding is consistent with previous reports that PV alkalinization impairs parasite PV escape (Ley et al., 1990; Stecconi-Silva et al., 2003). Rather than being released from PVs (as *T. cruzi* does), *Leishmania* spp. remain associated with PVs even during cell-to-cell parasite spreading. *L. amazonensis* takes advantage of host macrophage apoptosis to transfer from macrophage to macrophage *in vitro*, and remains associated with host lysosomal components on its surface that trigger anti-inflammatory cytokine production by recipient non-apoptotic macrophages (Real et al., 2014). PVs thus provide an additional shelter from the extracellular milieu and immune system surveillance, and participate in the late intracellular life cycle of parasites; i.e., egress from host cells and reinfection of new ones.

PARASITOPHOROUS VACUOLAR BIOGENESIS AND MAINTENANCE DEPEND ON HOST CELL MACHINERY

Several parasite species utilize a strategy based on formation of a specifically designed, customized PV during the process of cell infection. Intracellular persistence of trypanosomatids depends on several host-related features. In contrast to various intracellular pathogens that interfere with phagosome maturation to avoid transport to lysosomes, *Leishmania* spp. and *T. cruzi* recruit lysosome markers during the process of infection, and need an acidic environment to maintain their intracellular life cycle. This strategy requires that the parasites remodel and subvert the host endolysosomal pathway to benefit themselves.

In cells infected with *L. amazonensis*, an exchange of biomolecules (e.g., lipids, proteins, and sialoglycoproteins) between cells and parasites was observed following contact. The PV was labeled with the same molecular markers of the parasite, indicating that in addition to host cell internalized components, there is a shedding of proteins from the intracellular parasites to PV (Henriques and De Souza, 2000). Henriques et al. (2003) confirmed the transfer of lipids by labeling macrophages with ^{32}P and then exposing the cells to *L. amazonensis*. The main phospholipid component of PV was phosphatidylcholine. Changes were observed in PV protein composition in relation to time of infection and morphological form of the parasite (Henriques et al., 2003).

Gagnon et al. (2002) showed, based on observation of calnexin markers, that endoplasmic reticulum (ER) participates in formation of phagosomes in macrophages, by fusion with plasmatic membrane during early phagocytosis and its subsequent maturation. Entry of pathogens such as *L. donovani* into macrophages evidently required ER proteins such as calnexin and calreticulin, indicating participation of ER in the internalization process. Similarly, Canton et al. (2012) showed that ER elements are involved in PV formation in *L. amazonensis*, through action of SNARE protein.

Leishmania donovani also is able to upregulate Rab5a, an early endosome protein. The parasite retains Rab5a, along with its effector protein EEA1, in PVs, thereby forming and maintaining an early endosome compartment and delaying maturation (Verma et al., 2017). Such delay is observed in many other *Leishmania* species and is mediated by parasite surface components such as lipophosphoglycan (LPG; Lodge and Descoteaux, 2005), favoring differentiation into amastigote forms of promastigotes otherwise sensitive to the harsh environment of fully matured phagolysosomal vacuoles. In contrast, *L. amazonensis* acquires Rab5a and EEA1 soon after internalization but does not maintain these early endosome markers; rather, it rapidly acquires late endosome and lysosome markers (Courret et al., 2002; reviewed by Veras et al., 2019). For *L. amazonensis* (and possibly other members of the *L. mexicana* complex), PV maturation in terms of acquisition of lysosomal membrane markers and content is accompanied by a striking increase in PV volumetric size, which is dependent on host cell factors such as lysosomal traffic regulator LYST/Beige (Wilson et al., 2008), CD36 receptor (Okuda et al., 2016), and V-ATPase subunit d isoform 2 (ATP6V0d2; Pessoa et al., 2019). Lysosome marker recruitment and PV enlargement are impaired when the host cell lacks CD36 receptor, thereby impairing parasite multiplication as well (Okuda et al., 2016). In another mechanism possibly involving CD36, ATP6V0d2 knockdown depletes macrophage cholesterol and inhibits PV enlargement without impairing parasite multiplication (Pessoa et al., 2019). Increase of cholesterol level by addition of oxidized low-density lipoprotein (ox-LDL), of which CD36 is the receptor, results in PV enlargement and impaired parasite multiplication.

Initial parasite-host cell interaction leading to parasite internalization involves recognition of conserved parasite components, termed pathogen-associated molecular patterns (PAMPs), by host pattern recognition receptors (PRRs); the parasites then take advantage of adhesion to host cells to access safe intracellular environments (Bahia et al., 2018). Such interaction modifies cellular signaling pathways and thereby determines parasite fate. Activation of host signaling pathways [phosphatidylinositol-3-kinase/protein kinase C (PI3K/PKC) – mTOR pathway and endolysosomal pathway for *T. cruzi*; phagocytic pathway for *Leishmania* spp.] leads to parasite internalization and PV formation (Romano et al., 2009; Martins et al., 2011; Salassa and Romano, 2018; Ferreira et al., 2019).

Trypanosoma cruzi endocytic entry into non-professional phagocytic cells has been clearly shown to require lysosome recruitment (Meirelles et al., 1987; Carvalho and de Souza, 1989) and actin reorganization (Rosestolato et al., 2002). Metacyclic and culture-derived trypomastigote forms both depend on transient presence of Ca^{2+} during entry into cells driven by parasite surface molecules (gp82- MT/oligopeptidase B-CDT; Yoshida, 2006). Intact microtubule machinery is essential for *T. cruzi* internalization (Rodriguez et al., 1996; Rosestolato et al., 2002). During *T. cruzi* infection, microtubules play a role in directing lysosomes to PVs, which act as sites of microtubule organization (Tyler et al., 2005).

PV establishment in *T. cruzi* is directly related to its mechanism of entry into cells. Internalization of *T. cruzi* in non-phagocytic cells clearly depends on early lysosomal exocytosis to parasite infection sites (Tardieux et al., 1992). Following parasite-induced plasma membrane damage, membrane repair is stimulated via lysosomal exocytosis, and *T. cruzi* takes advantage of this process to enter the cell (Fernandes et al., 2011). Woolsey et al. (2003) demonstrated that trypomastigotes can also utilize a different invasion route which is dependent on phosphatidylinositol 3-phosphate (PIP-3) plasma membrane-associated molecules in non-phagocytic cells. Only 20% of the analyzed parasite population presented early endosomal markers (e.g., EEA1), in contrast to the 50% of the population that invaded via class I phosphatidylinositol-3-kinases (PI3K)-mediated PI3-P accumulation. These findings indicate that the main endocytic internalization pathway of *T. cruzi* in non-professional phagocytic cells does not require lysosomal exocytosis, contrary to previously proposed mechanisms.

Parasitophorous vacuole features formed during these two processes are distinctive. In the lysosome-dependent pathway (early lysosome fusion), Ca^{2+}-dependent exocytosis of lysosomes is activated and lysosomes fuse with nascent PVs (Tardieux et al., 1992; Fernandes et al., 2011). In contrast, in the lysosome-independent pathway (late lysosome fusion), parasite entry occurs through membrane invagination resulting from PIP3 accumulation, and lysosome markers are acquired only during PV maturation (Woolsey et al., 2003).

In HeLa cells, extracellular amastigotes induce PI3K pathway to promote rearrangement of actin cytoskeleton and their own phagocytosis (Ferreira et al., 2019). This process likely interferes with PV formation, although the mechanism remains unclear.

Martins et al. (2011) showed that both metacyclic and culture-derived trypomastigotes elicit lysosome recruitment during invasion by activating autophagy-related signaling pathways. Parasite surface glycoprotein gp82 and host actin remodeling are required for induction of lysosome recruitment to plasma membrane during metacyclic invasion through activation of PI3K/PKC-mTOR pathway (Martins et al., 2011). In contrast, invasion of culture-derived trypomastigotes depends on activation of autophagy-related proteins ATG5 and Beclin, independently of mTOR pathway (Romano et al., 2009; **Figure 1**).

Host autophagy processes, in addition to regulating invasion, have been shown to affect PV maturation (Ghartey-Kwansah et al., 2020). In *L. donovani*, both canonical and non-canonical autophagy are triggered, at different infection time points (Pitale et al., 2019). Salassa and Romano (2018) suggested that autophagy is involved in PV maturation in *T. cruzi* infection, based on observed recruitment of LC3 (an autophagosome marker) to PV. Confirmation of this idea will require elucidation of the process involved. e.g., canonical autophagy, xenophagy, or LC3-associated phagocytosis (Salassa and Romano, 2018).

Intracellular parasites exploit host membrane resources and organelles to promote PV maintenance and maturation, in order to complete their life cycle. Reignault et al. (2019) observed formation of PVs during the first 2 h (not later times) of internalization by peritoneal macrophages of *T. cruzi* amastigotes and trypomastigotes. Electron microscopic and 3D reconstruction techniques indicated that during biogenesis of *T. cruzi* PVs, ER and lysosomes act as membrane donors for generation of PVs. Morphological changes were observed in cellular distribution of Golgi complex and mitochondria during PV biogenesis; these organelles moved from the perinuclear region to the PV vicinity. No membrane fusion with Golgi complex or mitochondria was observed; however, it is conceivable that both organelles function in synchrony with PV development, in view of their proximity. In the context of PV development, the observed exchange of membranes between parasite and PV suggest occurrence of emergent signaling pathways between parasite and host cell, and indicate involvement of the host actin cytoskeleton, which surrounds the PV from its biogenesis until its rupture (Reignault et al., 2014, 2019).

Lysosome-mediated PV acidification is necessary for both PV maturation and trypomastigote-to-amastigote differentiation; it enables proper functioning of parasite-derived Tc-TOX protein (de Souza et al., 2010). Carvalho and de Souza (1989) were the first to suggest a *T. cruzi* mechanism of PV dissolution. Stecconi-Silva et al. (2003) demonstrated later that Tc-TOX induces formation of pores to degrade PV membrane, thereby promoting parasite release into host cell cytoplasm.

TRYPANOSOMATID STRATEGIES FOR OVERCOMING HOST CELL DEFENSES

Intracellular parasites are able to persist and overcome host cell defense mechanisms through a variety of strategies, e.g., secreting proteins, hijacking host proteins, and recruiting host proteins/structures. Certain parasite-derived factors have been implicated in subversion of host cell functions.

Lipophosphoglycan, a glycoconjugated virulence factor on *Leishmania* spp. surfaces, enhances parasite survival by targeting host defense proteins. During *L. donovani* phagocytosis, LPG delays PV maturation by inducing F-actin depolymerization around the PV site, resulting in inhibition of vesicular trafficking holding (e.g., lack of LAMP-1 marker; Winberg et al., 2009), and of recruitment to PV of protein kinase Cα (PKCα), a kinase involved in F-actin degradation and regulation of PV development (Holm et al., 2001). GP63, another virulence factor, is a metalloprotease surface protein that interferes with PV acidification. da Silva Vieira et al. (2019) reported that GP63 and

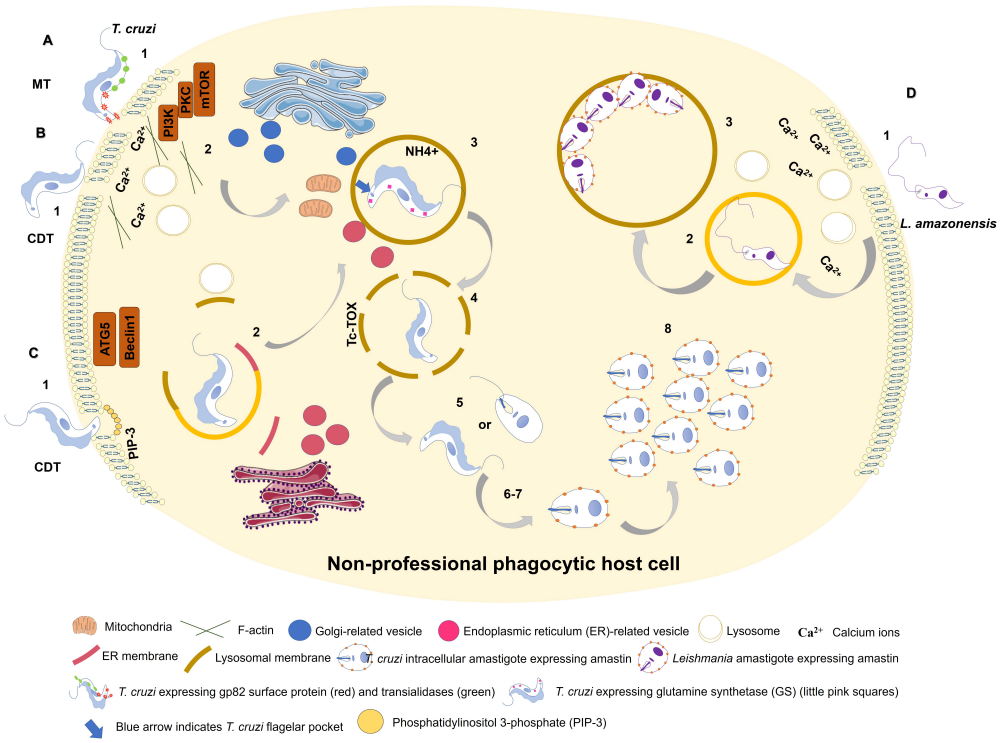

FIGURE 1 | Entry of *Trypanosoma cruzi* metacyclic trypomastigote (MT) forms into non-professional phagocytic cell **(A)**. 1: MT entry requires parasite surface protein gp82 and recruitment of lysosomes to the infection site in a Ca^{2+}-dependent manner. 2: MT invasion activates PI3K/PKC-mTOR signaling and F-actin disruption. 3: Acidic parasitophorous vacuole is formed as *T. cruzi* begins internalization. Mitochondria are localized near flagellar pocket (blue arrow). *T. cruzi* vacuolar closure and maturation/acidification involve continuous communication with ER/Golgi vesicles. Glutamine synthetase (GS) controls pH by regulating $NH4^+$ vacuolar content (small pink squares). 4: *T. cruzi* vacuolar degradation. 5: *T. cruzi* vacuolar escape into cytoplasm. MT form remains intact, or an intermediate form between MT and intracellular amastigote (IA) is present. 6: *T. cruzi* extravacuolar differentiation into IA forms. 7: Free *T. cruzi* IA in cytoplasm. 8: *T. cruzi* IA cytoplasmic replication. *T. cruzi* culture-derived trypomastigote (CDT) invasion by lysosome-dependent pathway (early lysosome fusion; **B)**. 1: CDT induces membrane damage. 2: CDT requires parasite oligopeptidase B surface protein and recruitment of lysosomes to the infection site in a Ca^{2+}-dependent manner. F-actin disruption also plays a role in CDT invasion. 3-8: Similar to **(A)**. *T. cruzi* culture-derived trypomastigote (CDT) invasion by lysosome-independent pathway (late lysosome fusion; **C)**. 1: CDT invades by membrane invagination resulting in a PI3K-dependent PIP3 accumulation. In deprivation of nutrients host cell increases CDT internalization through ATG5/Beclin1 pathway. 2: lysosome markers are acquired only during PV maturation. ER membrane is donated to PV during its membrane construction. 3-8: Similar to (A). Model of *L. amazonensis* non-phagocytic cell internalization as proposed by Cavalcante-Costa et al. (2019); **D)**. 1: *L. amazonensis* induces membrane damage and Ca^{2+} recruitment during invasion process. 2: *L. amazonensis* vacuolar formation and maturation. 3: *L. amazonensis* multiplication into large vacuoles.

LPG expression varies in *L. braziliensis*, and that these PV effects are strain-specific (da Silva Vieira et al., 2019).

Certain host ER- and Golgi-localized N-ethylmaleimide-sensitive-factor attachment protein receptors (SNAREs) are related to endosome/lysosome fusion and are coopted by trypanosomatids for PV biogenesis (Ndjamen et al., 2010; Canton and Kima, 2012; Cueto et al., 2017). Vacuoles containing either *L. donovani* or *L. pifanoi* recruit endoplasmic markers such as calnexin and SNARE Sec22b to PV formation sites during phagocytosis (Ndjamen et al., 2010). *L. amazonensis* engages SNAREs (syntaxin-5, Sec22b) that play important roles in PV development; syntaxin-5 inhibition blocked PV enlargement and reduced parasite burden (Canton and Kima, 2012), and Sec22b and syntaxin-5 participated in trafficking of parasite-derived molecules in host cells (Canton and Kima, 2012; Arango Duque et al., 2019).

Leishmania spp. metacyclic promastigotes utilize the host classic exocytic pathway (ER/Golgi complex) to deliver GP63 and LPG from PVs toward the extracellular milieu, thereby affecting parasite persistence (Arango Duque et al., 2019). Casgrain et al. (2016) observed that *L. mexicana* GP63 cleaved VAMP3 and VAMP8, two endocytic SNAREs associated with phagosome biogenesis and function, and helped maintain parasite intracellular development to allow PV expansion. Matte et al. (2016) reported that cleavage of VAMP8 by *L. major* GP63 was associated with inhibition of LC3 recruitment to phagosomes during LC3-associated phagocytosis (LAP). This pathway is typically activated by external particles already contained within a single-membraned phagosome or endosome, and leads to deposition of LC3 on the cytosolic side of the phagosome, thereby promoting more rapid fusion with lysosomes (Evans et al., 2018). Disruption resulting from VAMP8 cleavage impairs host cell antimicrobial machinery (Matte et al., 2016).

In *T. cruzi*, two SNAREs (VAMP3, VAMP7) are recruited to PVs at different times during PV development: VAMP3 appears only in early phases following parasite

internalization, whereas VAMP7 is readily recruited and maintained throughout PV maturation and maintenance, and is essential for parasite invasion and lysosome-PV fusion events (Cueto et al., 2017; **Figure 2**).

Amastin proteins, a family of stage-specific parasite surface factors first described in *T. cruzi* and showing upregulated expression in amastigote forms (Teixeira et al., 1994; Cruz et al., 2012), are reportedly involved in parasite intracellular survival and PV biogenesis (Cruz et al., 2012; de Paiva et al., 2015). The major amastin subfamily in *Leishmania* spp., termed δ-amastins, includes (˜42 isoforms. Genome analysis of *L. amazonensis* showed that amastin subfamilies are species-specific, and show correlations with disease outcomes and PV volumetric size (Real et al., 2013). In *L. braziliensis*, δ-amastin knockdown reduced parasite PV attachment, thereby inhibiting multiplication and release into cytosol both *in vitro* and *in vivo* (Teixeira et al., 1994; de Paiva et al., 2015). *T. cruzi* has a smaller number of δ-amastin gene copies (12 in total) than do *Leishmania* spp. δ-amastin superexpression in *T. cruzi in vitro* was correlated with rapid differentiation of culture-derived trypomastigotes into intracellular amastigote forms, and with host cell egress. Overexpression of δ-amastin in *T. cruzi* extracellular amastigotes *in vivo* led to earlier parasite tropism (relative to wild-type) toward livers of infected mice (Cruz et al., 2012). Thus,

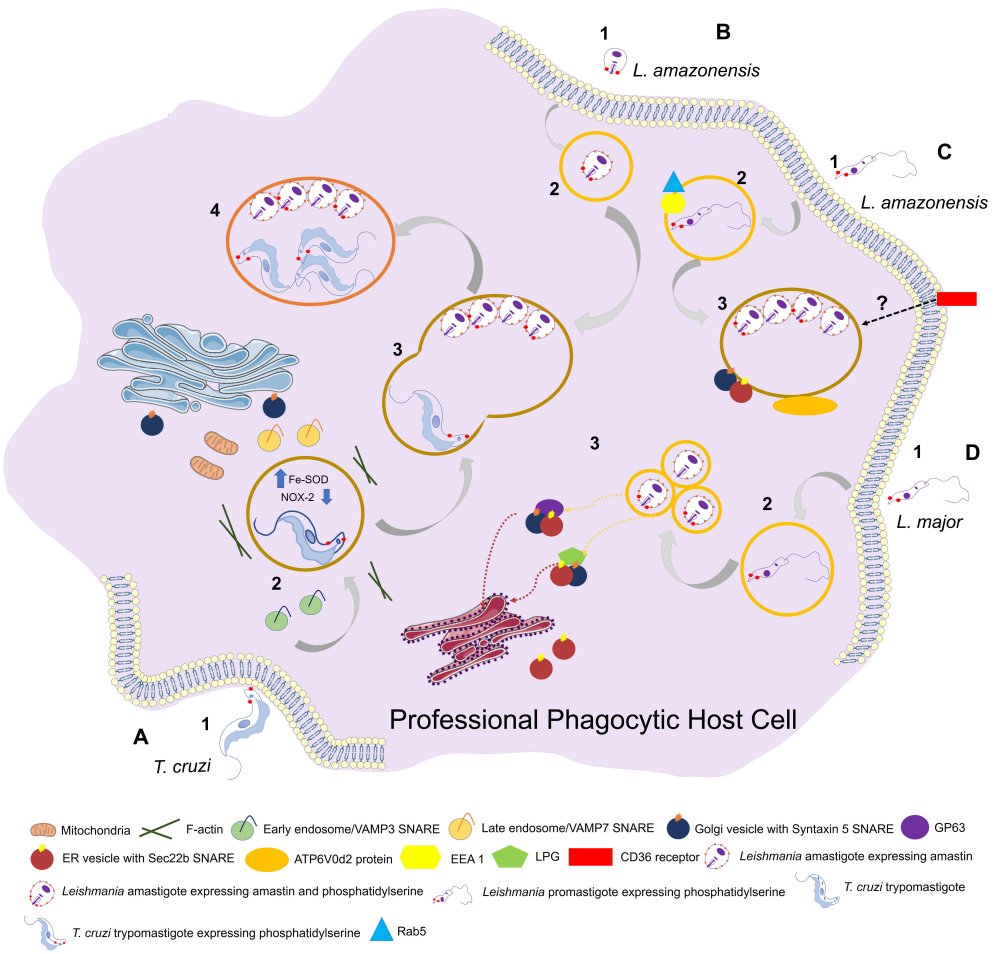

FIGURE 2 | Entry of trypanosomatids in a professional phagocytic cell. **(A)** 1: Uptake of *Trypanosoma cruzi* trypomastigote by phagocytosis. This process can be facilitated through expression of phosphatidylserine (PS) in parasite surface. VAMP3 (SNARE) recruitment to entry site in early-phase infection. 2: *T. cruzi* vacuolar closure and maturation. VAMP7 (SNARE) is recruited and maintained during PV maturation. Parasite uses Fe-SOD to reduce the amount of O_2^- produced by host (NOX-2) inside phagosome. PS exposition creates a permissive state to parasite survival. **(B)** 1: Uptake of *L. amazonensis* amastigote by phagocytosis. 2: *L. amazonensis* vacuolar formation and maturation. 3: *L. amazonensis* and *T. cruzi* vacuolar fusion. 4: Chimeric vacuole formation with *L. amazonensis* amastigotes and *T. cruzi* trypomastigotes. **(C)** 1: Uptake of *L. amazonensis* promastigote by phagocytosis. 2: *L. amazonensis* vacuolar formation and maturation. Rab5 and EEA1 endosome markers are acquired after internalization. 3: *L. amazonensis* multiplication into large vacuoles. ATP6V0d2 subunit of V-ATPase participates in cholesterol influx, an essential process in PV maintenance. Syntaxin 15 and Sec22b are SNAREs that play important roles in PV development. **(D)** 1: Uptake of *L. major* by phagocytosis. 2: *L. major* vacuolar formation and maturation. The parasite is developed in a single compact PV. 3: *L. major* multiplication into tight individual vacuoles. Parasite virulence factors GP63 and LPG are transferred to host cell (ER/ERGIC; "ER-Golgi intermediate compartment") by SNAREs. Both promastigotes and amastigotes of *L. amazonesis* and *L. major* can present PS in its surface with the same functions as in *T. cruzi* facilitating parasite phagocytosis and, once the parasite is inside the cell, aiding in its survival.

parasite-derived membrane factors display a wide variety of functions depending on trypanosomatid species, ranging from parasite extracellular morphological development and parasite tropism in host organisms, to intracellular multiplication and PV biogenesis.

Another family of proteins, the trans-sialidases (TSs), also play important roles in parasite-PV interactions. Freire-de-Lima et al. (2015) showed that *T. cruzi* TSs help the parasite salvage host cell sialic acid for its own benefit. Besides their well-documented involvement in adhesion, invasion, and immune modulation, TSs facilitate parasite escape from PVs to cytosol, but the mechanism for this is unclear (Freire-de-Lima et al., 2015, 2017; da Fonseca et al., 2019). *T. cruzi* culture-derived trypomastigotes, in comparison with metacyclic forms, express higher TS levels and escape earlier from PVs throughout their intracellular life cycle, suggesting a link between TSs and PV escape. In infected cells lacking surface sialic acid and lysosome membranes, TS-overexpressing metacyclic forms and culture-derived trypomastigotes with high native TS expression show similar PV escape kinetics (Rubin-de-Celis et al., 2006, Rubin-de-Celis and Schenkman, 2012).

Crispim et al. (2018) showed that the ATP-dependent enzyme glutamine synthetase (GS) is associated with PV evasion in *T. cruzi*. GS regulates the level of metabolites derived from amino acid consumption by converting accumulated $NH4^+$ and glutamate into glutamine. Blocking of GS by methionine sulfoximine (MS) inhibited trypomastigote PV escape into cytoplasm *in vitro*. *T. cruzi* PV escape is associated with acidic pH environment, and GS therefore may regulate intravacuolar $NH4^+$ content and acidification (Crispim et al., 2018). Another enzyme associated with parasite survival within PVs is cytosolic iron superoxide dismutase (Fe-SOD), an $O2^-$ catabolizing enzyme. In *T. cruzi*, Fe-SOD reduces the amount of $O2^-$ produced by host NADPH oxidase (NOX-2) inside phagosomes, thereby counteracting host cell oxidative stress involved in defense against intracellular pathogens. Fe-SOD overexpression in parasites *in vivo* resulted in increased parasitemia and parasite burden in infected mice (Martínez et al., 2019).

Last but not least, recognition of phosphatidylserine (PS) on the membrane surface of apoptotic cells (apoptosis) is necessary for its elimination by phagocytes (endocytosis) without causing inflammation. A reproduction of this mechanism, termed "apoptotic mimicry," is used by some intracellular parasites, including *T. cruzi* (trypomastigote forms) and *Leishmania* spp. (promastigote and amastigote forms), during the invasion process and maintenance of infection. In classical mimicry, the parasite expresses PS in order to be phagocytosed by macrophages, and a permissive state is created by decrease of NO production through induction of cytokines (e.g., TGF-β1; anti-inflammatory cytokine) and synthesis of IL-10, allowing the parasite to survive inside the host cell. In contrast, in non-classical mimicry the host cell expresses PS during the infection process. *Leishmania* spp., for example, initially colonizes a neutrophil and then induces its PS expression in order to be phagocytosed by a macrophage – the ideal host for the parasite. The amount of PS expressed determines the infection capacity of the parasite, and depends on an intrinsic pressure upon the host's immune system (De Freitas Balanco et al., 2001; DaMatta et al., 2007; El-Hani et al., 2012; Wanderley et al., 2020).

CONCLUSION

Trypanosoma cruzi and Leishmania spp. are trypanosomatid pathogens that depend on customized PV niches during the infection process. PV development mechanisms are complex, and vary among parasite species and strains. During evolution, mammalian host cells have adapted to resist invasion of intracellular parasites by establishment of hostile intracellular environments. Development of more efficient therapeutic strategies against Chagas disease and leishmaniasis will require better understanding of the PV processes related to such structural biogenesis, and the mechanisms whereby parasite factors subvert host cell responses.

AUTHOR CONTRIBUTIONS

MB, CN, IM, and DB conceived and wrote the manuscript.

FUNDING

This study was supported by funding from FAPEMIG (PPM-00604-16), CNPq (404182/2016-0), and CAPES. DB is a recipient of a CNPq fellowship.

ACKNOWLEDGMENTS

The authors are grateful to Dr. Fernando Real (Institut Cochin, INSERM U1016, Paris, France) for critical revision of the manuscript, and to Dr. S. Anderson for English editing.

REFERENCES

Andrade, L. O., and Andrews, N. W. (2004). Lysosomal fusion is essential for the retention of *Trypanosoma cruzi* inside host cells. *J. Exp. Med.* 200, 1135–1143. doi: 10.1084/jem.20041408

Arango Duque, G., Jardim, A., Gagnon, E., Fukuda, M., and Descoteaux, A. (2019). The host cell secretory pathway mediates the export of *Leishmania* virulence factors out of the parasitophorous vacuole. *PLoS Pathog.* 15:e1007982. doi: 10.1371/journal.ppat.1007982

Ashford, R. W. (2000). The leishmaniasis as emerging and reemerging zoonoses. *Int. J. Parasitol.* 30, 1269–1281. doi: 10.1016/B978-0-12-803265-7.00007-5

Bahia, D., Satoskar, A. R., and Dussurget, O. (2018). Editorial: cell signaling in host-pathogen interactions: the host point of view. *Front. Immunol.* 9:221. doi: 10.3389/fimmu.2018.00221

Barrias, E. S., de Carvalho, T. M. U., and De Souza, W. (2013). *Trypanosoma cruzi*: entry into mammalian host cells and parasitophorous vacuole formation. *Front. Immunol.* 4:186. doi: 10.3389/fimmu.2013.00186

Basu, M. K., and Ray, M. (2005). Macrophage and *Leishmania*: an unacceptable coexistence. *Crit. Rev. Microbiol.* 31, 145–154. doi: 10.1080/1040841059100510

Brener, Z. (1997). "*Trypanosoma cruzi*: morfologia e ciclo evolutivo," in *Clínica e Terapêutica da Doença de Chagas: uma Abordagem Prática Para o Clínico Geral*, eds J. C. P. Dias and J. R. Coura (Rio de Janeiro: FIOCRUZ), 24–31.

Burza, S., Croft, S. L., and Boeleart, M. (2018). Leishmaniasis. *Lancet* 392, 951–970.

Canton, J., and Kima, P. E. (2012). Targeting host syntaxin-5 preferentially blocks *Leishmania* parasitophorous vacuole development in infected cells and limits experimental *Leishmania* infections. *Am. J. Pathol.* 181, 1348–1355. doi: 10.1016/j.ajpath.2012.06.041

Canton, J., Ndjamen, B., Hatsuzawa, K., and Kima, P. E. (2012). Disruption of the fusion of *Leishmania* parasitophorous vacuoles with ER vesicles results in the control of the infection. *Cell. Microbiol.* 14, 937–948. doi: 10.1111/j.1462-5822.2012.01767.x

Caradonna, K. L., and Burleigh, B. A. (2011). Mechanisms of host cell invasion by *Trypanosoma cruzi*. *Adv. Parasitol.* 76, 33–61. doi: 10.1016/B978-0-12-385895-5.00002-5

Carvalho, T. M. U., and de Souza, W. (1989). Early events related with the behaviour of *Trypanosoma cruzi* within an endocytic vacuole in mouse peritoneal macrophages. *Cell Struct. Funct.* 14, 383–392. doi: 10.1247/csf.14.383

Casadevall, A. (2008). Evolution of intracellular pathogens. *Annu. Rev. Microbiol.* 62, 19–33. doi: 10.1146/annurev.micro.61.080706.093305

Casgrain, P. A., Martel, C., McMaster, W. R., Mottram, J. C., Olivier, M., and Descoteaux, A. (2016). Cysteine peptidase B regulates *Leishmania mexicana* virulence through the modulation of GP63 expression. *PLoS Pathog.* 12:e1005658. doi: 10.1371/journal.ppat.1005658

Cavalcante-Costa, V. S., Costa-Reginaldo, M., Queiroz-Oliveira, T., Oliveira, A. C. S., Couto, N. F., Dos Anjos, D. O., et al. (2019). *Leishmania amazonensis* hijacks host cell lysosomes involved in plasma membrane repair to induce invasion in fibroblasts. *J. Cell Sci.* 132:jcs226183. doi: 10.1242/jcs.226183

Chagas, C. (1909). Nova tripanozomiase humana: estudos sobre a morfolojia e o ciclo evolutivo do *Schizotrypanum cruzi*. Gen., n. Spp., ajente etiolojico de nova entidade morbida do homem. *Mem. Inst. Oswaldo Cruz* 1, 159–218. doi: 10.1590/S0074-02761909000200008

Chang, K. P., and Dwyer, D. M. (1976). Multiplication of a human parasite (*Leishmania donovani*) in phagolysosomes of hamster macrophages in vitro. *Science* 193, 678–680. doi: 10.1126/science.948742

Courret, N., Fréhel, C., Gouhier, N., Pouchelet, M., Prina, E., Roux, P., et al. (2002). Biogenesis of *Leishmania*-harbouring parasitophorous vacuoles following phagocytosis of the metacyclic promastigote or amastigote stages of the parasites. *J. Cell Sci.* 115, 2303–2316.

Crispim, M., Damasceno, F. S., Hernández, A., Barisón, M. J., Sauter, I. P., Pavani, R. S., et al. (2018). The glutamine synthetase of *Trypanosoma cruzi* is required for its resistance to ammonium accumulation and evasion of the parasitophorous vacuole during host-cell infection. *PLoS Negl. Trop. Dis.* 12:e0006170. doi: 10.1371/journal.pntd.0006170

Cruz, M. C., Souza-Melo, N., da Silva, C. V., DaRocha, W. D., Bahia, D., Araújo, P. R., et al. (2012). *Trypanosoma cruzi*: role of δ-amastin on extracellular amastigote cell invasion and differentiation. *PLoS One* 7:e51804. doi: 10.1371/journal.pone.0051804

Cueto, J. A., Vanrell, M. C., Salassa, B. N., Nola, S., Galli, T., Colombo, M. I., et al. (2017). Soluble *N*-ethylmaleimide-sensitive factor attachment protein receptors required during *Trypanosoma cruzi* parasitophorous vacuole development. *Cell. Microbiol.* 19:e12713. doi: 10.1111/cmi.12713

da Fonseca, L. M., da Costa, K. M., Chaves, V. S., Freire-de-Lima, C. G., Morrot, A., Mendonça-Previato, L., et al. (2019). Theft and reception of host cell's sialic acid: dynamics of *Trypanosoma cruzi* trans-sialidases and mucin-like molecules on chagas' disease immunomodulation. *Front. Immunol.* 10:164. doi: 10.3389/fimmu.2019.00164

da Silva Vieira, T. S., Arango Duque, G., Ory, K., Gontijo, C. M., Soares, R. P., and Descoteaux, A. (2019). *Leishmania braziliensis*: strain-specific modulation of phagosome maturation. *Front. Cell. Infect. Microbiol.* 9:319. doi: 10.3389/fcimb.2019.00319

DaMatta, R. A., Seabra, S. H., Deolindo, P., Arnholdt, A. C. V., Manhães, L., Goldenberg, S., et al. (2007). *Trypanosoma cruzi* exposes phosphatidylserine as an evasion mechanism. *FEMS Microbiol. Lett.* 266, 29–33. doi: 10.1111/j.1574-6968.2006.00495.x

De Freitas Balanco, J. M., Costa Moreira, M. E., Bonomo, A., Bozza, P. T., Amarante-Mendes, G., Pirmez, C., et al. (2001). Apoptotic mimicry by an obligate intracellular parasite downregulates macrophage microbicidal activity. *Curr. Biol.* 11, 1870–1873. doi: 10.1016/S0960-9822(01)00563-2

de Paiva, R. M. C., Grazielle-Silva, V., Cardoso, M. S., Nakagaki, B. N., Mendonça-Neto, R. P., Canavaci, A. M. C., et al. (2015). Amastin knockdown in *Leishmania braziliensis* affects parasite-macrophage interaction and results in impaired viability of intracellular amastigotes. *PLoS Pathog.* 11:e1005296. doi: 10.1371/journal.ppat.1005296

de Souza, W., de Carvalho, T. M. U., and Barrias, E. S. (2010). Review on *Trypanosoma cruzi*: host cell interaction. *Int. J. Cell Biol.* 2010:295394. doi: 10.1155/2010/295394

El-Hani, C. N., Borges, V. M., Wanderley, J. L. M., and Barcinski, M. A. (2012). Apoptosis and apoptotic mimicry in *Leishmania*: an evolutionary perspective. *Front. Cell. Infect. Microbiol.* 2:96. doi: 10.3389/fcimb.2012.00096

Evans, R. J., Sundaramurthy, V., and Frickel, E. M. (2018). The interplay of host autophagy and eukaryotic pathogens. *Front. Cell Dev. Biol.* 6:118. doi: 10.3389/fcell.2018.00118

Farah, F. S., Samra, S. A., and Nuwayri, N. S. (1975). The role of the macrophage in cutaneous *Leishmania*sis. *Immunol. Commun.* 29, 755–764.

Fernandes, M. C., and Andrews, N. W. (2012). Host cell invasion by *Trypanosoma cruzi*: a unique strategy that promotes persistence. *FEMS Microbiol. Rev.* 36, 734–747. doi: 10.1111/j.1574-6976.2012.00333.x

Fernandes, M. C., Corrotte, M., Miguel, D. C., Tam, C., and Andrews, N. W. (2015). The exocyst is required for trypanosome invasion and the repair of mechanical plasma membrane wounds. *J. Cell Sci.* 128, 27–32. doi: 10.1242/jcs.150573

Fernandes, M. C., Cortez, M., Flannery, A. R., Tam, C., Mortara, R. A., and Andrews, N. W. (2011). *Trypanosoma cruzi* subverts the sphingomyelinase-mediated plasma membrane repair pathway for cell invasion. *J. Exp. Med.* 208, 909–921. doi: 10.1084/jem.20102518

Fernandes, M. C., Flannery, A. R., Andrews, N. W., and Mortara, R. A. (2013). Extracellular amastigotes of *Trypanosoma cruzi* are potent inducers of phagocytosis in mammalian cells. *Cell. Microbiol.* 15, 977–991. doi: 10.1111/cmi.12090

Ferreira, B. L., Ferreira, É. R., Bonfim-Melo, A., Mortara, R. A., and Bahia, D. (2019). *Trypanosoma cruzi* extracellular amastigotes selectively trigger the PI3K/Akt and Erk pathways during HeLa cell invasion. *Microbes Infect.* 21, 485–489. doi: 10.1016/j.micinf.2019.06.003

Ferreira, E. R., Bonfim-Melo, A., Mortara, R. A., and Bahia, D. (2012). *Trypanosoma cruzi* extracellular amastigotes and host cell signaling: more pieces to the puzzle. *Front. Immunol.* 30:363. doi: 10.3389/fimmu.2012.00363

Freire-de-Lima, L., Fonseca, L. M., Oeltmann, T., Mendonca-Previato, L., and Previato, J. O. (2015). The trans-sialidase, the major *Trypanosoma cruzi* virulence factor: three decades of studies. *Glycobiology* 25, 1142–1149. doi: 10.1093/glycob/cwv057

Freire-de-Lima, L., Gentile, L. B., da Fonseca, L. M., da Costa, K. M., Lemos, J. S., Jacques, L. R., et al. (2017). Role of inactive and active *Trypanosoma cruzi* trans-sialidases on T cell homing and secretion of inflammatory cytokines. *Front. Microbiol.* 8:1307. doi: 10.3389/fmicb.2017.01307

Gagnon, E., Duclos, S., Rondeau, C., Chevet, E., Cameron, P. H., Steele-Mortimer, O., et al. (2002). Endoplasmic reticulum-mediated phagocytosis is a mechanism of entry into macrophages. *Cell* 110, 119–131.

Genois, M., Paquet, E. R., Laffitte, M. N., Maity, R., Rodrigue, A., Ouellette M., and Masson, J. (2014). DNA repair pathways in trypanosomatids: from DNA repair to drug resistance. *Microbiol. Mol. Biol. Rev.* 78, 40–73. doi: 10.1128/MMBR.00045-13

Ghartey-Kwansah, G., Aboagye, B., Adu-Nti, F., Opoku, Y. K., and Abu, E. K. (2020). Clearing or subverting the enemy: role of autophagy in protozoan infections. *Life Sci.* 247:117453. doi: 10.1016/j.lfs.2020.117453

Hamilton, P. B., Gibson, W. C., and Stevens, J. R. (2007). Patterns of co-evolution between trypanosomes and their hosts deduced from ribosomal RNA and protein-coding gene phylogenies. *Mol. Phylogenet. Evol.* 44, 15–25. doi: 10.1016/j.ympev.2007.03.023

Harmer, J., Yurchenko, V., Nenarokova, A., Lukeš, J., and Ginger, M. L. (2018). Farming, slaving and enslavement: histories of endosymbioses during kinetoplastid evolution. *Parasitology* 145, 1311–1323. doi: 10.1017/S0031182018000781

Henriques, C., Atella, G. C., Bonilha, V. L., and De Souza, W. (2003). Biochemical analysis of proteins and lipids found in parasitophorous vacuoles containing *Leishmania amazonensis*. *Parasitol. Res.* 89, 123–133. doi: 10.1007/s00436-002-0728-y

Henriques, C., and De Souza, W. (2000). Redistribution of plasma-membrane surface molecules during formation of the *Leishmania amazonensis*-containing parasitophorous vacuole. *Parasitol. Res.* 86, 215–225. doi: 10.1007/s004360050034

Holm, A., Tejle, K., Magnusson, K. E., Descoteaux, A., and Rasmusson, B. (2001). *Leishmania donovani* lipophosphoglycan causes periphagosomal actin accumulation: correlation with impaired translocation of PKCα and defective phagosome maturation. *Cell. Microbiol.* 3, 439–447. doi: 10.1046/j.1462-5822.2001.00127.x

Jaskowska, E., Butler, C., Preston, G., and Kelly, S. (2015). *Phytomonas*: trypanosomatids adapted to plant environments. *PLoS Pathog.* 11:e1004484. doi: 10.1371/journal.ppat.1004484

Kaufer, A., Ellis, J., Stark, D., and Barratt, J. (2017). The evolution of trypanosomatid taxonomy. *Parasit. Vectors* 10:287.

Kaufer, A., Stark, D., and Ellis, J. (2019). Evolutionary insight into the trypanosomatidae using alignment-free phylogenomics of the kinetoplast. *Pathogens* 8:157. doi: 10.3390/pathogens8030157

Laffitte, M. N., Leprohon, P., Papadopoulou, B., and Ouelletteb, M. (2016). Plasticity of the *Leishmania* genome leading to gene copy number variations and drug resistance. *F1000Res.* 5:2350. doi: 10.12688/f1000research.9218.1

Ley, V., Robbins, E. S., Nussenzweig, V., and Andrews, N. W. (1990). The exit of *Trypanosoma cruzi* from the phagosome is inhibited by raising the PH of acidic compartments. *J. Exp. Med.* 171, 401–413. doi: 10.1084/jem.171.2.401

Lima, F. M., Oliveira, P., Mortara, R. A., Silveira, J. F., and Bahia, D. (2010). The challenge of Chagas' disease: has the human pathogen, *Trypanosoma cruzi*, learned how to modulate signaling events to subvert host cells? *New Biotechnol.* 27, 837–843. doi: 10.1016/j.nbt.2010.02.003

Lodge, R., and Descoteaux, A. (2005). Modulation of phagolysosome biogenesis by the lipophosphoglycan of *Leishmania*. *Clin. Immunol.* 114, 256–265. doi: 10.1016/j.clim.2004.07.018

Martínez, A., Prolo, C., Estrada, D., Rios, N., Alvarez, M. N., Piñeyro, M. D., et al. (2019). Cytosolic Fe-superoxide dismutase safeguards *Trypanosoma cruzi* from macrophage-derived superoxide radical. *Proc. Natl. Acad. Sci. U.S.A.* 116, 8879–8888. doi: 10.1073/pnas.1821487116

Martins, R. M., Alves, R. M., Macedo, S., and Yoshida, N. (2011). Starvation and rapamycin differentially regulate host cell lysosome exocytosis and invasion by *Trypanosoma cruzi* metacyclic forms. *Cell. Microbiol.* 13, 943–954. doi: 10.1111/j.1462-5822.2011.01590.x

Matte, C., Casgrain, P. A., Séguin, O., Moradin, N., Hong, W. J., and Descoteaux, A. (2016). *Leishmania major* promastigotes evade LC3-associated phagocytosis through the action of GP63. *PLoS Pathog.* 12:e1005690. doi: 10.1371/journal.ppat.1005690

Meirelles, M. N. L., Araujo Jorge, T. C., de Souza, W., Moreira, A. L., and Barbosa, H. S. (1987). *Trypanosoma cruzi*: phagolysosomal fusion after invasion into non professional phagocytic cells. *Cell Struct. Funct.* 12, 387–393. doi: 10.1247/csf.12.387

Mortara, R. A. (1991). *Trypanosoma cruzi*: amastigotes and trypomastigotes interact with different structures on the surface of HeLa cells. *Exp. Parasitol.* 14, 1–14. doi: 10.1016/0014-4894(91)90002-e

Mortara, R. A., Andreoli, W. K., Fernandes, M. C. D. C., da Silva, C. V., Fernandes, A. B., L'Abbate, C., et al. (2008). Host cell actin remodeling in response to *Trypanosoma cruzi*: trypomastigote versus amastigote entry. *Subcell. Biochem.* 47, 92–100. doi: 10.1007/978-0-387-78267-6_7

Mortara, R. A., Andreoli, W. K., Taniwaki, N. N., Fernandes, A. B., da Silva, C. V., Fernandes, M. C. D. C., et al. (2005). Mammalian cell invasion and intracellular trafficking by *Trypanosoma cruzi* infective forms. *An. Acad. Bras. Ciênc.* 77, 77–94. doi: 10.1590/s0001-37652005000100006

Ndjamen, B., Kang, B., Hatsuzawa, K., and Kima, P. E. (2010). *Leishmania* parasitophorous vacuoles interact continuously with the host cell's endoplasmic reticulum; parasitophorous vacuoles are hybrid compartments. *Cell. Microbiol.* 12, 1480–1494. doi: 10.1038/jid.2014.371

Okuda, K., Tong, M., Dempsey, B., Moor, K. J., Gazzinelli, R. T., and Silverman, N. (2016). *Leishmania amazonensis* engages CD36 to drive parasitophorous vacuole maturation. *PLoS Pathog.* 12:e1005669. doi: 10.1371/journal.ppat.1005669

Pessoa, C. C., Ferreira, E. R., Bayer-Santos, E., Rabinovitch, M., Mortara, R. A., and Real, F. (2016). *Trypanosoma cruzi* differentiates and multiplies within chimeric parasitophorous vacuoles in macrophages coinfected with *Leishmania amazonensis*. Infect. Immun. 84, 1603–1614. doi: 10.1128/IAI.01470-15

Pessoa, C. C., Reis, L. C., Ramos-Sanchez, E. M., Orikaza, C. M., Cortez, C., de Castro Levatti, E. V., et al. (2019). ATP6V0d2 controls *Leishmania* parasitophorous vacuole biogenesis via cholesterol homeostasis. *PLoS Pathog.* 15:e1007834. doi: 10.1371/journal.ppat.1007834

Pitale, D. M., Gendalur, N. S., Descoteaux, A., and Shaha, C. (2019). *Leishmania donovani* induces autophagy in human blood–derived neutrophils. *J. Immunol.* 202, 1163–1175. doi: 10.4049/jimmunol.1801053

Real, F., Florentino, P. T. V., Reis, L. C., Ramos-Sanchez, E. M., Veras, P. S. T., Goto, H., et al. (2014). Cell-to-cell transfer of *Leishmania amazonensis* amastigotes is mediated by immunomodulatory LAMP-rich parasitophorous extrusions. *Cell. Microbiol.* 16, 1549–1564. doi: 10.1111/cmi.12311

Real, F., and Mortara, R. A. (2012). The diverse and dynamic nature of *Leishmania* parasitophorous vacuoles studied by multidimensional imaging. *PLoS Negl. Trop. Dis.* 6:e1518. doi: 10.1371/journal.pntd.0001518

Real, F., Mortara, R. A., and Rabinovitch, M. (2010). Fusion between *Leishmania amazonensis* and *Leishmania major* parasitophorous vacuoles: live imaging of coinfected macrophages. *PLoS Negl. Trop. Dis.* 4:e905. doi: 10.1371/journal.pntd.0000905

Real, F., Vidal, R. O., Carazzolle, M. F., Mondego, J. M. C., Costa, G. G. L., Herai, R. H., et al. (2013). The genome sequence of *Leishmania (Leishmania) amazonensis*: functional annotation and extended analysis of gene models. *DNA Res.* 20, 567–581. doi: 10.1093/dnares/dst031

Reignault, L. C., Alcantara, C. L., Barrias, E. S., and de Souza, W. (2019). 3D reconstruction of *Trypanosoma cruzi*-macrophage interaction shows the recruitment of host cell organelles towards parasitophorous vacuoles during its biogenesis. *J. Struct. Biol.* 205, 133–146. doi: 10.1016/j.jsb.2018.12.010

Reignault, L. C., Barrias, E. S., Soares Medeiros, L. C., De Souza, W., and De Carvalho, T. M. U. (2014). Structures containing galectin-3 are recruited to the parasitophorous vacuole containing *Trypanosoma cruzi* in mouse peritoneal macrophages. *Parasitol. Res.* 113, 2323–2333. doi: 10.1007/s00436-014-3887-8

Reis-Cunha, J. L., Rodrigues-Luiz, G. F., Valdivia, H. O., Baptista, R. P., Mendes, T. A. O., de Morais, G. L., et al. (2015). Chromosomal copy number variation reveals differential levels of genomic plasticity in distinct *Trypanosoma cruzi* strains. *BMC Genomics* 16:499. doi: 10.1186/s12864-015-1680-4

Reis-Cunha, J. L., Valdivia, H. O., and Bartholomeu, D. C. (2018). Gene and chromosomal copy number variations as an adaptive mechanism towards a parasitic lifestyle in trypanosomatids. *Curr. Genomics* 19, 87–97. doi: 10.2174/1389202918666170911161311

Ribeiro-Gomes, F. L., Otero, A. C., Gomes, N. A., Moniz-de-Souza, M. C. A., Cysne-Finkelstein, L., Arnholdt, A. C., et al. (2004). Macrophage interactions with neutrophils regulate *Leishmania major* infection. *J. Immunol.* 172, 4454–4462. doi: 10.4049/jimmunol.172.7.4454

Rodriguez, A., Samoff, E., Rioult, M. G., Chung, A., and Andrews, N. W. (1996). Host cell invasion by trypanosomes requires lysosomes and microtubule/kinesin-mediated transport. *J. Cell Biol.* 134, 349–362. doi: 10.1083/jcb.134.2.349

Romano, P. S., Arboit, M. A., Vázquez, C. L., and Colombo, M. I. (2009). The autophagic pathway is a key component in the lysosomal dependent entry of *Trypanosoma cruzi* into the host cell. *Autophagy* 5, 6–18. doi: 10.4161/auto.5.1.7160

Rosestolato, C. T. F., Dutra, J. M. F., de Souza, W., and Carvalho, T. M. U. (2002). Participation of host cell actin filaments during interaction of trypomastigote forms of *Trypanosoma Cruzi* with host cells. *Cell Struct. Funct.* 27, 91–98. doi: 10.1247/csf.27.91

Rubin-de-Celis, S. S., and Schenkman, S. (2012). T rypanosoma cruzi trans-sialidase as a multifunctional enzyme in Chagas' disease. *Cell. Microb.* 14, 1522–1530. doi: 10.1111/j.1462-5822.2012.01831.x

Rubin-de-Celis, S. S. C., Uemura, H., Yoshida, N., and Schenkman, S. (2006). Expression of trypomastigote trans-sialidase in metacyclic forms of *Trypanosoma cruzi* increases parasite escape from its parasitophorous vacuole. *Cell. Microbiol.* 8, 1888–1898. doi: 10.1111/j.1462-5822.2006.00755.x

Salassa, B. N., and Romano, P. S. (2018). Autophagy: a necessary process during the *Trypanosoma cruzi* life-cycle. *Virulence* 10, 460–469. doi: 10.1080/21505594.2018.1543517

Stecconi-Silva, R. B., Andreoli, W. K., and Mortara, R. A. (2003). Parameters affecting cellular invasion and escape from the parasitophorous vacuole by different infective forms of *Trypanosoma cruzi*. *Mem. Inst. Oswaldo Cruz* 98, 953–958. doi: 10.1590/s0074-02762003000700016

Stevens, J., Noyes, H., and Gibson, W. (1998). The Evolution of trypanosomes infecting humans and primates. *Mem. Inst. Oswaldo Cruz* 93, 669–676. doi: 10.1590/S0074-02761998000500019

Tardieux, I., Webster, P., Ravesloot, J., Boron, W., Lunn, J. A., Heuser, J. E., et al. (1992). Lysosome recruitment and fusion are early events required for trypanosome invasion of mammalian cells. *Cell* 71, 1117–1130. doi: 10.1016/s0092-8674(05)80061-3

Teixeira, S. M. R., Russell, D. G., Kirchhoffnll, L. V., and Donelson, J. E. (1994). A differentially expressed gene family encoding 'amastin', a surface protein of *Trypanosoma cruzi* amastigotes. *J. Biol. Chem.* 269, 20509–20516.

Tomlinson, S., Frevert, U., Vandekerckhove, F., and Nussenzweig, V. (1995). The induction of *Trypanosoma cruzi* trypomastigote to amastigote transformation by low PH. *Parasitology* 110, 547–554. doi: 10.1017/S0031182000065264

Tyler, K. M., Luxton, G. W. G., Applewhite, D. A., Murphy, S. C., and Engman, D. M. (2005). Responsive microtubule dynamics promote cell invasion by *Trypanosoma cruzi*. *Cell. Microbiol.* 7, 1579–1591. doi: 10.1111/j.1462-5822.2005.00576.x

Veras, P. S. T., de Menezes, J. P. B., and Dias, B. R. S. (2019). Deciphering the role played by autophagy in *Leishmania* infection. *Front. Immunol.* 10:2523. doi: 10.3389/fimmu.2019.02523

Verma, J. K., Rastogi, R., and Mukhopadhyay, A. (2017). *Leishmania donovani* resides in modified early endosomes by upregulating Rab5a expression via the downregulation of MiR-494. *PLoS Pathog.* 13:e1006459. doi: 10.1371/journal.ppat.1006459

Wanderley, J. L. M., Damatta, R. A., and Barcinski, M. A. (2020). Apoptotic mimicry as a strategy for the establishment of parasitic infections: parasite- and host-derived phosphatidylserine as key molecule. *Cell Commun. Signal.* 18:10. doi: 10.1186/s12964-019-0482-8

WHO (2020a). *Chagas Disease (American Trypanosomiasis)*. Available online at: https://www.who.int/chagas/epidemiology/en/ (accessed January 16, 2020).

WHO (2020b). *Leishmaniasis*. Available online at: https://www.who.int/news-room/fact-sheets/detail/leishmaniasis (accessed January 16, 2020).

Wilson, J., Huynh, C., Kennedy, K. A., Ward, D. M., Kaplan, J., Aderem, A., and Andrews, N. W. (2008). Control of parasitophorous vacuole expansion by *LYST/Beige* restricts the intracellular growth of *Leishmania amazonensis*. *PLoS pathog.* 4:e1000179. doi: 10.1371/journal.ppat.1000179

Winberg, M. E., Holm, A., Sarndahl, E., Vinet, A. F., Descoteaux, A., Magnusson, K. E., et al. (2009). *Leishmania donovani* lipophosphoglycan inhibits phagosomal maturation via action on membrane rafts. *Microbes Infect.* 11, 215–222. doi: 10.1016/j.micinf.2008.11.007

Woolsey, A. M., Sunwoo, L., Petersen, C. A., Brachmann, S. M., Cantley, L. C., and Burleigh, A. (2003). Novel Pl 3-kinase-dependent mechanisms of trypanosome invasion and vacuole maturation. *J. Cell Sci.* 116, 3611–3622. doi: 10.1242/jcs.00666

Yoshida, N. (2006). Molecular basis of mammalian cell invasion by *Trypanosoma cruzi*. *An. Acad. Bras. Ciênc.* 78, 87–111. doi: 10.1590/S0001-37652006000100010

Zingales, B., Miles, M. A., Campbell, D. A., Tibayrenc, M., Macedo, A. M., Teixeira, M. M. G., et al. (2012). The revised *Trypanosoma cruzi* subspecific nomenclature: rationale, epidemiological relevance and research applications. *Infect. Genet. Evol.* 12, 240–253. doi: 10.1016/j.meegid.2011.12.009

Conflict of Interest: The authors declare that the research was conducted in the absence of any commercial or financial relationships that could be construed as a potential conflict of interest.

frontiers in Medicine

ORIGINAL RESEARCH
published: 24 July 2020
doi: 10.3389/fmed.2020.00268

Long-Term Clinical, Audiological, Visual, Neurocognitive and Behavioral Outcome in Children With Symptomatic and Asymptomatic Congenital Cytomegalovirus Infection Treated With Valganciclovir

Arianna Turriziani Colonna[1], Danilo Buonsenso[2,3], Davide Pata[1], Gilda Salerno[1], Daniela P. R. Chieffo[1,4], Domenico M. Romeo[1,4], Valerio Faccia[5], Guido Conti[6,7], Fernando Molle[6,8], Antonio Baldascino[6,8], Chiara De Waure[9], Anna Acampora[1,10], Rita Luciano[1,2], Rosaria Santangelo[3,11] and Piero Valentini[1,2]*

[1] Istituto di Pediatria, Università Cattolica del Sacro Cuore, Rome, Italy, [2] Department of Woman and Child Health and Public Health, Fondazione Policlinico Universitario A. Gemelli IRCCS, Rome, Italy, [3] Istituto di Microbiologia, Università Cattolica del Sacro Cuore, Rome, Italy, [4] Istituto di Neuropsichiatria, Università Cattolica del Sacro Cuore, Rome, Italy, [5] Unit of Pediatrics, Department of Gynecologic, Pediatric and Neonatologic Sciences, "Sant'Andrea" University Hospital, University "Sapienza" of Rome, Rome, Italy, [6] Department of Aging, Neurologic, Orthopedic and Head and Neck Science, Fondazione Policlinico Universitario A. Gemelli, IRCCS, Rome, Italy, [7] Istituto di Otorinolaringoiatria, Università Cattolica del Sacro Cuore, Rome, Italy, [8] Istituto di Oculistica, Università Cattolica del Sacro Cuore, Rome, Italy, [9] Department of Experimental Medicine, University of Perugia, Perugia, Italy, [10] Istituto di Igiene, Università Cattolica del Sacro Cuore, Rome, Italy, [11] Department of Microbiology and Infectious Diseases, Fondazione Policlinico Universitario A. Gemelli IRCCS, Rome, Italy

Cytomegalovirus (CMV) is the most common cause of congenital infection in humans. There are no enough data on long-term outcome of newborns with congenital CMV (cCMV) infection, particularly for those asymptomatic at birth. For this reason, we performed this study to evaluate long-term audiological, visual, neurocognitive, and behavioral outcome in patients with symptomatic and asymptomatic cCMV infection treated with oral Valganciclovir (VGC). Thirty-six newborns with confirmed cCMV infection were evaluated: 12 (33.3%) symptomatic at birth and 24 asymptomatic (66.7%). No one had cognitive impairment. Cognitive assessment scales resulted abnormal in 4/35 patients (11.4%). 11/21 patients (52.4%) achieved abnormal scores in neuropsychological tests. The language evaluation gave pathological results in 6/21 (28.5%) patients. 6/35 patients (17.1%) developed SNHL, all symptomatic at birth except one. None of the 34 patients evaluated developed CMV retinopathy. Our study shows that both symptomatic and asymptomatic newborns with cCMV infection develop long-term sequelae, particularly in the behavioral and communicative areas, independently from the trimester of maternal infection.

Keywords: congenital cytomegalovirus, valganciclovir, hearing loss, congenital infections, neurocognitive outcome

OPEN ACCESS

Edited by:
Feng Lu,
Yangzhou University, China

Reviewed by:
Zdenek Novak,
University of Alabama at Birmingham, United States
SriSowmya Sanisetty,
Independent researcher, Boston, United States

***Correspondence:**
Davide Pata
davide.pata01@gmail.com

Specialty section:
This article was submitted to Infectious Diseases - Surveillance, Prevention and Treatment, a section of the journal Frontiers in Medicine

Received: *24 January 2020*
Accepted: *15 May 2020*
Published: *24 July 2020*

Citation:
Turriziani Colonna A, Buonsenso D, Pata D, Salerno G, Chieffo DPR, Romeo DM, Faccia V, Conti G, Molle F, Baldascino A, De Waure C, Acampora A, Luciano R, Santangelo R and Valentini P (2020) Long-Term Clinical, Audiological, Visual, Neurocognitive and Behavioral Outcome in Children With Symptomatic and Asymptomatic Congenital Cytomegalovirus Infection Treated With Valganciclovir. Front. Med. 7:268. doi: 10.3389/fmed.2020.00268

INTRODUCTION

Cytomegalovirus (CMV) is the most common cause of congenital infection in humans (1) and the leading cause of cognitive impairment and non-genetic sensorineural hearing loss (SNHL) in infancy (2). Congenital CMV (cCMV) infection is symptomatic in about 10–15% cases with a perinatal mortality of 10%; 90% of those who survive develop neurological sequelae, mainly defects of psychomotor development and SNHL (3). Eighty five to ninety percent of newborns does not present any symptoms at birth; however, 8–15% of these will show late signs related to cCMV, especially SNHL (4–8). Moreover, European and Asian studies have shown how cCMV infection can have repercussions on multiple developmental areas (9, 10), although the long-term outcome of newborns with asymptomatic infection is not well clear. Kimberlin et al. (11) demonstrated that intravenous (iv) Ganciclovir (GCV) for 6 weeks in symptomatic cCMV with CNS involvement prevents deterioration of the auditory and psychomotor function. Furthermore, antiviral therapy improved the neurological outcome during follow-up (12). However, this therapy requires prolonged hospitalization and vascular catheters with increased risk of nosocomial infections. Valganciclovir (VGC) is the pro drug of GCV (GCV L-valil-ester); first studies showed that a VGC dose of 15 mg/kg orally every 12 h is comparable to 6 mg/kg every 12 h iv of GCV (13). Several studies evaluated the effectiveness of oral VGC, but all of them aimed at symptomatic cCMV (14). Due to the lack of clear data on long-term follow-up of cCMV infection, we performed this study aiming to evaluate long-term, clinical, audiological, visual, neurocognitive, and behavioral outcome in patients with symptomatic and asymptomatic cCMV infection treated with VGC.

MATERIALS AND METHODS

We performed a retrospective study of patients with cCMV infection (both symptomatic and asymptomatic) treated with VGC, evaluated from October 2009 to February 2017. The study was approved by the Ethical Committee of our institution (prot 26317/19 ID 2629).

Maternal Diagnosis

Mothers have been considered infected in presence of at least one of the following:

- seroconversion with appearance of anti-CMV IgG antibodies documented during pregnancy,
- in case of positive anti-CMV IgG at the first serological control in pregnancy, if the IgG avidity index was compatible with an infection acquired after conception,
- presence of CMV-DNA in blood and urine (15).

Women with IgG positive antibodies before pregnancy and those with high IgG Avidity without IgM during the first 25 weeks of gestation were classified as having non-primary CMV infection.

Neonatal Diagnosis

Infants were considered infected if CMV-DNA was found in blood or urine using the Real TimePolymerase Chain Reaction method (RT-PCR), no later than the first 3 weeks of extra-uterine life (11, 16). It is a commercial assay and the analytical sensitivity allowed the quantification of 200 to 10^6molecules of the target DNA.

All infected newborns underwent clinical evaluation (17), blood tests, assessment of the ocular fundus, audiological screening using otoemissions (TEOAEs), auditory brainstem response (ABR), ultrasound of the brain and, in doubtful cases, encephalic magnetic resonance, and cranial radiography.

Newborns were classified as symptomatic if they had at least one of the following findings (18): petechiae, hepatomegaly, splenomegaly, abnormalities in blood chemistry (thrombocytopenia <100,000/μl, anemia, leukopenia, elevation of liver enzymes, conjugated hyperbilirubinemia), SGA <-2 DS status, neurologic and/or ophthalmologic examination anomalies, microcephaly, convulsions, neuroradiological abnormalities related to CMV infection, abnormalities in the ABR exam. Ultrasonographic signs indicative of symptoms included calcifications, cystic periventricular leukomalacia, subependymal pseudocysts, germinolytic cysts, white matter anomalies, cortical atrophy, migration disorders, cerebellar hypoplasia, and lenticulo-striatal vasculopathy (the latter only if in association with other signs) (19).

Treatment

Patients were treated with a galenic preparation of oral VGC based on data available in literature (13, 14, 20–22). The galenic was set up according to the dictates of rules of good preparation (N.B.P.) indicated on the Official Pharmacopoeia XII ed. following the procedure reported in the literature (23).

The treatment was started in the first month of age. Patients received VGC at a dose of 32 mg/kg/day divided into two daily doses, for a variable number of 6-week cycles (up to the persistently negative viremia, as stated below). At the beginning, on day 21 and at the end of the 6-week therapy cycle, the following parameters were monitored: viral load by RT-PCR performed on whole blood, urine and pharyngeal swab; creatinine, SGPT, amylase, gamma-GT, alkaline phosphatase and blood-cell count with formula.

At the end of each cycle, monthly and until the first year of age, patients underwent clinical evaluation and determination of viral load on blood and urine; if viremia was found positive again, a new 6-week therapy cycle was started, with the same modalities.

Patients born after the publication of Kimberlin's study in 2015 received the drug for 6 months, in accordance with the evidence that emerged from the study (14).

The administration of the drug was suspended in 1 case with peripheral blood neutrophil count lower than 500 cells/μl (reversible side effect).

Follow-Up

Patients with confirmed cCMV infection underwent audiological, neurocognitive, psychological, ocular, audiological,

and neurological assessments; tests performed are summarized in **Table 1**.

Primary Outcome

Evaluation of long-term clinical, audiological, visual, neurocognitive, and behavioral outcome in patients with symptomatic and asymptomatic cCMV infection treated with VGC.

Secondary Outcome

Association between outcome (clinical, audiological, visual, neurocognitive, and behavioral) and viremia, number of treatments performed and trimester of maternal infection.

Statistical Analyses

The analysis of data includes a descriptive part of the sample carried out by constructing frequency tables (absolute and

TABLE 1 | Tests performed for the evaluation of outcomes of primary and secondary interest, categories analyzed, and sample or sub-sample in which they are performed.

Outcome	Analyzed categories	Sample or subsample
NEUROCOGNITIVE OUTCOME		
Test 1: WPPSI-III: Wechsler Preschool and Primary Scale of Intelligence—III	IQ ≤ 69: score lower than normal; 70 ≤ IQ ≤ 84: borderline score; 85 ≤ IQ ≤ 115: normal score; IQ ≥ 116: higher than the norm score.	Patients from 2.6 to 7.3 years
Test 2: WISC-IV: Wechsler Intelligence Scale for Patients-IV	IQ ≤ 69: score lower than normal; 70 ≤ IQ ≤ 84: borderline score; 85 ≤ IQ ≤ 115: normal score; IQ ≥ 116: higher than the norm score.	Patients from 6 + 0 to 16 + 11 years
Test 3: Leiter-R: non-verbal scale	IQ ≤ 69: score lower than normal; 70 ≤ IQ ≤ 84: borderline score; 85 ≤ IQ ≤ 115: normal score; IQ ≥ 116: higher than the norm score.	Patients from 2 to 20 years of foreign language
NEUROPSYCHOLOGICAL OUTCOME		
Test 1: NEPSY-II	Scores from 1 to 4: deficit; from 5 to 7: lower than the norm; from 8 to 12: in the norm; from 13 upwards: above the norm.	Patients from 3 to 16 years
Test 2: Bells test	Result >-1.66 DS: normal; <-1.66: lower than the norm	Patients from 4 to 8 years
LANGUAGE		
Test 1: BVL_4–12: Battery for the evalaution of language in patients from 4 to 12 years	Result <-1.5 DS: lower than the norm; >-1.5 DS: normal	Patients from 4 to 12 years
Test 2: Phonolexical Test (TFL)	≤50° percentile: lower than normal; >50° percentile: normal; >90°: higher than normal.	Patients from 3 to 6 years
Test 3: Griffiths battery – C scale in five patients (comprehension and verbal production scale)	Score ≤ 69: score lower than normal; 70≤ score ≤84: borderline score; 85≤ score ≤115: score in the standard; score ≥ 116: score higher than normal.	Patients up to 3 years
BEHAVIOR		
Test 1: Child Behavior Checklist 1½−5 (CBCL)	>60: normal; =60: borderline; >60: lower than the norm.	Patients from 1 to 5 years
Test 2: Child Behavior Checklist 6–18 (CBCL)	>60: normal; =60: borderline; >60: lower than the norm.	Patients from 6 years upwards
RETINOPATHY		
Test 1: Fundus oculi examination	Present/absent retinopathy	All the patients
HEARING OUTCOME		
Test 1: TEOAEs	Pass (normal)/ Refer (pathological)	All patients at the 3rd day of life
Test 2: ABR Auditory threshold	Normoacusia if ≤20 dB Unilateral or bilateral hypoacusia: mild 21–40 dB; average 41–70 dB; severe 71–90 dB; deep > 90 dB.	0–2/3 years of age depending on the collaboration
Test 3: Audiometry Auditory threshold	Normal if ≤20 dB Unilateral or bilateral hypoacusia: mild 21–40 dB; average 41–70 dB; severe 71–90 dB; deep > 90 dB.	From 2 to 3 years of age upwards

percentages) for the categorical variables and with the mean ± standard deviation for the quantitative variables.

The association between the dependent and independent variables has been tested using statistical tests defined on the basis of the nature of the analyzed variables. For the analysis of the association between the symptomatic or asymptomatic condition at birth and the neurocognitive, neuropsychological, language, behavioral, auditory, and long-term retinopathy outcomes, a univariate analysis has been performed using the Chi-square test and the Fisher's exact test. These outcome variables have been categorized based on the score obtained in the tests and investigations carried out, previously described and reported in **Table 1**; the same tests have been used to study the association between the trimester of pregnancy in which the CMV infection occurred and the outcomes.

The Mann–Whitney test was used to analyze the endpoints regarding the number of therapy cycles administered.

For all analyses, a $p < 0.05$ was considered significant.

The analyses were performed using the STATA software version 13.1.

RESULTS

Study Population

Thirty-six newborns with confirmed cCMV infection: 12 symptomatic patients at birth (33.3%) and 24 asymptomatic (66.7%), who underwent oral VGC treatment were included in the study. The average age of the follow up is 4.23 years ± 1.57 SD. All patients were in good general health conditions, no endocrinological disorders were diagnosed.

Tables 2–4 summarize the characteristics of population, the treatment cycles, and the comparison between symptomatics and asymptomatics, respectively.

Based on the ESPID criteria (18), of the 12 symptomatic newborns, eight (66.5%) were severe symptomatic at birth, 1 (8%) moderate symptomatic and 1 (8%) mild symptomatic. Two patients (17%) were born with unilateral hearing loss, in association with subependymal pseudocysts in a newborn and isolated in another.

Timing of maternal infection was available for 35 patients (**Table 5**):

- first trimester for 15 women (41.7%), giving birth to 6 symptomatic newborns (40%);
- second trimester for 11 women (30.6%); at birth 3 newborns (27%) were symptomatic;
- third trimester for 9 women (25%), giving birth to 2 symptomatic newborns (22%) with CNS involvement.

Results of Neurocognitive and Behavioral Follow-Up

Neuropsychiatric evaluation was proposed to 35 patients, four of whom did not complete the tests. However, not all continued the follow-up in the following years and consequently performed the different tests, unlike the audiological follow-up. With regard to cognitive development, 30 out of 33 evaluated patients (90.9%) were normal (Intelligence Quotient, IQ, ≥85). The average IQ of patients in the group is 110.9. Specifically, 15 patients have a development above the norm with IQ ≥ 116 (45.5%) and 15 in the standard with 85 ≤ IQ ≤ 115 (45.5%). Among them, eight patients scored below the norm in at least one subtest. The major recurrence was observed in the test called Cifrario (10 patients out of 22–45.5%). Three patients achieved a borderline score: 70 ≤ IQ ≤ 84 (9.1%), one was severely symptomatic at birth. No one had cognitive impairment (IQ ≤ 69). The Symbols' Search (SS) test of cognitive assessment scales, given to 22 patients, was abnormal in 4 patients in whom the viremia for CMV had not become undetectable after the first course of therapy ($p = 0.017$, **Table 6**).

Of the 21 patients who underwent neuropsychological tests, 11 (52.4%) achieved an insufficient score in at least one subtest with a more frequent fall in the attention tests (7 out of 19−36.8%) and semantic fluency (8 out of 12−66.7%).

The language evaluation carried out on 32 patients gave normal results in all but in 6 patients, including 3 symptomatic at birth with CNS involvement; a significant difference emerged between those with language disorders and without in relation to the number of cycles of VGC administered. In particular, the median number of cycles is 3.50 with IQR = 2 in the first group and 2 with IQR = 1 in second group ($p = 0.042$ in the Mann–Whitney test).

Twenty-eight families completed the CBCL questionnaire for the analysis of the child's behavior. In the Total Scale of Problems, four patients (14.3%) obtained pathological results on the Internalizing scale and two patients (7.1%) also in the Externalizing scale. The same two patients were symptomatic at birth with CNS involvement.

Seven patients in total obtained an alarming score on the Internalizing scale (25%), three of them had a pathological score on the Externalizing scale and four of them were pathological on the Total scale.

The score on the Externalizing scale was noteworthy for four patients (14.3%), two of them already reported in the Total scale, and three also with internalizing problems.

Importantly, abnormal neurocognitive and behavioral tests were obtained both in newborns infected in the first trimester (9/15, 60%) and in the third trimester (4/9, 44%), $p > 0.05$.

Results of the Audiological Follow-Up

Thirty-five patients underwent audiological follow-up. It was assessed by Auditory Brainstem Response (ABR) within the 3rd month of age. The repetition of the exam was proposed at 6, 12, and 18 months of age and then annually until school age. The average age of the follow up is 4.23 years ± 1.57 SD.

Six patients (17.1%) developed SNHL, all symptomatic at birth except one ($p = 0.012$—**Table 7**). One child has had unilateral left-sided deep hearing loss (auditory threshold 95 dB−5 years of age at the last instrumental control) since the first control. Two patients, both 4 years old, have had severe unilateral left-sided hearing loss (auditory threshold 80 and 85 dB) since the first control, which has remained stable over time.

A child with normal ABR at birth, who had not performed controls in the first year of life, resulted affected by bilateral

TABLE 2 | Patient characteristics.

Patient	Gestational Age	Birth Weight (g)	AGA/ SGA/ LGA *	Symptomatic (S)/ Asymptomatic (A)	CMV PCR in urine, blood, pharynx	Viral load in blood (copies/mL)	Hearing status	Thrombocytopenia	Petechiae	Hepatomegaly	Splenomegaly	CNS involvement	Hepatitis	Trimester of infection
#1	40	3,470	AGA	A	+ U, B, P	930								2
#2	39	3,140	AGA	A	+ U, B, P	6,760								2
#3	40	2,660	SGA	A	+ U, B, P	17,190								2
#4	38	3,250	AGA	S	+ U, B, P	9,340	Left SNHL					White matter abnormalities		2
#5	40	2,830	AGA	S	+ U, B, P	152,800						White matter abnormalities, cysts, scars		1
#6	38	3,330	AGA	A	+ U, B, P	5,604								1
#7	40	3,700	AGA	A	+ U, B, P	1,880								3
#8	37	2,600	AGA	A	+ U, B, P	431								3
#9	38	3,240	AGA	A	+ U, B, P	486								2
#10	38	2,750	AGA	A	+ U, B, P	1,820								2
#11	37	3,250	AGA	A	+ U, B, P	2,000								1
#12	39	3,380	AGA	A	+ U, B, P	17,640								1
#13	40	3,930	LGA	A	+ U, B	#								1
#14	40	3,450	AGA	A	+ U, B, P	9,600								2
#15	38	2,740	SGA	S	+ U, B, P	9,200	Left SNHL							2
#16	40	4,220	LGA	A	+ U, B, P	810								3
#17	37	3,500	LGA	S	+ U, B, P	304						White matter abnormalities		3
#18	39	3,120	AGA	A	+ U, B, P	5,856		X		X		Subependymal pseudocysts		1
#19	39	2,920	SGA	S	+ U, B, P	8,684								3
#20	38	3,150	AGA	A	+ U, B, P	3,753						Lenticulostriatal vasculopathy		1
#21	#	#	#	A	+ U, B, P	1,987								3
#22	41	3,200	AGA	A	+ P	0								2
#23	#	#	#	A	+ U, P	0								1
#24	40	3,340	AGA	S	+ U, B, P	31,604	Left SNHL					Subependymal pseudocysts		1
#25	40	2,800	SGA	A	+ U, B, P	31,900	Left SNHL							1
#26	40	3,720	AGA	S	+ U, B, P	519						White matter abnormalities, lenticulostriatal vasculopathy		2
#27	#	#	#	S	+ U, B, P	3,610						Hypotonia, seizures		#
#28	39	4,000	LGA	A	+ U, B, P	#								3
#29	36	2,730	AGA	A	+ U, B, P	2,774								2
#30	35	1,750	<3	S	+ U, B, P and cerebrospinal fluid	1,746,873	Bilateral SNHL	X						1
#31	38	3,670	LGA	A	+ U, B, P	9,541								3
#32	38	3,130	AGA	S	+ U, B, P	3,883						White matter abnormalities, subependymal pseudocysts		1
#33	38	2,570	SGA	A	+ U, B, P	2,343								1
#34	38	3,580	AGA	S	+ U, B, P	#						Subependymal pseudocysts, lenticulostriatal vasculopathy		3
#35	37	4,180	LGA	S	+ U, B, P	774	Bilateral SNHL					White matter abnormalities, lenticulostriatal vasculopathy		1
#36	38	4,150	LGA	A	+ U, B, P	#								1

#*missing data.*

TABLE 3 | Treatment cycles.

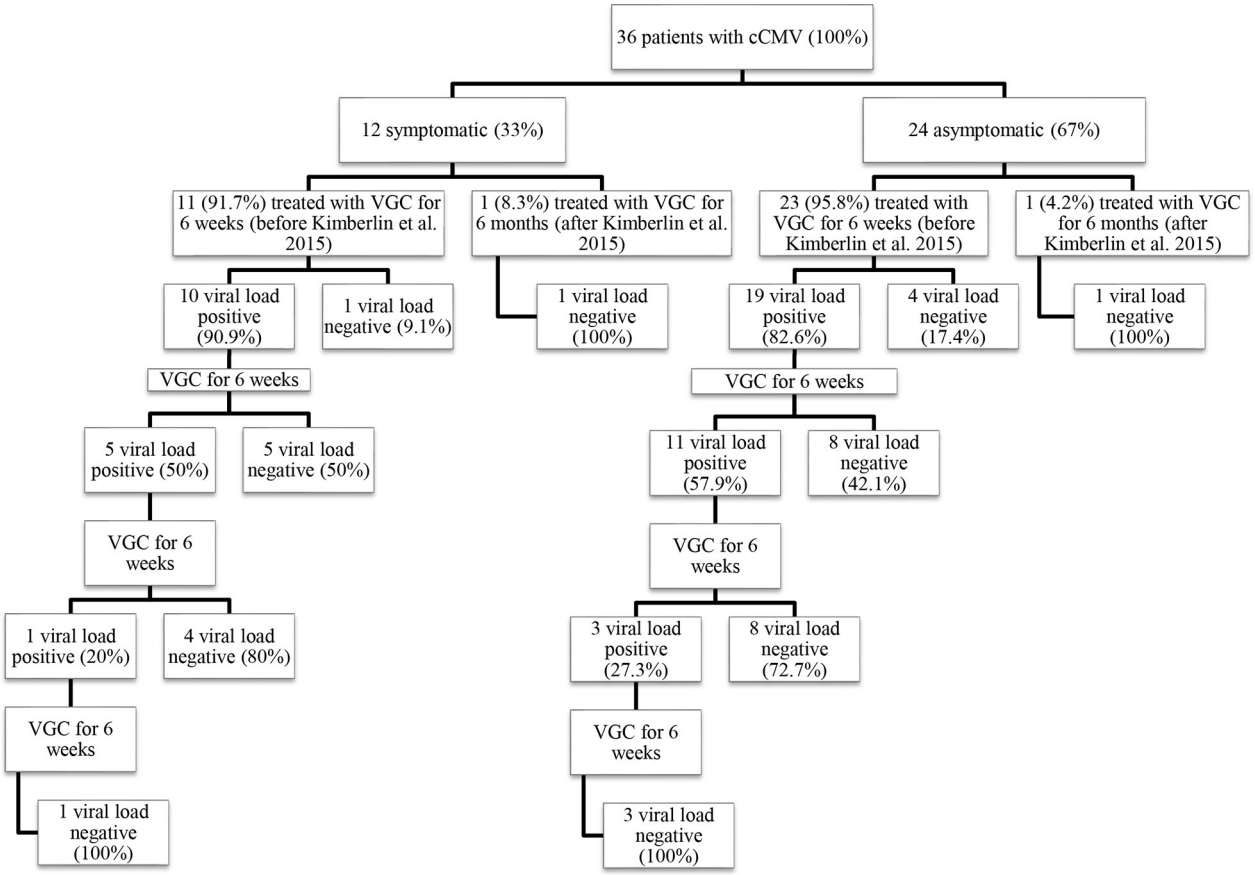

TABLE 4 | Comparison between Symptomatics and Asymptomatics.

	Gestational age (median)	Birth Weight (g, median)	Time of maternal infection (median trimester)	Viral load in blood (copies/mL)	Cycles of VGC (*n*)	SNHL (*n*)	Retinopathy (*n*)	Cognitive Impairment (*n*)	Abnormal neuropsycological tests (*n*)	Language disorders (*n*)	Abnormal behavioral tests (*n*)
Symptomatics	38.18	3,176	1.81	178,872	2.33	5	0	1	2	3	2
Asymptomatics	38.77	3,296	1.83	6,490	2.38	1	0	2	9	3	6

TABLE 5 | Study population according to trimester of maternal infection and symptoms at birth.

	Gestational age and symptoms at birth		
	Symptomatic	**Asymptomatic**	**Total (*n* = 36)**
First trimester	6 (16.7%)	9 (25%)	15 (41.7%)
Second trimester	3 (8.3%)	8 (22.2%)	11 (30.6%)
Third trimester	2 (5.6%)	7 (19.4%)	9 (25%)
Nondescript	1 (2.8%)		1 (2.8%)
Total	12 (33.3%)	24 (66.7%)	36

hypoacusia with 50 dB thresholds on the left and 60 dB on the right ear in the 2nd year of age.

In a child, symptomatic at birth, with known bilateral hearing loss since the first control and already wearing a prosthesis in the right ear, a worsening at the age of 3 years was observed (threshold 90 dB on the right and 50 dB on the left ear). He then started using a prosthesis also for the left ear and performed a 6-month course of therapy with VGC after which the hearing thresholds remained stable.

The remaining 29 patients (82.9%), including 7 symptomatic and 22 asymptomatic, had a physiological result at the auditory function control, showing a normal bilateral acoustic

TABLE 6 | Statistic analysis of the Symbols' Search subtest results (neurocognitive examination) and the zeroing of CMV viremia after 1 cycle of oral VGC ($n = 22$).

			CMV viremia after 1 cycle of oral VGC		
			Positive	**Negative**	***p*-value**
Neurocognitive subtest (Symbols' Search)	Normal	No. of patients	5	13	0.017
		%	55.6%	100.0%	
	Lower than normal	No. of patients	4	0	
		%	44.4%	0.0%	

TABLE 7 | Statistic analysis of the association between the presence of hearing loss and the presence of signs and symptoms of congenital CMV infection at birth.

			Symptoms at birth		
			No	**Yes**	***p*-value**
Hearing impairment	No	No. of patients	22	7	0.012
		%	95.7%	58.3%	
	Yes	No. of patients	1	5	
		%	4.3%	41.7%	

threshold (<20 dB) or slightly increased (25–30 dB) because of transmission problems for upper respiratory tract infections, as documented by the contextual clinical evaluation and by the results of the impedance test (tympanograms B or C).

Results of Ophthalmological Follow-Up

Thirty-four patients (12 symptomatic at birth) underwent examination of the fundus of the eye. No child developed CMV retinopathy.

DISCUSSION

Our study has analytically explored the long-term neurocognitive, behavioral, auditory, and ophthalmological outcome of a group of symptomatic and asymptomatic patients affected by cCMVand treated with VGC, showing a considerable impact of cCMV infection on social and individual child health.

As regards the cognitive domain, except for the case of a child with severe nervous system involvement since birth, patients achieved excellent results. There was no finding of overt cognitive deficit and only three patients obtained a borderline score (IQ = 71, 77, and 79). Two of these patients were asymptomatic at birth and one was diagnosed with Language and Attention Deficit and Disorder of Language Understanding.

Fifteen patients out of 33 brilliantly faced cognitive tests, reaching scores above the norm. Overall, the average IQ of patients in the group is in the standard. Interestingly, our values are significantly higher than the average IQ of the group of asymptomatic infected, not treated with VGC, studied by Zhang et al. (10): IQ of 89.43 ± 12.78 among 49 patients between 2 and 6 years.

Korndewal's et al. (9) published in 2017 data on a 6-year multidisciplinary follow-up of a group of patients with untreated symptomatic and asymptomatic cCMV. We compared our results with Korndewal study, although there are intrinsic methodological differences between the two projects, such as sample size, classification of symptomatic and asymptomatic at birth, evaluation tests, characteristics of the population, cultures. In our series a better neuropsychiatric outcome emerges, in particular the absence of cognitive deficit vs 6% (3.7% among asymptomatic patients) in the Dutch group. However, our patients still presented specific falls in the SS test of cognitive assessment scales (4 patients). The SS test helps assess the child's processing speed, measures the ability to focus attention, speed of analysis and capacity for discrimination (24). Interestingly, there was an association between lower scores and the lack of negative viremia after the first cycle of VGC ($p = 0.017$ at Fisher's exact test).

On the contrary, the rate of generic language disorder was similar: 18.8% of patients in our group vs. 16.5% (14.3 against 12.2% among asymptomatic people). Although it is not possible to make conclusions from this comparison, the possibility that VGC treatment gave us good results on this specific follow-up must be considered.

The language evaluation was normal in all but six patients, three of whom were symptomatic at birth with CNS involvement. A significant difference emerged between those with and without language disorders ($p = 0.042$ at the Mann–Whitney test) in relation to the number of VGC cycles needed to achieve persistent negative viremia. Importantly, total non-negligible lower scores in semantic fluency tests were found. Examining only the asymptomatic, seven patients out of nine showed low scores.

Focusing attention on the results of the behavioral questionnaire (CBCL), a quarter of patients has a trait of weak psychic structure on the internalizing side, with a tendency toward anxiety and social withdrawal. None of the patients was diagnosed with autism spectrum disorder (as in 3% of the Korndewal's group, not treated with VGC) (9). The behavioral and emotional spheres are obviously multifactorial. Furthermore, the sequelae of cCMV in the auditory and ophthalmologic areas and the consequent possible need to wear hearing aids and/or glasses and performing rehabilitative therapies are sources of stress for the child and embarrassment with peers. A recent study from Switzerland confirmed the abnormal neuro-development of patients with cCMV (25).

The outcome of post-treatment audiological evaluations did not show the onset of SNHL in normal hearing patients or its deterioration in those in whom it was already present at birth, except in one case. This observation suggests that the control of viral replication in the first year of life, through the administration of VGC, may limit the direct or immune-mediated damage caused by CMV. Only one child had post-treatment worsening of auditory function. Symptomatic at birth (thrombocytopenia, neutropenia, and petechiae), he developed

hearing loss during the 1st year of life. At 15 months of age, hearing function worsened and the use of a right prosthesis was implemented in the second year of life. Following a new deterioration at the age of 3 he began using a prosthesis also for the left ear. On this occasion, we administered VGC for 6 months, after which the hearing thresholds were confirmed stable. Our choice was based on the hypothesis that the observed damage could be the result of long lasting inflammation and, therefore, the control of viral replication could influence the audiological outcome, as hypothesized by the study of Kimberlin et al. (14). They compared VGC treatment (six weeks vs. six months) in patients with symptomatic cCMV infection. This study demonstrated comparable efficacy in terms of 6-month audiological outcome in the two groups. Instead, the prolonged treatment demonstrated a statistically significant superiority for the same outcome at 12 and 24 months, with a maintenance of the hearing benefit. In addition, a statistically significant superiority of the 6-month treatment in linguistic and communicative-behavioral development was reported (14).

Our data confirm what is already known in literature: symptomatic cCMV is a risk factor for the presence of damage to the auditory function ($p = 0.012$). Comparing with the Korndewal's group of untreated patients, the prevalence of hearing loss is proportionally greater in our sample. However, the picture of the audiological status of the patients examined by us after years of treatment reflects in almost all cases what has already been present at birth, or pre-treatment (9).

Regarding the ophthalmological follow-up, the absence of development of chorioretinitis, possible outcome of the infection, is also a positive finding. The results are undoubtedly encouraging, especially when compared with a recent publication of ophthalmological interest in which the development of retinal damage was recorded in 7.8% of symptomatic and in 3.7% of asymptomatic untreated patients (26).

Finally, some considerations are important regarding the trimester of maternal infection. As already described, cCMV infection is more severe in newborns born to pregnant women with first trimester infection. However, the long-term outcome shows a varied distribution of falls in specific scales of cognitive development, language and behavioral sphere. An extremely important finding is that neither a group of patients is free from problems nor it is characterized by a recurrence of specific sequelae.

Our study has some limitations: first, we describe a small sample size; secondly, we do not have a control group of not treated newborns with cCMV to compare with those treated. Despite these limits, our study clearly shows that both symptomatic and asymptomatic newborns with cCMV infection develop long-term sequelae, particularly in the behavioral and communicative areas, no matter the trimester of maternal infection. Importantly, our study also shows a possible association between the entity of viral replication and future sequelae, suggesting that controlling it with antiviral treatment appears a reasonable strategy. Finally, although no comparison with untreated cCMV has been done, our series of treated patients shows a better neuro-cognitive and audiological long-term outcome compared to available data from literature about untreated patients.

New studies evaluating more patients with symptomatic and asymptomatic CCMV and including a randomization of different treatment strategies are needed to better define the best way to manage this increasingly common and characterized condition.

DATA AVAILABILITY STATEMENT

The datasets generated for this study are available on request to the corresponding author.

ETHICS STATEMENT

The Ethics Committee of Catholic University of Sacred Heart/Fondazione Policlinico Universitario Agostino Gemelli IRCCS approved this study.

AUTHOR CONTRIBUTIONS

AT, VF, DP, and PV contributed conception and design of the study. GS, DC, DR, GC, FM, AB, RL, and RS collected the data. AT and VF organized the database. CD and AA performed the statistical analysis. AT wrote the first draft of the manuscript. DB and DP wrote sections of the manuscript. All authors contributed to manuscript revision, read, and approved the submitted version.

REFERENCES

1. Kenneson A, Cannon MJ. Review and meta-analysis of the epidemiology of congenital cytomegalovirus (CMV) infection. *Rev Med Virol.* (2007) 17:253–76. doi: 10.1002/rmv.535
2. Fowler KB, McCollister FP, Dahle AJ, Boppana S, Britt WJ, Pass RF. Progressive fluctuating sensorineural hearing loss in patients with asymptomatic congenital cytomegalovirus infection. *J Pediatr.* (1997) 130:624–30 doi: 10.1016/S0022-3476(97)70248-8
3. Mocarski ES, Shenk T. Cytomegalovirus. In: Howley PM, Knipe DM, editors. *Fields Virology*. Vol. 2. Philadelphia, PA: Lippincott Williams and Wilkins (2007). p. 2701–72.
4. Dollard SC, Grosse SD, Ross DS. New estimates of the prevalence of neurological and sensory sequelae and mortality associated with congenital cytomegalovirus infection. *Rev Med Virol.* (2007) 17:355–63. doi: 10.1002/rmv.544
5. Goderis J, De Leenheer E, Smets K, Van Hoecke H, Keymeulen A, Dhooge I. Hearing loss and congenital CMV infection: a systematic review. *Pediatrics.* (2014) 134:972–82. doi: 10.1542/peds.2014-1173
6. Fowler KB, Boppana SB. Congenital cytomegalovirus (CMV) infection and hearing deficit. *J Clin Virol.* (2006) 35:226–31. doi: 10.1016/j.jcv.2005.09.016
7. Fowler KB, Dahle AJ, Boppana SB, Pass RF. Newborn hearing screening: will patients with hearingloss caused by congenital cytomegalovirus infection be missed? *J Pediatr.* (1999) 135:60–4. doi: 10.1016/S0022-3476(99)70328-8
8. American Academy of Pediatrics, Joint Committee on Infant Hearing. Year 2007 position statement: principles and guidelines for early hearing detection and intervention programs. *Pediatrics.* (2007) 120:898–921. doi: 10.1542/peds.2007-2333

9. Korndewal MJ, Oudesluys-Murphy AM, Kroes ACM, van der Sande MAB, de Melker HE, Vossen ACTM. Long-term impairment attributable to congenital cytomegalovirus infection: a retrospective cohort study. *Dev Med Child Neurol*. (2017) 59:1261–8. doi: 10.1111/dmcn.13556
10. Zhang XW, Li F, Yu XW, Shi XW, Shi J, Zhang JP. Physical and intellectual development in patients with asymptomatic congenital cytomegalovirus infection: a longitudinal cohort study in Qinba mountain area, China. *J Clin Virol.* (2007) 40:180–5. doi: 10.1016/j.jcv.2007.08.018
11. Kimberlin DW, Lin CY, Sánchez PJ, Demmler GJ, Dankner W, Shelton M, et al. Effect of ganciclovir therapy on hearing in symptomatic congenital cytomegalovirus disease involving the central nervous system: a randomized, controlled trial. *J Pediatr.* (2003) 143:16–25. doi: 10.1016/S0022-3476(03)00192-6
12. Ross SA, Boppana SB. Congenital cytomegalovirus infection: outcome and diagnosis. *Semin Pediat Infect Dis.* (2005) 16:44–9. doi: 10.1053/j.spid.2004.09.011
13. Kimberlin DW, Acosta EP, Sànchez PJ, Sood S, Agrawal V, Homans J, et al. Pharmacokinetic and pharmacodynamic assessment of oral valganciclovir in the treatment of symptomatic congenital cytomegalovirus disease. *J Infect Dis.* (2008) 197:836–45. doi: 10.1086/528376
14. Kimberlin DW, Jester PM, Sànchez PJ, Ahmed A, Arav-Boger R, Michaels MG, et al. Valganciclovir for symptomatic congenital cytomegalovirus disease. *N Engl J Med*. (2015) 372:933–43. doi: 10.1056/NEJMoa1404599
15. Revello MG, Fabbri E, Furione M, Zavattoni M, Lilleri D, Tassis B, et al. Role of prenatal diagnosis and counseling in the management of 735 pregnancies complicated by primary human cytomegalovirus infection: a 20-year experience. *J Clin Virol.* (2011) 50:303–7. doi: 10.1016/j.jcv.2010.12.012
16. Bhatia P, Narang A, Minz RW. Neonatal cytomegalovirus infection: diagnostic modalities available for early disease detection. *Indian J Pediatr.* (2010) 77:77–9. doi: 10.1007/s12098-009-0255-2
17. Bertino E, Spada E, Occhi L, Coscia A, Giuliani F, Gagliardi L, et al. Neonatal anthropometric charts: the Italian neonatal study compared with other European studies. (2010). *J Pediatr Gastroenterol Nutr*. (2010) 51:353–61 doi: 10.1097/MPG.0b013e3181da213e
18. Luck SE, Wieringa JW, Blázquez-Gamero D, Henneke P, Schuster K, Butler K, et al. Congenital cytomegalovirus - a European expert consensus statement on diagnosis and management. *Pediatr Infect Dis J*. (2017) 36:1205–213. doi: 10.1097/INF.0000000000001763
19. Schleiss MR. Congenital cytomegalovirus infection: update on management strategies. *Curr Treat Options Neurol.* (2008) 10:186–92. doi: 10.1007/s11940-008-0020-2
20. Lombardi G, Garofoli F, Villani, P. Oral valganciclovir treatment in newborns with symptomatic congenital cytomegalovirus infection. *Eur J Clin Microbiol Infect Dis.* (2009) 28:1465–70. doi: 10.1007/s10096-009-0806-5
21. Amir J, Wolf DG, Levy I. Treatment of symptomatic congenital cytomegalovirus infection with intravenous ganciclovir followed by long term oral valganciclovir. *Eur J Pediatr.* (2010) 169:1061–7. doi: 10.1007/s00431-010-1176-9
22. Buonsenso D, Serranti D, Gargiullo L, Ceccarelli M, Ranno O, Valentini P. Congenital cytomegalovirus infection: current strategies and future perspectives. *Eur Rev Med Pharmacol Sci.* (2012) 16:919–35.
23. Henkin CC, Griener JC, Ten Eick AP. Stability of valganciclovir in extemporaneously compounded liquid formulations. *Am J Health Syst Pharm.* (2003) 60:687–90 doi: 10.1093/ajhp/60.7.687
24. *Giunti Psychometrics*. Avalaible online at https://www.giuntios.it/
25. Kobas M, Bickle Graz M, Truttmann AC, Giannoni E, Meylan P, Asner SA. Clinical characteristics, audiological and neurodevelopmental outcomes of newborns with congenital cytomegalovirus infection. *Swiss Med Wkly.* (2018) 148:w14627. doi: 10.4414/smw.2018.14627
26. Jin HD, Demmler-Harrison GJ, Coats DK, Paysse EA, Bhatt A, Edmond JC, et al. Long-term visual and ocular sequelae in patients with congenital cytomegalovirus. *Pediatr Infect Dis J.* (2017) 36:877–82. doi: 10.1097/INF.0000000000001599

Conflict of Interest: The authors declare that the research was conducted in the absence of any commercial or financial relationships that could be construed as a potential conflict of interest.

frontiers in Public Health

ORIGINAL RESEARCH
published: 30 October 2020
doi: 10.3389/fpubh.2020.558283

Anaplasma phagocytophilum Activates NF-κB Signaling via Redundant Pathways

J. Stephen Dumler[1,2]*, *Marguerite Lichay*[2], *Wan-Hsin Chen*[2], *Kristen E. Rennoll-Bankert*[2] *and Jin-ho Park*[2]

[1] *Department of Pathology, F. Edward Hébert School of Medicine, Uniformed Services University for the Health Sciences, Bethesda, MD, United States,* [2] *Division of Medical Microbiology, Department of Pathology, The Johns Hopkins University School of Medicine, Baltimore, MD, United States*

Anaplasma phagocytophilum subverts neutrophil function permitting intracellular survival, propagation and transmission. Sustained pro-inflammatory response, recruitment of new host cells for population expansion, and delayed apoptosis are associated with prolonged nuclear presence of NF-κB. We investigated NF-κB signaling and transcriptional activity with *A. phagocytophilum* infection using inhibitors of NF-κB signaling pathways, and through silencing of signaling pathway genes. How inhibitors or silencing affected *A. phagocytophilum* growth, inflammatory response (transcription of the κB-enhanced genes *CXCL8* and *MMP9*), and NF-κB signaling pathway gene expression were tested. Among *A. phagocytophilum*-infected HL-60 cells, nuclear NF-κB p50, p65, and p52 were detected by immunoblots or iTRAQ proteomics. *A. phagocytophilum* growth was affected most by the IKKαβ inhibitor wedelolactone (reductions of 96 to 99%) as compared with SC-514 that selectively inhibits IKKβ, illustrating a role for the non-canonical pathway. Wedelolactone inhibited transcription of both *CXCL8* ($p = 0.001$) and *MMP9* ($p = 0.002$) in infected cells. Compared to uninfected THP-1 cells, *A. phagocytophilum* infection led to >2-fold down regulation of 64 of 92 NF-κB signaling pathway genes, and >2-fold increased expression in only 4. Wedelolactone and SC-514 reversed downregulation in all 64 and 45, respectively, of the genes down-regulated by infection, but decreased expression in 1 gene with SC-514 only. Silencing of 20 NF-κB signal pathway genes increased bacterial growth in 12 (*IRAK1*, *MAP3K1*, *NFKB1B*, *MAP3K7*, *TICAM2*, *TLR3*, *TRADD*, *TRAF3*, *CHUK*, *IRAK2*, *LTBR*, and *MALT1*). Most findings support canonical pathway activation; however, the presence of NFKB2 in infected cell nuclei, selective non-canonical pathway inhibitors that dampen *CXCL8* and *MMP9* transcription with infection, upregulation of non-canonical pathway target genes *CCL13* and *CCL19*, enhanced bacterial growth with *TRAF3* and *LTBR* silencing provide evidence for non-canonical pathway signaling. Whether this impacts distinct inflammatory processes that underlie disease, and whether and how *A. phagocytophilum* subverts NF-κB signaling via these pathways, need to be investigated.

Keywords: ***Anaplasma phagocytophilum*, NF-κB, signaling, neutrophil, inflammation**

OPEN ACCESS

Edited by:
Shaobin Shang,
Yangzhou University, China

Reviewed by:
Mingqun Lin,
The Ohio State University, United States
Jason A. Carlyon,
Virginia Commonwealth University, United States

***Correspondence:**
J. Stephen Dumler
john.dumler@usuhs.edu

Specialty section:
This article was submitted to Infectious Diseases - Surveillance, Prevention and Treatment, a section of the journal Frontiers in Public Health

Received: *01 May 2020*
Accepted: *22 September 2020*
Published: *30 October 2020*

Citation:
Dumler JS, Lichay M, Chen W-H, Rennoll-Bankert KE and Park J-h (2020) Anaplasma phagocytophilum Activates NF-κB Signaling via Redundant Pathways. Front. Public Health 8:558283. doi: 10.3389/fpubh.2020.558283

INTRODUCTION

Anaplasma phagocytophilum is an *Ixodes* spp. tick-transmitted zoonotic rickettsia of small mammals, cervids, and ruminants (1). Infection of co-evolved mammalian reservoirs often results in mild, subclinical, and persistent infections (2). However, granulocytic anaplasmosis is a mild to severe disease of humans, horses, and dogs, characterized in humans by fever, headache, myalgias, thrombocytopenia, leukopenia, and liver injury (1). This obligate intracellular rickettsial bacterium infects and propagates within granulocytes, largely neutrophils, in blood and bone marrow after it is acquired by tick bite and disseminated into the blood.

A. phagocytophilum evolved to survive within the antimicrobial confines of neutrophils by co-opting a number of pathways that regulate endosomal entry, vacuolar trafficking, and signals that lead to delayed apoptosis and reduced antimicrobial activities, while promoting an inflammatory environment that recruits new host cells to expand bacterial populations and inducing inflammatory cell injury as a mechanism for disease pathogenesis (3–5). The mechanisms by which *A. phagocytophilum* subverts its mammalian host cell, the neutrophil, to achieve all of these functions has been greatly studied, with a deep understanding of some microbial mechanisms and control over host functions. A key for understanding how disease occurs with *A. phagocytophilum* is the observation that clinical signs of illness in humans and animal models are not closely linked to bacterial loads, but are more closely associated with stimulation of host immune and inflammatory signaling such as with upregulation of the genes for *interleukin 1* (*IL1*), *C-X-C motif chemokine ligand 8* (*CXCL8*), *matrix metalloprotease−9* (*MMP9*), or innate immune responses, and subversion of regulatory aspects of cytotoxic lymphocytes (6–12).

How *A. phagocytophilum* triggers or directly influences immune and inflammatory processes is of some debate, but appears tied to the ability to regulate inflammatory gene transcriptional programs, including those that operate through key transcription factors such as signal transducer and activator of transcription 1 (STAT1) or the nuclear factor kappa B (NF-κB) (8, 13–16). While it is likely that inflammatory signaling after *A. phagocytophilum* infection involves multiple pathways, as a major pathway, NF-κB signaling is likely to be central to either death or survival of the pathogen and as a mechanism by which innate immune-mediated injury occurs. Two major pathways exist for NF-κB activation, the canonical pathway chiefly leading to p50/RELA dimer transcription factor, and the non-canonical pathway, largely dependent on the generation of p52/RELB dimers. While both can be generated simultaneously, there are key differences in the specific programs incited (17–19). Canonical pathway activation is associated with classical inflammatory processes, but non-canonical activation seems to be a feature of differentiation of lymphoid cells, processing in dendritic cells, and associations with immune dysregulation and autoimmunity. Owing to the diverse clinical inflammatory manifestations of infection by *A. phagocytophilum* in humans and animals, the major objective of this study was to identify specific NF-κB signaling molecules and pathways triggered or targeted by *A. phagocytophilum* and how their alterations affect sustained bacterial growth while increasing pro-inflammatory responses of host neutrophils. Here, we examine NF-κB signaling of infected cells to determine whether *A. phagocytophilum* impacts canonical, non-canonical, or atypical NF-κB signaling. We hypothesize that inhibition or silencing of *A. phagocytophilum*-interacting pathways or genes will (i) adversely affect intracellular bacterial growth, and (ii) subsequently reverse pro-inflammatory neutrophil phenotypes. We sought to identify molecular targets that detect and signal, or at which *A. phagocytophilum* could exert influence over sustained inflammatory responses and severe disease.

METHODS

Cell Lines and *A. phagocytophilum* Infection

The promyelocytic HL-60 (ATCC CCL-240) and myelomonocytic THP-1 (ATCC TIB-202) cell lines were purchased from American Type Culture Collection (Manassas, VA), and grown in RPMI 1640 medium (Hyclone, Thermo Fisher Scientific, Waltham, MA) supplemented with 5–10% fetal bovine serum (Thermo Fisher Scientific, Waltham, MA) and Glutamax (Life Technologies, Carlsbad, CA). All cells were grown in a humidified incubator at 37°C with 5% CO_2. Cell density was kept $<10^6$ cells/mL by diluting with fresh medium. *A. phagocytophilum* (Webster^T strain)-infected HL-60 or THP-1 cells were maintained as previously described (20, 21). Cell-free *A. phagocytophilum* were harvested and purified from heavily infected cells, as previously described (21), and used to infect THP-1 cells at an MOI of 100:1. For all experiments *A. phagocytophilum* was passed <10 times *in vitro*. To simulate infection over short and longer intervals of time, we used cultures at 50% (between 2 and 4 days after subculture) and 90% (4–7 days of culture) infected cells.

Cell Fractionation, Immunoblotting, and Nuclear Proteomics Evaluation

Nuclear extracts from *A. phagocytophilum*-infected, uninfected, or LPS-stimulated HL-60 cells were prepared using NE-PER Nuclear and Cytoplasmic Extraction Reagents (Thermo Scientific/Pierce Biotechnology, Rockford, IL). Samples of the cytoplasmic and nuclear fractions were analyzed by immunoblotting for the presence of NF-κB components. Ten microgram total protein from nuclear extracts of infected and uninfected HL-60 cells was electrophoresed in 10–12% SDS-PAGE gels and transferred to nitrocellulose membranes. The membranes were blocked with 5% non-fat dried milk, probed with either NF-κB p50/p105, NF-κB p65, and IκBα rabbit polyclonal antibodies (Santa Cruz Biotechnology) and incubated with goat anti-rabbit IgG or anti-mouse IgM alkaline phosphatase conjugate (KPL, Gaithersburg, MD); loading controls were not used for these initial studies. The immunoblots were visualized by incubation with BCIP/NBT substrate (Bio-Rad, USA), and the migration of the specific bands was compared with that of Jurkat nuclear extract positive control (Santa Cruz

Biotechnology) or with nuclear protein isolated from LPS-stimulated HL-60 cells. These experiments were repeated 3 times.

We further examined data extracted from a proteomics (iTRAQ [isobaric tag for relative and absolute quantitation protein profiling technology; Applied Biosystems]) study using *A. phagocytophilum*-infected and uninfected cells HL-60 cells that identified nuclear proteins in infected and uninfected HL-60 cells and their ratios (22). For each protein identified, two types of scores were reported: unused ProtScore and total ProtScore. The total ProtScore measures all peptide evidence for a protein analogous to protein scores reported by other protein identification software programs. However, the unused ProtScore measures all peptide evidence for a protein not better explained by a higher ranking protein, and was the method of choice. The protein confidence threshold cutoff for this study was set at an unused score of 2.0 with at least one peptide with 99% confidence. A ratio of infected to uninfected (Aph:HL-60) score was used to identify differential presence of human proteins in nuclear lysates. To do this, we averaged the ratios of uninfected HL-60 nuclear lysate replicates (isobaric isotope labels 115:114) and ratios of nuclear lysate replicates from *A. phagocytophilum*-infected HL-60 cells (116:114 and 117:114) to create the composite Aph:HL-60 mean ratio. Proteins identified with mean ratios (fold change infected/uninfected) > 2 or < 0.5 were considered to be significantly differentially present in the nucleus. This experiment was done once with biological replicates.

Finally, we compared gene expression profiles among 4 separate studies that examined *A. phagocytophilum* infection in neutrophils (GSE2405; GPL570) (8, 14) HL-60 cells, all trans-retinoic acid (ATRA)-differentiated HL-60 cells (23) (GSE107770), and NB4 promyelocytic cells (24) (GSE2600) to identify differential expression of 104 genes associated with NF-κB signaling in the KEGG (Kyoto Encyclopedia of Genes and Genomes) database (https://www.genome.jp/dbget-bin/www_bget?pathway+hsa04064). This pathway is roughly divided into "canonical," "atypical," and" non-canonical." The downloaded list was manually annotated for each protein/gene with regard to the 3 pathways in which each participates for signaling. The set was examined for consensus differential transcript in two of the three studies examined, with up- and downregulation considered as per authors, in all 3 cases, a 2-fold change compared to control uninfected neutrophils or HL-60 cells; *p*-values or false discovery rate were collected as available (**Supplementary Table 1C**).

Inhibitors and Toxicity Studies

In order to determine which of the NF-κB activation pathways was utilized by *A. phagocytophilum*, we selected specific pharmacologic inhibitors that could differentially block either (i) the proteasome, using MG132 (N-[(Phenylmethoxy)carbonyl]-L-leucyl-N-[(1S)-1-formyl-3-methylbutyl]-L-leucinamide); (ii) the canonical pathway at NF-κB essential modulator/inhibitor of nuclear factor kappa B kinase regulatory subunit gamma (NEMO/IKKγ), using NEMO-Binding Domain Binding Peptide (NBD peptide; DRQIKIWFQNRRMKWKKTALDWSWLQTE, and control peptide DRQIKIWFQNRRMKWKK-TALDASALQTE); (iii) the non-canonical pathway using either wedelolactone (1,8,9-Trihydroxy-3-methoxy-6H-benzofuro[3,2-c][1]benzopyran-6-one, 7-Methoxy-5,11,12-trihydroxycoumestan; an inhibitor of both inhibitor of nuclear factor kappa-B kinase subunit alpha [IKKα,IKK1,CHUK]) and nuclear factor kappa-B kinase subunit beta [IKKβ,IKK2] (25) or SC 514 (4-Amino-[2′,3′-bithiophene]-5-carboxamide; a selective ATP-competitive inhibitor of IKKβ (26); or (iv) the atypical pathway (inhibitor of nuclear factor kappa-B kinase [IKK]-independent) using Casein Kinase II Inhibitor I (CK2i; 4,5,6,7-Tetrabromobenzotriazole), a high affinity, cell-permeable inhibitor of casein kinase 2 (CK2) (all from Millipore/Sigma, USA). To implement these studies, we selected to use the myelomonocytic cell line THP-1, owing to its ready ability for manipulation and transfection. Initially, all drugs were tested over the range of 12.5, 25.0, and 50.0 μM concentrations to assess both THP-1 and *A. phagocytophilum*-infected THP-1 cell (4×10^5 cells) toxicity using the ToxiLight Bioassay Kit (Lonza) compared to cells treated with 1% Triton X and untreated cells. Percent cytotoxicity was calculated (luminescence units of cells with or without drug/luminescence units of cells treated with Triton X) and then normalized to untreated cells. Normalized values >2 (50% cytotoxicity) were considered toxic.

Quantitative Measurement of *A. phagocytophilum* Growth and Inhibitor Impact on Defense Gene Transcription

A. phagocytophilum was quantified by three methods: (1) cytocentrifugation of infected THP-1 cells, followed by Romanowsky staining (LeukoStat) and enumeration of the proportion of infected cells (repeated 3 times); (2) quantitative real-time 5′-nuclease PCR, targeting *A. phagocytophilum msp2* DNA, as previously described (27, 28) (repeated 3 times in triplicate); and (3) quantitative reverse transcriptase PCR, targeting *A. phagocytophilum major surface protein-2* (*msp2*) mRNA using the same 5′ nuclease method (repeated twice in triplicate). Quantification of PCR assays was accomplished using the BioRad CFX384 Real time PCR analyzer, by comparing mean Cq values of known concentrations of cloned *A. phagocytophilum msp2* as a single copy in a plasmid, and dividing by a factor of 84 (the approximate number of *msp2* paralogs detectable by this assay in the *A. phagocytophilum* Webster strain genome) for DNA. All samples were tested in at least duplicate.

To determine whether specific pharmacologic inhibition of pathways in the canonical, non-canonical, or the "atypical" IKK-independent pathway would impact infection, growth or survival of *A. phagocytophilum*, infected THP-1 cells were pretreated with a range of non-toxic doses of drugs targeting each pathway, infected with cell-free *A. phagocytophilum* at an MOI of 100:1, and examined after 24 h of growth *in vitro* by qPCR or after 6 days of growth for microscopic examination, comparing untreated to treated cells. Similarly, cells were harvested from triplicate cultures for preparation of RNA and analysis of relative transcription of cellular *CXCL8* and *MMP9*, markers of κB-driven pro-inflammatory gene regulation with *A. phagocytophilum* infection. Transcriptional responses were normalized (ΔCt) to housekeeping genes for infected

and uninfected cells separately, then to *CXCL8* and *MMP9* transcription (ΔΔCt) for no inhibitor vs. inhibitor in infected and uninfected cells separately. To extend the findings of pharmacologic inhibitors of NF-κB signaling genes, similar studies were conducted in a high-throughput screen using 96 distinct target genes, including 92 related to NF-κB signaling (**Supplementary Table 1A**) and 4 housekeeping genes previously shown to be largely unaffected by *A. phagocytophilum* infection (*ACTB, B2M, GAPDH,* and *HPRT1*) (29, 30). Assays were conducted as above in smaller scales comparing uninfected THP-1 cell gene transcription to that of *A. phagocytophilum*-infected THP-1 cells with or without 25 μM SC-514 or wedelolactone. Transcription for each of the 96 genes was measured by preparing RNA from duplicate cultures after 24 h of infection and testing each culture in technical replicates, measuring increase in SYBR green fluorescence at the Ct values for each culture and technical replicate. Final values for relative transcription were calculated after averaging the housekeeping gene expression Ct values to calculate initial ΔCt values (housekeeping gene Ct—target gene Ct), and using the ΔΔCt method by comparing ΔCt expression values of all variables to ΔCt values for uninfected or infected cells (21). In general, a 2-fold increase or decrease in transcription was considered significant. However, statistical analysis was conducted by comparing transcription in replicate cultures using the Student's *t*-test with and without the Benjamini-Hochberg method for False Discovery rate (FDR) correction (http://www.real-statistics.com/). FDR < 0.05 was considered significant. These experiments were done twice.

NF-κB Signaling Pathway Gene Silencing

To determine the impact of genes involved in NF-κB signaling on the propagation of *A. phagocytophilum*, we used the SureSilencing™ siRNA Array Human NF-κB Signaling Pathway- Validated Gene Knockdown RNA Interference kit (SABiosciences/Qiagen), according to manufacturer instructions. Here, 6.4×10^3 to 1.28×10^4 THP-1 cells were aliquoted into the respective wells after reagent rehydration with SureFECT Transfection Reagent in medium and allowed to become transfected for 12 h. Thereafter, cell-free *A. phagocytophilum* was added at an MOI of 200:1 (2×10^6 bacteria) and incubated for 6 h. This MOI reproducibly yielded a significant and discernable increase in bacterial quantity within 6 h in pilot experiments (not shown). At 18 h, samples were removed for microscopy and quantitation of infected cells; the remainder was used for RNA preparation and reverse transcriptase PCR. Relative gene transcription was evaluated by SYBR green reverse transcriptase PCR targeting mRNA transcripts included for silencing in the SureSilencing™ siRNA Array Human NF-κB Signaling Pathway kit; *GAPDH* and *HRPT1* were used as housekeeping genes. Melt curve analysis was used to assure specificity of the SYBR green PCR reactions. Silencing efficiency was evaluated as per manufacturer's instructions for THP-1 cells, and only those targets for which significant reduction of at least 75% expression was observed were evaluated for changes in *A. phagocytophilum* RNA quantity as an estimate of bacterial viability and propagation in gene-silenced cells; data for selected gene targets with >55% reduction in expression were also evaluated. *A. phagocytophilum* growth or suppression was monitored by simultaneous reverse transcriptase amplification of *msp2* transcripts within the RNA preparations, using the factor of 119 (number of *msp2* RNA transcripts for each *msp2* genome equivalent) to convert to genome equivalents based on comparative RNA and DNA PCR using known quantities of bacteria after 18–24 h active replication (data not shown). This experiment was done twice.

RESULTS

Prolonged Nuclear Localization of NF-κB in *A. phagocytophilum*-Infected HL-60 Cells

As shown in **Figure 1**, uninfected HL-60 cells demonstrated presence of RELA p65 but lacked detectable NF-κB p50 (and precursor p105) in nuclei and cytoplasm. In contrast, infection of HL-60 cells of sufficient duration to achieve 50% infected cells (∼2–4 days) or 90% infected cells (∼4–7 days) demonstrated the presence of both nuclear p65 and the presence and persistence of p50 in infected cell nuclei. While p50 was detected also as a higher molecular weight mobility, likely as precursor p105, p65 was detected predominantly as a monomer, with possible isoforms or post-translational modifications in both the nucleus and cytoplasm (31). Similarly, IκBα was marginally detectable as a 36–41 kDa monomer in the cytoplasm of uninfected, infected, and LPS-stimulated HL-60 cell; however, in the nucleus, IκBα was not detected in either uninfected or LPS-stimulated HL-60 cells, but was present within high molecular weight bands at ∼100 to 150 kDa among *A. phagocytophilum*-infected cells, likely reflecting ubiquitylation (32, 33).

Using the iTRAQ proteomics approach, infected HL-60 cells demonstrated 848 human nuclear protein signatures, of which 26 were present in 2-fold greater or lesser amounts than in uninfected cells; of note, NF-κB2 was identified expressed 2.5-fold higher than in uninfected cell nuclei, but among 11 NF-κB signaling signatures (**Supplementary Table 1B**) detected in the nuclear preparations, 10 were not differentially expressed >2-fold. IκBα, the inhibitor of NF-κB in the cytoplasm and nucleus (33, 34), was not identified, perhaps owing to stimulation of the canonical pathway leading to its ubiquitylation and degradation. When transcriptional profiles of *A. phagocytophilum*-infected myeloid cells were queried for differential expression of a set of 104 NF-κB signaling pathway genes, 9 were upregulated >2-fold and none were downregulated more than 2-fold in 3 of 4 datasets evaluated (**Supplementary Table 1C**).

Toxicity of Pharmacologic Reagents

THP-1 cells, infected or not by *A. phagocytophilum*, generally tolerated up to 25 to 50 μg/mL of NF-κB inhibitors, except MG-132, which was cytotoxic in all concentrations tested for uninfected, but not infected cells (**Supplementary Figure 1**), and NBD peptide, which was toxic at concentrations >12.5 μM in uninfected cells (**Supplementary Figure 1**); NBD peptide was not further tested. The optimal concentrations of each inhibitor were determined by the highest concentration of the inhibitor that was not cytotoxic for uninfected or infected cells. In general,

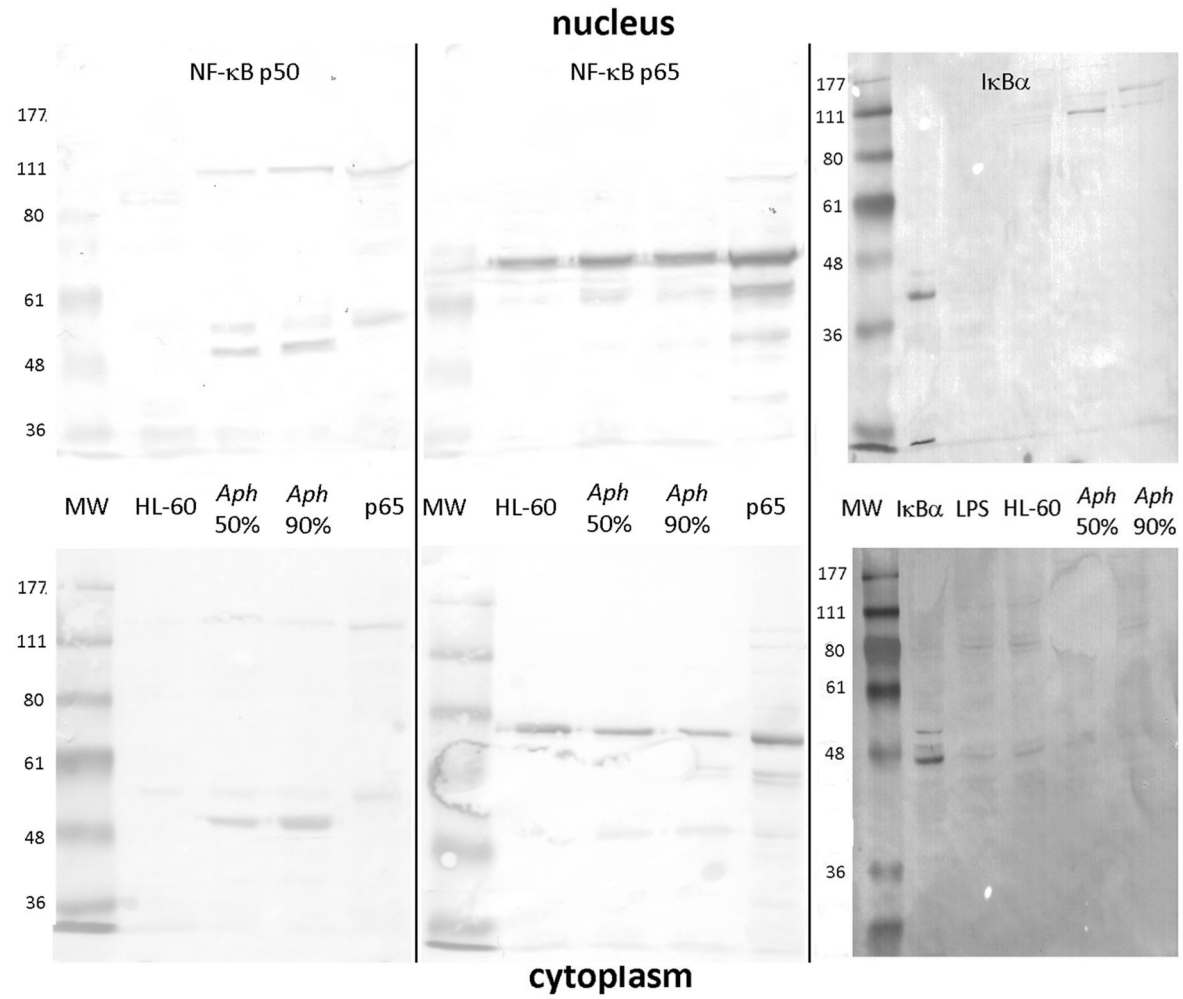

FIGURE 1 | NF-κB p50/p105, RELA (p65), and IκB analysis in the nucleus and cytoplasm of *A. phagocytophilum*-infected and uninfected HL-60 cells. The p50 component of p105 is expressed as two isoforms in infected HL-60 cells, and qualitatively lower density in uninfected than in infected cells; p50 is also detected as its precursor, p105 in both nucleus and cytoplasm (left panels). Unlike p50 and p105, RELA (p65) is qualitatively similar in uninfected and infected HL-60 cell nuclei and cytoplasm (middle panel). IκBα is also detected qualitatively at very low band density in the cytoplasm but not nuclei of uninfected, LPS-stimulated, and infected HL-60 cells as monomers; it is also detected in the nuclei of infected HL-60 cells but only as high molecular weight complexes, likely reflecting ubiquitylation. The antibody used to detect bands for each vertical nuclear (top panels) and cytoplasm (bottom panels) extract pair is labeled at the top. Jurkat cell nuclear lysate positive control = pos. The image represents a composite of six separate gel images, altered only for decreased brightness to visualize all bands, applied equally to all panels. No other manipulations were used.

each drug was tested over the range of concentrations including 12.5, 25.0, and of 50.0 μM.

Effects of Pharmacologic Inhibitors of NF-κB Signaling on *A. phagocytophilum* Infection and Growth

The effects of inhibitors of NF-κB signaling on *A. phagocytophilum* infection and growth was greatest for wedelolactone and to a lesser degree for SC-514, with no effect for CK2i. The impact of inhibition of the non-canonical pathway by wedelolactone and SC-514 was most dramatic in the microscopic evaluations (**Figure 2**) where growth was reduced between 99 and 96% ($p = 0.035$ and 0.015, respectively). In contrast, growth was not significantly different compared to no drug for CK2i that impacts the IKK-independent pathway. The proteasome inhibitor, MG-132, which targets both the canonical and non-canonical NF-κB pathways, was cytotoxic in the high drug concentration used for the microscopic studies. Because of this limitation, *A. phagocytophilum* growth was also assessed by qPCR using pharmacologic inhibitors over a range of drug doses shown to lack cytotoxicity. In general, bacterial quantity/cell was lower with wedelolactone at high concentrations (**Figure 3**). Unlike the observations by microscopy, SC-514 had no significant impact on *A. phagocytophilum* growth at any dosage. Triplicate experiments with the CK2 inhibitor CK2i revealed no

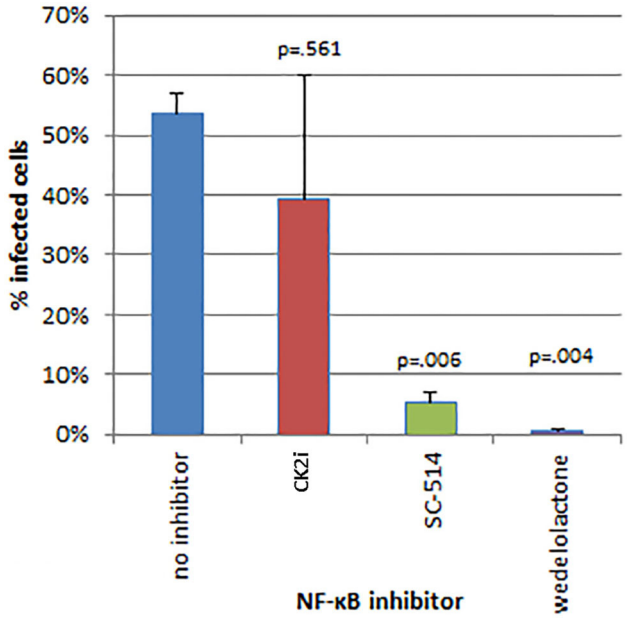

FIGURE 2 | Inhibitors of the alternative or non-canonical NF-κB signaling pathway (wedelolactone—inhibitor of IKKα/β; SC-514—selective inhibitor of IKKβ) significantly inhibit *A. phagocytophilum* growth when examined microscopically for the presence of morulae (intravacuolar bacterial colonies). The casein kinase 2 inhibitor of the IKK-independent pathway (CK2i), did not significantly affect bacterial growth. Error bars are SEM; *p*-values were calculated comparing to no inhibitor.

significant changes in *A. phagocytophilum* growth for any of the 3 concentrations tested.

The effects of pharmacologic inhibition of NF-κB signaling inhibitors on downstream expression of *CXCL8* and *MMP9*, genes known to be upregulated with and important for *A. phagocytophilum* pathogenesis (6–8, 23, 35), were evaluated. Increasing concentrations of the NF-κB signaling pathway inhibitors had marginal reproducible effects for all drugs tested in infected cells, with the exception of wedelolactone, for which concentrations higher than 12.5 μM significantly diminished *CXCL8* transcription, and also dampened transcription of *MMP9*. *CXCL8* transcription was also significantly reduced in uninfected THP-1 cells with all doses of wedelolactone. When confirmed with optimized doses of drug based on initial experiments (Wedelolactone 31.8 μM, SC-514 50 μM, and CK2i 20 μM), the silencing of *CXCL8* and *MMP9* was greater among infected cells (∼100-fold reduced) than uninfected cells (**Figure 4**), with significant reductions only observed for wedelolactone ($p = 0.001$ to 0.002).

To discern whether *A. phagocytophilum* also influences the transcription of genes involved in NF-κB signaling, and whether this could be impacted by pharmacologic inhibition by either Wedelolactone or SC-514, RNA from uninfected, and *A. phagocytophilum*-infected THP-1 cells with our without 25 μM wedelolactone or 25 μM SC-514 were assayed by RT-PCR. A majority (64/92) of NF-κB signaling pathway genes were downregulated more than 2-fold with infection, whereas only 5 of 92 were upregulated, *BCL2A1*, *IL1B, CXCL8, MMP9,* and *SOD2* (**Supplementary Figure 2**). Eight of 92 genes were downregulated more than 6.25-fold (*CCL23, FGF8, IFNG, MADCAM1, MAP3K3, PGR, PRKCG,* and *PTPN13*); only *BCL2A1* had a $p < 0.05$, and no gene expression was significantly changed when analyzed by the Benjamini-Hochberg method for False Discovery rate (FDR) (**Supplementary Figure 2**). When normalized to uninfected cells, of the 92 genes assayed in infected cells treated with SC-514, 24 were upregulated and 11 downregulated more than 2-fold, but only 4 achieved unadjusted $p < 0.05$ (*AKT1, FADD, MADCAM1,* and *MAP3K1*), and none were significant when adjusted for FDR. Wedelolactone had more dramatic effects, increasing expression of 15 and decreasing expression of 23 out of the 92 genes examined. Of these, only 10 showed upregulated expression with unadjusted $p < 0.05$, including *AKTA, BCL2A1, CCL23, CHUK, IRAK2, MAP3K1, RPL13A, TICAM1, TNFRSF10B,* and *TNFRSF1A*, but only *RPL13A* ($p = 0.0144$) and *TICAM1* ($p = 0.0058$) were significantly upregulated compared to infected cells after adjustment for FDR (**Figure 5**). It should be noted that *CXCL8* and *MMP9* that were downregulated in infected cells treated with wedelolactone, but not SC-514 (**Figure 4**), were not significantly changed by similar inhibitor treatments in the high-throughput study. This observation could be an effect of the differing assay sensitivities, uncontrolled biological variables over time that perhaps lead to differential activation of canonical and non-canonical pathways in the same experiments, all potentially confounding interpretations.

NF-κB Signaling Pathway Gene Silencing

To discern whether broader effects of *A. phagocytophilum* infection resulted in transcriptional regulation of a variety of genes involved in NF-κB signaling, a transcriptional profiling array was employed to analyze the effects of infection in silenced THP-1 cells vs. effects in cells with control siRNA. Of the 41 NF-κB signaling pathway genes targeted in the SureSilencing™ siRNA Array kit (**Supplementary Table 2**), 16 genes were silenced by 75% or greater. Among the NF-κB signaling pathway genes successfully silenced in THP-1 cells, *A. phagocytophilum* levels increased by more than 30% and with $p < 0.05$ with silencing of *TRADD*, *TRAF3*, *MAP3K1*, *MAP3K7*, *IRAK1*, *TLR3*, *TICAM2*, and *NFKB1*, and of 4 with growth decreased by 20% or more, none were significantly different than mock silenced cells (**Figure 6**). Five additional genes silenced >55% were also considered, and 4 of these demonstrated a significant increase in *A. phagocytophilum* growth as compared with mock-silenced controls; these included *CHUK* (*IKKA*), *IRAK2, LTBR,* and *MALT1*. Their inclusion allowed an improved analysis of the non-canonical pathway.

DISCUSSION

A. phagocytophilum has a remarkable capacity to survive within the harsh niche of the primary innate immune antimicrobial cell, the neutrophil. It does this by virtue of altering fundamental functions of this cell, including reprogramming of

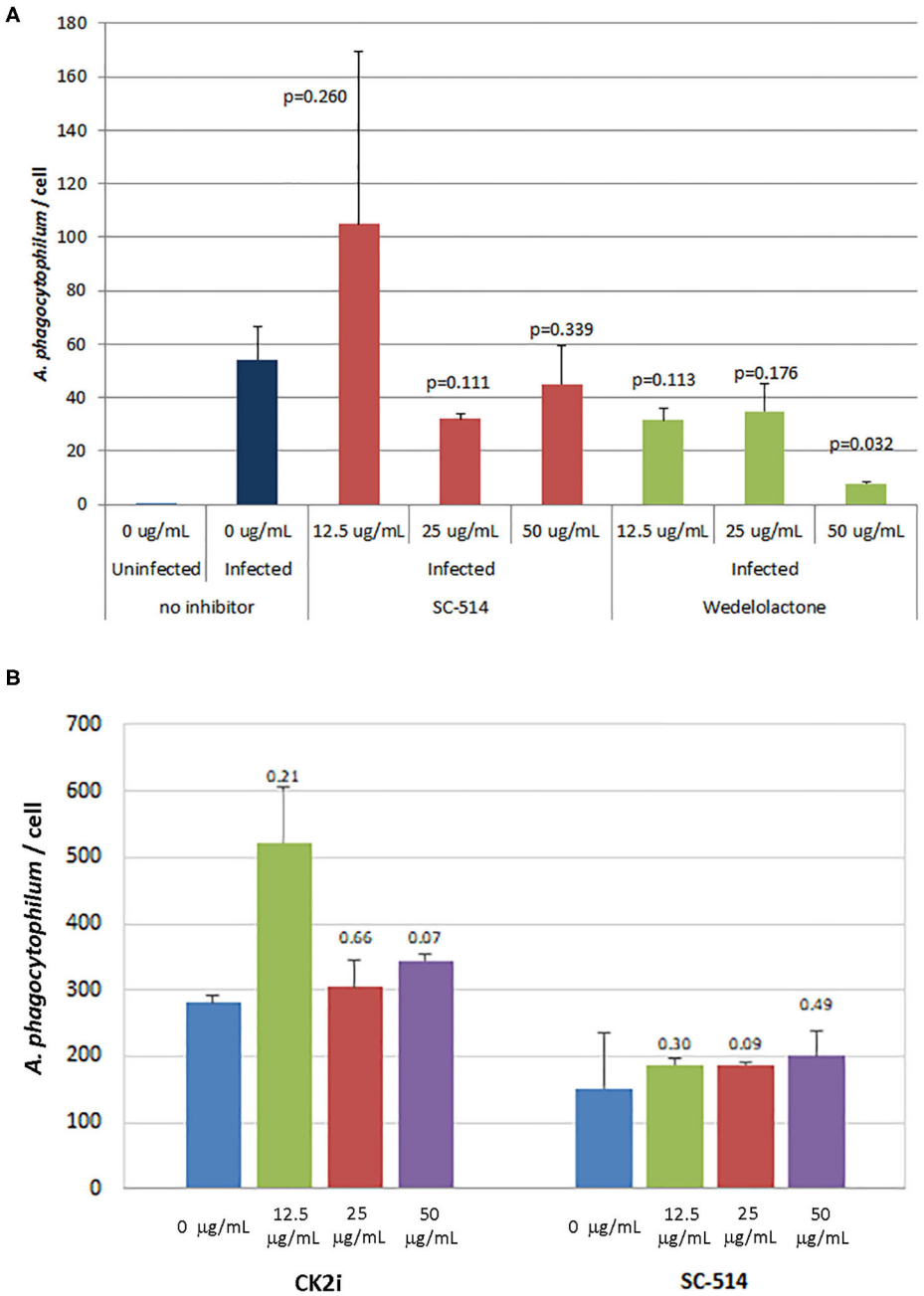

FIGURE 3 | Wedelolactone, a non-selective IKKα/β inhibitor of the alternative or non-canonical NF-κB signaling pathway **(A)**, but not SC-514 that selectively inhibits IKKβ in the non-canonical pathway **(A,B)**, or CK2i, and inhibitor of the IKK-independent pathway **(B)**, significantly inhibits *A. phagocytophilum* growth when used in high concentrations and when assessed by quantitative PCR. Error bars are SEM; *p*-values were calculated comparing to no inhibitor and are listed above each average measurement.

(i) pro-inflammatory responses; (ii) apoptosis; (iii) antimicrobial responses; and (iv) reduction of tethering/arrest and emigration capacity. The overall fitness benefit to the bacterium is (i) pro-inflammatory responses and recruitment of new host neutrophils into which it can pass and propagate (6, 10, 15, 16, 35, 36); (ii) dampening of mechanisms that could lead to bacterial killing within the neutrophil (21, 30, 37–41); (iii) prolongation of neutrophil survival through delayed apoptosis to permit increased bacterial doubling (8, 42–44); and (iv) increased retention of infected cells within the vasculature accessible for transmission during a subsequent tick blood meal (7, 45–49). Each of these distinct functions has been

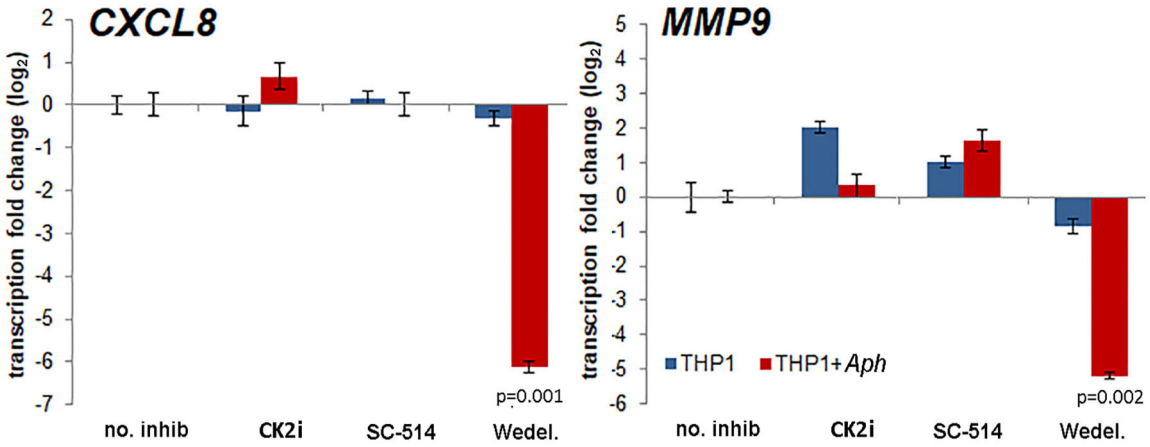

FIGURE 4 | Activation of the non-canonical NF-κB signaling pathway mediates upregulation of downstream gene expression important for *A. phagocytophilum* immune pathogenicity. Differential transcription from *CXCL8* encoding the key chemokine that recruits new host neutrophils, and from *MMP9* encoding an important protease in neutrophils that is secreted as part of the inflammatory process after *A. phagocytophilum* infection, are significantly dampened by the non-selective IKKα/β inhibitor, wedelolactone (Wedel.), but not by other inhibitors of NF-κB signaling, and a similar effect was not present with uninfected cells. Error bars represent SEM; *p*-values infected vs. uninfected THP-1 are shown when <0.05.

examined to some degree and many depend intrinsically on host gene expression and transcriptional programs, modulation of signaling pathways, or subversion of intracellular trafficking, some proven to be regulated by microbial manipulation of host gene transcription (21, 30, 41). While it would be anticipated that *A. phagocytophilum* should initiate pro-inflammatory responses via interactions with toll-like receptors and other microbial sensors, coordination of host inflammation ordinarily results in parallel activation of both inflammatory and antimicrobial activities as well as the ability of activated cells to transmigrate microvascular barriers in response to chemotactic gradients. Moreover, the lack of most differential transcription elicited when cells are stimulated by heat-killed *A. phagocytophilum* (8), suggests that active infection and host cell manipulation are key to not only pathogen survival, but to pro-inflammatory responses. These events are coordinated by a number of mechanisms; but most converge with activation and nuclear translocation of NF-κB, and binding of its active components to κB consensus sequences over a spectrum of gene promoters that execute the neutrophil's inflammatory, survival, and antimicrobial activities.

An overriding concept in intracellular infections is that pathogens modulate host signal transduction and transcriptional responses to change host cell function and improve bacterial survival. Intracellular pathogens that alter host signaling are best studied in macrophages and epithelial cells, while little is known about bacteria that propagate within neutrophils. In macrophages, bacterial proteins introduced into host cells influence phagocytosis, vacuolar trafficking, and promote or dampen inflammation, apoptosis and cytotoxicity, among other effects. One strategy targets signal transduction of important pro-inflammatory pathways, particularly by interfering with activation of NF-κB (50). The full spectrum of NF-κB-responsive genes has not been described, but important targets include those involved in innate and adaptive immunity, such as genes for cytokines, chemokines, adhesion molecules, acute phase proteins (SAA), inducible effectors (iNOS, COX-2), adaptive immune response, and regulators of apoptosis and cell proliferation (51), many of which comprise the transcriptional reprogramming phenotype of *A. phagocytophilum*-infected neutrophils. NF-κB is a target for bacterial and viral subversion of host cells (50), where, for example, *Yersinia enterocolitica* YopP binds to IKKβ, the kinase that phosphorylates IκBα before proteolysis and release of activated NF-κB (52). Likewise, *Mycobacterium ulcerans* affects NF-κB transactivation by preventing nuclear localization or by interfering with DNA binding (53), and NF-κB can be regulated by viral IκBα mimics suppressing inflammatory response (54).

NF-κB/REL proteins comprise a family of dimeric transcription factors, including RELA (p65), RELB, c-REL, NF-κB1 p50 (and p105 precursor), and NF-κB2 p49/52 (and p100 precursor) (51). Most abundant is the p50/p65 heterodimer that rapidly transactivates genes for transcription; p50/p50 and p52/p52 homodimers can repress target gene transcription. NF-κB/REL proteins possess a conserved N-terminal Rel homology domain (RHD) that mediates DNA binding, dimerization, and interaction with IκB inhibitory proteins, to which they are bound in an inactive state in the cytoplasm. The RHD also has nuclear localization sequences (NLS) usually masked by interaction with IκBs. IκBs comprise a family with several members, IκBα, IκBβ, IκBε, IκBγ, Bcl-3, and the Rel precursors, p100 and p105. Control of NF-κB gene transactivation is based on phosphorylation of IκBs at specific sites that targets them for ubiquitylation and proteasome degradation, unmasking the NLS on NF-κB to allow transport into the nucleus where transcriptional effects are mediated (51).

NF-κB activation is affected by a number of signals including receptors such as toll-like (TLR) or tumor necrosis factor (TNFR)

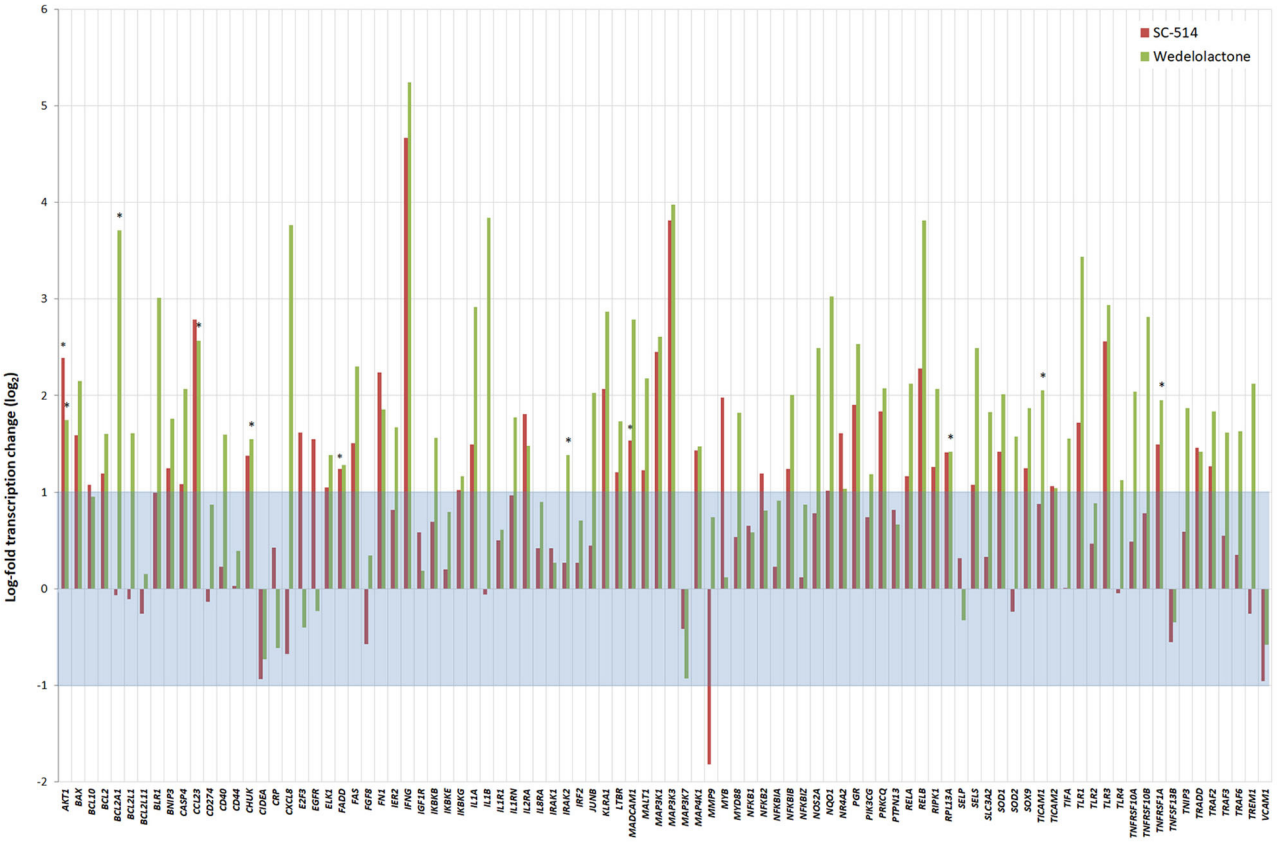

FIGURE 5 | Inhibition of non-canonical NF-κB activation with wedelolactone or SC-514 reverses suppression of many genes transcriptionally dampened with *A. phagocytophilum* infection (see **Supplementary Figure 2**). Here, gene expression was normalized to that observed in *A. phagocytophilum*-infected THP-1 cells. Beyond the borders of the blue zone depicts >2-fold change compared to transcription in infected cells without the pharmacologic inhibitors. The most highly impacted genes were all upregulated by either wedelolactone (IKKα/β inhibitor) or SC-514 (IKKβ inhibitor) and included *AKT1, FADD, MADCAM11, MAP3K1, BCL2A1, CCL23, CHUK, IRAK2, RPL13A, TICAM1, TNFRSF1A,* and *TNFRSF10A*. Values that represent a significant difference ($p < 0.05$) compared to infected cells are denoted by an asterisk "*".

receptors, and is propagated by signaling through MyD88-dependent or -independent pathways resulting in IKK complex activation and eventual phosphorylation of IκBα in the canonical pathway (55, 56). The alternative or non-canonical pathway to NF-κB activation, particularly for p49/52 (NF-κB2) and RELB, results from stimuli through TNFR family members, such as CD40, lymphotoxin-β receptor, or those for LPS, via NIK (MAP3K14) upregulation and activation of IKKα or via receptor-induced degradation of TRAF2 and TRAF3 that under steady state conditions degrade NIK (18, 57). Additional activation of NF-κB occurs through intracellular interactions with NOD1 and NOD2, but whether this involves IKK complex activation is unclear (58–61). Although NF-κB activation occasionally occurs without IKK complex activation, activation of the IKK complex is often the key to NF-κB activation. A key distinction between canonical and non-canonical activation is the sole utilization of IKKα dimers in the non-canonical pathway, allowing their distinction by comparing the effects of the IKK-non-selective inhibitor wedelolactone to those of the IKKβ-selective inhibitor SC-514. This unique pharmacologic inhibition would predict that more dramatic effects with wedelolactone than for SC-514 are the result of non-canonical pathway inhibition. It is obvious that *A. phagocytophilum*, which benefits when inflammation is modulated, is provided ample targets for pathogen effectors in NF-κB signaling pathways.

Here, we demonstrate that both p65 and p50 are present in the nuclei of *A. phagocytophilum*-infected cells for at least 7 days of infection, although p65 is constitutively expressed in uninfected HL-60 cells (62). The presence of NF-κB p105 in nuclear lysates was not anticipated, but is well-documented with stimulation (63–65); whether it would provide IκB-like inhibitory function in this circumstance is not known, but likely. While neutrophils when stimulated with LPS or TNF will demonstrate nuclear p50 and p65 over periods that persist for 12 h or longer, this is in part controlled by the simultaneous nuclear retention of IκBα (33, 34), and ultimately such neutrophils become

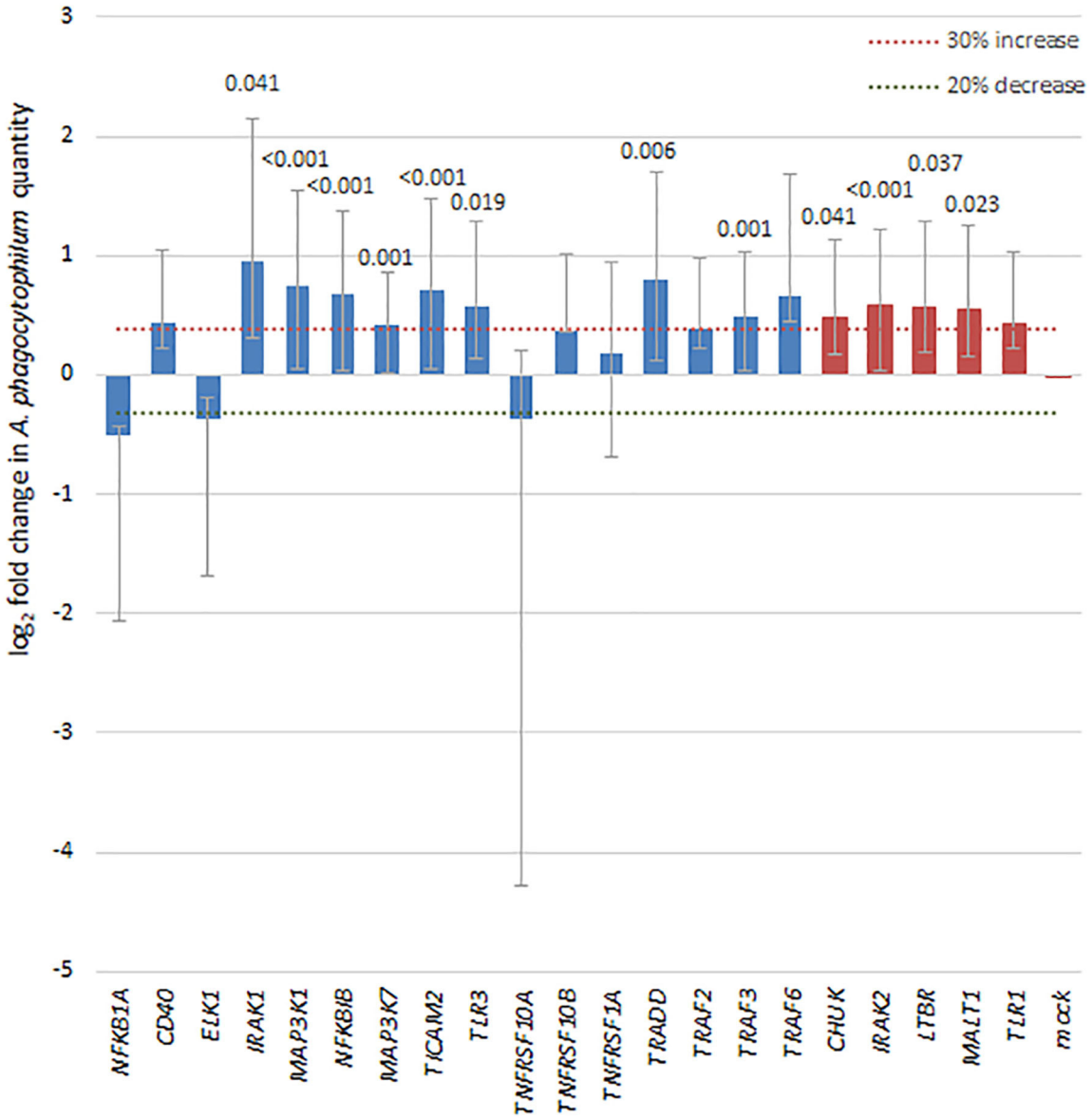

FIGURE 6 | Silencing of NF-κB signaling pathway genes by siRNA leads to a 30% or greater increase in *A. phagocytophilum* growth, as measured by qPCR in 8 of 16 genes with silencing >75% (blue bars), including *IRAK1* (canonical), *MAP3K1* (canonical), *NFKBIB* (both), *TLR3* (both), *TRADD* (canonical), *TRAF3* (both), and *MAP3K7* (canonical), involved largely with the canonical pathway via TNF receptor or TLR signaling pathways. In addition, among 5 other genes silenced to at least 55% (red bars), 4 (*CHUK, IRAK2, LTBR,* and *MALT1*) also demonstrated significant increases in *A. phagocytophilum* growth. Error bars represent SEM; when significantly different from the mock-silenced control ($p < 0.05$), *p*-values are provided above each bar.

apoptotic owing to the inhibition of κB site transcriptional activation with prolonged IκBα binding (33, 34). Additionally, extrapolation from THP-1 or HL-60 cells to neutrophils is challenging; however, *A. phagocytophilum* can delay apoptosis in infected neutrophils for as long as 96 h via mechanisms active in MAP kinase signaling, sustained *BCL2* gene family transcription, and through mitochondrial stabilization (43, 44, 66). In contrast to our hypothesis, silencing of NF-κB signaling genes and inhibition of their protein products, when effective, largely increased bacterial propagation suggesting that their presence with activated NF-κB signaling lowers the fitness of *A. phagocytophilum*. For 8 of these silenced genes, *A. phagocytophilum* burden increased 30% or greater, including with silencing of *TRAF3* and *TRADD*, confirming that the canonical NF-κB signaling pathway is impacted by *A. phagocytophilum* infection. The major unexplained discrepancy for this finding is the diminished transcription of both *CXCL8* and *MMP9* in infected cells treated with the non-selective IKK inhibitor

wedelolactone. This observation is of interest since CXCL8 and MMP9 are implicated as important for *A. phagocytophilum* fitness by enhancing bacterial expansion *in vitro* and *in vivo* (6, 7, 35, 67).

In contrast with the concurrent increase of RELA (p65), NFKB1 p50 and IκBα in the nuclei of activated or infected HL-60 cells and evidence that the canonical NF-κB pathway is active, is the increased detection of a NF-κB2 protein in infected vs. uninfected HL-60 cell nuclei as long as 7 days after infection, and increases in *NFKB2* transcription among transcriptional profiling studies (**Supplementary Table 1C**). Inhibition of *A. phagocytophilum* propagation and differential expression of κB-driven genes by the non-selective IKKα/β inhibitor wedelolactone and less robustly by the IKKβ inhibitor SC-514 was reproducible. Because signaling for the non-canonical pathway depends predominantly on IKKα, which selectively phosphorylates p100 when associated with RELB (68), the more consistent impact of wedelolactone than the IKKβ-selective inhibitor SC-514 further supports a role for signaling through the non-canonical pathway.

The non-canonical pathway is typically linked to stimulation of cell surface receptors such as the TNF receptor family CD40 (TNFRSF5) or RANK (TNFRSF11A), via lymphotoxin-β (LTB) or the B-cell TNF-family cytokine BAFF (TNFSF13B) (57, 69). Of the TNFR family, silencing of *TNFRSF10A, TNFRSF10B,* and *TNFRSF1* did not alter *A. phagocytophilum* growth *in vitro*. However, *CD40*, *CD40L*, *TNFRSF11A* (RANK), *TNFSF14*, EDAR associated death domain (*EDARADD*), and baculoviral IAP repeat containing 3 (*BIRC3*) are significantly upregulated with *A. phagocytophilum* infection in several transcriptional profiling studies, and all are involved in the induction of or propagation of non-canonical NF-κB signaling (8, 14, 23). Non-canonical pathway-specific gene targets that are upregulated with *A. phagocytophilum* infection include both *CCL13*, which recruits inflammatory leukocytes except neutrophils, and *CCL19*, which impacts lymphocyte recruitment and homing in the thymus or lymph nodes.

Additionally, of the key TNFR signaling adaptors *TRAF2*, *TRAF3*, and *TRAF6*, expression is not significantly upregulated with *A. phagocytophilum* infection of HL-60 or human neutrophils (**Supplementary Table 1C**). NIK (MAP3K14) stabilization after TNFRs aggregate TRAF2, TRAF3 and/or TRAF6, the major adaptors for non-canonical signaling, permits their ubiquitylation by cIAP1/2 and degradation, ultimately allowing NIK to degrade IKKα (CHUK) and release of p100/p52 dimers in the non-canonical pathway. Here, silencing of both *TRAF3* and *TRAF6* leads to a more productive *A. phagocytophilum* infection. This finding further suggests that activation of non-canonical (or canonical) pathway is host-protective rather than an enhancer of bacterial fitness. While the finding does not inform about microbial fitness, it could be a potentially important observation given the recognition that non-canonical pathway activation is associated with unique transcriptional programs that in part guide lymphoid cell differentiation, dendritic cell function, and distinct inflammatory phenotypes, including chronic inflammatory conditions, autoimmune diseases such inflammatory bowel disease, acute kidney and lung injury, immunodeficiency syndromes, and even cancer (17, 69–72).

Of course, other possibilities exist for mechanisms by which *A. phagocytophilum* could influence NF-κB signaling. Ligation of innate immune receptors such as toll-like or NOD-like intracellular receptors can also lead to activation (73), and NLRC4 activates the inflammasome in *A. phagocytophilum* infection (74). We previously showed *A. phagocytophilum* triggered NF-κB-driven target gene expression through TLR2 but not TLR4 in primary *ex vivo* human monocytes (36). Prior transcriptional profiling of *A. phagocytophilum*-infected ATRA-differentiated HL-60 cells also demonstrated significant upregulation of *TLR2, TLR1, TLR3,* and *TLR6*, as well as *NOD2* and *NLRP3* (23). In fact, treatment of infected cells with wedelolactone and SC-514 led to increased transcription of *TLR1* and *TLR3*, but not *TLR2* in infected cells. The recent evaluation of differentially regulated NF-κB-related genes in response to various TLR ligands shows distinctive patterns for each TLR (75). When these genes were queried using the *A. phagocytophilum* transcriptional profiling in infected ATRA-differentiated HL-60 cells (23), the highest proportion of differentially expressed genes was found among the group observed when cells were stimulated by the TLR2 agonist, PAM-2CSK4 (data not shown). It is likely that responses triggered by PAMPs contribute to the sustained activation of NF-κB pro-inflammatory signaling in infected *A. phagocytophilum* cells. Finally, it is further recognized that cross-talk exists between the canonical and non-canonical pathways that could be regulatory or have other yet to be discerned purposes (72).

To synthesize a working model from these data, it is reasonable to start from the signal origin for ligands. The clear evidence of canonical pathway activation likely results from interactions with pathogen recognition receptors such as TLRs (36), NLRs (74), formyl-peptide and Fc receptors (40), or cytokines released from other stimulated cells that amplify the response. With regard to the non-canonical NF-κB pathway, signaling is initiated by ligands binding to TNFR superfamily members, for which there is evidence with *A. phagocytophilum* infection, including upregulated expression of several ligands and receptors. Although silencing of several of these TNFR superfamily members did not change *A. phagocytophilum* growth, with the possible exception of *LTBR*, of 8 TNFR superfamily genes detected in expression profiling of *A. phagocytophilum*-infected ATRA-differentiated HL-60 cells, 7 are upregulated from 2.9- to 178-fold, providing ample opportunity for non-canonical NF-κB signaling (23).

Aside from initiating signaling via PAMPs and related processes, pathogens can manipulate NF-κB signaling to their advantage, such as with viral RNAs that are detected by the cytoplasmic RNA sensor retinoic acid inducible gene I (RIG-I), or via production of viral proteins that interact with and alter various NF-κB signaling pathway proteins (18). Whether *A. phagocytophilum* or its effectors interfere with normal cellular functions or lead to transcriptional regulation of key NF-κB pathway genes is not proven, but given the evidence of activation

of both canonical and non-canonical pathways, such extended studies might be fruitful. Despite increased *A. phagocytophilum* growth with silencing of some NF-κB signaling pathway genes, the ongoing differential transcription that yields significant upregulation of chemokine genes or those associated with suppression of apoptosis clearly benefit the pathogen, even if simply a component of physiologic NF-κB function. In fact, while the inhibitor and silencing data seem to argue for a protective role of NF-κB signaling, a majority of genes in these pathways are downregulated by *A. phagocytophilum* infection, reminiscent of the role that the type IV secretion system nuclear effector AnkA plays in dampening transcription of host defense genes, although no data here directly support that hypothesis (21, 41).

These observations provide evidence for NF-κB signaling via the canonical and non-canonical pathways as targets for control of infection or by which *A. phagocytophilum* could subvert host cell functions to impact microbial fitness. There are weaknesses in our study, including the lack of direct evidence of RELB in the nucleus of infected cells, and the ambiguity that is increasingly recognized in NF-κB signaling pathways that potentially confounded some studies leading to discrepant results. An increasing body of literature examines the cross-talk between the canonical and non-canonical NF-κB signaling pathways, and an emerging view is one of co-regulation and balance between acute and chronic inflammation and healing. Specifically how this occurs is still open for much additional research since inhibitors of NF-κB-mediated inflammatory suppression are in development (17). Moreover, an improved understanding of these inflammatory pathways could result from a clearer picture as to how *A. phagocytophilum* interacts with and reprograms its mammalian host cells while promoting a diversity of inflammatory responses that link closely to the diverse outcomes and human disease severity (4, 11, 76–78).

DATA AVAILABILITY STATEMENT

The datasets presented in this study can be found in online repositories. The names of the repository/repositories and accession number(s) can be found in the article/**Supplementary Material**.

AUTHOR CONTRIBUTIONS

JSD conceived and coordinated all research activities, interpreted results, and wrote the manuscript. ML conducted the majority of the experiments related to bacterial growth effects with pharmacologic inhibition and siRNA. W-HC conducted most of the experiments related to effects of pharmacologic inhibitors on transcriptional activity with infection. KR-B helped with the proteomics experiments and analyses. J-hP conducted and interpreted results from the initial experiments on NF-kappa B expression among nuclear and cytoplasmic preparations by protein immunoblotting. All authors contributed to the article and approved the submitted version.

FUNDING

The work was supported in part by grants R21AI080911, R01AI044102, and R01AI041213 to JSD from the National Institutes of Allergy and Infectious Diseases.

ACKNOWLEDGMENTS

The authors acknowledge the excellent technical advice and assistance of Jose Carlos Garcia-Garcia, Ph.D. and Dennis Grab, Ph.D. ML and W-HC are no longer employed by The Johns Hopkins University School of Medicine; KR-B is currently employed at Becton Dickinson, Sparks, MD; J-hP is currently Professor in the Department of Veterinary Internal Medicine, College of Veterinary Medicine, Jeonbuk National University, Jeonbuk, Republic of South Korea. The opinions expressed herein are those of the author(s) and are not necessarily representative of those of the Uniformed Services University of the Health Sciences (USUHS), the Department of Defense (DOD); or, the United States Army, Navy, or Air Force.

SUPPLEMENTARY MATERIAL

The Supplementary Material for this article can be found online at: https://www.frontiersin.org/articles/10.3389/fpubh.2020.558283/full#supplementary-material

REFERENCES

1. Bakken JS, Dumler JS. Human granulocytic anaplasmosis. *Infect Dis Clin North Am.* (2015) 29:341–55. doi: 10.1016/j.idc.2015.02.007
2. Stephenson N, Foley J. Parallelisms and contrasts in the diverse ecologies of the *Anaplasma phagocytophilum* and *Borrelia burgdorferi* complexes of bacteria in the far western United States. *Vet Sci.* (2016) 3:26. doi: 10.3390/vetsci3040026
3. Rikihisa Y. Mechanisms of obligatory intracellular infection with *Anaplasma phagocytophilum*. *Clin Microbiol Rev.* (2011) 24:469–89. doi: 10.1128/CMR.00064-10
4. Dumler JS. The biological basis of severe outcomes in *Anaplasma phagocytophilum* infection. *FEMS Immunol Med Microbiol.* (2012) 64:13–20. doi: 10.1111/j.1574-695X.2011.00909.x
5. Truchan HK, Cockburn CL, Hebert KS, Magunda F, Noh SM, Carlyon JA. The pathogen-pccupied vacuoles of *Anaplasma phagocytophilum* and *Anaplasma marginale* interact with the endoplasmic reticulum. *Front Cell Infect Microbiol.* (2016) 6:22. doi: 10.3389/fcimb.2016.00022
6. Akkoyunlu M, Malawista SE, Anguita J, Fikrig E. Exploitation of interleukin-8-induced neutrophil chemotaxis by the agent of human granulocytic ehrlichiosis. *Infect Immun.* (2001) 69:5577–88. doi: 10.1128/IAI.69.9.5577-5588.2001
7. Choi KS, Grab DJ, Dumler JS. *Anaplasma phagocytophilum* infection induces protracted neutrophil degranulation. *Infect Immun.* (2004) 72:3680–3. doi: 10.1128/IAI.72.6.3680-3683.2004
8. Borjesson DL, Kobayashi SD, Whitney AR, Voyich JM, Argue CM, Deleo FR. Insights into pathogen immune evasion mechanisms: *Anaplasma phagocytophilum* fails to induce an apoptosis differentiation

program in human neutrophils. *J Immunol.* (2005) 174:6364–72. doi: 10.4049/jimmunol.174.10.6364
9. Scorpio DG, von Loewenich FD, Gobel H, Bogdan C, Dumler JS. Innate immune response to *Anaplasma phagocytophilum* contributes to hepatic injury. *Clin Vaccine Immunol.* (2006) 13:806–9. doi: 10.1128/CVI.00092-06
10. Choi KS, Webb T, Oelke M, Scorpio DG, Dumler JS. Differential innate immune cell activation and proinflammatory response in *Anaplasma phagocytophilum* infection. *Infect Immun.* (2007) 75:3124–30. doi: 10.1128/IAI.00098-07
11. Dumler JS, Barat NC, Barat CE, Bakken JS. Human granulocytic anaplasmosis and macrophage activation. *Clin Infect Dis.* (2007) 45:199–204. doi: 10.1086/518834
12. Scorpio DG, Choi KS, Dumler JS. *Anaplasma phagocytophilum*-related defects in CD8, NKT, and NK lymphocyte cytotoxicity. *Front Immunol.* (2018) 9:710. doi: 10.3389/fimmu.2018.00710
13. de la Fuente J, Ayoubi P, Blouin EF, Almazan C, Naranjo V, Kocan KM. Gene expression profiling of human promyelocytic cells in response to infection with *Anaplasma phagocytophilum*. *Cell Microbiol.* (2005) 7:549–59. doi: 10.1111/j.1462-5822.2004.00485.x
14. Lee HC, Kioi M, Han J, Puri RK, Goodman JL. *Anaplasma phagocytophilum*-induced gene expression in both human neutrophils and HL-60 cells. *Genomics.* (2008) 92:144–51. doi: 10.1016/j.ygeno.2008.05.005
15. Choi KS, Dumler JS. *Anaplasma phagocytophilum*, interferon gamma production and Stat1 signaling. *Microbiol Immunol.* (2013) 57:207–12. doi: 10.1111/1348-0421.12023
16. Choi KS, Scorpio DG, Dumler JS. Stat1 negatively regulates immune-mediated injury with *Anaplasma phagocytophilum* infection. *J Immunol.* (2014) 193:5088–98. doi: 10.4049/jimmunol.1401381
17. Cildir G, Low KC, Tergaonkar V. Noncanonical NF-kappaB signaling in health and disease. *Trends Mol Med.* (2016) 22:414–29. doi: 10.1016/j.molmed.2016.03.002
18. Sun S-C. The non-canonical NF-κB pathway in immunity and inflammation. *Nat Rev Immunol.* (2017) 17:545–58. doi: 10.1038/nri.2017.52
19. Mulero MC, Wang VY-F, Huxford T, Ghosh G. Genome reading by the NF-κB transcription factors. *Nucl Acids Res.* (2019) 47:9967–89. doi: 10.1093/nar/gkz739
20. Goodman JL, Nelson C, Vitale B, Madigan JE, Dumler JS, Kurtti TJ, et al. Direct cultivation of the causative agent of human granulocytic ehrlichiosis. *N Engl J Med.* (1996) 334:209–15. doi: 10.1056/NEJM199601253340401
21. Garcia-Garcia JC, Barat NC, Trembley SJ, Dumler JS. Epigenetic silencing of host cell defense genes enhances intracellular survival of the rickettsial pathogen *Anaplasma phagocytophilum*. *PLoS Pathog.* (2009) 5:e1000488. doi: 10.1371/journal.ppat.1000488
22. Sinclair SH, Garcia-Garcia JC, Dumler JS. Bioinformatic and mass spectrometry identification of *Anaplasma phagocytophilum* proteins translocated into host cell nuclei. *Front Microbiol.* (2015) 6:55. doi: 10.3389/fmicb.2015.00055
23. Dumler JS, Sinclair SH, Shetty AC. Alternative splicing of differentiated myeloid cell transcripts after infection by *Anaplasma phagocytophilum* impacts a selective group of cellular programs. *Front Cell Infect Microbiol.* (2018) 8:14. doi: 10.3389/fcimb.2018.00014
24. Pedra JH, Sukumaran B, Carlyon JA, Berliner N, Fikrig E. Modulation of NB4 promyelocytic leukemic cell machinery by *Anaplasma phagocytophilum*. *Genomics.* (2005) 86:365–77. doi: 10.1016/j.ygeno.2005.05.008
25. Kobori M, Yang Z, Gong D, Heissmeyer V, Zhu H, Jung YK, et al. Wedelolactone suppresses LPS-induced caspase-11 expression by directly inhibiting the IKK Complex. *Cell Death Differ.* (2004) 11:123–30. doi: 10.1038/sj.cdd.4401325
26. Kishore N, Sommers C, Mathialagan S, Guzova J, Yao M, Hauser S, et al. A selective IKK-2 inhibitor blocks NF-kappa B-dependent gene expression in interleukin-1 beta-stimulated synovial fibroblasts. *J Biol Chem.* (2003) 278:32861–71. doi: 10.1074/jbc.M211439200
27. Scorpio DG, Caspersen K, Ogata H, Park J, Dumler JS. Restricted changes in major surface protein-2 (*msp2*) transcription after prolonged *in vitro* passage of *Anaplasma phagocytophilum*. *BMC Microbiol.* (2004) 4:1. doi: 10.1186/1471-2180-4-1
28. Scorpio DG, Leutenegger C, Berger J, Barat N, Madigan JE, Dumler JS. Sequential analysis of *Anaplasma phagocytophilum* msp2 transcription in murine and equine models of human granulocytic anaplasmosis. *Clin Vaccine Immunol.* (2008) 15:418–24. doi: 10.1128/CVI.00417-07
29. Rennoll-Bankert KE, Sinclair SH, Lichay MA, Dumler JS. Comparison and characterization of granulocyte cell models for *Anaplasma phagocytophilum* infection. *Pathog Dis.* (2014) 71:55–64. doi: 10.1111/2049-632X.12111
30. Rennoll-Bankert KE, Garcia-Garcia JC, Sinclair SH, Dumler JS. Chromatin-bound bacterial effector ankyrin A recruits histone deacetylase 1 and modifies host gene expression. *Cell Microbiol.* (2015) 17:1640–52. doi: 10.1111/cmi.12461
31. Grumont RJ, Gerondakis S. Alternative splicing of RNA transcripts encoded by the murine p105 NF-kappa B gene generates I kappa B gamma isoforms with different inhibitory activities. *Proc Natl Acad Sci USA.* (1994) 91:4367–71. doi: 10.1073/pnas.91.10.4367
32. Alkalay I, Yaron A, Hatzubai A, Orian A, Ciechanover A, Ben-Neriah Y. Stimulation-dependent I kappa B alpha phosphorylation marks the NF-kappa B inhibitor for degradation via the ubiquitin-proteasome pathway. *Proc Nat Acad Sci U.S.A.* (1995) 92:10599–603. doi: 10.1073/pnas.92.23.10599
33. Vancurova I, Vancura A. Regulation and function of nuclear IkappaBalpha in inflammation and cancer. *Am J Clin Exp Immunol.* (2012) 1:56–66.
34. Miskolci V, Rollins J, Vu HY, Ghosh CC, Davidson D, Vancurova I. NFkappaB is persistently activated in continuously stimulated human neutrophils. *Mol Med.* (2007) 13:134–42. doi: 10.2119/2006-00072.Miskolci
35. Scorpio DG, Akkoyunlu M, Fikrig E, Dumler JS. CXCR2 blockade influences *Anaplasma phagocytophilum* propagation but not histopathology in the mouse model of human granulocytic anaplasmosis. *Clin Diagn Lab Immunol.* (2004) 11:963–8. doi: 10.1128/CDLI.11.5.963-968.2004
36. Choi KS, Scorpio DG, Dumler JS. *Anaplasma phagocytophilum* ligation to toll-like receptor (TLR) 2, but not to TLR4, activates macrophages for nuclear factor-kappa B nuclear translocation. *J Infect Dis.* (2004) 189:1921–5. doi: 10.1086/386284
37. Carlyon JA, Chan WT, Galan J, Roos D, Fikrig E. Repression of rac2 mRNA expression by *Anaplasma phagocytophila* is essential to the inhibition of superoxide production and bacterial proliferation. *J Immunol.* (2002) 169:7009–18. doi: 10.4049/jimmunol.169.12.7009
38. Choi KS, Dumler JS. Early induction and late abrogation of respiratory burst in *A. phagocytophilum*-infected neutrophils. *Ann N Y Acad Sci.* (2003) 990:488–93. doi: 10.1111/j.1749-6632.2003.tb07415.x
39. Garyu JW, Choi KS, Grab DJ, Dumler JS. Defective phagocytosis in *Anaplasma phagocytophilum*-infected neutrophils. *Infect Immun.* (2005) 73:1187–90. doi: 10.1128/IAI.73.2.1187-1190.2005
40. Garyu JW, Dumler JS. *Anaplasma phagocytophilum* infection reduces expression of phagocytosis-related receptors on neutrophils. *Ann N Y Acad Sci.* (2005) 1063:416–9. doi: 10.1196/annals.1355.075
41. Garcia-Garcia JC, Rennoll-Bankert KE, Pelly S, Milstone AM, Dumler JS. Silencing of host cell *CYBB* gene expression by the nuclear effector AnkA of the intracellular pathogen *Anaplasma phagocytophilum*. *Infect Immun.* (2009) 77:2385–91. doi: 10.1128/IAI.00023-09
42. Scaife H, Woldehiwet Z, Hart CA, Edwards SW. *Anaplasma phagocytophilum* reduces neutrophil apoptosis *in vivo*. *Infect Immun.* (2003) 71:1995–2001. doi: 10.1128/IAI.71.4.1995-2001.2003
43. Choi KS, Park JT, Dumler JS. *Anaplasma phagocytophilum* delay of neutrophil apoptosis through the p38 mitogen-activated protein kinase signal pathway. *Infect Immun.* (2005) 73:8209–18. doi: 10.1128/IAI.73.12.8209-8218.2005
44. Ge Y, Yoshiie K, Kuribayashi F, Lin M, Rikihisa Y. *Anaplasma phagocytophilum* inhibits human neutrophil apoptosis via upregulation of bfl-1, maintenance of mitochondrial membrane potential and prevention of caspase 3 activation. *Cell Microbiol.* (2005) 7:29–38. doi: 10.1111/j.1462-5822.2004.00427.x
45. Choi KS, Garyu J, Park J, Dumler JS. Diminished adhesion of *Anaplasma phagocytophilum*-infected neutrophils to endothelial cells is associated with reduced expression of leukocyte surface selectin. *Infect Immun.* (2003) 71:4586–94. doi: 10.1128/IAI.71.8.4586-4594.2003
46. Park J, Choi KS, Grab DJ, Dumler JS. Divergent interactions of *Ehrlichia chaffeensis*- and *Anaplasma phagocytophilum*-infected leukocytes

with endothelial cell barriers. *Infect Immun.* (2003) 71:6728–33. doi: 10.1128/IAI.71.12.6728-6733.2003
47. Munderloh UG, Lynch MJ, Herron MJ, Palmer AT, Kurtti TJ, Nelson RD, et al. Infection of endothelial cells with *Anaplasma marginale* and *A. phagocytophilum.Vet Microbiol.* (2004) 101:53–64. doi: 10.1016/j.vetmic.2004.02.011
48. Herron MJ, Ericson ME, Kurtti TJ, Munderloh UG. The interactions of *Anaplasma phagocytophilum*, endothelial cells, and human neutrophils. *Ann N Y Acad Sci.* (2005) 1063:374–82. doi: 10.1196/annals.1355.090
49. Schaff UY, Trott KA, Chase S, Tam K, Johns JL, Carlyon JA, et al. Neutrophils exposed to *A. phagocytophilum* under shear stress fail to fully activate, polarize, and transmigrate across inflamed endothelium. *Am J Physiol Cell Physiol.* (2010) 299:C87–96. doi: 10.1152/ajpcell.00165.2009
50. Rosenberger CM, Finlay BB. Phagocyte sabotage: disruption of macrophage signalling by bacterial pathogens. *Nat Rev Mol Cell Biol.* (2003) 4:385–96. doi: 10.1038/nrm1104
51. Ghosh S, Karin M. Missing pieces in the NF-kappaB puzzle. *Cell.* (2002) 109:S81–96. doi: 10.1016/S0092-8674(02)00703-1
52. Ruckdeschel K, Harb S, Roggenkamp A, Hornef M, Zumbihl R, Kohler S, et al. *Yersinia enterocolitica* impairs activation of transcription factor NF-kappaB: involvement in the induction of programmed cell death and in the suppression of the macrophage tumor necrosis factor alpha production. *J Exp Med.* (1998) 187:1069–79. doi: 10.1084/jem.187.7.1069
53. Pahlevan AA, Wright DJ, Andrews C, George KM, Small PL, Foxwell BM. The inhibitory action of *Mycobacterium ulcerans* soluble factor on monocyte/T cell cytokine production and NF-kappa B function. *J Immunol.* (1999) 163:3928–35.
54. Tait SW, Reid EB, Greaves DR, Wileman TE, Powell PP. Mechanism of inactivation of NF-kB by a viral homologue of Ikappa-Balpha. *J Biol Chem.* (2000) 275:34656–64. doi: 10.1074/jbc.M000320200
55. Perkins ND. Post-translational modifications regulating the activity and function of the nuclear factor kappa B pathway. *Oncogene.* (2006) 25:6717–30. doi: 10.1038/sj.onc.1209937
56. Perkins ND. Integrating cell-signalling pathways with NF-kappaB and IKK function. *Nat Rev Mol Cell Biol.* (2007) 8:49–62. doi: 10.1038/nrm2083
57. Sun SC. The noncanonical NF-kappaB pathway. *Immunol Rev.* (2012) 246:125–40. doi: 10.1111/j.1600-065X.2011.01088.x
58. Girardin SE, Tournebize R, Mavris M, Page AL, Li X, Stark GR, et al. CARD4/Nod1 mediates NF-kappaB and JNK activation by invasive *Shigella. flexneri EMBO Rep.* (2001) 2:736–42. doi: 10.1093/embo-reports/kve155
59. Philpott DJ, Girardin SE. The role of Toll-like receptors and Nod proteins in bacterial infection. *Mol Immunol.* (2004) 41:1099–108. doi: 10.1016/j.molimm.2004.06.012
60. Hasegawa M, Fujimoto Y, Lucas PC, Nakano H, Fukase K, Nunez G, et al. A critical role of RICK/RIP2 polyubiquitination in Nod-induced NF-kappaB activation. *EMBO J.* (2008) 27:373–83. doi: 10.1038/sj.emboj.7601962
61. Newton K, Dixit VM. Signaling in innate immunity and inflammation. *Cold Spring Harb Perspect Biol.* (2012) 4:a006049. doi: 10.1101/cshperspect.a006049
62. Luo X, Xu L, Wu X, Tan H, Liu L. Decreased SATB1 expression promotes AML cell proliferation through NF-κB activation. *Cancer Cell Int.* (2019) 19:134. doi: 10.1186/s12935-019-0850-x
63. Tenjinbaru K, Furuno T, Hirashima N, Nakanishi M. Nuclear translocation of green fluorescent protein-nuclear factor kappaB with a distinct lag time in living cells. *FEBS Lett.* (1999) 444:1–4. doi: 10.1016/S0014-5793(99)00002-2
64. Nelson G, Paraoan L, Spiller DG, Wilde GJC, Browne MA, Djali PK, et al. Multi-parameter analysis of the kinetics of NF-κB signalling and transcription in single living cells. *J Cell Sci.* (2002) 115:1137–48.
65. Savinova OV, Hoffmann A, Ghosh G. The Nfkb1 and Nfkb2 proteins p105 and p100 function as the core of high-molecular-weight heterogeneous complexes. *Mol Cell.* (2009) 34:591–602. doi: 10.1016/j.molcel.2009.04.033
66. Ge Y, Rikihisa Y. *Anaplasma phagocytophilum* delays spontaneous human neutrophil apoptosis by modulation of multiple apoptotic pathways. *Cell Microbiol.* (2006) 8:1406–16. doi: 10.1111/j.1462-5822.2006.00720.x
67. Grab DJ, Nyarko E, Barat NC, Nikolskaia OV, Dumler JS. *Anaplasma phagocytophilum-Borrelia burgdorferi* coinfection enhances chemokine, cytokine, and matrix metalloprotease expression by human brain microvascular endothelial cells. *Clin Vaccine Immunol.* (2007) 14:1420–4. doi: 10.1128/CVI.00308-07
68. Oeckinghaus A, Ghosh S. The NF-kappaB family of transcription factors and its regulation. *Cold Spring Harb Perspect Biol.* (2009) 1:a000034. doi: 10.1101/cshperspect.a000034
69. Song N, Thaiss F, Guo L. NFkappaB and kidney injury. *Front Immunol.* (2019) 10:815. doi: 10.3389/fimmu.2019.00815
70. McDaniel DK, Eden K, Ringel VM, Allen IC. Emerging roles for noncanonical NF-kappaB signaling in the modulation of inflammatory bowel disease pathobiology. *Inflamm Bowel Dis.* (2016) 22:2265–79. doi: 10.1097/MIB.0000000000000858
71. Li TJ, Zhao LL, Qiu J, Zhang HY, Bai GX, Chen L. Interleukin-17 antagonist attenuates lung inflammation through inhibition of the ERK1/2 and NF-kappaB pathway in LPS-induced acute lung injury. *Mol Med Rep.* (2017) 16:2225–32. doi: 10.3892/mmr.2017.6837
72. Tegowski M, Baldwin A. Noncanonical NF-kappaB in cancer. *Biomedicines.* (2018) 6:66. doi: 10.3390/biomedicines6020066
73. Ghosh S, Dass JFP. Study of pathway cross-talk interactions with NF-kappaB leading to its activation via ubiquitination or phosphorylation: a brief review. *Gene.* (2016) 584:97–109. doi: 10.1016/j.gene.2016.03.008
74. Wang X, Shaw DK, Sakhon OS, Snyder GA, Sundberg EJ, Santambrogio L, et al. The tick protein sialostatin L2 binds to annexin A2 and inhibits NLRC4-mediated inflammasome activation. *Infect Immun.* (2016) 84:1796–805. doi: 10.1128/IAI.01526-15
75. Borghini L, Lu J, Hibberd M, Davila S. Variation in genome-wide NF-kappaB RELA binding sites upon microbial stimuli and identification of a virus response profile. *J Immunol.* (2018) 201:1295–305. doi: 10.4049/jimmunol.1800246
76. Marko D, Perry AM, Ponnampalam A, Nasr MR. Cytopenias and clonal expansion of gamma/delta T-cells in a patient with anaplasmosis: a potential diagnostic pitfall. *J Clin Exp Hematop.* (2017) 56:160–4. doi: 10.3960/jslrt.56.160
77. Yi J, Kim KH, Ko MK, Lee EY, Choi SJ, Oh MD. Human gGranulocytic anaplasmosis as a cause of febrile illness in Korea since at least 2006. *Am J Trop Med Hyg.* (2017) 96:777–82. doi: 10.4269/ajtmh.16-0309
78. Camacci ML, Panganiban RP, Pattison Z, Haghayeghi K, Daly A, Ojevwe C, et al. Severe human granulocytic anaplasmosis with significantly elevated ferritin levels in an immunocompetent host in pennsylvania: a case rReport. *J Investig Med High Impact Case Rep.* (2018) 6:2324709618758350. doi: 10.1177/2324709618758350

Conflict of Interest: The authors declare that the research was conducted in the absence of any commercial or financial relationships that could be construed as a potential conflict of interest.

Advantages of publishing in Frontiers

OPEN ACCESS
Articles are free to read for greatest visibility and readership

FAST PUBLICATION
Around 90 days from submission to decision

HIGH QUALITY PEER-REVIEW
Rigorous, collaborative, and constructive peer-review

TRANSPARENT PEER-REVIEW
Editors and reviewers acknowledged by name on published articles

Frontiers
Avenue du Tribunal-Fédéral 34
1005 Lausanne | Switzerland

Visit us: www.frontiersin.org
Contact us: frontiersin.org/about/contact

REPRODUCIBILITY OF RESEARCH
Support open data and methods to enhance research reproducibility

DIGITAL PUBLISHING
Articles designed for optimal readership across devices

FOLLOW US
@frontiersin

IMPACT METRICS
Advanced article metrics track visibility across digital media

EXTENSIVE PROMOTION
Marketing and promotion of impactful research

LOOP RESEARCH NETWORK
Our network increases your article's readership